REFINEMENT OF THE NOCTURNAL BOUNDARY LAYER BUDGET METHOD FOR QUANTIFYING AGRICULTURAL GREENHOUSE GAS EMISSIONS

Laura A. Wittebol

Department of Natural Resource Sciences
McGill University, Montreal

September 2009

A thesis submitted to McGill University in partial fulfillment of the requirements for the degree of Doctor of Philosophy

Suggested short title:

Refinement of NBL Budget Method for Agricultural GHGs

ABSTRACT

Measuring greenhouse gas (GHG) emissions directly at the farm scale is most relevant to the agricultural sector and has the potential to eliminate some of the uncertainty arising from scaling up from plot or field studies or down from regional or national levels. The stable nighttime atmosphere acts as a chamber within which sequentially-measured GHG concentration profiles determine the flux of GHGs. With the overall goal of refining the nocturnal boundary layer (NBL) budget method to obtain reliable flux estimates at a scale representative of the typical eastern Canadian farm (approximately 1 km^2), fluxes of CO_2, N_2O, and CH_4 were measured at two agricultural farms in Eastern Canada. Field sites in 1998 and 2002 were located on an experimental farm adjacent to a suburb southwest of the city of Ottawa, ON, a relatively flat area with corn, hay, and soy as the dominant crops. The field site in 2003 was located in the rural community of Coteau-du-Lac, QC, about 20 km southwest of the island of Montreal, a fairly flat area bordered by the St. Lawrence River to the south, consisting mainly of corn and hay with a mixture of soy and vegetable crops. A good agreement was obtained between the overall mean NBL budget-measured CO_2 flux at both sites, near-in-time windy night eddy covariance data and previously published results. The mean NBL-measured N_2O flux from all wind directions and farming management was of the same order of magnitude as, but slightly higher than, previously published baseline N_2O emissions from agroecosystems. Methane fluxes results were judged to be invalid as they were extremely sensitive to wind direction change. Spatial sampling of CO_2, N_2O, and CH_4 around the two sites confirmed that [CH_4] distribution was particularly sensitive to the nature of the emission source, field conditions, and wind direction. Optimal NBL conditions for measuring GHG fluxes, present approximately 60% of the time in this study, consisted of a very stable boundary layer in which GHG profiles converged at the top of the layer allowing a quick determination of the NBL flux integration height. For suboptimal NBL conditions consisting of intermittent turbulence where GHG profiles did not converge, a flux integration method was developed which yielded estimates similar to those obtained during optimal conditions. Eighty percent of the GHG flux in optimal NBL conditions corresponded to a footprint-modelled source area of approximately 2 km upwind, slightly beyond the typical length of a farm in Coteau-du-Lac. A large portion (50%) of the flux came from within 1 km upwind of the measurement site, showing the influence of local sources. 'Top-down' NBL-measured flux values were compared with aggregated field, literature and IPCC flux values for four footprint model-defined areas across both sites, with results indicating that in baseline climatic and farm management conditions, with no apparent intermittent NBL phenomena, the aggregated flux was a good approximation of the NBL-measured flux.

RÉSUMÉ

Les données sur les émissions des gaz à effet de serre (GES) obtenues au niveau des fermes entières agricoles sont pertinentes au secteur agricole et ont le potentiel d'éliminer une partie de l'incertitude qui se produit quant à l'extrapolation du niveau de la parcelle jusqu'au niveau du champ. La couche limite nocturne (CLN) agit comme une chambre virtuelle dans laquelle on fait plusieurs ascensions pour déterminer les fluxes de GES. Dans le but géneral de raffiner la méthode du budget de la CLN afin d'obtenir de plus fiables estimées au niveau de la ferme typique (environ 1 kilomètre carré), les fluxes de CO_2, N_2O, et CH_4 ont été mesurés sur deux fermes agricoles dans l'est du Canada. En 1998 et 2002, les sites d'étude se trouvaient sur une ferme près d'une banlieue au sud-ouest d'Ottawa (Ontario), où le terrain est relativement plat et les principales cultures sont le maïs, le foin et le soya. En 2003, le site d'étude se situait dans la communauté rurale de Coteau-du-Lac (Québec), environ 20 km au sud-ouest de Montréal. Bordé par le fleuve St-Laurent au sud, ce terrain est plat et on y cultive surtout le maïs, le foin et un mélange de soya et de légumes. Le flux moyen de CO_2 mesuré aux deux sites par la méthode du budget de la CLN correspondait bien avec celui mesuré par la technique de la covariance des fluctuations et aussi avec ce qui est rapporté dans la littérature. Considérant toutes les directions de vent et toutes les pratiques agricoles, la moyenne des flux de N_2O mesurés par la technique de NBL était du même ordre de grandeur, quoiqu'un peu plus élevée, que ce qui est rapporté dans la littérature pour les émissions de base de N_2O des écosystèmes agricoles. Les résultats pour le CH_4 ont été jugés non-valides car l'échantillonage concurrente des trois gaz aux alentours des deux sites a confirmé que le CH_4 était particulièrement sensible à la variabilité spatiale selon la nature de la source d’émission, les conditions du terrain, et la direction du vent. Les conditions optimales, donnant les meilleurs résultats pour le budget de la CLN consistaient d’une très stable couche limite nocturne avec profils de CO_2 convergents, présentes 60% du temps. Une méthode pour l’intégration du flux en conditions non-optimales de profils non-convergents a été développée et a donnée des résultats semblables à ceux obtenus en conditions optimales. La majorité du flux total mesuré par le budget de la CLN durant les conditions optimales de la CLN correspondait, selon une simulation de la zone-source, à une région de source d’approximativement 2 kilometres en amont, dépassant la longueur typique d’une ferme à Coteau-du-Lac. Pourtant, une grande portion, 50%, du flux venait d’une distance de 1 km amont, ce qui confirme l’influence prononcée de l’environnement immédiat. Les flux mesurés par la méthode du budget de la CLN ont été comparés contre les estimés provenant de données experimentales, de la littérature, et du GIEC (Groupe d’experts intergouvernemental sur l’évolution du climat) agrégées pour quatre régions definiés par une simulation de zone-source à travers les deux sites. Les résultats ont démontré que dans les conditions climatiques et agricoles de base avec aucun phénomène discontinu relié à la CLN, le flux agrégé était une bonne approximation du flux mesuré par la méthode du budget de la CLN.

ACKNOWLEDGEMENTS

This thesis is the culmination of the efforts of many.

First and foremost I would like to thank my supervisor, Ian Strachan, for sticking with me throughout this long process! Thank you for your scholarly guidance and direction, your good practical advice, and for taking the time to be involved with me and my work. Thanks also to you and your wife Nancy for your kindness and generosity toward me and my family. In support of this Ph.D., Dr. Strachan provided me with: a computer, desk space, and lab space (in a newly refurbished lab!); the Coteau-du-Lac field site, field, lab, and analytical equipment for NBL data, including a CIRAS-SC CO_2 analyzer and GC-FID for methane, and other ancillary equipment ranging from a golf cart to Exetainer tubes to a shelter for the inflated blimp at the Coteau-du-Lac site; research assistants; funding for gas mileage to the field sites, accommodations in Ottawa, and a food/snack allowance for NBL nights; opportunities to travel and present at scientific conferences, as well as attend an intensive micrometeorology workshop given by Dr. Tom Denmead (hosted by Dr. Monique Leclerc); and a much appreciated graduate stipend. Dr. Strachan was very involved in field work, data processing and analysis, and especially the writing of this thesis. He was always available for guidance.

Many thanks also go to Dr. Elizabeth Pattey, my co-supervisor, for her valuable and helpful guidance both in field work, data processing and analysis, and in the written thesis. In support of this Ph.D., Dr. Pattey provided: the Ottawa field site and electricity at the Coteau-du-Lac site; previously and/or concurrently collected eddy covariance, flux gradient, and NBL data; most of the analytical instruments including a CIRAS-SC CO_2 analyzer, TDL for N_2O and CH_4, and various LI-COR CO_2 analyzers; field equipment including the tethered blimp tethersonde system, golf cart, and other ancillary equipment; research assistants, and lab assistance.

This project was primarily funded through a grant to Drs. Strachan, Pattey, and Leclerc from the Canadian Foundation for Climate and Atmospheric Sciences (CFCAS, GR-229). Additional funding for this Ph.D. was received in the form of a graduate scholarship from the Fonds québécois de la recherche sur la nature et les technologies (FQRNT).

A very earnest thank you to the following people who helped me in the course of this Ph.D. (in a somewhat chronological order): Drs. Peter Schuepp and David Lewis for their help in applying for the FQRNT scholarship; Bano Mehdi, Abdirashid Elmi, and Dr. Jim Fyles for providing a GC and help in the analysis of N_2O; Hélène Lalande, Khosro Mousavi, and Dr. Caroline Begg for providing equipment and help in soil sample analyses and/or with GPS; Dr. Roger Knowles and Mike Dalva, for their help regarding GC analysis of methane; Dr. Philippe Rochette and Normand Bertrand, for their help with GC analysis and sample tube evacuation; Herman Wittebol, for his help with GC analysis; Dr. Monique Leclerc, for graciously hosting me at The University of Georgia and for her helpful comments on NBL data; Dave Dow, for technical and lab assistance; Peter Kirby, for computer help; Lynda Blackburn, Matt Hinther, Christophe Forget, Melissa Valiquette, Diane Poon, Yao Hua Law, M. Hairabedian, Kathleen Lysyshyn, and Clare Salustro, for their help in the collection of field samples, lab analysis, and/or data processing; Mr. Guy Vincent, for allowing us access to his farm to perform our NBL work and for receiving us at his home a number of times to give us information on his own farm management practices and those in the area surrounding his farm, as well as soil analysis data; Drs. Sam Kaharabata, Tom Horst, and Natascha Kljun, for advice on the use of footprint models in stable conditions.

A very special thank you to my lab partner Nathalie Mathieu for her help and support in the lab and in the field, all our helpful discussions, and most of all for her friendship as we journeyed through graduate studies together.

The completion of this thesis would not have been possible without the invaluable aid and support of my parents, Cory and Louise Wittebol, who very kindly and generously provided a home, financial support, and childcare, and my parents-in-law, Ben and Marge Bruno, who very kindly provided childcare, most notably three days a week in the fall of 2008 and winter of 2009.

I would like to dedicate this thesis to my husband Marco Bruno and our three beautiful children, Simona (May 2004), Darius, (April 2006), and Hayden (February 2008), who make it all worthwhile.

TABLE OF CONTENTS

ABSTRACT i
RÉSUMÉ iii
ACKNOWLEDGEMENTS v
TABLE OF CONTENTS viii
LIST OF TABLES xiii
LIST OF FIGURES xvi
STATEMENT OF ORIGINAL CONTRIBUTION xxii

CHAPTER 1. INTRODUCTION 1
1.1 Uncertainties Related to Scale 1
1.2 Importance of Measuring CO_2, N_2O, and CH_4 on Farms 2
1.3 Experimental Approach: Micrometeorology 3
1.4 Hypotheses and Research Objectives 3
1.5 Thesis Format 5

CHAPTER 2. LITERATURE REVIEW
2.1 Greenhouse Gases in Canadian Agriculture 8
2.1.1 Overall Trends 8
2.1.2 CO_2 on a Farm 9
2.1.2.1 Diurnal and Seasonal Variations: CO_2 10
2.1.3 CH_4 on a Farm 10
2.1.3.1 Diurnal and Seasonal Variations: CH_4 12
2.1.4 N_2O on a Farm 13
2.1.4.1 Diurnal and Seasonal Variations: N_2O 16
2.2 Methods of Gas Flux Determination and The Nocturnal Boundary Layer 17
2.2.1 Overview 17
2.2.2 The Nocturnal Boundary Layer 20
2.2.2.1 The Low-Level Nocturnal Jet and Shallow Drainage Flow 21
2.2.2.2 Exact Definition of the NBL 22
2.2.2.3 Classification of NBL Regimes 23

2.3 The NBL Budget Method ... 25
2.4 Determination of Source Area of Fluxes ... 26
2.4.1 Footprint Models ... 26
2.4.2 Limitations of Footprint Models ... 29
2.4.2.1 Footprint Model Limitations Specific to this Project ... 30
CHAPTER 3. NBL OPERATIONAL METHODOLOGY
3.1 Introduction ... 37
3.2 Key Aspects of NBL Budget Method ... 40
3.2.1 Conditions Favouring Well-Defined Trace Gas Build-Up Within the NBL.. 40
3.3 Field Work ... 42
3.3.1 Procedure for Determining Atmospheric Conditions Suitable for NBL Launches ... 42
3.3.2 Field Sites 1998 and 2002: CFIA Farm, Ottawa, ON ... 43
3.3.3 Field Site 2003: Private Producer's Farm, Coteau-du-Lac, QC ... 45
3.3.4 Equipment, Sample Collection, and Analysis ... 47
3.3.4.1 Vertical Profile Measurements ... 47
3.3.4.2 Spatial Measurements ... 50
3.3.5 Measurements Required: Change in Trace Gas Concentration and Height of NBL ... 51
3.3.6 Flux Calculation ... 53
CHAPTER 4. VERTICAL AND SPATIAL COMPONENTS OF THE NBL BUDGET METHOD IN CONDITIONS VARYING FROM OPTIMAL TO SUBOPTIMAL
4.1 Introduction ... 69
4.2 Materials and Methods ... 71
4.2.1 CH_4 Detailed Profile ... 71
4.2.2 Flux Footprint Parameterization ... 72
4.3 Typical Profiles of Temperature, Wind Speed, and Carbon Dioxide in the NBL ... 73
4.3.1 Potential Temperature (θ) Profiles ... 73
4.3.2 Wind Speed (u) Profiles ... 74
4.3.3 CO_2 Concentration Profiles ... 76

4.4 Study-Specific Classification of Bulk NBL Structure during Calm, Clear Conditions ... 77
4.5 Method for Choosing Flux Integration Height ... 78
4.5.1 Optimal NBL Conditions: Very Stable Upside-Down Boundary Layer, Converging CO_2 Profiles ... 79
4.5.2 Suboptimal NBL Conditions: Very Stable Upside-Down Boundary Layer, Non-Converging CO_2 Profiles ... 80
4.6 Comparative Contribution of Normalized NBL Height Intervals (*z/h*) to GHG Flux ... 83
4.7 Preliminary 'Bottom-Up' Verification of NBL Budget Method ... 85
4.8 Summary and Conclusions ... 88

CHAPTER 5. NBL FLUXES OF CO_2, N_2O, AND CH_4 WITH SURFACE SPATIAL VARIABILITY
5.1 Introduction ... 102
5.2 NBL Budget for CO_2, N_2O, and CH_4 ... 102
5.2.1 CO_2 Fluxes ... 103
5.2.1.1 July 22-23, 2003 Results (Coteau-du-Lac) ... 104
5.2.2 N_2O Fluxes ... 106
5.2.3 CH_4 Fluxes ... 109
5.2.4 Comparison Between NBL Budget Method and Eddy Covariance Data ... 111
5.2.5 Effects of Seasonality and NBL Structure on GHG Fluxes ... 112
5.3 Near-Surface Spatial Variability of GHGs ... 115
5.3.1 Spatial Results: Ottawa, ON ... 116
5.3.2 Spatial Results: Coteau-du-Lac, QC ... 119
5.3.3 Use of Spatial Results to Represent Surface Measurements in NBL Profile ... 119
5.4 Conclusion ... 120

CHAPTER 6. A 'BOTTOM-UP' VERIFICATION OF THE NBL BUDGET METHOD
6.1 Introduction ... 135
6.2 Materials and Methods ... 137
6.2.1 Source Area Mapping ... 137
6.2.1.1 Farmland and Crops in Ottawa and Coteau-du-Lac Regions ... 138

6.2.2 Methods of Obtaining GHG Emissions Estimates 139
6.2.2.1 Field-Based Estimates 139
6.2.2.2 Literature-Based Estimates 140
6.2.2.3 IPCC Emission Factors 141
6.2.3 NBL Data 143
6.2.3.1 Ottawa, ON, June 28-29, 2002—23:00-0:45 143
6.2.3.2 Ottawa, ON, June 28-29, 2002—3:30-4:45 144
6.2.3.3 Coteau-du-Lac, QC, June 17-18, 2003—20:45-21:45 144
6.2.3.4 Coteau-du-Lac, QC, July 9-10, 2003—19:30-20:45 145
6.2.4 Footprint Model Description, Assumptions, and Simplifications 146
6.2.4.1 Footprint Parameterization Output 147
6.2.5 Weighting of Source Area and Flux Aggregation 148
6.3 Results and Discussion 151
6.3.1 Footprint-Aggregated Flux vs. NBL-Measured Flux 151
6.3.1.1 Ottawa, ON, June 28-29, 2002—23:00-0:45 151
6.3.1.2 Ottawa, ON, June 28-29, 2002—3:30-4:45 153
6.3.1.3 Coteau-du-Lac, QC, June 17-18, 2003—20:45, 21:45, 22:30 157
6.3.1.4 Coteau-du-Lac, QC, July 9-10, 2003—19:30-20:45 158
6.4 Conclusion 158
CHAPTER 7. CONCLUSIONS, SUMMARY, AND SCOPE FOR FUTURE RESEARCH 178
7.1 Hypotheses and Summary of Findings 178
7.2 Specific Contributions Furthering the Advancement of NBL Budget Research 182
7.3 Scope for Future Study 184
LITERATURE CITED 186
APPENDIX A: EXETAINER TUBE EVACUATION EFFICIENCY TEST
A.1 Procedure for Evacuation Efficiency Test A-2
A.1.1 Goal of Procedure A-2
A.1.2 Materials A-2
A.1.3 Procedure Followed A-2

A.2 Evacuation Test Results A-6
A.2.1 July 3, 2003 .... A-6
A.2.2 July 18, 2003 .... A-6
A.2.3 Discussion A-6

APPENDIX B: ANALYTICAL METHODS FOR GAS CHROMATOGRAPHY
B.1 CH_4 Method for Shimadzu GC-8AIF (Flame Ionization Detector-FID) B-2
B.2 N_2O Method for HP 5890 (Electron Capture Detector-ECD) B-4
B.3 Comparison of Results Generated by GC and TDL-TGA B-6

APPENDIX C: SOURCES OF ERROR AND UNCERTAINTY IN CO_2 FLUX CALCULATION
C.1 Coordination Between Instruments C-1
C.2 Interpolation of CO_2 Concentration to Global z Axis C-2
C.3 Conversion from ppmv to mg m^{-3} C-3
C.4 Non-Stationarity C-3

APPENDIX D: IMPACT OF TETHERSONDE TEMPERATURE HYSTERESIS ON NOCTURNAL SOUNDINGS
D.1 Introduction D-1
D.2 Tethersonde Temperature Sensor: The Thermistor D-2
D.3 Experimental Set-Up D-2
D.4 Results D-3
D.4.1 Rate of Response to Temperature Change D-4
D.4.2 Rate of Response to Relative Humidity Change D-5
D.4.3 Step-Change During Last Temperature Transition D-5
D.5 Discussion D-5
D.6 Conclusion D-8

APPENDIX E: GHG SOURCE STRENGTH CALCULATION
E.1 Table 5.1 Footnotes E-1
E.2 Calculation Method for CO_2 and N_2O Contributions from Daytime Vehicular Traffic in Suburban Portion of Flux Footprint: Ottawa, ON, June 28-29, 2002 .... E-3

LIST OF TABLES

Table No.		Page
	CHAPTER 2	
2.1	Overall level-uncertainty in greenhouse gas emissions for subcategories of the agriculture sector, as per Hutchinson *et al.* (2007) in the 2005 Canadian Greenhouse Gas Inventory (Environment Canada, 2007).	33
2.2	Characteristics of three broadly defined classifications of the stable nocturnal boundary layer, summarized from Mahrt (1998, 1999).	34
	CHAPTER 4	
4.1	Carbon dioxide flux values for three cases of NBL/CO_2 structure. Type 1 = stable upside down boundary layer: CO_2 profiles converging. Type 2 = same but CO_2 not converging. Type 3 = turbulence down to ground. Time intervals rounded to nearest quarter hour. Eddy covariance (EC) results are averaged from data available from windy periods on the NBL night and from one to three nights before and after. "±" is 95% confidence interval. "–" means data not available.	91
4.2	Average heights with associated cumulative % contribution to total measured flux and 80% flux footprint distance (using parameterization of Kljun *et al.,* 2004) on nights exhibiting a very stable upside-down boundary layer with converging CO_2 profiles at the Ottawa (1998, 2002) and Coteau-du-Lac sites (2003).	92
4.3	Height, wind direction (u dir) with variation, concentrations, and comparative source strength from detailed CH_4 profiles measured on the night of August 18-19, 2003, at Coteau-du-Lac, QC. Source strength estimation methods (footnotes a-h) can be found in Appendix E.	93
	CHAPTER 5	
5.1	Nitrous oxide (F_{N2O}) and CH_4 (F_{CH4}) fluxes using NBL method. Time intervals rounded to nearest quarter hour. CI 95 is 95%	122

confidence interval, SD is standard deviation. FG means flux gradient-measured data (for N_2O), given as available. Three N_2O values for each night are given: (1) the afternoon prior to NBL measurements (12:00-18:00), (2) the next afternoon, and (3) the next night (21:00-4:30). Exceptions are footnoted. Integration height (h_i) is the height to which bags were filled. – is data not available (for N_2O, u *at* h_i, or for CH_4 where wind direction exceeded 45°). P1 is profile 1. u dir is mean wind direction from surface to z ≈ 20 m. Times are average profile times. Nightly flux is given for periods with constant source area type.

5.2 Carbon dioxide fluxes: Comparison of NBL vs. eddy covariance (EC)-measured values at both Ottawa and Coteau-du-Lac sites. STB CONV = very stable upside-down boundary layer with convergent CO_2 profiles, STB NON-CONV = very stable upside-down boundary layer with non-convergent CO_2 profiles, TURBULENT = turbulent layer at surface. CI is the 95% confidence interval. 124

5.3 (a) NBL flux data averages from Coteau-du-Lac, 2003, combined for all three observed NBL structures and sorted by month. 125

5.3 (b) NBL flux data averages from Coteau-du-Lac, 2003, combined for the entire season and sorted by observed NBL structure. STB CONV = very stable upside-down boundary layer with convergent CO_2 profiles, STB NON-CONV = very stable upside-down boundary layer with non-convergent CO_2 profiles, TURBULENT = turbulent layer at surface. 125

5.4 Results from spatial measurements of CO_2, N_2O and CH_4, where ST1 is spatial transect 1 (start time and duration of transects indicated in hh:mm local time). CI 95 is 95% confidence interval, SD is standard deviation, Rep is replicate. 126

5.5 Carbon dioxide concentration (mg m^{-3}) in first 12 m of vertical profile, compared with spatial average at z =12 m, July 18-19, 2002. 127

CHAPTER 6

6.1 Example of CO_2 flux aggregation with areal weighting of sources assigned within each footprint-weighted segment, 3:30 and 4:45 162

	profiles, Ottawa, June 28-29, 2002. Segment and areal weightings listed here are applied to flux estimates for each source which are given in Table 6.2a, yielding a weighted flux for each footprint segment which is then summed to give the total flux for the footprint (Equation 6.3).	
6.2 (a)	Estimated fluxes of CO_2, and N_2O from sources within footprints on June 28-29, 2002, June 17-18, 2003, and July 9-10, 2003. Indirect sources of N_2O (from leaching, runoff, volatilization) are already included in estimates for each source.	163
6.2 (b)	Example of N_2O calculation from crop fields, Ottawa, June 28-29, 2002.	165
6.3	Results of flux aggregation vs. NBL flux measurements for Ottawa, June 28-29, 2002, and Coteau-du-Lac, June 17-18, 2003, and July 9-10, 2003.	166

APPENDIX B

B-1	Methane results: GC vs. TDL.	B-6

APPENDIX D

D-1	Temperature difference (T diff): Three tethersondes (TS) vs. thermocouple reference.	D-9
D-2	Response times and rates for tethersonde (TS) and thermocouple (TC) for temperature (T) change when moving from warm to cold to warm locations.	D-9

APPENDIX E

E-1	Calculation of CO_2, N_2O, and CH_4 emissions from mobile fuel combustion from National Capital Region.	E-5

LIST OF FIGURES

Figure No. **Page**

CHAPTER 2

2.1 Idealized contrast of the vertical temperature structure of the weakly stable and very stable boundary layers. σ_w is the standard deviation of the vertical velocity fluctuations and θ is the potential temperature. From Mahrt (1998). 35

2.2 Schematic diagram of the source area function (Schmid, 1994). Maximum contribution of source area (f_{max}) occurs at a certain distance upwind (x_m) from the measurement at height z_m. Contribution decreases to all sides from the maximum. 35

2.3 Analytical footprint model of Schuepp *et al.* (1990) run for 3 measurement heights under neutral atmospheric conditions, with a surface roughness (z_0) of 0.06 m and a zero plane displacement (d) of 0.3 m. From Schuepp *et al.* (1990). 36

2.4 Footprint prediction of numerical model by Leclerc and Thurtell (1990) for different thermal stability conditions at a given measurement height, surface roughness, and zero-plane displacement. From Leclerc and Thurtell (1990). 36

CHAPTER 3

3.1 Diagram depicting agricultural layout within 1 to 4 km of Ottawa site, June-July 2002. 55

3.2 Eddy covariance tower measuring fluxes of CO_2 at Coteau-du-Lac field site in April 2003 (Credit: E. Pattey, 2003). 56

3.3 Flux gradient tower measuring fluxes of N_2O over edible green peas at Coteau-du-Lac field site in June-July 2003. 57

3.4 Ottawa 2002 field site (viewed looking approximately to the NNW) showing rain gauge and wind speed instruments wind direction. 58

3.5 Diagram depicting agricultural layout within 2 to 3 km of Coteau-du-Lac site, summer of 2003 59

3.6 Eastward view of Coteau-du-Lac field site, showing edible green peas, flux gradient tower, trailer housing TDL, tent shelter 60 for tethered blimp, and barn, July 2003.

3.7 (a) Blimps (large and small) tethered to electric winches in early morning hours bordering the corn field at the Ottawa site, June-July 2002. Large blimp making its descent (monitored by Nathalie Mathieu) shows CIRAS analyzer and tethersonde attached to tetherline. 61

3.7 (b) Blimp tethered to electric winch, during snowmelt, Coteau-du-Lac, April 2003. Sonde is attached to tetherline. Standing next to winch are Nathalie Mathieu and Ian Strachan. 62

3.7 (c) Blimp tethered to electric winch, sonde attached to tetherline, in middle of field of edible green peas, early June 2003, next to housing for tile drainage measurement system. Standing near tent are Nathalie Mathieu and Melissa Valiquette. 63

3.8 AAFC's A.I.R. tethersonde system shown with laptop, receiver, and antenna. 64

3.9 CIRAS-SC portable infra-red CO_2 analyzer in protective casing. 65

3.10 In-house developed bag filling system (Pattey *et al.,* 2006). 66

3.11 (a) Electric golf cart with tethered blimp for spatial measurements viewed from front, on south side of Ottawa field site (looking eastward). 67

3.11 (b) Golf cart viewed from the back (looking westward), showing left to right, top to bottom: LI-COR CO_2 analyzer, laptop computer, GPS (orange vest), zero gas cylinder, marine batteries, and electric winch with tubing and tethersonde attached to tetherline. 68

CHAPTER 4

4.1 (a)-(l) Examples of NBL profiles of potential temperature (θ), horizontal wind speed (u), and CO_2 concentration ([CO_2]) for the Ottawa (2002) and Coteau-du-Lac (2003) field sites. 94

4.2 CO_2 profile over agricultural field in Ottawa, ON, from Pattey *et al.* (2002). Arrows indicate balloon ascent and descent. 95

4.3 Profiles of nocturnal CO_2 concentrations over pasture in NSW, Australia, from Denmead *et al.* (1996). Shaded area represents the CO_2 accumulated between profile times. 96

4.4 (a)-(c) Case examples of $u/Ri/CO_2$ patterns from 22 NBL profile pairs that met criteria of constant upwind source area and intact NBL.

(a) Very stable upside-down boundary layer, decoupled low-level jet: Ottawa, June 28-29, 2002. 97

(b) Very stable upside-down boundary layer, u maxima, $[CO_2]$ convergence: Ottawa, June 28-29, 2002. 98

(c) Very stable upside-down boundary layer, non-convergent $[CO_2]$ profiles: Coteau-du-Lac, July 9-10, 2003, with wind direction (*u dir*). Height of co-located variables using second approach for choosing integration height in suboptimal conditions (Section 4.5.2). 99

4.5 Non-cumulative (a) and cumulative (b) contribution (%) of normalized NBL height intervals (z/h) to total flux measured for the height interval z = 2.5 m to h, where z is measurement height and h is the height of the NBL (integration heigh). Data bars represent 3 situations of $u/Ri/CO_2$ patterns: STB CONV = very stable upside-down boundary layer with convergent CO_2 profiles, STB NON-CONV = very stable upside-down boundary layer with non-convergent CO_2 profiles, Turbulent = turbulent layer at surface. Error bars are 95% confidence interval. 100

4.6 Detailed CH_4 profiles: Aerial photo labeled with crops, CH_4 point sources, overlain by 80% footprints and x_{max}, for given heights of detailed vertical CH_4 profiles on Aug. 18, 2003 (Coteau-du-Lac, QC). 101

CHAPTER 5

5.1 (a) Richardson number profiles for July 22-23, 2003, Coteau-du-Lac. 128

5.1 (b) Wind direction profiles, July 22, 2003, Coteau-du-Lac. 129

5.2 Comparison of NBL- and eddy-covariance (EC)-measured CO_2 fluxes plotted with 1:1 line. Error bars are 95% confidence interval. STB CONV = very stable upside-down boundary layer with convergent CO_2 profiles, STB NON-CONV = very stable upside-down boundary layer with non-convergent CO_2 profiles, Turbulent = turbulent layer at surface. 130

5.3 (a)-(c) Diagram depicting layout of spatial sampling at experimental 131

	site (approximately 450 × 600 m) at CFIA Farm, Ottawa, ON, Canada, June-July 2002. Star indicates blimp launch site. Dots indicate spatial sampling points. Striped triangle is location of manure pile, sheep in pentagon shape is sheep housing. Numbers in boxes at each sampling point indicate GHG concentrations. Top number is for first transect, bottom number is for second transect. Mean wind speeds and mean wind directions (dashed arrows in compass roses) are given for each transect (u_1 for ST1, u_2 for ST2). See Section 5.3.1 for explanation of wind direction. Times are given in Table 5.4.	
	(a) Methane sampling at Ottawa site, June 24-25, 2002 (± 0.06 ppmv).	131
	(b) Nitrous oxide sampling at Ottawa site, June 24-25, 2002 (± 0.01 ppmv).	132
	(c) Methane sampling at Ottawa site, July 18-19, 2002 (± 0.06 ppmv).	133
5.4	As in Figure 5.3 but for Coteau-du-Lac field site (240 × 1000 m). Cow indicates location of cattle housing. Numbers in boxes at each sampling point indicate CH_4 concentrations (+/- 0.06 ppmv) measured night of Aug. 28-29, 2003.	134

CHAPTER 6

6.1 (a)	Carbon dioxide, *u*, and *Ri* profiles for Ottawa, ON, June 28-29, 2002, 23:00-0:45.	167
6.1 (b)	Carbon dioxide, *u*, and *Ri* profiles for Ottawa, ON, June 28-29, 2002, 3:30-4:45.	168
6.1 (c)	Carbon dioxide, *u*, and *Ri* profiles for Coteau-du-Lac, QC, June 17-18, 2003, 20:45-22:30.	169
6.1 (d)	Carbon dioxide, *u*, and *Ri* profiles for Coteau-du-Lac, QC, July 9-10, 2003, 19:30-20:45.	170
6.2 (a)	Illustration of flux footprint parameterization-generated results, for u* = 0.2 m s^{-1}, σ_w = 0.07 m s^{-1}, and other settings indicated in figure.	171
6.2 (b)	Illustration of consistent relationship between relative upwind distance and relative contribution (same settings as 6.5 a).	172
6.3	Example of cumulative 80% footprint obtained following	173

	procedure outlined in Section 6.2.5, for z_m = 10, 20, 30, 40, and 50 m (0.2 *h* to 1.0 *h*), u^* = 0.2 m s^{-1}, z_0 = 0.2 m, and σ_w of 0.07 m s^{-1}. Start of each gap signals drop below 50% level of previous footprint (*i.e.,* previous footprint is no longer included in cumulative weighting).	
6.4 (a)	Approximate flux footprint for Ottawa, ON, June 28-29, 2002, 23:00-0:45. Numbers denote footprint weighting (relative contribution).	174
6.4 (b)	Same as in (a), but for Ottawa, ON, June 28-29, 2002, 3:30-4:45.	175
6.4 (c)	Same as in (a) but for Coteau-du-Lac, QC, June 17-18, 2003, 20:45-21:45.	176
6.4 (d)	Same as in (a) but for Coteau-du-Lac, QC, July 9-10, 2003, 19:30-20:45. St. Lawrence River is located approximately 2 km south of blimp launch site.	177

APPENDIX A

A-1	In-house-assembled evacuation manifold, consisting of ten 26G needles on Luer-Lok ports inserted into a plastic tube and fastened with silicone, vacuum pressure gauge, and end connector for tubing from vacuum pump (not shown). Additional taping to minimize leaks at joints where sampling ports meet plastic tube. A double septum-sealed Exetainer tube is inserted on each sampling port and the vacuum pump turned on.	A-8

APPENDIX B

B-1	Correspondence of GC to TDL values for methane.	B-7

APPENDIX D

D-1	Air temperature over time for three tethersondes and a thermocouple, moved between several locations varying in ambient temperature.	D-10
D-2	Correlation of tethersonde and thermocouple results outside of	D-11

transition periods.

D-3 %RH plotted for three sondes over time and across varying locations. D-12

D-4 Temperature difference (red line) between thermocouple wire and sonde 2. Peaks and dips in T diff correspond to periods where the SD in temperature for each respective sonde was greater than 0.175 °C. D-13

STATEMENT OF ORIGINAL CONTRIBUTION TO SCIENCE

The following are elements of the thesis that are considered to constitute original scholarship and an advancement of knowledge in the domain of micrometeorology, specifically regarding the quantification of greenhouse gas emissions at the landscape scale (approximately 1 km^2) in an agricultural environment.

The technique used was the nocturnal boundary layer (NBL) budget method, a method previously documented but in need of further exploration and refinement in particular with regard to 1) its use in suboptimal atmospheric conditions where intermittent turbulence may cause entrainment or loss of traces gases through the top of the NBL, 2) the extent of its spatial representation, and 3) a general ground-based verification of the fluxes it measures.

The original contributions of this thesis are as follows:

1. CO_2, N_2O, and CH_4 have previously been measured separately in the NBL. This thesis presents an operational technique using the NBL budget method for the simultaneous measurement of CO_2, N_2O, and CH_4 by concomitantly measuring vertical concentration profiles of these gases in the NBL using a portable CO_2 analyzer and a bag air sampling system for N_2O and CH_4. This technique could be adapted for other non-reactive trace gases by employing different in-situ gas analyzers or by analyzing air collected in bags for other species of interest.

2. While it has been shown previously that a certain level of intermittency can take place without invalidating the NBL approach, this thesis addresses how during specifically defined suboptimal NBL conditions, where intermittent turbulence may cause the

downward entrainment of trace gas-enriched air through the top of the NBL, the NBL budget technique can still be used to produce representative estimates of GHG fluxes. It is shown that this can be done through careful choice of the flux integration height by examining in detail the progression of vertical profiles over time, with specific reference to the co-location of the following: (1) u maxima, (2) shear and turbulent layers, and (3) where $\Delta CO_2/\Delta z$ approaches zero for a given profile.

3. The height-contribution within the vertical profile of NBL-measured GHG flux has not previously been examined in relation to the upwind area of influence. This thesis shows that the trace gas source contribution to the vertical flux, under stable atmospheric conditions, varies spatially with the local sources exerting the most influence on the measured flux:

   - by identifying the contribution of vertical profile height intervals to the total measured NBL flux at both field sites, during optimal conditions exhibiting a sustained, very stable NBL and

   - by using a footprint model to show that 50% of the flux came from local sources within 1 km upwind and that 80% of the flux came from within 2 km upwind of the launch site.

4. With support from spatial sampling data showing the sensitivity of CH_4 measurements to wind direction change, this thesis shows that the NBL budget method as performed here with vertical concentration profiles in a single location fails to measure trace gas fluxes from strong point sources such as methane.

5. Prior to this study, no ground-based verification of the NBL budget method has been conducted. This thesis verifies the 'top-down' NBL budget method using two 'bottom-up' approaches:

   - by showing that point sources within two to three km were reflected in respective detailed CH_4 concentration profiles as their footprints moved closer to and further from these sources, and
   - by comparing and showing the agreement, during baseline atmospheric and farm management conditions, between NBL-measured fluxes of CO_2 and N_2O and footprint-weighted and aggregated individual ground-level sources of these gases, within four footprint model-defined upwind source areas.

1. INTRODUCTION

According to the Fourth Assessment Report of the Intergovernmental Panel on Climate Change, there is now very high confidence that anthropogenic increases in emissions of greenhouse gases (GHGs) are causing global warming (IPCC, 2007). In an effort to quantify the rise in atmospheric concentrations of carbon dioxide (CO_2), methane (CH_4), and nitrous oxide (N_2O), the three most prevalent GHGs, countries, including Canada, participating in the United Nations Framework Convention on Climate Change (UNFCCC) (adopted in 1992) have established emissions inventories. However, as these inventories are based primarily on estimates derived from a combination of national statistics, measured emission factors, and scientific or engineering models, many sources of uncertainty may arise (Environment Canada, 1999).

1.1 UNCERTAINTIES RELATED TO SCALE

A certain portion of the uncertainty in emissions estimates from the agriculture sector comes from the scaling-up of emissions determined from small-scale plot studies (*e.g.,* tens of square meters) to obtain estimates of emissions at national levels. Regional estimates of fluxes have been studied using flux-instrumented aircraft (*e.g.,* Desjardins *et al.*, 2000) and tall towers (*e.g.,* Chen *et al.,* 2007). This thesis presents a methodology for providing information within the gap between plot and regional scale by simultaneously measuring the three main agricultural greenhouse gases (CO_2, N_2O, and CH_4) from agricultural ecosystems at the farm scale, that is, approximately one square kilometer, the average size of the typical agricultural farm in eastern Ontario and western Quebec (Statistics Canada, 2004). This is considered the most relevant scale for the agricultural sector.

1.2 IMPORTANCE OF MEASURING CO_2, N_2O, AND CH_4 ON FARMS

While agriculture is responsible primarily for N_2O and CH_4 emissions, it is important to measure all three gases because they play important roles in the GHG source and sink balance of a typical agroecosystem: CO_2 is taken up by growing plants during the day through photosynthesis. Plant, or crop, residue and its derivatives, for example, compost, or animal manure, after consumption of plants, returned to the soil provide organic matter, containing C and N, for soil microbial consumption (Brady and Weil, 2002). Microbial decomposition releases CO_2 once again and also makes other essential nutrients available for plants, including ammonium (NH_4^+) and nitrate (NO_3^-) (Brady and Weil, 2002). The latter can then undergo microbial nitrification and denitrification, respectively, releasing N_2O to the atmosphere (Brady and Weil, 2002). Ammonium and nitrate and can also be added to the soil through chemical fertilizers. Methanotrophic bacteria can take CH_4 from the atmosphere into the soil for oxidization (Topp and Pattey, 1997). The soil in a dry upland agroecosystem, unless inundated, is not a source of CH_4 which is typically produced under anaerobic conditions (Topp and Pattey, 1997). Methane is emitted from ruminant livestock and manure management facilities frequently found on a farm (Environment Canada, 2006). Carbon dioxide, methane, and nitrous oxide can also be emitted from adjacent drainage ditches and rivers (*e.g.,* Silvennoinen *et al.,* 2008). In summary, agricultural farms constitute both sources and sinks for the major greenhouse gases. Measuring all three gases, therefore, in particular using larger scale methods, allows us to obtain a "whole farm" estimate. In addition, the measurement of detailed vertical profiles of CO_2 concentration allows us to follow the development of the nocturnal boundary layer (NBL) and verify the principal method used in this project, the NBL budget method (Section 1.3).

1.3 EXPERIMENTAL APPROACH: MICROMETEOROLOGY

The approach used here to quantify GHG fluxes is a direct micrometeorological technique called the NBL budget method (Denmead *et al.,* 1996). The NBL budgeting approach makes use of atmospheric properties at night during stable conditions to quantify emissions at the landscape scale. GHG fluxes are calculated by integrating the concentration change over time with respect to NBL height, obtained from vertical profiles of the NBL. This technique is useful because it integrates any "hot spots" or point sources of emissions in surrounding fields or within the farm complex into the flux measurement, thus providing flux values that are more representative of the farm as a whole (Pattey *et al.*, 2002).

While several studies have used the NBL budget method over a variety of landscapes with a tethered balloon or tower-based vertical profiling technique (*e.g.,* Choularton *et al.,* 1995, Denmead *et al*., 1996, 2000, Beswick *et al.,* 1998, Fisch *et al*., 2000, Eugster and Siegrist, 2000, Pattey *et al*., 2002, Griffith *et al.,* 2002, Acevedo *et al.,* 2004, Mathieu *et al.,* 2005, and Pattey *et al.,* 2006), very few focus on the validity and conditions of application of using the NBL budget method in the ever-varying NBL. The principal goal of this thesis is to address this issue, to increase the level of confidence in the flux measured and to demonstrate that the results are acceptable at the farm scale.

1.4 HYPOTHESES AND RESEARCH OBJECTIVES

While it is generally understood that the vertical movement of trace gases is impeded under very stable conditions (*e.g.,* Mathieu *et al.,* 2005), several issues remain unresolved. In particular, the spatial contribution and scale of the technique along with its applicability in suboptimal conditions have not yet been adequately identified. This thesis will address the following hypotheses:

1. During optimal conditions demonstrating a sustained, very stable NBL, the NBL budget technique provides estimates of GHGs that are comparable to other methods of measurement (*e.g.,* eddy covariance, flux gradient methods, *etc.,* bearing in mind scale differences).
2. During suboptimal conditions consisting of elevated intermittent turbulence which may cause downward entrainment of trace gas-enriched air through the top of the NBL, the NBL budget technique can still produce representative estimates of GHG fluxes if the choice of integration height is made based on structural pattern indicators in the NBL.
3. The trace gas source contribution to a vertical flux, under stable atmospheric conditions, varies spatially with the local sources exerting the most influence on the measured flux.
4. The spatial scale of the fluxes measured using the NBL budget technique is in the range of the typical farm size in Eastern Canada (*i.e.,* 1 km^2).
5. The 'top-down' NBL budget method gives values that accurately reflect fluxes originating at the surface within an appropriately defined source area.

This study therefore expands our knowledge of the NBL conditions necessary for the application of the NBL budget method within the context of CO_2, N_2O, and CH_4 measurements over agricultural fields typical to Eastern Canada, with the following research objectives designed to address the stated hypotheses:

1. To refine and document in detail the NBL operational methodology for the simultaneous measurement of fluxes of CO_2, N_2O and CH_4 from agroecosystems using a tethered balloon, including the NBL conditions required to obtain fluxes representative of the source area of interest, the farm,
2. To demonstrate how the NBL budget method may, in conditions of evelated intermittent turbulence which may cause the downward entrainment of trace gas-enriched air through the top of the NBL, still be applied to yield fluxes representative of the farm,
3. To give a preliminary estimate of the minimum spatial extent of the NBL budget footprint,
4. To identify the impact and quantify the contribution of spatial heterogeneity of GHG concentrations near the surface on the NBL budget, and
5. To verify the 'top-down' NBL budget method.

1.5 THESIS FORMAT

This thesis consists of seven chapters within which the objectives are addressed. A literature review (Chapter 2) provides an overview of the processes underlying the exchanges of GHG on farms, nighttime atmospheric exchange processes, NBL budget theory, and the footprint concept.

Chapter 3 addresses Objective 1 through a reporting of the NBL methodology applied in this study, and focuses on the NBL conditions, measurements, and calculations necessary for its application.

Chapter 4 presents a description of typical NBL profile data measured in this study, including potential temperature, wind speed, and CO_2 concentration. A detailed examination of this NBL data, in terms of vertical profiles of wind speed, Richardson number, and CO_2 concentration, leads to recommendations on how to proceed with NBL budget flux calculation in the optimal and suboptimal NBL conditions seen in our data (Objective 2). This chapter also presents an examination of the spatial scale of the NBL budget method (Objective 3) in terms of both horizontal and vertical zones of importance. The key contributing height interval of the NBL vertical profile flux is determined and related to an effective horizontal upwind distance using a flux footprint parameterization. A preliminary ground-based or 'bottom-up' verification of the NBL budget method using local CH_4 point sources as tracers is then presented.

Chapter 5 presents the CO_2, N_2O, and CH_4 flux results obtained using the NBL budget method at two farms. NBL-measured CO_2 and N_2O fluxes are compared with results from near-in-time-measured fluxes from the eddy covariance and flux gradient techniques and are also examined in terms of bulk NBL structure and seasonality. Results addressing the spatial heterogeneity of GHG concentration (Objective 4) through near-surface spatial sampling of GHG around the NBL launch site are also given.

Chapter 6 presents an in-depth verification of the 'top-down' NBL budget method (Objective 5). A flux footprint parameterization is used once again, in more detail, to compare ground-based, or 'bottom-up', GHG fluxes, weighted and aggregated within a footprint-defined upwind agricultural source area, to the total flux measured by the NBL budget method. Ground-based fluxes of CO_2, N_2O, and CH_4 were estimated from field and literature data as well as IPCC emission factors.

The thesis concludes in Chapter 7 with a summary of findings and scope for future study.

2. LITERATURE REVIEW

2.1 GREENHOUSE GASES IN CANADIAN AGRICULTURE

2.1.1 Overall Trends

In 2004, agricultural sources (soils, enteric fermentation, and manure management) were responsible for 25% and 66% of total anthropogenic CH_4 and N_2O emissions, respectively, in Canada (Environment Canada, 2007). Total emissions from agriculture (with sectoral emissions of 51% N_2O and 49% CH_4) have increased by 24% since 1990, because of increases in cattle, swine, and poultry production and in synthetic nitrogen fertilizer use in Canada (Environment Canada, 2007). There are large uncertainties in CH_4 and N_2O emissions from the agriculture sector (Hutchinson *et al.,* 2007) (Table 2.1). These uncertainties can be due to problems commonly encountered in the compilation of an emissions inventory, including (1) differences in: (a) interpretation of source and sink categories and definitions, (b) assumptions, (c) units, etc., (2) inadequate and incorrect socio-economic information, (3) inappropriate application of emission factors, and (4) empirical uncertainty in measurements and incomplete understanding of basic processes involved in emissions (Environment Canada, 2002).

Despite high uncertainties, promising advances are being made for reducing GHG emissions in the agriculture sector, such as precision agriculture for N fertilizer management (*e.g.,* Pattey *et al.,* 2001) and conservative tilling practices to increase C sequestration (*e.g.,* review by Batjes, 1998).

2.1.2 CO_2 on a Farm

The elevated CO_2 levels seen in the atmosphere are due to the burning of fossil fuels and removal of sinks for CO_2, for example, through the disturbance of forests and soils (Janzen *et al.,* 1998, 2008). Carbon dioxide on a farm is produced through plant, animal, and microbial respiration, as well as from fuel combustion from farm vehicles and machinery. Plants exchange CO_2 with the atmosphere in the processes of photosynthesis and respiration (Ingenhousz, 1779; Warburg, 1919-1920; van Niel, 1929). Respiration by soil microorganisms (first observed by Ingenhousz, 1779) is also a major contributor to CO_2 release from the soil. Organic matter (*e.g.,* from plant residues and microbial biomass) in soils and manure is decomposed by microorganisms either to CO_2 in aerobic conditions or to CH_4 in anaerobic conditions ((*e.g.*, Liebig, 1840; Pasteur, 1857; and reviews by Conrad, 1996; Brady and Weil, 2002). However, in a stable agroecosystem this carbon loss is usually balanced by carbon input into the soil as plant residues (Brady and Weil, 2002). CO_2 is also emitted (along with small amounts of CH_4) by ruminant livestock (*e.g.,* Kinsman *et al.,* 1995).

Currently the main concern in agriculture regarding carbon is how to increase its levels in the soil, through management practices such as crop rotation, fertilizer or manure application, and reduced tillage or fall tillage (*e.g.,* Fortin *et al.,* 1996; Paustian *et al.,* 1997; Batjes *et al.,* 1998; Swift, 2001; Smith *et al.,* 2001; West and Post, 2002; Prior *et al.,* 2004; Bronick and Lal, 2005; Wang and Dalal, 2006), afforestation and permanent pastures (*e.g.,* Martens *et al.,* 2003) or even the planting of crops for biofuel use (*e.g.,* Lemus and Lal, 2005; Sartori *et al.,* 2006). Increasing the sequestration of carbon in soil would be considered beneficial in maintaining soil productivity as well as reducing increases in atmospheric CO_2.

2.1.2.1 Diurnal and Seasonal Variations: CO_2

During the growing season, in the daytime there is a decrease in the ambient concentration of CO_2 whereas, at night, there is an increase in the ambient concentration of CO_2 (*e.g.,* Eugster and Siegrist, 2000; Fisch *et al.,* 2000). Seasonally, atmospheric CO_2 levels drop during the summer when the plants are growing and absorbing CO_2 and rise again during the winter after plants die (Steele *et al.,* 2007). Soil microbes decompose carbon compounds continually, although rates of decomposition are dependent upon soil temperature (Kirschbaum, 1995), and the primary product of decomposition (CO_2 or CH_4) is also dependent upon the level of moisture, which modulates the oxygen availability in the soil (Moore and Knowles, 1989; Yu *et al.,* 2007) A minimum temperature of 5°C is generally considered necessary for microbial processes to occur and different processes have different optimal temperatures (Brady and Weil, 2002). Microbial respiration has an optimum temperature of 35-40°C (Nyhan, 1976; Kirschbaum, 1995; Brady and Weil, 2002).

For livestock production, a diurnal trend has been seen in dairy cattle with CO_2 and CH_4 emissions peaking at times of feeding and declining over the night (Kinsman *et al.,* 1995).

2.1.3 CH_4 on a Farm

Methane is produced in soils through the microbial reduction of either CO_2 or organic carbon in anaerobic conditions (Mah *et al.,* 1993; reviews by Conrad, 1996 and Dalal *et al.,* 2008). Methane emissions from soils are thought to occur when methanogenesis exceeds methanotropism (the microbial oxidation of CH_4 to CO_2) (Topp and Pattey, 1997). Since methanogenesis only occurs in anaerobic conditions, typically a well-aerated agricultural soil would be a weak sink for methane while a water-saturated soil such as a wetland or peat bog would be a significant source of methane (Conrad, 1996; Topp and Pattey, 1997). Soil may have a decreased methane uptake after precipitation (*e.g.,* Mosier *et al.,* 1991) and it is even possible for a well-drained soil to become a weak source of methane after snowmelt or a heavy rainfall (Wang and Bettany, 1995). Nitrogen fertilization has been found to decrease CH_4 uptake as well (*e.g.,* Mosier *et al.,* 1991). Manure application to soil appears to have an effect on methane flux dynamics, but overall seems to only decrease the net CH_4 uptake by a soil (Lessard *et al.*, 1997; Hansen *et al.*, 1993), except for a few days post-application when it has been seen to increase greatly (Rochette and Côté, 2000).

It remains that the primary source of methane emission on a farm would typically be ruminant digestion (enteric fermentation) and stored manure (Gregorich *et al.,* 2005; Environment Canada, 2008). In fact, about 88% of CH_4 emitted from Canadian farms is estimated to come from livestock and the remaining 12% from livestock manure (Environment Canada, 2008). Methane emission from livestock will vary with type, age, feed, *etc.* (Kinsman *et al.,* 1995; Monteny *et al.,* 2001, Janzen *et al.,* 2008). Methane can be emitted from stored manure as a result of microbial decomposition, where the method of storing manure (*e.g.,* aerated vs. non-aerated) can affect the rate of CH_4 emission (Monteny *et al.,* 2001; Pattey *et al.,* 2005; review by Kebreab *et al*. 2006). In general, well-aerated manure produces less methane than anaerobic liquid manure, but the amount of CH_4 released will depend on the length of the transport path to the surface and opportunities for the CH_4 to become oxidized along the way (Conrad, 1989; Hao *et al.,* 2001b). Strategies to reduce emissions from manure include composting, anaerobic digestion, diet manipulation by ruminants, the use of covers, and solid-liquid separation (Kebreab *et al.,* 2006).

2.1.3.1 Diurnal and Seasonal Variations: CH_4

Dunfield *et al.* (1993) found that methane oxidation in peat soils was not strongly affected by a large soil temperature range, but that methane production, in contrast, was. Therefore, even if soil temperature were to change drastically between day and night (or throughout the season), there would be little difference in methane uptake (which would be the process of interest in a well-aerated soil) (*e.g.,* Mosier *et al.,* 1991). Distinct diurnal and seasonal differences in methane emission are evident in wetland environments (which are strong sources of methane) (Kuhlmann *et al.,* 1998; Worthy *et al.,* 1998). However, while the soil-warming and drying transition from winter to spring thaw has coincided with increases in methane uptake (Dörsch *et al.,* 2004), overall seasonal variation does not seem to be the case for an arable soil farm (Rochette and Côté, 2000).

Methanogenic processes in stored manure, on the other hand, are more sensitive to temperature and could be emitting more during the day when temperatures are warmer (Kaharabata *et al.,* 1998; Massé *et al.,* 2003). In turn, a seasonal difference can also be inferred for methane production from manure, with more emissions occurring with warmer temperatures during the summer. A study of the seasonal variations in methane emissions from stored slurry and solid manures showed a strong seasonal variation that strongly correlated with air temperature but for slurry, also depended on the formation of a crust (Husted, 1994). Amon *et al.* (2001) also found that methane emissions from farmyard-stacked manure strongly correlated with internal manure pile temperatures, *i.e.,* more methane was emitted in the summertime.

As mentioned previously, a diurnal difference has been found in ruminant emissions of CH_4, with emissions peaking immediately after each feeding time (Kinsman *et al.*, 1995; Amon *et al.,* 2001). Kinsman *et al.,* (1995) found that while CO_2 followed the same diurnal pattern, CH_4 had greater peaks and declines. A similar diurnal pattern for CH_4 emission has been seen in sheep (Judd *et al.,* 1999).

2.1.4 N_2O on a Farm

The agricultural soil sector is the primary source of nitrous oxide emission in Canada (Environment Canada, 2008). According to the IPCC (IPCC, 2006), N_2O from agricultural sources comes primarily from (1) direct emissions from soil nitrogen, *e.g.,* soils applied with manure and chemically fixed N fertilizers, N deposited by grazing animals, crop residue decomposition, and the cultivation of highly organic soils, (2) animal waste management, and (3) indirect sources, from N lost to the agricultural system (*e.g.,* leaching, runoff, atmospheric deposition).

Nitrous oxide is a by-product of the microbial processes of nitrification and denitrification (Knowles, 1982; Conrad, 1996). Nitrification is the microbial oxidation of ammonium (NH_4^+) to nitrate (NO_3^-) in aerobic conditions (Schloesing and Müntz, 1877; Warington, 1878-1891; Winogradsky, 1890), while denitrification is the microbial reduction of NO_3^- to dinitrogen (N_2) under anaerobic conditions (Schloesing and Müntz, 1877; Warington 1878-1891). A number of complex chemical and physical interactions affect the rates of these processes (*e.g.,* reviews by Conrad, 1996; Beauchamp, 1997). Nitrous oxide fluxes are regulated by the quantities of available substrates for nitrification and denitrification (*e.g.,* organic C, ammonium, and nitrate), the ratio of N_2O produced under different soil chemical and physical conditions (*e.g.,* soil moisture, temperature, pH, redox potential, oxygen availability), and the diffusion and consumption of N_2O before its escape to the atmosphere (Beauchamp, 1997). These factors contribute to the great spatial and temporal variability seen in field measurements of these fluxes (*e.g.,* Grant and Pattey, 2003).

The processes of nitrification and denitrification have important implications for plants which can only absorb the N they require in the form of NH_4^+ and NO_3^- (Touraine *et al.,* 2001; von Wiren *et al.,* 2001). As nitrate can easily be transformed to N_2 which is unusable by the plant, or leached out in ground water, nitrogen fertilizers added to agricultural soils are usually in the form of NH_4^+, which can form complexes and be thus bound in the soil (Janzen *et al.,* 2008; van Spanning *et al.,* 2005). However, it is believed that denitrification is the principal route for the loss of N_2O from the soil (Janzen *et al.,* 2008). Inefficient use of N fertilizers in agricultural soils, for example, adding more N without regard to timing, placement, or residual N in the soil, leads to leaching of NO_3^-, which will eventually be denitrified, producing N_2 or N_2O as a by-product (Mengel, 1992; Beauchamp, 1997; Janzen *et al.,* 2008).

Nitrous oxide can also be released from stored manure from the ammonification of urea followed by the nitrification of the resulting ammonium to nitrate by nitrifying bacteria, and finally through the denitrification of nitrate by denitrifying organisms (Monteny *et al.,* 2001). Studies have found N_2O production in manure samples was strongly correlated with NO_2^- + NO_3^- content (substrates for denitrification) (Brown, H.A., *et al.,* 2000; Tenuta *et al*., 2001). The state of aeration of the manure, solid vs. liquid, also has an impact on the production of N_2O (Kebreab *et al.,* 2006). Strategies to reduce N_2O emissions from manure include composting, livestock diet manipulation, and the use of covers (review by Kebreab *et al.,* 2006). For example, Brown H.A. *et al.,* (2000) found that incorporation of straw into manure increased aeration and decreased N_2O production. A study by Hao *et al.* (2001b) showed that composted feedlot cattle manure emitted significantly less for a passive treatment than for an active treatment involving turning of the manure. In a study comparing storage of dairy and beef manure as slurry, in stockpile and by passive composting, Pattey *et al.* (2005) found that emissions were highest only for the initial phase of composting, when nitrification was dominant.

Studies have also been conducted to see the effects of fertilizer application timing, manure application to soils, tillage vs. no tillage, and crop residue management on N_2O emissions, with highly variable results from study to study and site to site (Janzen *et al.,* 1998). For example, a study by Burton *et al.* (1997) found that, according to soil N_2O profiles, a field cropped to alfalfa had greater total N_2O emission, while a manured fallow field in the same study had the least N_2O emission. However, concurrent measurements of the same fields using soil cores and micrometeorological methods showed the opposite results (Burton *et al.,* 1997). The timing of N_2O release events coincided with all three methods; differences in magnitude were attributed to the nature of N_2O production in each of the three field management systems (Burton *et al.,* 1997). Wagner-Riddle *et al.* (2007), using the flux gradient method in a 5-year study of a corn-soybean-wheat rotation, found a significant reduction in growing season N_2O emissions in a no-till, precision N application situation compared to conventional tillage and N fertilization. Gregorich *et al.* (2005), in their Canadian multi-study analysis, found that conservation tillage, generally considered beneficial for CO_2 sequestration, appears to affect N_2O

emission as well, but depends highly on soil and climate factors, with dry climates showing a decrease in N_2O emission but the reverse for wetter climates (see also Helgason *et al.,* 2005). They also found that conservation tillage appears to increase spatial variability of N_2O emissions (Gregorich *et al.,* 2005). Spatial and temporal heterogeneity (related to soil and climate factors) appear to be a key issue in obtaining consistent results for N_2O emission from soils under varying management practices. This problem can only be addressed through long-term studies consisting of measurement schemes that are adequate spatially and temporally to cover this heterogeneity (Gregorich *et al.,* 2005).

2.1.4.1 Diurnal and Seasonal Variations: N_2O

Nitrous oxide fluxes from soils have been noted to peak after a period of rainfall (*e.g.,* Burton *et al.,* 1997; Pattey *et al.,* 2008) and also have coincided with N fertilizer application (*e.g.,* Hao *et al.,* 2001a). Apart from this, diurnal changes in N_2O production would seem to be due primarily to changing surface temperatures and their effect on biological processes (as seen in Meyer *et al.,* 1997; Brown, H.A. *et al.,* 2002; Petersen *et al.,* 1998). Pattey *et al.* (2006b), using the flux gradient method over a cornfield fertilized with urea, measured fluxes of less than 35 ng N_2O m^{-2} s^{-1} with little diurnal variation during a "baseline" period of little rain and low fertilizer volatility. However, they observed considerable diurnal variation in fluxes after key field management events combined with periods of heavier rainfall (Pattey *et al.,* 2006b).

Nitrous oxide fluxes are generally greatest in the spring (Goodroad and Keeney, 1984; Parsons *et al.,* 1991; Groffman *et al*., 2000, Burton and Beauchamp 1994; Corre *et al.,* 1996; Nyborg *et al.,* 1997; Grant and Pattey, 1999; Hao *et al.,* 2001, Wagner-Riddle *et al.,* 2007; Pattey *et al.,* 2007). This is thought to be due to greater denitrification because of higher soil moisture from snowmelt, or to the release of N_2O trapped under the snow upon snowmelt (Goodroad and Keeney, 1984; Burton and Beauchamp, 1994; van Bochove *et al.,* 2000; Teepe *et al.,* 2001; Dörsch *et al.,* 2004). Freeze-thaw cycles can disrupt soil aggregates and lyse microbial cells resulting in higher levels of dissolved organic carbon and N (substrates for denitrification) (Smith *et al.,* 2002). Low plant activity at springtime may mean that more N is available (Smith *et al*., 2002).

Wagner-Riddle *et al.* (1997) used a flux gradient technique to measure fluxes from a selection of differently cropped and managed agricultural fields at a site in Elora, Ontario (near Guelph) for a period of 28 months. Fluxes were lower than 0.2 kg N ha^{-1} mo^{-1} (7.7 ng N_2O-N m^{-2} s^{-1}) 70% of the time, while during peak emission periods (spring thaw, manure addition, and crop (alfalfa) plowing) fluxes as high as 3.23 kg N_2O-N ha^{-1} mo^{-1} (125 ng N_2O-N m^{-2} s^{-1}) were measured. Wagner-Riddle *et al.* (2007), using the flux gradient method, measured fluxes between -5 and 5 g N_2O-N ha^{-1} day^{-1} (-5.8 to 5.8 ng N_2O-N m^{-2} s^{-1}) 68-77% of the time during a five-year period over a corn-soybean-wheat rotation in the same area. Peak emissions (*e.g.,* up to 255 g N_2O-N ha^{-1} day^{-1} or 295 ng N_2O-N m^{-2} s^{-1}) were seen during spring thaw periods.

2.2 METHODS OF GAS FLUX DETERMINATION AND THE NOCTURNAL BOUNDARY LAYER

2.2.1 Overview

The flux density (F_s) of a trace gas can be expressed as

$$F_S = \overline{w's'} + \int_0^z \frac{\partial s}{\partial t} \partial z + A \qquad (2.1)$$

where the first term is the vertical turbulent exchange represented by a covariance between the vertical wind speed w and the gas mixing ratio s, the second term is the storage within the boundary layer (defined as having height z from the surface) represented by the concentration s change with time t and the third term represents advection A (*e.g.,* Lee, 1998; Baldocchi*,* 2003; Pattey *et al.,* 2006a). In general, the first term is most important in turbulent atmospheric conditions while the storage term becomes important in calm conditions. Storage of trace gases can also occur through the physical trapping of these gases, for example, under a dense plant canopy. The advection term is often assumed to be zero in flat, homogeneous terrain (*e.g.,* Baldocchi, 2003, Pattey *et al.,* 2006a) as any horizontal transport in this case will not cause the vertical flux to change with height (Baldocchi, 2003). The exclusion of advection from the NBL budget equation in this study is addressed in Section 2.3.

Under turbulent conditions, eddy covariance (EC) is the technique of choice (Baldocchi, 2003). Fast response sensors provide high frequency measurements of vertical wind speed and gas concentration. Flux density is calculated continuously through time. The eddy covariance system spatially integrates the flux over an upwind source area whose exact dimensions are governed by the sensor height, the surface roughness and the atmospheric stability. However, because the EC method relies on turbulent exchange, during periods of weak or intermittent turbulence, the technique fails to provide accurate measurements of trace gas exchange (*e.g.,* Pattey *et al.,* 1997; 2001; 2002; Eugster and Siegrist, 2000). Turbulent flux data are usually screened using threshold criteria such as a minimum friction velocity or standard deviation of the vertical wind speed in order to consider that turbulence is high enough for using the EC technique. As stable atmospheric conditions are dominant at night, many nights do not permit eddy flux measurements. Furthermore, fluxes measured by turbulent methods, such as EC, at a single height, do not incorporate gases stored in the interval between the surface and the height of the sensor, which is crucial to capturing the stable nighttime flux.

The flux gradient technique is also frequently used to measure turbulent trace gas fluxes (equivalent to Term 1 in Equation 2.1). This technique consists of measuring the gradient of the trace gas concentration profile and applies an eddy diffusivity coefficient to determine the trace gas flux (Businger, 1973; 1986). However, this method relies on the Monin-Obukhov similarity theory, which fails in very stable conditions (Mahrt *et al.,* 1999).

The storage term of Equation 2.1 can be measured using methods that measure the change in trace gas concentration over time. For small-scale studies, closed chambers can be used to determine gas exchange by measuring slope of gas concentration with time in the enclosure. Samples can either be extracted at fixed time intervals or measured dynamically using portable analyzers (Rochette *et al.,* 1997). This technique has been used extensively for plot-scale studies involving different treatments (*e.g.,* Allaire *et al.,* 2008; Roberson *et al.,* 2008) and for determining gas exchange from different sub-units of an ecosystem (*e.g.* Pelletier *et al.,* 2007; Saurette *et al.,* 2006). The emission of some trace gases (*e.g.,* N_2O) varies widely spatially leading to large ranges in measured values using small chambers (*e.g.,* Henault et al., 1998; Laville et al., 1999) which are restricted in the areal extent that they represent. The spatial inhomogeneity of surface emissions over a large area on the order of several square kilometers is accounted for by the NBL technique and will include any high-emission ("hot") spots, especially for CH_4 and N_2O (Pattey *et al*., 2002).

Trace gas fluxes can also be simulated at daily or hourly timesteps using process-based trace gas flux models (*e.g.,* DNDC, Li *et al.,* 1992a,b; 1994; DAYCENT, Parton *et al.,* 1998, DelGrosso *et al.,* 2002; Smith *et al.,* 2008; *ecosys*, Grant and Nalder, 2004). Process-based models are particularly useful to summarize our understanding of the ecosystem and can provide independent field-scale estimates with which to compare top-down micrometeorological methods (see Chapter 6). Atmospheric physics-based models such as ZINST (Wilson *et al.,* 1981) can be used to find the source emission strength. Models predicting the upwind source area of fluxes are discussed in Section 2.4.

2.2.2 The Nocturnal Boundary Layer

With the removal of the supply of radiative energy from the sun, sensible heat flux from the surface into the atmosphere becomes stalled. The temperature of the ground becomes approximately equal to the temperature of the air just above it, and the atmosphere becomes neutral (Sorbjan, 1989). After this point, especially on clear nights, radiative cooling of the surface begins (net upward long-wave radiative flux) (Funk, 1960). Net downward sensible heat flux occurs from the air (Businger 1973), and a radiative temperature inversion layer slowly forms. This layer deepens into the lower atmosphere over the course of the night (*e.g.,* Mahrt *et al.,* 1979). Air temperature increases with height as the increasing net downward heat flux continuously reduces the temperature at the base of the residual layer (Garratt, 1992).

The result, as the night progresses, is a reversal of the previous day's near-surface temperature gradient where temperature normally decreases with height. The strength of the inversion, measured as the temperature difference between the ground and the top of the inversion layer, will depend on the strength of turbulence in the NBL and any mesoscale factors (Mahrt, 1998). An illustration of a weak vs. a strong inversion is shown in Figure 2.1. At the top of the inversion, the temperature decreases with height as in the daytime (Oke, 1987). As the depth of the NBL on land continuously evolves over the night it is termed non-stationary (Stull, 1988). It does not have time before the night ends to reach a height where it will be in a steady state/equilibrium condition such as the convective boundary layer (CBL) may reach during the day (Derbyshire, 1990). Typically the height of the NBL will reach anywhere from 5 to 500 m (Mahrt, 1998).

There is little turbulence in the NBL compared to the daytime CBL because of the lack of buoyant convection (Businger, 1973). On clear nights, turbulence may only be generated mechanically by wind shear (Businger, 1973). Wind shear in the NBL can be induced by friction as air passes over the surface or at the underside of a low-level nocturnal jet (Mahrt *et al.,* 1979). The nighttime presence of clouds, however, will impact long-wave radiative flux divergence, thus affecting boundary layer dynamics and the generation and evolution of turbulence (Stull, 1988).

2.2.2.1 The Low-Level Nocturnal Jet and Shallow Drainage Flow

Wind speeds in the NBL typically increase with height, reaching a maximum near the top of the inversion layer. When this maximum speed exceeds that of the geostrophic wind, the mean wind driven by pressure gradient and Coriolis forces, it is termed the 'low-level nocturnal jet' (Stull, 1988). The jet is thought to form from flow acceleration due to decreased turbulence aloft (inertial oscillation) (Blackadar, 1957) or sloping terrain (baroclinicity) (Lettau and Davidson, 1957). Above the jet, wind speed and direction smoothly decrease to that of the geostrophic wind (Stull, 1988).

A cold, down-slope, shallow drainage, or katabatic, surface flow can occur in the lowest 2-10 m of a stable boundary layer, with wind speed depending upon friction from the surface and entrainment from air above the wind (Stull, 1988). These winds are formed when cold dense air caused by nighttime radiative surface cooling is accelerated down-slope by gravity (Oke, 1987; Stull, 1988; Garratt, 1992). Sometimes drainage flows can be thinner than 2 m, and can transport heat and trace gases (Mahrt *et al.,* 2001). Even gentle slopes such as 0.001 or 0.01 over a large area can generate katabatic winds of 1 to 2 m s^{-1} (Brost and Wyngaard, 1978; Mahrt, 1981).

2.2.2.2 Exact Definition of the NBL

The NBL can be defined according to different characteristics found in this developing surface boundary layer. In his introductory boundary-layer text, Stull (1988) tends to consider the NBL a "nocturnal inversion" (referring to the temperature inversion), and gives a list of definitions of NBL height (also referred to as "depth"). For example, the top of the NBL could be the height where the lapse rate is adiabatic or where it becomes isothermal. It can also be defined as the height where turbulent kinetic energy goes to zero or where it is reduced to 5% of its surface value. The top of the NBL can also be defined in terms of a nocturnal jet or geostrophic winds, or the height at which SODAR returns disappear.

On the other hand, in his introductory text, Garratt (1992) defined the NBL as the shallow, turbulent layer above which the mean shear stress and heat flux are negligibly small and differentiates this from the temperature inversion, the height of which is generally greater than that of the turbulent layer. The shallow turbulent layer Garratt (1992) refers to is the 'constant flux' or 'thin surface' layer, a traditional boundary layer where turbulence is generated immediately adjacent to the surface by the interaction between air flow and the rough elements of the surface (Businger, 1973; Mahrt, 1999; Mahrt and Vickers, 2002). The layer above this is the stable nocturnal boundary layer where turbulence is weak and intermittent (André and Mahrt 1982; Mahrt, 1999). At night, however, the constant flux layer is usually very thin and can even disappear altogether (Mahrt, 1999). In this thesis, following Mahrt (1999), reference to the nocturnal boundary layer includes both the thin surface boundary layer and the stable boundary layer above it.

Not surprisingly, Stull (1988) points out that there has been difficulty in comparing data sets due to different definitions being used by different investigators.

2.2.2.3 Classification of NBL Regimes

Mahrt (1998; 1999) and Mahrt and Vickers (2002) give a good review of the classifications and vertical structure of stable nocturnal boundary layers with regard to basic features such as radiative cooling, wind and clouds, temperature profile, turbulence, NBL height, mesoscale motions, and vegetation canopy effects. While emphasizing that any attempt to classify stable boundary layers into a few classes is an oversimplification, Mahrt (1998; 1999) defines three broad categories: the weakly stable boundary layer, the transition stable layer, and the very stable layer. The main characteristics thought to be attributable to each class of stable boundary layer are given in Table 2.2.

The characteristics of such classifications vary by author but typically wind speeds are reported to be within the range of 0 and 4 m s^{-1} for conditions to be classified as stable. Early evening can be more stable than the latter part of the night, due to increasing wind speeds (Mahrt *et al.,* 1998; 2000). In general, vertical turbulent transport decreases with increasing stability (Mahrt, 1998). In the weakly stable case, that is, when winds are stronger, turbulence over the NBL can occur in a continuous/contiguous manner. At the other extreme, the very stable case, turbulence can exist as patchy, intermittent bursts throughout the layer, which are governed by local shears and stability at a particular height, rather than from forcings at the surface (Stull, 1988, Mahrt, 1999). For the weakly stable boundary layer, overall turbulence decreases with height (Caughey *et al,* 1979; Mahrt, 1999; Mahrt and Vickers, 2002). For the strongly stable boundary layer, the turbulence energy will increase with height, which is opposite to a traditional boundary layer (Mahrt and Vickers, 2002). Mahrt (1999) has termed this a very stable 'upside-down' boundary layer, where the elevated turbulence originates from shear generated by a low-level jet. Vertical turbulent transfer on the underside is towards the surface along the momentum gradient while vertical turbulent transport is upwards from the top of the jet (Mahrt and Vickers, 2002).

The top of the NBL becomes more difficult to define as stability increases over time (Figure 2.1). However, Mathieu *et al.* (2005) and the current study find that the NBL height for the purposes of a GHG budget can be defined best using maxima in the wind profile rather than the potential temperature profile as previously suggested.

Mahrt (1998; 1999) indicates that most studies have been done on the weakly stable case, so that knowledge of the structure of the very stable boundary layer is limited and does not present a unified picture or theory, due to the limitations of atmospheric scaling theories, the difficulties in measuring weak intermittent turbulence with existing instrumentation, and also the fact that there is a complex interaction of different physical processes such as radiative cooling and flux divergence, intermittent turbulence, gravity waves, the nocturnal jet, katabatic winds, and the absence of a well-defined NBL top, all occurring simultaneously in the stable boundary layer. Surface heterogeneity, including heterogeneity in vegetation and soil, adds a further complicating dimension (Mahrt 1998; 1999).

2.3 THE NBL BUDGET METHOD

The NBL budget technique relies on changes in trace gas concentration over time at the landscape scale. It performs well for stable nocturnal conditions and has the potential to provide flux measurements when conventional turbulent measurements, taken at a fixed height, are not applicable.

In stable conditions, strong temperature stratification actively suppresses any buoyant stirring, which keeps gases from migrating vertically (Oke, 1987; Stull, 1988). Low winds can also limit the turbulent diffusion and transport of greenhouse gases in the NBL (*i.e.,* $\bar{u}$ less than 2 m s^{-1}, Anfossi *et al.,* 2005). For example, in low wind and turbulence conditions, Denmead and Raupach (1993) found that CO_2 concentrations built up to 100 ppmv above the baseline large-scale average. A low-level nocturnal jet or wind speed maximum can also trap surface-emitted gases beneath it (Beyrich et al., 1997; Corsmeier et al., 1997; Mathieu *et al.,* 2005; Banta *et al.,* 2002; 2007).

Several tethered balloon soundings are conducted in the NBL in one night, following the development of the NBL (Denmead *et al*., 1996). The difference in GHG concentration between successive NBL profiles ($\partial s/\partial t$) is integrated over the NBL height (z) (Term 2 of Equation 2.1) (Denmead *et al.,* 1996) making the assumption that the turbulent vertical flux is negligible under calm conditions.

While advection is excluded from NBL budget measurement and flux calculation here and in previously published NBL budget studies (*e.g.,* Denmead et al., 1996; Pattey *et al.,* 2002), in reality, the contribution of advection to the NBL budget is not zero. Current research indicates that advection can be significant (Finnigan, 2008; Foken, 2008; Aubinet, 2008). The principal form of horizontal exchange in the NBL is shallow drainage flow, which can occur with slight slopes (Finnigan, 2008; Foken, 2008; Aubinet, 2008) Other forms of advection can include gravity waves and nighttime regional (*e.g.,* land-water, urban-rural) circulation events (*e.g.,* Goulden *et al.,* 1996; Sun *et al.,* 1998; Mahrt *et al.,* 2001; Finnigan, 2008; Foken, 2008; Aubinet, 2008). The main challenge in including the advective component in the NBL budget equation is the associated measurement difficulty as advection, when present varies spatially and requires a comprehensive, site-specific measurement setup (Finnigan, 2008; Foken, 2008; Aubinet, 2008). The impact excluding the advective component on the NBL-measured fluxes in this study cannot be estimated.

Limitations of the NBL approach include the probability that there will be many nights when the use of this technique will be unsuitable, for example, when winds are strong and the NBL is turbulent (Pattey *et al*., 2002), or when cloudy skies restrain strong radiative cooling from the surface. There also may be an uncertainty about the extent of the surface that the budget represents (Denmead *et al*., 1996). Exploring the latter issue is one of the objectives of this thesis.

2.4 DETERMINATION OF SOURCE AREA OF FLUXES

2.4.1 Footprint Models

The footprint of a measured concentration or flux is the area of the surface which constitutes the source/sink of the measured value. Mathematical modeling of concentration and flux footprints has been studied progressively since the work of

Pasquill (1972) through to the work of Schuepp *et al.* (1990) and Leclerc and Thurtell (1990) who presented a simple analytical footprint model readily applicable for field situations. Subsequent studies have aimed at providing improved footprint prediction, to account for more complex surface flows and a greater range of atmospheric stability (*e.g.,* Schmid and Oke, 1990; Horst and Weil, 1992; 1994; Schmid, 1994, 1997; Flesch *et al.,* 1995; Leclerc *et al.*, 1997; Baldocchi, 1997; Rannik *et al.* 2000; 2003; Kormann and Meixner, 2001; Kljun *et al.*, 2002; and Sogachev and Lloyd, 2004).

There are essentially three types of footprint models. An analytical/numerical model uses differential solutions to the advection-diffusion problem (*e.g.,* Schuepp *et al.,* 1990; Schmid and Oke, 1990; Wilson and Swaters, 1991; Horst and Weil, 1992). A Lagrangian stochastic diffusion model involves the numerical simulation of the trajectories of independent particles that follow a Lagrangian dispersion pattern (*e.g.,* Leclerc and Thurtell, 1990; Horst and Weil, 1992; Flesch *et al.,* 1995; Rannik *et al.,* 2000; Kljun *et al.,* 2002). Large eddy simulation (LES) models can also be used to characterize footprints by calculating, from Navier-Stokes equations (describing atmospheric motion), the contribution of large eddies in the planetary boundary layer to momentum and energy transfer (*e.g.,* Moeng, 1984; Leclerc *et al.,* 1997; Piomelli, 1999). Related to LES models are 'closure' models which are designed to perform well in heterogeneous terrain (Sogachev *et al.,* 2002). Schmid (2002), Foken and Leclerc (2004), and Vesala *et al.* (2008) give reviews of the history and current state of footprint modeling, including the general characteristics, assumptions, and limitations of each type of footprint model.

Footprint functions describe the contribution of the source area to the measured value. In other words, a certain distance or location (*x, y*) upwind will contribute a certain percentage of the measured value. An example of a weighted source area model by Schmid (1994) is shown in Figure 2.2.

The area contributing to the flux will vary with the height of measurement. A concern in micrometeorology is the correct placement of sensors within the fetch, the area upwind of the sensors. In general, for a given surface roughness, the greater the height of measurement, the greater the area of contribution and also the distance of the maximum source contribution will be. An example is shown in Figure 2.3 (Schuepp *et al.,* 1990).

In unstable conditions, strong vertical motions are present and a maximum percentage of the source area contribution will occur at a distance relatively close to the measurement location. An example is given in Figure 2.4 (Leclerc and Thurtell, 1990). Conversely, in stable conditions where vertical motions are suppressed, the source area will be more spread out, with a small percentage of contribution occurring over a large surface area (Figure 2.4).

In stable conditions where stratification of the atmosphere occurs (*i.e.,* in the nocturnal boundary layer), a point measurement at a given height may be measuring something that has originated quite far away and traveled horizontally along the mean wind to the sensor. Concentration profiles with a tethered balloon beginning near the ground and moving upward in the atmosphere are therefore suitable to make sure that both the surface near the sensor location and the surface further upwind are being “seen”.

Surface heterogeneity, expressed as the patchwork of surfaces of different roughness found on a typical farm, has an influence on footprints as well (Schuepp *et al.,* 1990; Leclerc and Thurtell, 1990). The smoother the surface, the greater is the extent of upwind influence on the measured value (Leclerc and Thurtell, 1990). This has implications for micrometeorological techniques (daytime and nighttime) that assume measurement areas are surrounded by large homogeneous surfaces for the measurement to be representative of the surface. Where typically a 100:1 fetch to measurement height ratio was previously thought sufficient in a variety of conditions, it seems that over relatively smooth surfaces (*e.g.,* grass or short crops) and under stable conditions, the ratio is found to underestimate the amount of upwind homogeneous surface needed (Leclerc and Thurtell, 1990).

2.4.2 Limitations of Footprint Models

There are a number of limitations in the use of footprint models, which are currently optimized for unstable atmospheric conditions. The footprint model gives the upwind location/distance of the greatest contribution from the source area, based on horizontally homogeneous turbulent diffusion, atmospheric stability, and surface aerodynamic parameters. Models also usually assume there is no vertical flux divergence (*e.g.,* Schuepp *et al.,* 1990; Schmid 1994, 1997) and the advective component (*i.e.,* horizontal flux divergence) is also ignored (Vesala *et al.,* 2008). Analytical and stochastic footprint models also assume that the source area is of equal emission strength everywhere. In reality, of course, variations in a surface affect all turbulent exchange, whether it is the flux of momentum, heat, or mass (Schmid, 1997). These models cannot tell us, then, precisely where sources of scalar concentrations or fluxes are located, given multiple strongly-emitting sources within the source area. However, a recently proposed "closure"-type footprint model (Sogachev *et al.,* 2002; Sogachev and Lloyd, 2004) attempts to account for different contributions in a heterogeneous source area. Validation of footprint models with real field data remains a priority (Schmid, 2002; Foken and Leclerc 2004; Vesala *et al.,* 2008).

2.4.2.1 Footprint Model Limitations Specific to this Project

Beyond the immediate field site, the agricultural landscape is a patchwork of different crops, that is, it is a surface of varying roughness and trace gas source strengths. We might assume, then, that the source area determination may be susceptible to misrepresentation due to the footprint model assumption of surface homogeneity. However, Schmid (1997) discusses the issue of scale regarding the viewing of a surface as homogeneous, at least as far as roughness and flow conditions are concerned. For example, if a surface is viewed on a large horizontal scale, the surface roughness by comparison might be considered homogeneous (Schmid, 1997). This is good news for NBL budget measurements which have footprints on the order of kilometers. As the NBL develops into its stratified layers, horizontal movement in each layer may encourage blending within that layer. Furthermore, layers higher up will also become horizontally integrated and have even larger footprints, further rendering the surface seemingly homogeneous and in this way meeting the assumption of the footprint model.

Ideally, determining the source area for a concentration or flux measurement in the nocturnal boundary layer would require a footprint model optimized for stable conditions. Such a model does not currently exist (Vesala *et al.,* 2007). Despite this, for the purposes of this project, an easy-to-use on-line parameterization of a Lagrangian-based flux footprint model by Kljun *et al.* (2004), with input parameters set as close to stable conditions as possible, has been used (Chapter 4). This is justified because footprint models have a physical basis and are helpful to provide a first-order confirmation of the main source area of measured concentrations and fluxes.

A further limitation in this project is that the flux footprint parameterization has been used in this project to estimate the source area of both concentration (Chapter 5) and flux measurements (Chapter 6). In reality concentration and flux footprint models contain equations and variables specific to concentration and flux behavior and do not give the same results (*e.g.,* Griffis *et al.,* 2007). Both analytical and stochastic footprint simulations have shown that concentration footprints extend much farther upwind than flux footprints (*e.g.,* Schmid, 1994; Rannik *et al.,* 2000; Kljun *et al.,* 2002), by as much as an order of magnitude (Schmid, 1994). Finnigan (2004) stated that a concentration model is actually better suited for finding the footprint of fluxes in conditions where storage is important (*e.g.,* the very stable boundary layer). Chen *et al.* (2008) used a concentration footprint model for concentration profile-derived fluxes based on a model of vertical diffusion.

An additional assumption is the equivalence of the flux footprint predicted by the model for a directly measured flux (*e.g.,* by EC) to that of a flux measured from a concentration profile. Horst (1999), using the analytical footprint model of Horst and Weil, 1994) showed that the footprint for a concentration profile-derived flux is equivalent to that of a directly-measured flux if the footprint for the directly-measured flux is modeled for the mean measurement height of the concentration profile. However, while inter-model (Lagrangian-analytical) comparisons have given similar output (*e.g.,* Leclerc *et al.,* 2003b; Cai and Leclerc, 2007), we will assume here that the footprint of turbulence- and concentration-profile-derived fluxes are the same and use the NBL height to model the footprint. Also, considering recent comments that during strong storage conditions a concentration footprint should be used (*e.g.,* Finnigan, 2004), using Horst's (1999) method with the mean measurement height instead of the NBL height may lead to further underestimation of an already underestimated source area, because Kljun's model is not designed to be used for stable conditions.

Despite all this, the flux footprint model is used in this project to give a minimum estimate of the upwind boundary of the source area which includes the most important, near-field contributions to a concentration profile (Chapter 4). For continuous, relatively homogeneous agricultural land, there should be minimal impact on the interpretation of the results (Chapter 4). We consider the use of the flux footprint is acceptable (aforementioned limitations notwithstanding) when finding the source area of the NBL-measured flux, where the flux is the difference between two concentration profiles, as used in Chapter 6.

Further pertinent assumptions, limitations, or simplifications of this model will be addressed in Chapters 4 and 6.

TABLES

Table 2.1. Overall level-uncertainty in greenhouse gas emissions for subcategories of the agriculture sector, as per Hutchinson *et al.* (2007) in the 2005 Canadian Greenhouse Gas Inventory (Environment Canada, 2007).

Agriculture Subcategory	**Overall Uncertainty**
CH_4-enteric fermentation	±18%
CH_4-manure management	±23%
N_2O-manure management	-31 to 40%
N_2O -synthetic N fertilizers	-39 to 49%
N_2O -manure as fertilizer	-35 to 41%
N_2O -crop residue decomp.	-44 to 48%
N_2O -cultivation organic soil	±50%
N_2O -manure pasture or paddock	-26 to 33%
N_2O -indirect emissions	-45 to 45%
N_2O -leaching	-45 to 57%

Table 2.2. Characteristics of three broadly defined classifications of the stable nocturnal boundary layer, summarized from Mahrt (1998, 1999).

Characteristic	WEAKLY STABLE	TRANSITION	VERY STABLE
Net Radiative Cooling	Slow[a]	Downward heat flux reaches maximum (See Fig. 2.1)	Strong
Wind/Clouds[b]	Windy and/or cloudy	Skies clearing, winds diminished	Calm and clear
Temperature profile (See also Fig. 2.1)	Weak inversion, shallow, well-mixed	Weak inversion, shallow, better defined	Strong inversion, not mixed
Turbulence	Continuous near surface and globally intermittent at higher levels Decreases with height	Still some continuous near surface but now more dominated by intermittent turbulence throughout the BL[a]	Globally intermittent throughout the BL May only originate from nocturnal jet (not surface); increases with height
Richardson Number (*Ri*)[c]	Less than 0.25		Greater than 0.25
NBL Height	Definable	Not well-defined	Not well-defined
Mesoscale Influences[d]	Less important due to dominance of turbulence	Increasing in importance	More important (weak turbulence, phenomena more active)

a Holtslag & Nieuwstadt (1986)
b Wyngaard (1973)
c Dimensionless stability parameter which considers the proportions of shear production and buoyant production of turbulent kinetic energy (Richardson, 1920), defined in Chapter 3.The critical Richardson number of 0.25 represents the transition from turbulent ($Ri < 0.25$) to laminar flow ($Ri > 0.25$).
d Nieuwstadt (1984)

FIGURES

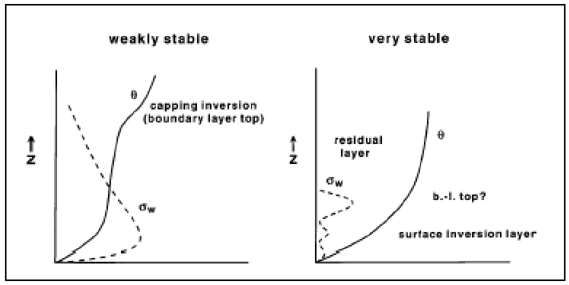

Figure 2.1. Idealized contrast of the vertical temperature structure of the weakly stable and very stable boundary layers. σ_w is the standard deviation of the vertical velocity fluctuations and θ is the potential temperature. From Mahrt (1998).

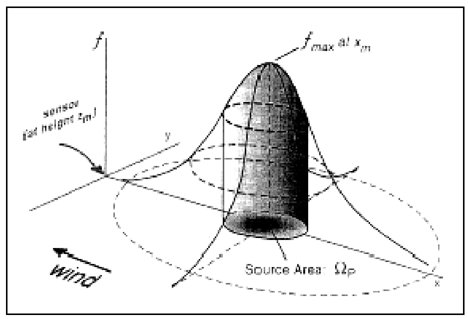

Figure 2.2. Schematic diagram of the source area function (from Schmid, 1994). Maximum contribution of source area (f_{max}) occurs at a certain distance upwind (x_m) from the measurement at height z_m. Contribution decreases to all sides from the maximum.

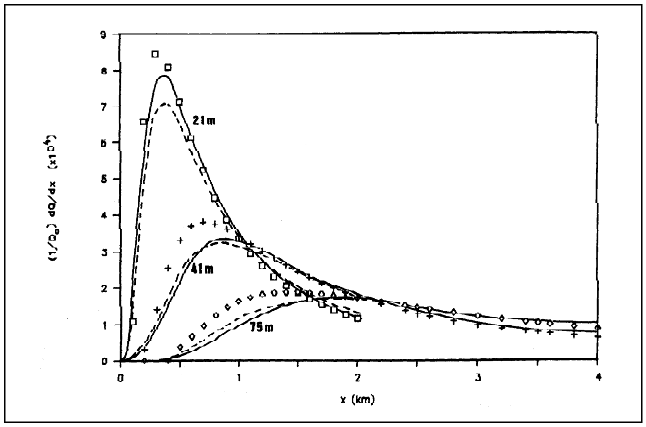

Figure 2.3. Analytical footprint model of Schuepp *et al.* (1990) run for 3 measurement heights under neutral atmospheric conditions, with a surface roughness (z_0) of 0.06 m and a zero plane displacement (*d*) of 0.3 m. From Schuepp *et al.* (1990).

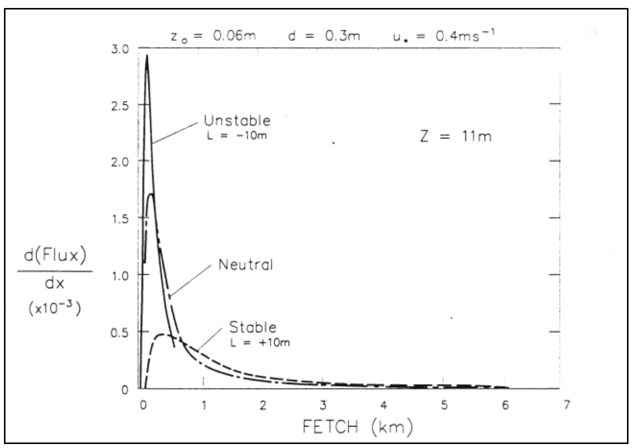

Figure 2.4. Footprint prediction of numerical model by Leclerc and Thurtell (1990) for different thermal stability conditions at a given measurement height, surface roughness, and zero-plane displacement. From Leclerc and Thurtell (1990).

3. NBL OPERATIONAL METHODOLOGY

3.1 INTRODUCTION

The NBL budget method has been used by many research teams to measure CO_2 fluxes over relatively flat, dry upland agricultural land including pasture and cereal crops (Denmead *et al*., 1996), soybean and corn fields (Pattey *et al*., 2002), alfalfa pasture (Griffith *et al.*, 2002), grass pasture in Brazil (Acevedo *et al.*, 2004), and less frequently for the measurement of other greenhouse gases over field crops to obtain N_2O flux (Pattey *et al.*, 2006), and over pasture grazed by sheep and cattle, to measure CH_4 flux (Denmead *et al.,* 2000a). The NBL method has also been used to measure GHG fluxes in other environments such as wetlands (Choularton *et al.,* 1995) and mires (Beswick *et al.,* 1998), a mountain plateau (Eugster and Siegrist, 2000), forests (Fisch *et al.,* 2000; Pattey *et al.,* 2002), and even urban settings (Zinchenko *et al.,* 2002).

While both the theory and methodology of the NBL budget method are relatively simple compared to other flux measurement techniques, several issues interfere with the application of this technique. These issues include primarily (1) the requirement for optimal atmospheric conditions and stability, (2) the inherent intermittent behaviour of the very stable nocturnal boundary layer, (3) the entrainment or loss of gases from the NBL and (4) the uncertain source area (footprint) of NBL-measured fluxes.

Atmospheric conditions on a given night will determine the degree of stability of the NBL, and therefore potential gas accumulation. The intermittent behaviour of the NBL stems from a complex interaction of different physical processes including radiative cooling and flux divergence, intermittent turbulence, gravity waves, low-level nocturnal jets (LLJ), and shallow drainage flow occurring simultaneously in the NBL (Mahrt, 1998;

1999). In particular, horizontal advective exchange from shallow drainage flow, gravity waves, or other mesoscale motions (*e.g.,* Eugster and Siegrist, 2000; Mahrt and Vickers, 2002; Sun *et al.,* 2004) and a sudden breakdown of the NBL, *e.g.,* from shear originating at the underside of a LLJ (*e.g.,* Mathieu *et al.,* 2005), from advection, or other mesoscale motion appearing over a deep layer, can contribute to the loss of accumulated gases at the surface or entrainment of trace gas-enriched air at the top of the NBL and uncertainty in the surface representativeness of NBL-measured GHG fluxes. These features, along with intermittent shear-associated turbulence at varying heights in the NBL can also directly affect the choice of height to which NBL fluxes are integrated (*i.e.,* the effective height of the NBL). Uncertainty around the upwind source area contribution within the NBL is also attributable to changing wind direction and current footprint model limitations (Schmid, 2002).

The agricultural surface should also be representative of the area over which GHGs need to be quantified. For any micrometeorological technique, the surface should be flat, homogeneous in nature, and spatially infinite, so that no horizontal gradients exist and all fluxes are only vertical (Oke, 1987). These conditions are rarely met since the agricultural landscape is heterogeneous and made up of a 'patchwork' of fields, each cropped and managed differently, with its own radiative, thermal, moisture, and aerodynamic properties. As the mean horizontal wind crosses over each field toward the measurement location, it adopts features (*e.g.,* air temperature, trace gas concentration, relative humidity) derived from the field, forming an internal boundary layer (Oke, 1987). This layer grows vertically and retains the signature of the underlying land up to a height where it will then blend completely with overlying air (*e.g.,* Oke, 1987; Mason, 1988; Wood and Mason, 1991; Mahrt, 1996; Schmid and Lloyd, 1999). Usually, when aggregated (*i.e.,* heterogeneous) ecosystem-scale fluxes are desired, it is considered important to ensure that flux measurements are taken above the blending height; this ensures that fluxes measured are not biased to an individual field within the ecosystem (*e.g.,*Mahrt, 1996; Schmid and Lloyd, 1999). At a scale of horizontal measurement much larger than both the scale of surface roughness elements and the height of observation, as in this study, a heterogeneous surface can be described as homogeneous (Wood and Mason, 1991; Mahrt, 1996). This, along with limited vertical mixing during strongly stable conditions, most likely limits the blending height to well-below the height of observation, here the NBL height. This would be a reasonable assumption in complement to findings that sensor height and location bias are considerable during strongly unstable conditions, becoming less biased toward neutral conditions (Schmid and Lloyd, 1999). In any case, for the NBL budget method, the fact that the well-defined NBL 'traps' any gases migrating vertically from the source area may override the importance of the observation height encompassing the blending height; as long as the measured vertical profile of GHG concentrations extends to the top of the NBL, an averaged flux representing the heterogeneous farm ecosystem may be obtained.

Changes in surface roughness also affect wind speed and direction. The NBL budget integrates these characteristics from many fields upwind. However, major topographic variation (*e.g.,* hills) or the presence of isolated strong point sources of trace gases (*e.g.,* factory urban center) could cause unrepresentative budget measurements by the NBL budget method.

To determine GHGs at the farm scale, any effect resulting from the patchwork of fields is in fact desirable in the selection of a relevant agricultural site. If the make-up of the agricultural 'patchwork' is consistent throughout the region it allows some flexibility in the restriction for wind direction consistency, as the source area type will remain steady.

Very few of the NBL studies (*e.g.,* Eugster and Siegrist, 2000, Pattey *et al.,* 2002; Acevedo *et al.,* 2004, and Mathieu *et al.,* 2005) address in detail the impact of intermittent turbulence and of footprint heterogeneity on the results obtained using the NBL budget method. This chapter focuses on the key aspects of the NBL methodology for the simultaneous measurement of CO_2, N_2O, and CH_4 fluxes from agroecosystems, previously measured separately in the NBL, including the NBL conditions necessary for its application. Following this review the chapter covers the field sites, equipment, measurements, and calculations used during the field campaigns.

3.2 KEY ASPECTS OF THE NBL BUDGET METHOD

As described in Chapter 2, the NBL budget method operates through measurements of the retention of surface-emitted trace gases within the NBL over a certain period of time. The change in trace gas concentration is measured and the 'effective' height of the NBL, the flux integration height, needs to be identified for the trace gas flux to be calculated (Equation 2.2). The NBL should remain intact between profile measurements so that uninterrupted trace gas accumulation can be quantified. Furthermore, the source area, by wind direction or land/vegetation type, should remain consistent for the resulting trace gas flux to be considered representative of the surface of interest.

3.2.1 Conditions Favouring Well-Defined Trace Gas Build-Up Within the NBL

A strongly stable nocturnal boundary layer will favour gas accumulation. Different degrees of stability exist within the strongly stable category (see Chapter 2,

Table 2.1). From our observations, the synoptic conditions leading to the development of strong stability allowing appreciable gas accumulation are as follows: 1) clear nights associated with high-pressure systems, with 2) surface winds less than 2 m s^{-1} and 3) a strong temperature inversion at the surface (at least 5-10°C).

While trace gases may accumulate near the surface simply because of the nature of the stably stratified layers (very slow upward diffusion), the rate of accumulation is enhanced considerably by a well-defined NBL. Here, the effective NBL height can be easily defined and forms a 'cap' or 'lid' that hinders the upward migration of surface-emitted trace gases and also may prevent their dilution by the entrainment of gases from above the NBL. Banta *et al.* (2006) argue that there is likely some transport through the LLJ due to small, non-zero turbulence in the nose of the jet, but in our observations the transport through the LLJ was minimal compared to the gas retention induced by the LLJ (Mathieu *et al.,* 2005). Horizontal wind speed maxima in conjunction with associated stable and shear layers can be used to determine the effective height of accumulation (Mathieu *et al.,* 2005). This concept is described briefly in Chapter 4, §4.2.2 and 4.2.3, and in more detail in Chapter 5.

Once established, the very stable NBL and horizontal wind speed maximum must remain established for the period of time covered by at least one pair of NBL profile measurements. Periodic breakdowns in NBL stability may lead to the upward loss of near-surface accumulated gases and downward contamination by gases from aloft. The NBL can, however, re-establish itself in the same night (Mahrt, 1999). For example, Griffith *et al.* (2002) observed that overall nocturnal increase in surface CO_2 concentration is interrupted periodically due to changes in storage near the surface. As a result they did not include all half-hourly measurements and instead calculated average nocturnal fluxes using measurements from “suitable” periods (not defined, presumably when there was no reduction).

Lastly, when measuring diffusely-emitted gases (*e.g.,* CO_2, N_2O), the source area type should remain the same for the period covered by the set of profile measurements. For gases from point sources (*e.g.,* CH_4), the wind direction must remain the same.

3.3 FIELD WORK

Field work for this study was conducted during the summer of 1998 by Dr. Pattey’s team from AAFC and in 2002 and 2003 by the candidate at two agricultural farms in eastern Canada. Results from the NBL budget method for 1998, 2002, and 2003 are available for a total of 21 nights representing conditions in June, July, August, and/or September.

3.3.1 Procedure for Determining Atmospheric Conditions Suitable for NBL Launches

A limited number of nights meet suitable conditions for using the NBL technique (Pattey *et al*., 2002). It is also difficult to predict which nights will meet all the above conditions; in our study the NBL budget method was attempted when a clear night and wind speeds of 0 (calm) to 5 km h^{-1} were forecasted by the Environment Canada weather office. Some NBL attempts were also made on borderline (slightly cloudy, slightly breezy) nights relying on the chance that conditions might improve at some point. Given the first two criteria (clear and calm, strong inversion), the development of any wind speed maxima was something that could only be witnessed *in situ* and analyzed later in conjunction with stability and trace gas accumulation data.

3.3.2 Field Sites 1998 and 2002: CFIA Farm, Ottawa, ON

The locations of field sites from 1998 and 2002 within the CFIA farm are shown in Figure 3.1. Results from the NBL budget method were available for six nights from July and August of 1998 and three nights in June and July of 2002. The NBL field site in 1998 is described in Pattey *et al.* (2001). Briefly, the field used in 1998 was planted with corn and was surrounded by similar corn fields.

The 2002 27-ha field site (Figure 3.2) was located on an experimental farm of 1000 ha managed by the Canadian Food Inspection Agency (CFIA) located southwest of Ottawa, Ontario, Canada (45°23'N, 75°43'W). The average farm size in the Ottawa region was 0.9 km^2 (Statistics Canada, 2004). The field site was surrounded by agricultural lands and wetlands several km to the west, 3 km of agricultural land to the north and east, and approximately 750 m to the south, with suburban housing beyond (Figure 3.1). The topography of the farmland in the area varied less than 2 m for the most part. Drainage flow could, in theory, still be present even with this relatively flat topography but was assumed to be negligible for the purposes of this study. The tethered blimp launch site (Figure 3.1) was located on the border of a 27-ha field planted with corn and bordered by a farm road, animal housing and feedlot, a manure pile, a wooded area, and other crop fields and pasture. With the given layout of the region, measurements with wind directions from the southwest to east directions favoured agricultural sources. As all the different elements making up this farm could be found on a typical farm in the region, they were considered as part of the 'patchwork' of the overall agricultural landscape. More information on field management activities (in relation to N_2O and CH_4 fluxes) is given in Chapter 4, Table 4.2.

Flux towers were installed in the field adjacent to the launch site to continuously measure trace gas fluxes (Pattey *et al.,* 2006) using the eddy covariance technique for CO_2 (Figure 3.2) and the flux gradient technique for N_2O (Figure 3.3). The flux towers, operated by AAFC, were equipped with three-dimensional sonic anemometers (DAT-310, Kaijo Denki and HS-3 Solent), closed-path IRGAs (LI-6262, LI-COR Inc., Lincoln, NE) and a tunable diode laser (TDL) trace gas analyzer (TGA 100, Campbell Scientific, Logan, UT). The eddy covariance towers measured fluxes of momentum, CO_2, and sensible and latent heat recorded every 30 minutes at a height of 2 m above the canopy (Grant and Pattey, 2003). The flux gradient towers measuring N_2O fluxes had two inlets separated by 0.50 m which were maintained in the inertial sublayer (Grant and Pattey, 2003). N_2O flux gradients were measured for 30-minute averaging periods alternately between areas of different fertilization levels (Grant and Pattey, 2003). Nighttime flux tower data used for analyses in this study were screened for a minimum friction velocity (u*) of 0.1 m s^{-1} and standard deviation of vertical wind speed (σ_w) of 0.075 m s^{-1} (after Pattey *et al.,* 2002). Data from a minimum of four consecutive half-hourly periods meeting these criteria were kept (after Pattey *et al.,* 2008), to avoid the inclusion of 'bursts' of gas at the onset of a turbulent period after a period of calm conditions (*e.g.,* Aubinet, 2008). The storage flux below the height of tower measurement was not added to the tower flux.

Standard meteorological variables were measured (Figure 3.4), as were soil moisture and temperature profiles. Daytime maximum air temperatures throughout the period of June and July were about 25°C, while night time minima were about 15°C. Soil temperatures ranged from 22 to 27°C at 5 and 10 cm, and ranged from 17 to 25 °C at 20 cm. More information on precipitation (in relation to N_2O and CH_4 fluxes) is given in Chapter 4, Table 4.2.

3.3.3 Field Site 2003: Private Producer's Farm, Coteau-du-Lac, QC

Measurements throughout the summer of 2003 were conducted at a private farm in the rural municipality of Coteau-du-Lac, Quebec, Canada (45°19' N, 74°10' W) (Figure 3.5), some 20 km southwest of the city of Montreal, QC, where the average farm size was approximately 0.9 km^2 (Statistics Canada, 2004). A total of twelve nights of NBL budget method results were available for this field site, from late May to early September 2003.

The St. Lawrence River was located approximately 2.2 to 2.6 km to the south and southeast of the farm (Figure 3.5). A narrow, winding river (the Rivière Rouge) lay 2 to 2.5 km to the west of the site as well. The Trans-Canada highway was located about 1 km south of the launch site, and between the highway and the river, about 1.25 km away, was the rural municipality of Coteau-du-Lac (population approximately 6500). Otherwise, the launch site was surrounded by agricultural land, with small rural residential clusters, for several kilometres. Desired fetch directions were from the southwest to east, to reflect emissions from agricultural land. Land elevation was within 1 to 2 m for several km around the site except where it dropped by about 4 m in close proximity to the rivers. The effects of drainage flow were assumed negligible. The farm was bordered on the east by a farm road along which the residences of local farmers were situated. Animal housing and manure storage facilities in the area are described in Chapter 5, Table 5.3 and Figure 5.3. The elements found on this farm were considered to be commonly found on the typical farm in this region and part of the overall patchwork of agricultural land.

The field site had an area of approximately 60 ha. The surrounding fields were fertilized and planted with corn in early to mid-May. The crop reached a maximum height of approximately 2 to 2.5 m by the end of July and the fields were harvested in October. The field adjacent to the blimp launch site was fertilized in mid-May and planted with edible green peas. The peas (Figure 3.6) were harvested at the end of July and had reached a height of approximately 25 cm. Following the pea harvest, cereals (a combination of barley, alfalfa, and timothy) were planted. This crop was allowed to grow to a height of 12 cm and was maintained at this height to be later ploughed under as green manure. More information on field management activities (in relation to N_2O and CH_4 fluxes) is given in Chapter 5, Table 5.1.

Eddy covariance and flux gradient towers (for instrumentation see Section 3.3.2) and meteorological instrumentation similar to the Ottawa site were also deployed by AAFC (Figures 3.2 and 3.3). Eddy fluxes were measured in 30-minute averages at a height of 2.6 m above the ground. Two towers measured the N_2O gradient at 3 m and 2 m above the surface for 5 s at each height, sampling sequentially for 30 minutes each hour (Pattey *et al.,* 2008). The procedure of screening of data was as described in Section 3.3.2.

Daytime maximum air temperatures at this site in July of 2003 ranged from 21 to 30°C, nighttime minimum ranged from 11-20 °C. Soil temperature data were not available. More information on precipitation, in relation to N_2O and CH_4 fluxes, is given in Chapter 5, Table 5.1.

3.3.4 Equipment, Sample Collection, and Analysis

3.3.4.1 Vertical Profile Measurements

Profile measurements of the NBL were taken several times throughout the nights of measurement, using a tethered blimp from the launch site in each study field (Figure 3.7 a to c) Typically four to six GHG profiles were performed each night (minimum two, maximum eight) with an interval of approximately 1 hour between launches (or two hours when CO_2 and N_2O/CH_4 profiles alternated), to allow for changes in trace gas concentration at the surface without too much potential disturbance of the NBL by the tethered blimp. Launches with the tethersonde alone were occasionally done in between GHG-measurement launches to better characterise the state of the lower atmosphere. Profiles started at sunset and continued until sunrise or until conditions were no longer compatible with the technique (*i.e.,* stronger winds, cloud cover).

The general setup of AAFC's tethered blimp system is shown in Figures 3.7 (a) to (c). A tethersonde (Model 5A, A.I.R., Boulder, CO, U.S.A., Figure 3.8), CO_2 analyzer (CIRAS-SC infra-red gas analyzer (IRGA), PP Systems, Amesbury, MA, Figure 3.9), and/or in-house developed air sampling equipment (Pattey *et al*., 2006, Figure 3.10) were attached to the blimp (TIF-460, Aerostar, Sioux Falls, SD) which had a maximum lift of 7.26 kg (16 lbs). Prior to launch, the CO_2 analyzer was connected to a cylinder of compressed air of very low CO_2 concentration (approximately 7 ppmv) as an aid in determining the start time of launch in the data. Immediately upon launching, the CO_2 analyzer was disconnected from the air cylinder and the tethersonde system began to collect data. The tethersonde (bead thermistor) measured temperature (to the nearest 0.01 °C), pressure (to the nearest 0.01 mb), relative humidity (%), horizontal wind speed (cup anemometer) (to the nearest 0.1 m s^{-1}), and compass direction (to the nearest 0.1°). All references to wind speed in this thesis refer to the horizontal wind speed (u). The magnetic declination (part of the initial tethersonde input, providing correction of magnetic north to true north) was 14.7° for 2002 and 15.2° for 2003 (<http://www.geolab.nrcan.gc.ca/geomag/apps/mdcal_e.php>). The tethersonde also measured altitude, but this was frequently incorrect due to some conflict between the initial surface pressure and surface elevation (both part of initial tethersonde input). The height was instead calculated using the hypsometric equation (Equation 3.1), using T and P from the sonde and e from the CO_2 IRGA. All parameters were measured and signals transmitted at 0.5 Hz and were displayed in real time on a laptop computer at the experimental site. This allowed immediate, in-progress viewing and evaluation of NBL conditions which aided in determining the height and frequency of NBL profiles conducted during that particular evening.

In 2002, the CO_2 analyzer was calibrated prior to each flight using known concentrations of CO_2 and water vapour pressure. In 2003, having previously shown good stability, the CO_2 IRGA was calibrated for CO_2 once daily, prior to use in the field, and once weekly for water vapour pressure. Data were measured at 0.6 Hz, averaged and recorded every 10 s in the internal storage module of the instrument. The stored CO_2 data were downloaded to a laptop computer following each flight. Both CO_2 analyzer and tethersonde data output contained a date/time stamp which could be used to link these data, after proper synchronization of their respective clocks (see Appendix C for more detail).

During launches with air sample collection, the pump was switched on to collect air into the sample bag. This platform was raised vertically at a rate of approximately 0.12

m s^{-1} from the surface up to between 100 to 130 m height, according to the observations of the temperature or CO_2 concentration profile, to encompass the top of the NBL. The air sampling system (Pattey *et al.,* 2006) collected air in a PTFE bag using a pump and a 2-way valve activated by a timer/controller, which automatically closed the bag intake by activating the valve after a prescribed length of time (10 minutes). The air collected in each bag represented an average concentration of the NBL from the surface to approximately 80 m at that location and point in time. Air sample bags were later analyzed for concentration difference in N_2O and CH_4 using a TDL installed in an environmentally controlled chamber at AAFC (Pattey *et al.,* 2006). Sub-samples of air from the PTFE bags were taken for analysis using gas chromatography (GC) at Macdonald campus. These sub-samples were injected by syringe into previously evacuated and double-septum-sealed glass Exetainer-brand tubes. At least 20 mL of sample air were injected into each 12-mL tube to ensure that internal tube pressure exceeded ambient pressure to prevent contamination of the sample due to intake of outside air while the septum puncture healed following the methodology of Rochette and Bertrand (2004). Testing of our in-house evacuation procedure was performed and is presented in Appendix A. GC analysis for N_2O was performed on an HP 5890 equipped with a Poropak-Q column (80/100) and an electron capture detector (ECD). Methane analysis was performed on a Shimadzu GC-8AIF (Kyoto, Japan) equipped with a Poropak-Q column (80/100) and a flame ionization detector (FID). Standard curves consisted of concentrations bracketing observed field sample concentrations: 0.1, 0.5, and 1 ppm for N_2O, and 1.2, 10.4, and 21.4 ppm for CH_4. Methods for CH_4 and N_2O GC analysis, as well as a comparison of TDL and GC values for CH_4 and N_2O, are included in Appendix B.

Samples of reference gases for GC analysis were also taken in Exetainer tubes at the time of field sampling in order to monitor the effect of field and transport conditions on field samples (field standards/blanks). Samples were analyzed as soon as possible after collection (within 24-48 hours). Field sample concentrations were then corrected by multiplying the concentrations by the % difference between the lab reference sample and the field reference sample. Appendix C presents sources of error or uncertainty in the collection and processing of vertical profile data.

The tethersonde's thermistor was verified against an independent fast-response thermistor and showed very good correspondence. A stronger hysteretic effect was seen in tethersonde temperature measurements going from warmer to cooler temperatures (Appendix D) therefore only results from the blimp ascent (cooler to warmer air) are considered for describing the NBL structure. A description of the test verifying tethersonde temperature function is given in Appendix D.

3.3.4.2. Spatial Measurements

Measurements of GHG were occasionally made along the perimeter of the field while vertical profiles were being conducted. Equipment for gas sampling and geo-referencing was loaded onto a battery-powered golf cart (Figure 3.11 (a) and (b)) and driven around the perimeter of the crop field, stopping periodically at georeferenced locations. At the Ottawa site, a small tethered balloon held a length of Tygon tubing and a mini-pump aloft at a height of 12 m. At the Coteau-du-Lac site, a length of Tygon tubing was held aloft by PVC piping at a height of 3 m. In both situations, two 12 V "marine" batteries with an AC/DC power inverter powered a laptop computer, CO_2 IRGA (LI-6252, LI-COR, Lincoln, NE or CIRAS-SC), and the pumps. Air was drawn down by a pump toward the surface through the tubing and passed through the CO_2 IRGA which measured and recorded concentrations continuously as the cart was driven around the perimeter of the field. Air samples for later N_2O and CH_4 analysis were taken by syringe through a sampling port near the bottom of the tubing. Sample collection and analysis were performed in the same way as described in the previous section.

3.3.5 Measurements Required: Change in Trace Gas Concentration and Height of NBL

The vertical profile of trace gas concentration is measured at intervals of one to two hours, in order to allow appreciable gas accumulation, throughout the night. Air temperature (*T*), atmospheric pressure (*P*), relative humidity (*RH*) and/or water vapour pressure (*e*), horizontal wind speed (*u*), and wind direction are measured concurrently in each profile. The first three variables are used to identify the actual height of concurrent trace gas measurement using the hypsometric equation,

$$\Delta z = \frac{R_d}{g} \times \overline{T_v}(z_1, z_2) \times \ln\left(\frac{P_{z_1}}{P_{z_2}}\right) \tag{3.1}$$

with

$$T_v = T \times (1 + 0.61w) \tag{3.2}$$

and

$$w = \frac{m_v}{m_d} \times \frac{e}{P - e} \tag{3.3}$$

where z is the height of measurement (m), z_1 is z at height 1, z_2 is z at height 2, R_d is ideal gas coefficient for dry air (287.04 J kg^{-1} K^{-1}), g is acceleration due to gravity (9.8 m s^{-2}), T is the air temperature (K), T_v is the virtual temperature (accounting for variation of water vapour content of total air) (K), P is total atmospheric pressure (kPa), w is the water vapour mixing ratio (g g^{-1} dry air), m_v is the molecular mass of water vapour (18.01 g

mol^{-1}), m_d is the molecular mass of dry air (28.97 g mol^{-1}), and e is the water vapour pressure (kPa).

T, P, and e are also used to convert the trace gas concentration expressed in ppmv to mass density mg m^{-3}. Temperature and atmospheric pressure can also be used to generate a potential temperature (θ) profile, which accounts for the effect of pressure decrease with height,

$$\theta = T \times \left(\frac{1000}{P} \right)^{\frac{R_d}{C_p}} \tag{3.4}$$

(where C_p is the specific heat of dry air at constant pressure, 1004.7 J K^{-1} kg^{-1}) to determine the nocturnal temperature inversion (the top of the inversion being where the rate of change of potential temperature becomes zero with height). The wind direction profile, measured in degrees, is straightforward and is used to identify the upwind source area of the trace gas being measured.

The vertical concentration profile is also used to identify trace gas capping heights (where the profiles merge to a single concentration from one ascent to the next), in relation to the stable cores of wind speed maxima (LLJ or otherwise) and their associated shear layers. Stable and shear layers are identified by quantifying the profiles of the bulk Richardson number (Ri), calculated from temperature and horizontal wind speed measurements as:

$$Ri = \frac{g}{\overline{\theta}} \times \frac{\left(\Delta\overline{\theta} / \Delta z \right)}{\left(\Delta\overline{u} / \Delta z \right)^2} \tag{3.5}$$

Ri profiles are also used to determine the state of the NBL from one profile to the next, to see whether stability was maintained.

Capping heights did not generally coincide with the top of the temperature inversion layer, but were, in all but a few cases, within the temperature inversion layer. Specific examples of how to use capping height, wind speed maxima, and stable and shear layers to choose the flux integration height in the most prevalently observed form of the stable NBL are explored in Chapter 5.

3.3.6 Flux Calculation

With the turbulent vertical flux and advection assumed negligible, Term 2 of Equation 2.1 states that to obtain the flux of the desired scalar, the derivative of the scalar concentration with respect to time is integrated over the height of the NBL. In practice, the NBL trace gas flux (F_s) is estimated as the difference of the average trace gas concentration between each vertical concentration profile ($\overline{C}_2 - \overline{C}_1$) up to a chosen common integration height (h_i), over the time between profiles ($t_2 - t_1$), as:

$$F_s = \frac{\left(\overline{C}_2 - \overline{C}_1\right) \times h_i}{t_2 - t_1} . \tag{3.6}$$

The flux integration height (h_i) is the height up to which gases emitted from the surface accumulate between profiles, determined from trace gas concentration, wind speed and Ri profiles. The method for choice of integration height varied according to the bulk state of the NBL and is described in Chapter 4.

In this study, carbon dioxide fluxes were integrated starting from z = 2.5 m upward in steps of 1 m, acquired from a light-weight infra-red CO_2 analyzer, while N_2O and CH_4 fluxes were derived from the average concentration of the profile, as air was collected in a bag throughout each ascent. Concentrations below 2.5 m were not measured as the risk of local contamination from operators was too high and because the physical location of the IRGA on the tether line in relation to the winch made reliable measurements nearer to the surface difficult. Using detailed CO_2 profiles, simulations were made to compare two techniques: the calculation of the difference in concentration at each metre versus the difference in the average concentration of the entire profiles; results from both methods were found to be identical (data not shown). Therefore, during periods where the very stable upside-down boundary layer and converging CO_2 profiles were observed, as long as the bags had air collected at least as high as the CO_2 flux integration height, fluxes measured using this method were considered reliable.

FIGURES

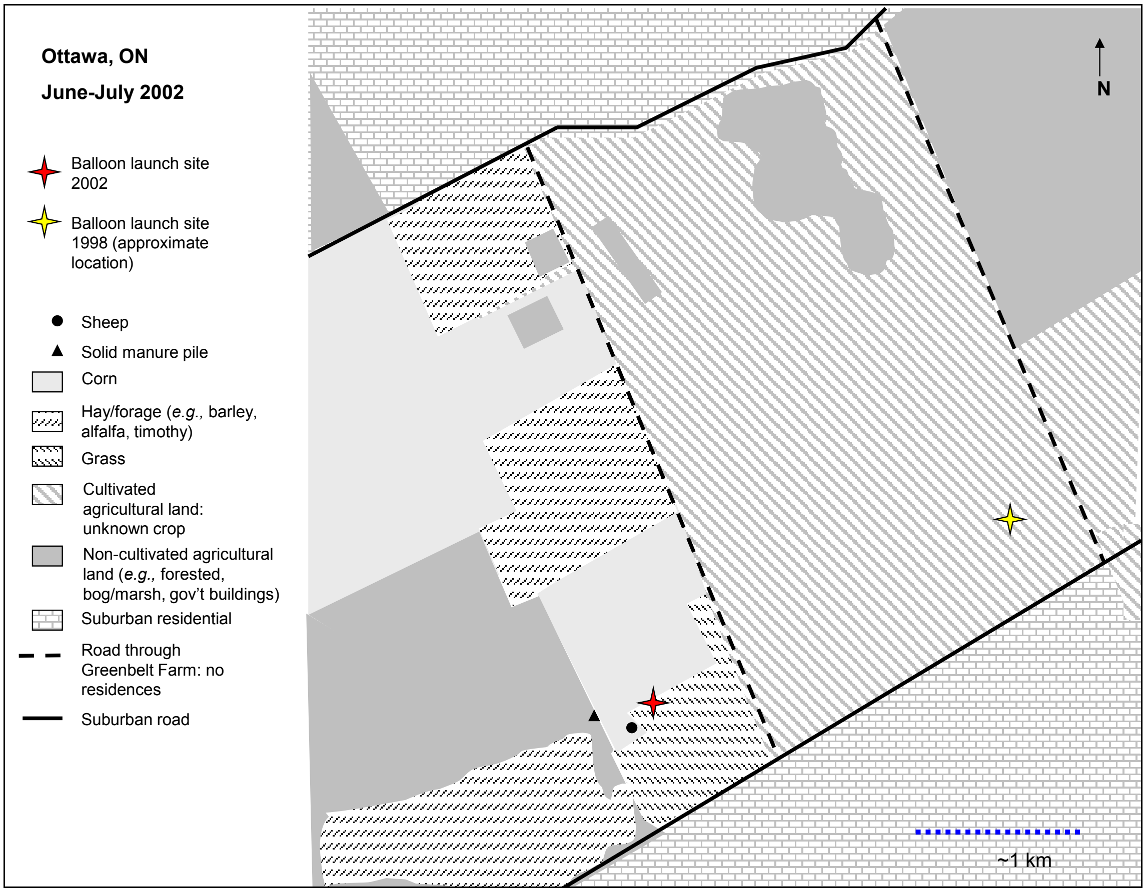

Figure 3.1 Diagram depicting agricultural layout within 1 to 4 km of Ottawa site, June-July 2002.

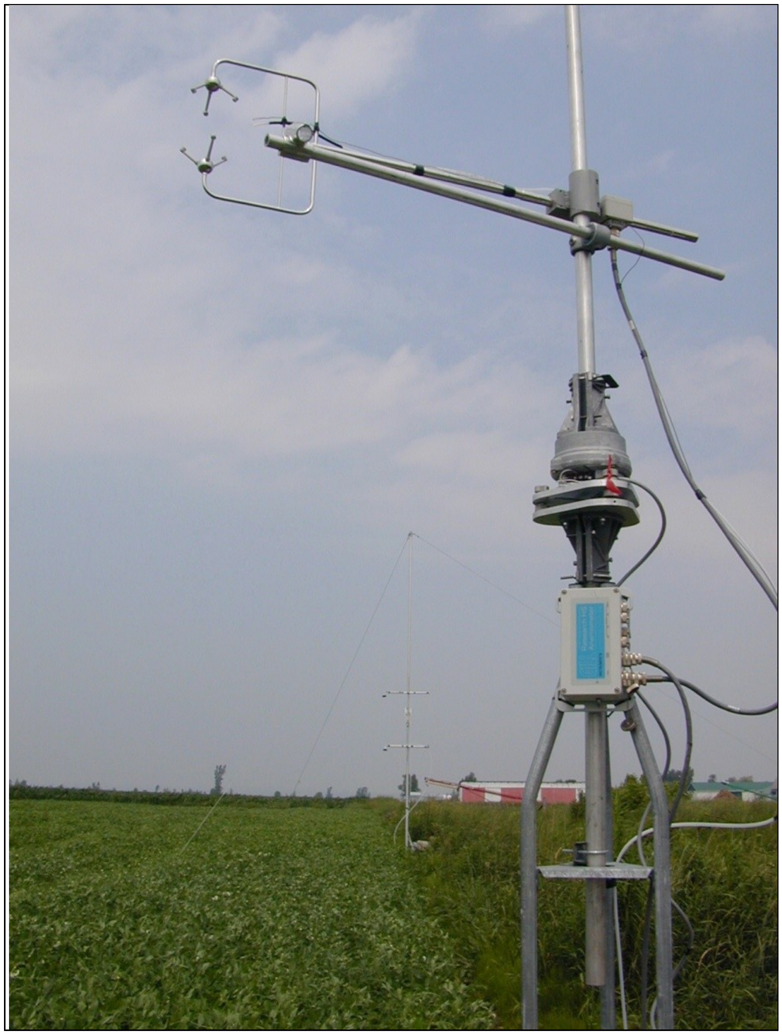

Figure 3.2 Eddy covariance tower measuring fluxes of CO_2 at Coteau-du-Lac field site in April 2003 (Credit: E. Pattey, 2003).

Figure 3.3 Flux gradient tower measuring fluxes of N_2O over edible green peas at Coteau-du-Lac field site in June-July 2003 (Pattey *et al.,* 2006).

Figure 3.4 Ottawa, June 2002 field site (viewed looking approximately to the NNW) showing rain gauge and wind speed instruments.

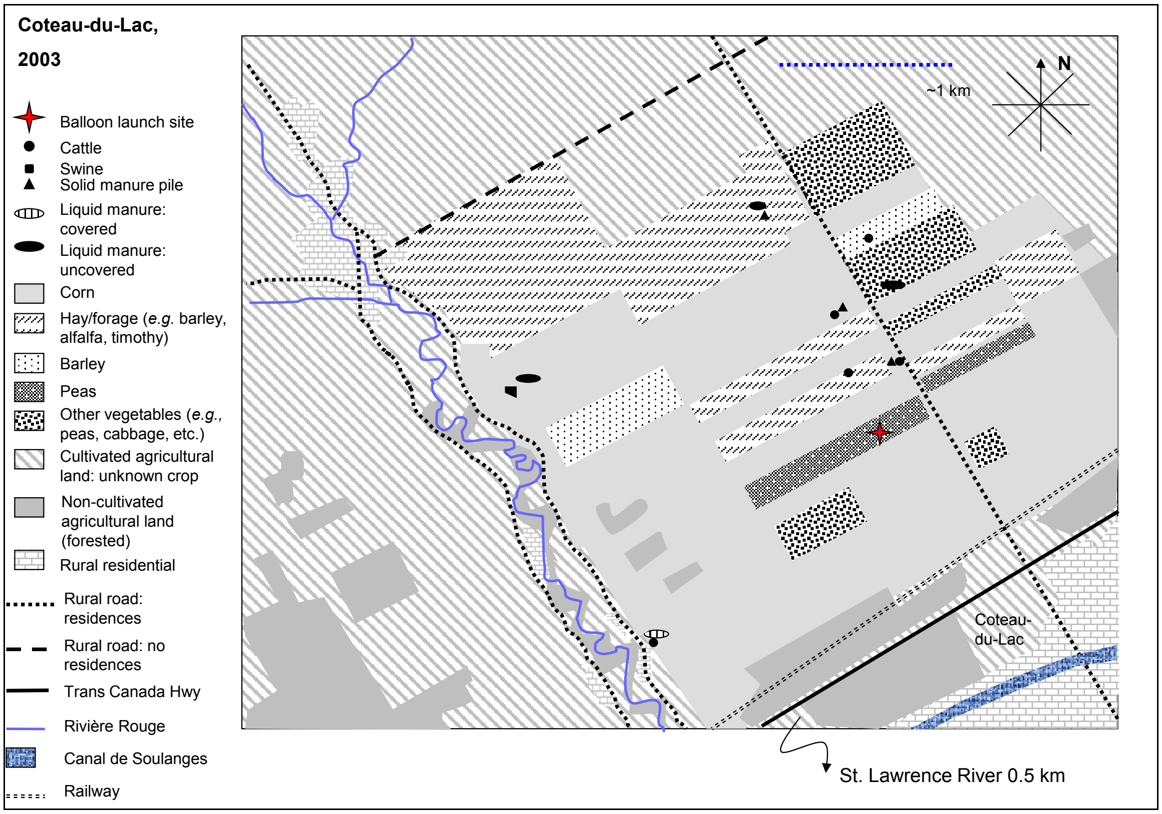

Figure 3.5 Diagram depicting agricultural layout within 2 to 3 km of Coteau-du-Lac site, summer of 2003.

Figure 3.6 Eastward view of Coteau-du-Lac field site, showing edible green peas, flux gradient tower, trailer housing TDL, tent shelter for tethered blimp, and barn, July 2003.

Figure 3.7 (a) Helium-filled blimps (large and small) tethered to electric winches in early morning hours bordering the corn field at the Ottawa site, June-July 2002. Large blimp making its descent (monitored by Nathalie Mathieu) shows CIRAS analyzer and tethersonde attached to tetherline.

Figure 3.7 (b) Blimp tethered to electric winch, during snowmelt, Coteau-du-Lac, April 2003. Sonde is attached to tetherline. Standing next to winch are Nathalie Mathieu and Ian Strachan.

Figure 3.7 (c) Blimp tethered to electric winch, sonde attached to tetherline, in middle of field of edible green peas, early June 2003, next to housing for tile drainage measurement system. Standing near tent are Nathalie Mathieu and Melissa Valiquette.

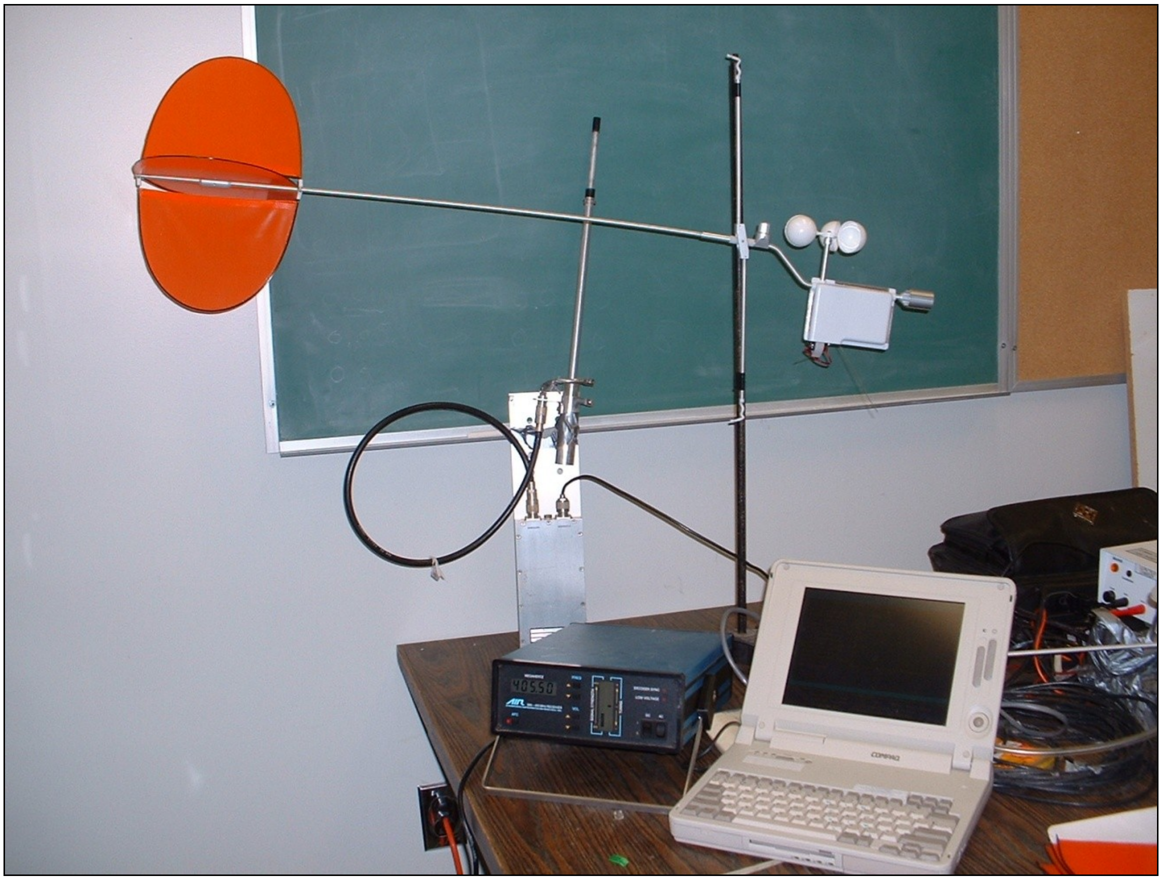

Figure 3.8 AAFC's A.I.R. tethersonde system shown with laptop, receiver, and antenna.

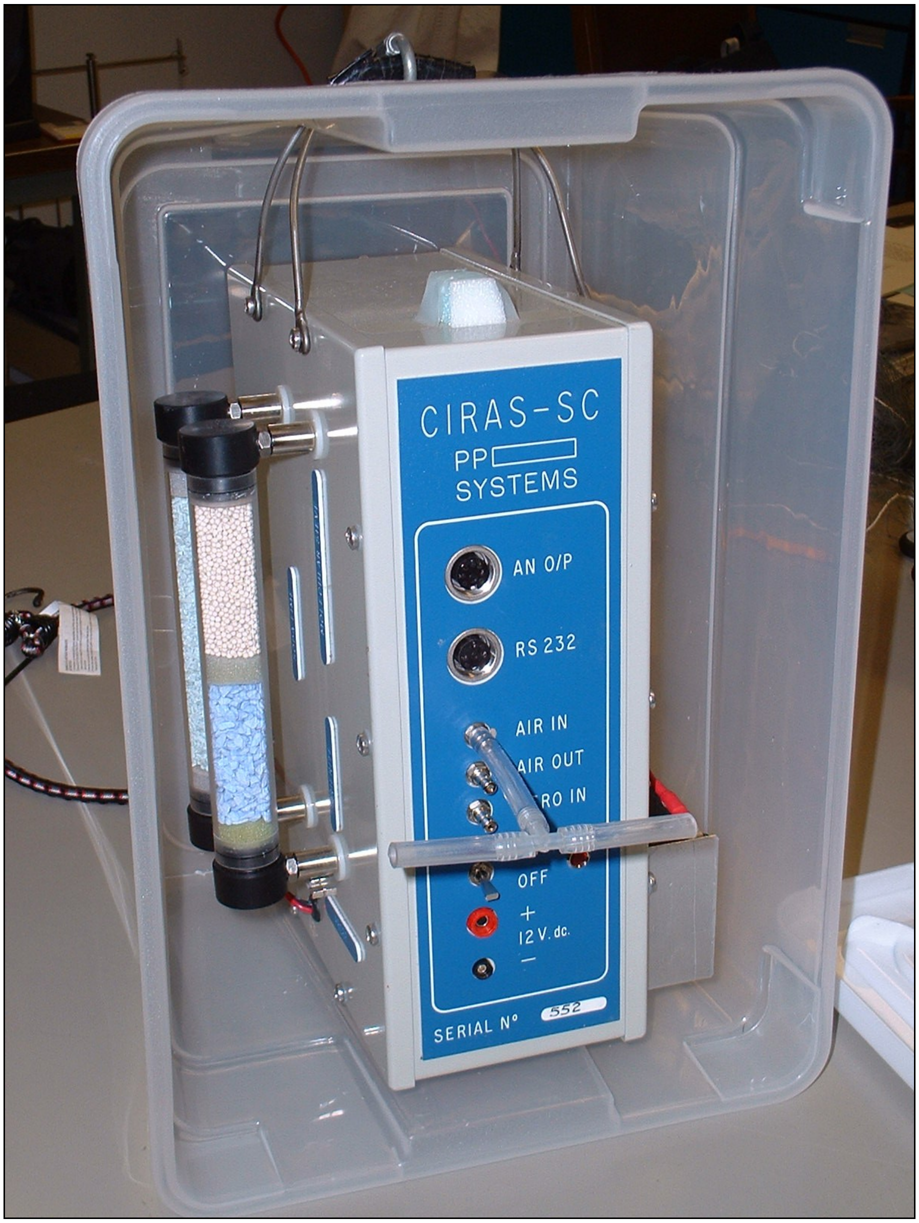

Figure 3.9 CIRAS-SC portable infra-red CO_2 analyzer in protective casing.

Figure 3.10 In-house developed bag filling system (Pattey *et al.,* 2006).

Figure 3.11 (a) Electric golf cart with tethered blimp for spatial measurements viewed from front, on south side of Ottawa field site (looking eastward).

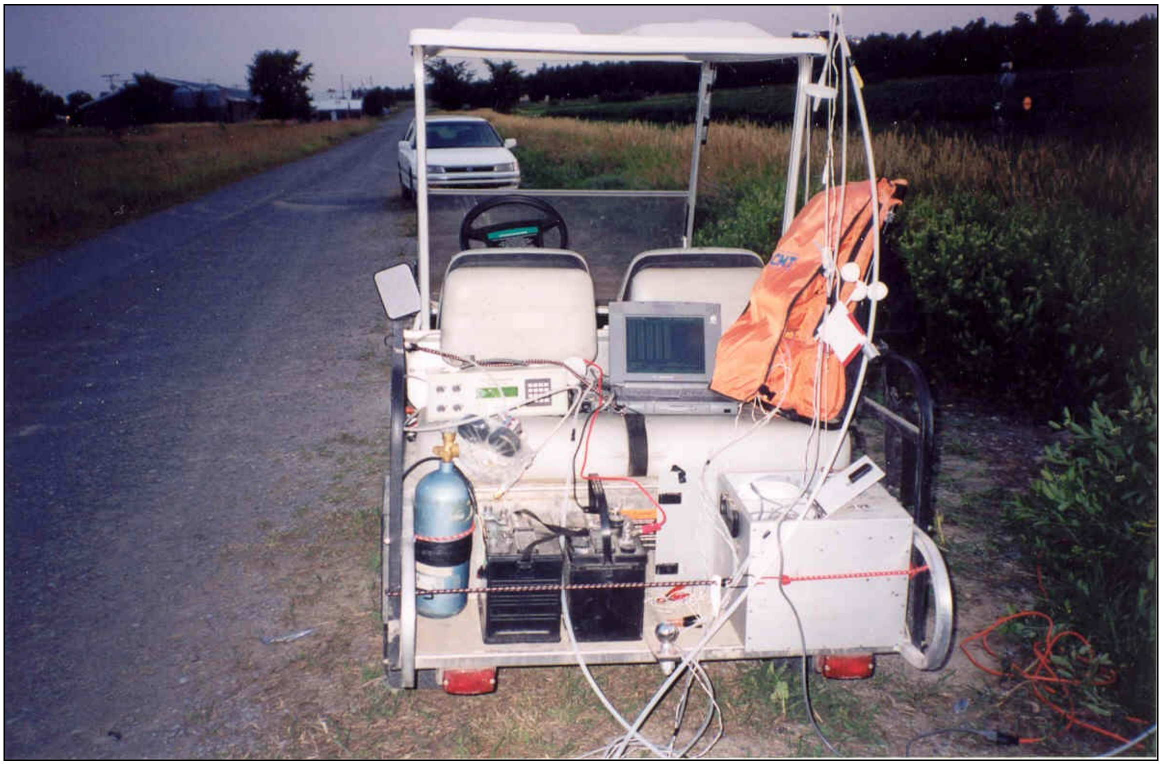

Figure 3.11 (b) Golf cart viewed from the back (looking westward), showing left to right, top to bottom: LI-COR CO_2 analyzer, laptop computer, GPS (orange vest), zero gas cylinder, marine batteries, and electric winch with tubing and tethersonde attached to tetherline.

4. VERTICAL AND SPATIAL COMPONENTS OF THE NBL BUDGET METHOD IN CONDITIONS VARYING FROM OPTIMAL TO SUBOPTIMAL

4.1 INTRODUCTION

The nocturnal boundary layer has been studied over the last 50 years beginning with the fundamental work of Blackadar (1957) and continuing through the research by Kaimal (1973), Brost and Wyngaard (1978), Mahrt *et al.* (1979), Nieuwstadt (1984), Smedman (1988), Coulter (1990), and Derbyshire (1995) to the more recent works of contemporary NBL researchers (Mahrt, 1999; Mahrt and Vickers, 2002; Sun *et al.*, 2004: Grachev *et al.*, 2005; Karipot *et al.*, 2006; Banta *et al.*, 2002; 2007).

Today, while many basic characteristics of the NBL have been established, a definitive, all-encompassing characterization of the turbulent and non-turbulent transport of scalars within the NBL remains elusive, as evidenced by the lack of footprint models for the NBL. The intermittency of the NBL makes it difficult to understand.

One mesoscale phenomenon particularly relevant to this study that may form in the nocturnal boundary layer is the low-level jet, due to either inertial oscillations developing during the evening transition of the NBL or cooling over sloped terrain (Blackadar, 1957; Stull, 1988; Mahrt, 1999). The formation of the LLJ creates turbulence decoupled from the very stable surface (Ri > critical Ri of 0.25), forming what Mahrt (1999) refers to as the 'very stable upside-down boundary layer'. After some time, the shear generated at the underside of the LLJ may lead to the extension of turbulence right down to the ground, transforming the previously decoupled jet into a jet that is coupled with the surface (Smedman, 1988; Mahrt, 1999; Mahrt and Vickers, 2002). While both of these situations were observed in our NBL profiles, the very stable upside-down boundary layer was the predominant state on these very calm and clear nights.

Mathieu *et al.* (2005) examined two detailed cases of the role of the fully-formed nocturnal LLJ and its particular influence on vertical CO_2 distribution, in relation to CO_2 flux calculation using the NBL budget method over agricultural land. They found that conditions providing the best opportunity for good NBL budget application include clear nights with 1) surface winds less than 1-2 m s^{-1}, 2) a strong surface temperature inversion at the surface and 3) presence of a steady horizontal wind speed maximum or low-level jet which is decoupled from the surface (where a stable surface layer underlies the jet) and located within the surface temperature inversion layer (Mathieu *et al.*, 2005). Under these conditions, the NBL technique is readily applied because the depth of the NBL can be clearly defined and GHG concentration changes over the course of the night are large for significant emissions. Our observations suggest that in cases where the first two conditions were met but a LLJ was not present within the vertical profile interval, a LLJ may have formed at a greater height beyond the tethered blimp's detection. Whether or not this was the case, smaller wind speed maxima within the wind speed profile were sufficient to cap surface-emitted CO_2 (see also Mathieu *et al.,* 2005).

This thesis chapter presents considerations for CO_2 flux calculation using the NBL budget in cases where the first two optimal NBL conditions were met (calm and clear, strong inversion), but a LLJ had not necessarily formed within the vertical height measurement interval. Within this context, the relative contribution of vertical and spatial components to the total NBL-measured flux is examined.

First, field results are given for vertical profiles of the NBL. Examples of typical results for temperature, wind speed and CO_2 profiles are presented. Following this is a classification of NBL conditions typically observed during the field work. Next, flux calculation is discussed with regard to choice of integration height for one night during optimal conditions with a LLJ (briefly) and two examples of nights, one during optimal conditions, the other suboptimal, when no LLJ was present. The height-contribution of the total measured flux in terms of typically observed NBL conditions is then discussed and the largest contributing height interval for flux calculation identified. The spatial extent of this critical height interval is examined through the use of a flux footprint model. A preliminary ground-based verification of the NBL budget method is then presented.

4.2 MATERIALS AND METHODS

4.2.1 CH_4 Detailed Profile

The procedure for general vertical profile data collection and analysis is as described in Chapter 3. On two nights, a detailed vertical profile of methane concentrations was created by sampling air every 10 m from a line of flexible tubing as it was being lifted by the tethered balloon up to a height of approximately 70 m. The air was drawn down through the tubing by a small pump and sampled with a syringe and needle at a rubber septum-sealed sampling port. At the time of each sampling, the elapsed ascent time given by the tethersonde system was recorded. A lag time correction, to account for the travel time of the sample through the tube down to the sampling port, was then applied to each sampling time and the tethersonde height associated with the new corrected time was considered to be the actual height of the sample. Samples were analyzed by gas chromatography in the manner described in Chapter 3.

4.2.2 Flux Footprint Parameterization

While footprint models are still considered suboptimal for very stable conditions (*e.g.,* Schmid 2002), the on-line flux footprint parameterization of Kljun *et al.* (2004) provided a convenient way to estimate the upwind extent of the footprint.

The model requires six input variables: the standard deviation of the vertical wind speed (σ_w), friction velocity (u*), NBL height (h), measurement height (z_m), surface roughness length (z_o), and the desired percentage of the footprint to include in the output. Neither σ_w nor u* were measured directly by the NBL budget instrumentation used in this study. A value of 0.07 m s^{-1} was used for σ_w which is a typical value used for screening nighttime eddy covariance data into non-turbulent periods over agricultural fields (Pattey *et al.,* 2002) and u* was set at 0.2 m s^{-1} which was the minimum value allowed in the model. h was set to 80 m and was always greater than the measurement height and z_0 was set to 0.2 m to reflect the composite agricultural surface upwind.

A number of simplifications and assumptions are required in the use of this model in conditions studied here (see Chapter 2). The model does not provide estimates of the lateral extent of the footprint. An assumption of Gaussian distribution of turbulence has been used to generate crosswind footprints in the models SAM and F-SAM by Schmid (1994, 1997). While this distribution is not valid in stable conditions, it still has a physical basis and could have provided a rough estimate of lateral distribution. However, these and other models required the input of certain stability parameters, for example, the Obukhov length, L, which was not derivable from NBL profile data. Obukhov length was measured by the eddy covariance system but was considered to be unreliable in stable nighttime conditions. Instead, a simple scheme was employed whereby for each degree of deviation in the measured direction of the horizontal wind speed, the footprint was widened on both sides of the centre axis by 1% of its length *(e.g.*, a standard deviation of 5 degrees resulted in a 1000 m footprint having a width of 50 m) forming a rectangular shape. In general, considering the homogeneously patchy agricultural landscape, the impact of using this lateral approximation in the interpretation of footprint results is probably minor. More detail regarding the model and further simplifications will be presented in Chapter 6.

4.3 TYPICAL PROFILES OF TEMPERATURE, WIND SPEED, AND CARBON DIOXIDE IN THE NBL

Profiles of potential temperature (θ), wind speed (u), and CO_2 concentration followed typical patterns on the strongly stable nights where the NBL budget could be performed or calculated. Examples of profiles and the interaction between these variables are given for four nights: 1) June 16-17, 2003 (low u, highly variable u maxima) (Figure 4.1 a-c), 2) July 22-23, 2003 (low u, relatively fixed u maxima) (Figure 4.1 d-f), 3) June 17-18, 2003 (higher u, somewhat variable u maxima) (Figure 4.1 g-i), and 4) June 28-29, 2002 (formation of LLJ) (Figure 4.1 j-l).

4.3.1 Potential Temperature (θ) Profiles (Figures 4.1: a, d, g, j)

Temperature profiles revealed an initial decrease in temperature due to radiative cooling starting at the surface, with overall temperature decreasing over time upward from the surface, giving a positive exponential-type shape. The inversion strength is primarily related to the degree of longwave radiation loss from the surface, which is determined by the degree of cloud cover. The overall temperature at the top of the NBL usually decreased due to clear air radiative cooling and vertical mixing due to shear from developing wind speed maxima.

Early in the evening, the potential temperature profile typically became constant with height at around 70-120 m, signaling the top of the temperature inversion. During this early evening period, under conditions exhibiting a normal wind profile at the surface (*e.g.,* one without a maximum near the surface), the rate of inversion growth was approximately 1.3°C h^{-1} and was fairly constant over time. As the evening continued, however, the inversion top was frequently beyond measurement and therefore the rate of inversion growth could not be calculated. The overall observable range of inversion strengths at the two field sites was approximately 4 to 10 °C.

The exponential shape of the potential temperature profile can be altered by vertical air mixing caused by changes in the wind speed profile, as shown in Figures 4.1 j and k, where, upon an increase in wind speeds in the 3:30 and 4:45 profiles, the corresponding temperature inversions spread over an increased NBL height, compared with earlier profiles on that night. The 4:45 profile (Figure 4.1 j) actually shows an increase in temperature at the top: radiative cooling may have been offset due to the downward movement of warmer air from aloft by the strong shear on the upper side of the strong wind maximum in the corresponding wind speed profile (Figure 4.1 k).

For example, June 16-17 and July 22-23, 2002, both had very low wind speeds (Figures 4.1 b and e) but the inversion strength (Figures 4.1 a and d) was weaker on the night of June 16-17, 2002 because of very thin cloud cover present on that night.

4.3.2 Wind Speed (*u*) Profiles (Figures 4.1 b, e, h, and k)

The horizontal wind speed typically increased with height, with speeds near the surface between 0 and 1 m s^{-1}. The degree of increase in speed with height varied nightly, but for the most part u at z = 60-100 m was approximately 4 to 8 m s^{-1}. Wind speed maxima of differing magnitude routinely formed at different heights. Over time, these wind speed maxima could appear briefly and recede (*e.g.,* from one profile to the next, Figures 4.1 b and h) or remain relatively constant at a certain height (*e.g.,* over several profiles, Figure 4.1 e). On a few occasions, a LLJ developed with a well-defined nose and a difference of at least 2 m s^{-1} above and below the nose (Andreas *et al.,* 2000) within our measurement range. An example of this occurred on the night of June 28-29, 2002, and is shown in Figure 4.1 k (3:30 and 4:45 profiles).

While the temperature inversion allows gases to accumulate near the ground, it can be seen quite readily, in all examples given in Figure 4.1, that wind maxima play a significant role in 'capping' and thereby enhancing the accumulation of gases below a certain height. For example, on June 16-17, 2003, low wind speed combined with the wind maximum at about z = 35 m (Figure 4.1 b) corresponded to a ground-level CO_2 accumulation of 625 ppmv (Figure 4.1 c, beyond scale of graph). On July 22-23, 2003, a clear cap can be seen at about z = 50 m for all three profiles, where the height of wind speed maxima (again of relatively low speed) and CO_2 profile convergence are co-located, leading to a high ground-level CO_2 accumulation (Figures 4.1 e and f). High accumulation at low wind speeds was also noted by Acevedo *et al.* (2004). On nights with higher wind speeds, the CO_2 accumulation, moderated by the relative inversion strength, can be less, but can still remain capped by wind maxima (*e.g.,* Figures 4.1 h and i, 20:45-22:30, and 4.1 k and l, 23:00 to 4:45). This is because the downward momentum gradient in the shear on the underside of the wind maximum is still sufficient to keep the CO_2 from mixing aloft (Mathieu *et al.*, 2005).

4.3.3 CO_2 Concentration Profiles (Figures 4.1 c, f, i, and l)

Carbon dioxide concentration exhibited well-mixed profiles prior to sunset (constant concentration from surface to maximum measurement height) (*e.g.,* Figure 4.1 c, 18:45). The CO_2 concentration of the initial well-mixed vertical profile was within 5-10 ppmv of the eddy-covariance tower-measured CO_2 concentration taken at the same time. On nights where the NBL method could be applied, CO_2 accumulation began at the surface, increasing from the surface upward over time.

The shape of the CO_2 profile was quite variable and, as discussed in the previous section, was quite dependent upon the actions of the wind speed profile. In fact, the vertical CO_2 distribution can reveal much of the state of the NBL (Mahrt, 1999). Relatively high surface wind speeds precluded surface CO_2 accumulation (*e.g.,* Figures 4.1 h and i). When a low-level jet had formed, a particular 'box-shape' in the profile resulted from the increased upward mixing of gases accumulated in high concentration immediately adjacent to the surface (*e.g.,* within plant canopies) by the strong shear at the underside of the jet nose (Figures 4.1 k and l, 3:30 and 4:45), resembling profiles shown in Pattey *et al.* (2002) (Figure 4.2). Otherwise, the CO_2 profile showed a more or less sharp exponential decrease from the surface up to the capping height (Figures 4.1 c, f, and l), similar to results from Denmead *et al.* (1996) (22:00 profile in Figure 4.3).

The wind direction should always be taken into consideration in interpretation of CO_2 accumulation because of possible changes in source area type. On nights with very low wind speeds, however, it is difficult to obtain a reliable wind direction observation at the surface. This was the case for June 16-17, 2003 (Figure 4.1 a-c), and July 22-23, 2003 (Figure 4.1 d-f), where readings showed fluctuating wind directions (within 45-90°) at the surface over the course of the NBL measurements. For calm conditions, the CO_2 emissions computed from the CO_2 profiles can be associated with a specific agricultural regional pattern insofar as the agricultural landscape is homogeneous in most directions. However, when there were distinct differences in source area type according to direction, a change in wind direction between CO_2 profile measurements did not allow us to assign the measured flux to a given source. This occurred, for example, when at either site the wind direction changed between approximately south/southeast and any other direction. A suburban area was located approximately 675 m to the south of the field site in Ottawa. In Coteau-du-Lac, a suburban area was located approximately 1.25 km away and the St. Lawrence River approximately 2.2 to 2.6 km away, to the south/southeast. This contrasted with the agricultural landscape found in the other directions.

4.4 STUDY-SPECIFIC CLASSIFICATION OF BULK NBL STRUCTURE DURING CALM, CLEAR CONDITIONS

For the most part, u, Ri, and CO_2 profiles varied with height in a way that indicated the possible existence of a LLJ above the upper limit of our measurements, an issue noted as well by Banta *et al.,* 2002. Only a few classic LLJ patterns (with a distinct nose and unmistakable decrease in u above it) were seen within the measurement range of our vertical profiles ($z \approx$ surface to 120 m), either coupled to or decoupled from the surface, representing eight of the 39 individual profiles used for NBL budget method. These occurred throughout the night but were mostly concentrated around 21:00-23:00 and 3:00-4:45.

Most of the non-LLJ profiles exhibited a stable layer at the surface beneath a turbulent layer (*i.e.,* a very stable upside-down boundary layer). The remaining profiles exhibited turbulence at the surface underneath a u maximum and represent the most uncertainty and therefore the least desirable conditions for NBL flux calculation; an example will not be given here.

Amid these different types of wind and turbulence profiles three general states, or bulk structures, of the stable NBL were defined for our study: 1) a very stable upside-down boundary layer with converging CO_2 concentration profiles (optimal conditions), 2) a very stable upside-down boundary layer with non-converging CO_2 concentration profiles (suboptimal conditions where intermittent turbulence may cause the downward entrainment of trace gas-enriched air through the top of the NBL), and 3) turbulence extending down to surface from the underside of a jet or *u* maximum. The results of the current study indicate that the first two states allow for maximum trace gas accumulation and profiles measured in the third state have consistently shown lower flux values (see Section 5.2.4).

4.5 METHOD FOR CHOOSING FLUX INTEGRATION HEIGHT

The method for choosing the flux integration height was based on the examination of NBL CO_2 profile data in terms of vertical profiles of horizontal wind speed (u), wind shear ($\Delta u/\Delta z$), and bulk Richardson number (Ri) (Equation 3.5). Variations in shear and stability in turbulent layers corresponded strongly to u profile shape. The location of wind speed maxima (and corresponding stable layers) over a total of 22 profile pairs almost always corresponded with CO_2 profile convergence heights, making it apparent that non-LLJ u maxima were indeed effective at stopping CO_2 vertical migration (Figures 5.1b, 5.1c). Following are two examples showing the choice of flux integration height based on [CO_2], u, $\Delta u/\Delta z$, and Ri for the first two NBL states only; the third, turbulent state is not considered a state optimal for NBL gas measurement.

4.5.1 Optimal NBL Conditions: Very Stable Upside-Down Boundary Layer, Converging CO_2 Profiles

The profile pair shown in Figure 4.4a (Ottawa, June 28-29, 2002, 3:30 and 4:45) exhibits a fully-formed LLJ that is decoupled from the surface. It is easy to see that CO_2 accumulates up to a distinct height: the well-defined nose of the LLJ (z = ~65 m). In the large shear layer under the strongly stable jet nose, *Ri* values become sub-critical ($Ri <$ 0.25), causing mixing and forming a distinctive 'box' shape in the CO_2 profiles. The box shape may result from the flushing upward of CO_2 accumulated at very high concentrations immediately adjacent to the surface, within crop and forest canopies in the upwind source area (see Section 6.3.1.2). Apart from a slight accumulation of CO_2 past the height of the jet nose amounting to a flux of approximately 0.01 mg CO_2 m^{-2} s^{-1}, CO_2 upward migration was inhibited by the LLJ, and this case provided very good opportunity to apply the NBL budget method. The resulting CO_2 flux was 0.40 mg CO_2 m^{-2} s^{-1}.

The case of a very stable upside-down boundary layer where the CO_2 profiles converge without an observable LLJ within the measured vertical profile is shown in Figure 4.4b. The two CO_2 profiles (Ottawa, June 28-29, 2002, 0:45 and 2:15) converge distinctly at a height of about 40 m, corresponding to the height of the 2:15 *u* maximum and the top of its associated shear layer. Once again, here, as for the case in Figure 4.4a, the NBL budget method can be easily applied, resulting in a CO_2 flux of 0.09 mg CO_2 m^{-2} s^{-1}. (This comparatively lower flux prior to the onset of the LLJ later this night is discussed in Sections 6.3.1.1 and 6.3.1.2.) Similar profile patterns were observed in 14 out of 22 NBL profile pairs used for NBL budget calculations, resulting in fluxes ranging from 0.07 to 0.40 mg CO_2 m^{-2} s^{-1}, across all field sites (Table 4.1).

4.5.2 Suboptimal NBL Conditions: Very Stable Upside-Down Boundary Layer-Non-Converging CO_2 Profiles

In the case presented in Figure 4.4c (Coteau-du-Lac, July 9-10, 2003, 00:15 and 1:45), a very stable upside-down boundary layer is present without a measured concentration convergence height. In general, the reason for non-convergence is probably the transport of CO_2-enriched air from outside the agricultural area of interest, higher up in the vertical profile. Intermittent turbulence at the top of the NBL could allow the downward entrainment of CO_2 into the vertical zone of accumulated gas from agricultural sources, resulting in a blending of the CO_2 profile at the top of the NBL with that above it. In three of our four profile pairs in very stable conditions showing non-convergence, the wind direction aloft was downwind of an urban or suburban area. The goal here was therefore to try to find the upper limit of accumulation of trace gases originating from our surface of interest.

The first profile (00:15) is largely stable ($Ri > 0.25$), with a single, thin, well-defined layer of turbulence resulting from the shear beneath the u maximum at 40 m. The second profile (1:45) shows turbulent layers ($Ri < 0.25$) starting at $z = 33$ m, again, each associated with the shear from the underside of a u maximum. If the vertical profile had been measured to a greater height, we may have seen this turbulent layer resulted from the shear at the underside of a LLJ which had its maximum higher up. However, our restriction of wanting local farm conditions remains. To apply the NBL budget method in this case, two approaches can be taken: 1) assume that there is a LLJ in the 1:45 profile and that the CO_2 profiles will converge at the jet's nose (height unknown but approaching); or 2) assume that there is no LLJ and that the steady concentration gap in the upper portion of the CO_2 profiles is sustained from downward movement of advected CO_2 from aloft, along the *u* gradient.

In the first approach, the flux would be calculated using the full height of the profile, realizing that this would be an underestimation of the flux due to the missing height interval at the top. The resulting CO_2 flux using this approach is 0.48 mg CO_2 m^{-2} s^{-1}.

In the second approach, the integration height could be chosen by examining several physical pattern indicators that we have seen recurring in our data. These patterns involve the co-location of the following at a given height: (1) *u* maxima, (2) shear and turbulent layers, and (3) where $\Delta CO_2/\Delta z$ approaches zero for a given profile. The height where $\Delta CO_2/\Delta z$ approaches zero usually coincides with the height of a shear layer and *u* maximum, making the choice of integration height clearer. Ideally both profiles will have a common height where co-located indicators occur. When this does not occur, the integration height must be chosen considering the 'normal' theoretical progression in CO_2 profile over time, where CO_2 migrates upward over time as the NBL height increases. An illustration of the process for choice of integration height using this second approach is described as follows and shown in Figure 4.4c.

As mentioned above, the first profile (00:15) is almost completely stable and has only a brief turbulent layer coinciding with a peak in $\Delta u/\Delta z$ (data not shown) from the underside of the *u* maximum at z = 40 m (Height 1_A, Figure 4.4c). $\Delta CO_2/\Delta z$ at this height is approximately -0.2 ppm m^{-1}. However, $\Delta CO_2/\Delta z$ becomes even smaller at z = 50 m (Height $1_{B,}$ Figure 4.4c) with a concentration change of less than -0.02 ppm m^{-1}, coinciding with a smaller *u* maximum at precisely that height. A peak in shear (data not shown) is also found at the underside of this *u* maximum (but *Ri* remains close to but greater than 0.25). $\Delta CO_2/\Delta z$ stays within -0.1 ppm m^{-1} above this height so other minor *u* maxima higher up are not considered. In the first profile, therefore, co-located indicators of interest exist at both z = 40 m and z = 50 m.

In the second profile (1:45), the first *u* maximum of interest is at z = 56 m (Height 2_A, Figure 4.4c). Maximum shear from its underside occurs at z = 52 m (data not shown). $\Delta CO_2/\Delta z$ at z = 56 m is -0.05 ppm m^{-1}. $\Delta CO_2/\Delta z$ actually comes closest to zero at z = 40 m, but this indicator does not fit with any others: in particular, there is no coinciding *u* maximum. In the second profile, therefore, z = 56 m is the height of our co-located indicators of interest.

Therefore, having examined our two profiles, we would choose z = 56 m (Height 2_A, Figure 4.4c) as the integration height for this profile pair. We choose the height of co-located variables from the second profile to allow for gas migration upward between these successive profiles. This height is also fairly close to z = 50 m (Height 1_B, Figure 4.4c), which was a height of co-located variables in the first profile. Upward migration would likely be evident if the two profiles were converging as, for example, in Figure 4.4b. For this reason, given any non-convergent pair of profiles, we would probably always choose the height of co-located variables from the second profile. The resultant flux using the second approach would be 0.36 mg CO_2 m^{-2} s^{-1}.

This example demonstrates the importance in the choice of integration height in the flux calculation for suboptimal conditions exhibiting non-convergent CO_2 profiles: there is a 30% difference between the values from each approach. While the first approach may actually be closer to reality as far as NBL structure at the time of the soundings is concerned, the chances remain that the gas accumulated in the upper profile region is from an area outside of the scale of interest, the agricultural farm. Above the integration height of z = 56 m, the wind direction was fairly constant between profiles, coming from approximately ENE (Figure 4.4c), placing the field site 20 km directly downwind of the island of Montreal, which may be the origin of the increase in CO_2 concentration aloft. It may therefore be more prudent to use the second approach, which at least increases the probability that gases are from the surface of interest.

While flux values from both methods are at the higher end of the range of fluxes seen for this site (Coteau-du-Lac, QC) (Table 4.1), the value using the second approach is closer to the average value of about 0.26 mg CO_2 m^{-2} s^{-1} seen in converging profiles in our study.

4.6 COMPARATIVE CONTRIBUTION OF NORMALIZED NBL HEIGHT INTERVALS (*z/h*) TO GHG FLUX

The vertical distribution of CO_2 varies according to which bulk NBL structure is occurring at the time of the sounding. The distribution of percent contribution to the measured flux was calculated for normalized intervals of NBL profile height (z/h; where z is measurement height starting from the surface and h is the CO_2 flux integration height) using the three basic types of NBL structures listed previously (Figure 4.5). The observed uneven distribution of flux with height demonstrates that in stable conditions, the flux is not independent of height (*i.e.,* there is vertical flux divergence). This counters the assumption of current footprint models, where for unstable conditions, the flux may be considered independent of height, pointing out yet again the need for a footprint model based on stable conditions.

For the most prevalent case, optimal NBL conditions (a very stable upside down boundary layer with converging CO_2 profiles), the trend was for the maximum contribution to occur near to the surface with the contribution rapidly diminishing as h was approached. This corresponds with the simulations of Horst (1999) who, using an analytical diffusion model, noted that the flux from a concentration profile was mostly highly influenced by concentration measurements made in the lowest proportion of the profile. For suboptimal NBL conditions, the very stable upside-down boundary layer with non-converging CO_2 profiles, the percent contribution was more evenly distributed with height. This class of profiles was observed less than half as often as the first class containing converging profiles. Lastly, the least prevalent case, where turbulence extended to the ground from a u maximum, in most cases showed a loss of CO_2 at the surface from one profile to the next, with the largest contribution occurring near the top of the flux integration interval. This near-surface CO_2 decrease might be caused by the release of accumulated CO_2 upon the breakdown of the existing LLJ or u maximum. The large error bars reflect the extent of differing shapes of these turbulent profile pairs.

Optimal NBL conditions occurred in about 64% of our observed NBL profile pairs with constant wind direction and/or source area type. The average z_m for each z/h interval was calculated and the heights for cumulative 10% contributions were determined (Table 4.2). 80% of the total NBL-measured GHG flux was represented, on average, in the interval from the surface to 29.5 m (Table 4.2). The 80%-probability flux footprint distance for this height was 1948 m. This distance was greater than the length of most farm fields within about 3 km around the Coteau-du-Lac launch site, about 1000 to 1500 m. This distance may, though, still reasonably encompass a farming area of approximately 1 km^2, corresponding to the average farm size in eastern Ontario and western Quebec, the scale of interest in this project. A large portion (50%) of the total NBL-measured flux came from local sources within 1000 m upwind of the measurement site.

Studies using only near-surface profile measurements (*e.g.,* Griffith *et al.,* 2002) cannot verify NBL structure and hence vertical GHG distribution aloft; they do not have a complete picture of the NBL flux. For example, Griffiths *et al.* (2002) measured the build-up of trace gases up to z = 22 m on eleven "suitable" nights over a lucerne pasture with a "clear, flat fetch" of 200 m distance. If we assume these were nights with a very stable upside-down boundary layer and that CO_2 profile structure was similar to our study, according to our results (Table 4.2) they may have been capturing about 60% of the total flux. They were likely including areas beyond their target pasture, even at this low measurement height. The fact that their NBL results were quite close to their flux gradient results (measured on windy nights) and darkened chamber results (which cover a much smaller scale) is likely an indication of the spatial homogeneity of respiration rates of the larger area at their location.

4.7 PRELIMINARY 'BOTTOM-UP' VERIFICATION OF NBL BUDGET METHOD

With evidence to suggest that 80% of the emitted flux originates from an upwind distance of approximately 2 km, the next step was to provide ground-based evidence confirming that we were indeed measuring fluxes from sources within this footprint. Tracer experiments involving the upwind release and downwind measurement of naturally or non-naturally occurring gases have been used previously to develop measurement methodologies (*e.g.* Desjardins *et al.,* 2004 with CH_4) to determine the exact extent of the upwind footprint (*e.g.,* Finn *et al.,* 1996; Leclerc *et al.,* 2003a; Göckede *et al.,* 2005). In the current study, the existing release of CH_4 is used as a passive or natural tracer to identify the occurrence of point sources within the upwind footprint. Göckede *et al.* (2005) point out that the use of natural tracers is applicable when variable sources of the gas to be used as a tracer exist in the region surrounding the sensor. They continue by stating that the ultimate success of such measurements will depend on the differences in the emission rates and the size and arrangement of the sources. These criteria are met at our agricultural sites as methane does not come from diffuse sources but rather from point sources such as animal housing and manure piles which should have elevated concentrations. Detailed vertical profile concentration data for CH_4 and flux footprint predictions were used to associate point sources at known upwind locations with the CH_4 concentration measured at a particular height.

A pair of vertical CH_4 concentration profiles (23:50, 1:54 EST) was measured on the night of August 18-19, 2003, at the Coteau-du-Lac field site. *Ri* profiles at these times (data not shown) demonstrated a very stable upside down boundary layer and optimal measurement conditions for the NBL budget. The modeled footprints were overlaid on a scaled map of the Coteau-du-Lac area showing the potential emission point sources of CH_4, such as animal housing facilities, manure piles, and liquid manure tanks (Figure 5.3). Information on the location of these sources including the type of source and livestock numbers was obtained from the private producer at our Coteau-du-Lac field site.

Both profiles moved from east to west with height, moving into and out of known point source areas (Figure 4.6). Nighttime CH_4 concentrations from the detailed profiles (Table 4.3) were elevated compared to daytime concentrations (1.9 ppmv; measured 1 m above the surface at noon and 17:00), particularly in the lowest part of the profile, as might be expected for optimal NBL conditions where there is not much vertical dispersion of gases. The high near-surface concentration might be due to the accumulation of methane in the water-filled drainage ditch running along the NE side of the fields which was within the z_m= 2 m modeled footprint distance from the launch site for both profiles. In mid-summer the flow within this ditch was fairly still and these conditions may have produced methane; alternatively, methane could have come from animal waste found within the ditch. Samples were taken on one occasion at night from the air immediately above the water in the drainage ditch and showed concentrations of approximately 3.0 ppmv. Air samples from immediately above the bank beside the ditch had concentrations of about 2.5 ppmv (comparable to the z_m = 2 m NBL measurements).

While not markedly different from one height to the next (except for z_m = 2 and 13 m in the 1:54 EST profile), the average CH_4 concentration for each measurement height (z_m) in the detailed CH_4 profile tended to reflect the sources within each respective footprint (Table 4.3). CH_4 concentration tended to be higher particularly when the wind direction was from the north where 100 head of cattle were housed (*e.g.,* Profile 1, z_m = 10 m, and Profile 2, z_m = 13 m, with 2.48 and 2.42 ppmv respectively) and west, where a slurry tank accompanied a facility of 2500 head swine (*e.g.,* Profile 1, z_m = 45 m, with 2.47 ppmv) (Figure 4.6, Table 4.3). While the point sources contributing to measurements in Profile 2, z_m= 13 m, were only bordering the assigned footprint area, we should remember that this footprint is a static representation and over the course of time the footprint did actually move over these locations and they therefore still influenced the measured concentration (Figure 4.6). Concentration was also higher when the wind was from the NW (*e.g.,* Profile 2, z_m = 24m, 2.40 ppmv), and likely passed over the cattle housing in this direction (Figure 4.6). Lower concentrations for Profile 1, z_m = 24 m (2.34 ppmv), and Profile 2, z_m = 45 m (2.29 ppmv), were seen where there was clearly no point source within the footprint (Figure 4.6, Table 4.3). While these lower concentrations may also be related to the typically expected decrease in trace gas concentration with height in the NBL as one moves away from surface sources, the concentration jump seen in Profile 1, z_m = 45 m (2.47 ppmv), indicates that directionality is important at any height and that a point source of CH_4 will increase the measured concentration.

In summary, the two CH_4 profiles measured on the night of Aug. 18-19, 2003, include specific sources of methane, which in this region of arable agricultural land cannot be from a source other than animal housing, manure storage, or standing water (possibly the drainage ditches). This therefore serves as a preliminary 'bottom-up' confirmation that the NBL budget method was measuring emissions from the upwind area within approximately 1 km from the launch site, and also from the surface of several farms within at least approximately 3 km upwind distance (for z_m = up to 45 m). Although the wind direction changed with height, the consistency of crop mixture covered in the east to west upwind area in this case was such that fluxes of CO_2 and N_2O would still be considered as representative as if the wind direction had stayed uniform with height.

4.8 SUMMARY AND CONCLUSIONS

Examples of typical patterns of potential temperature (θ), wind speed (u), and CO_2 concentration profiles and the interaction between these variables were given for four nights. Detailed vertical profiles of CO_2, Ri, and u, were classified into three main types of bulk NBL structure in calm, clear conditions: 1) a very stable upside-down boundary layer with convergent CO_2 profiles (optimal conditions); 2) a very stable upside-down boundary layer with non-convergent CO_2 profiles (suboptimal conditions where intermittent turbulence may cause the downward entrainment of trace gas-enriched air through the top of the NBL); and 3) turbulence extending to the surface from the underside of a LLJ or *u* maximum. The choice of integration height by examining in detail the progression of vertical profiles over time, with specific reference to the co-location of the following: (1) *u* maxima and/or the height were CO_2 profiles converge, (2) shear and turbulent layers, and (3) where $\Delta CO_2/\Delta z$ approaches zero for a given profile was discussed in relation to the first two types of bulk structure. Sixty-four percent of the dataset of profile pairs with a constant wind direction and/or source area type used for NBL budget measurement were observed to correspond to the first class (optimal conditions with converging profiles). In these NBL conditions the layer extending from the surface to 29.5 m contributed 80% of the flux measured at our field sites. The footprint distance for the height representing this major portion of the flux (z_m = 29.5 m) was modeled using a flux footprint parameterization (Kljun *et al.,* 2004) showing that this fell within 1948 km of the site, greater than the average length of a private farm in Coteau-du-Lac but still within the desired 'farm-scale' area. However, a large portion of the flux (50%) came from more local sources within 1 km of the measurement site. In addition, detailed CH_4 profiles were used to show that point sources within a 2 to 3 km radius were reflected in each respective profile as the footprint moved closer to and further away from these areas.

Defining the type of profile pattern of the NBL structure which in turn directly influences the pattern of CO_2 accumulation enables us to identify two critical height intervals in the CO_2 flux calculation: the integration height, and the interval contributing most to the total measured flux. This leads to a flux estimate that can be more readily related to the upwind source areas. We may assume that CO_2 and N_2O vertical distributions are similar as they are both gases emitted relatively diffusely and therefore these methods can also be applied for detailed N_2O profile measurements. Flux measurement can be further enhanced if surface spatial point measurements of concentration are available to substitute or to corroborate the lower profile measurements (Section 5.3.3) since the lowest portion of the profile often constitutes the largest contributing portion of the total measured flux. Information on the advective component of trace gas exchange would also be important to give a complete characterization of the lowest portion of the profile.

The preliminary 'bottom-up' verification of the NBL budget method, where CH_4 point source influence was seen in detailed CH_4 profiles, also increases confidence in the technique's applicability during stable atmospheric conditions. While the upper part of the NBL profile undoubtedly measures beyond the farm scale, it was shown that most of the flux originates from proximal sources and the resulting flux estimate can be considered to approximate the farm.

TABLES

Table 4.1. Carbon dioxide flux values for three cases of NBL/CO_2 structure. Type 1 = stable upside down boundary layer: CO_2 profiles converging. Type 2 = same but CO_2 not converging. Type 3 = turbulence down to ground. Time intervals rounded to nearest quarter hour. Eddy covariance (EC) results are averaged from data available from windy periods on the NBL night and from one to three nights before and after. "±" is 95% confidence interval. "–" means data not available.

Location Date	NBL/Vertical CO_2 Distribution Case	Time Interval (hh:mm) (EST)	CO_2 Flux (NBL Method) (mg m^{-2} s^{-1})	F_{EC} (mg m^{-2} s^{-1})	h_i (m)
Ottawa					
20-Jul-98	1	22:15-0:00	0.37	0.36±0.03	47
12-Aug-98	2	22:00-0:00	0.12	0.22±0.02	26
27-Aug-98	1	21:00-22:00	0.30	0.29±0.08	57
28-Jun-02	2	21:15-23:00	0.07	0.19±0.03	33
	1	23:00-0:45	0.07		32
	1	0:45-2:15	0.09		34
	1	2:15-3:30	0.36		76
	1	3:30-4:45	0.40		65
Coteau-du-Lac					
16-Jun-03	1	18:45-20:45	0.15	–	47
17-Jun-03	1	19:45-20:45	0.23	–	46
	1	20:45-21:45	0.15		46
	3	21:45-22:30	0.07		75
20-Jun-03	1	3:00-4:30	0.40	–	60
9-Jul-03	1	19:30-20:45	0.19	0.39±0.04	56
	2	0:15-1:45	0.36		56
	1	1:45-3:15	0.26		77
22-Jul-03	1	21:45-22:15	0.96	0.46±0.12	50
	1	22:15-23:45	-0.23		47
30-Jul-03	3	21:00-22:30	0.09	0.33±0.06	70
	3	3:30-4:15	0.12		41
18-Aug-03	3	19:15-20:30	0.15	0.29±0.04	55
	2	0:45-4:15	0.20		39

Table 4.2. Average heights with associated cumulative % contribution to total measured flux and 80% flux footprint distance (using parameterization of Kljun *et al.,* 2004) on nights exhibiting a very stable upside-down boundary layer with converging CO_2 profiles at the Ottawa (1998, 2002) and Coteau-du-Lac sites (2003).

z (m) from z = 2.5 m to:	% Contribution to Total Measured NBL Flux	80% Footprint Distance[a] (m)
5.7	10	376
8.1	20	535
10.8	30	713
13.6	40	898
16.7	50	1103
20.3	60	1341
24.4	70	1611
29.5	80	1948
36.4	90	2404
52.1	100	3440

input parameters as described in Section 4.2.2 except h = 52.1 m

Table 4.3. Height, wind direction (u dir) with variation, concentrations, and comparative source strength from detailed CH_4 profiles measured on the night of August 18-19, 2003, at Coteau-du-Lac, QC. Source strength estimation methods (footnotes a-h) can be found in Appendix E.

Profile (time, hh:mm)	Height z_m (m)	u dir (°)	CH_4 conc. +/- SD (ppmv)	σ (u dir) (°)	Point source in footprint?	Estimated Source Strength	
						Observations from Literature	IPCC Estimate
1 (23:50)	2	47	2.53 +/- 0.10	n/a	Drainage ditch at edge of field [a]	—	—
	10	13	2.48 +/- 0.15	4.5	Cattle housing (100 head, 75 LU) (non-dairy) Dry manure pile (estimated 107 t) [d]	22500 g CH_4 day^{-1} [b] 79 g CH_4 day^{-1} [e]	24700 g CH_4 day^{-1} [c] 960 g CH_4 day^{-1} [c]
	24	306	2.34 +/- 0.06	4.7	None	—	—
	45	269	2.47 +/- 0.11	7.9	Swine (2500 head, 300 LU) Open liquid manure tank (unknown volume and surface area)	— 5 to 317 g CH_4 m^{-2} day^{-1} [g] *or* 10900-25300 g CH_4 day^{-1} [h]	10300 g CH_4 day^{-1} [f] 33800 g CH_4 day^{-1} [i]
2 (1:54)	2	90	2.67 +/- 0.01	n/a	Drainage ditch at edge of field [a]	—	—
	13	358	2.42 +/- 0.07	12.9	Cattle housing (100 head, 75 LU) (non-dairy) Dry manure pile (estimated 107 t) [d]	22500 g CH_4 day^{-1} [b] 79 g CH_4 day^{-1} [e]	24700 g CH_4 day^{-1} [c] 960 g CH_4 day^{-1} [c]
	24	322	2.40 +/- 0.07	4.7	Cattle housing (non-dairy) (50 head, 38 LU)	11400 g CH_4 day^{-1}	12300 g CH_4 day^{-1}
	45	298	2.29 +/- 0.06	1.9	None	—	—

FIGURES

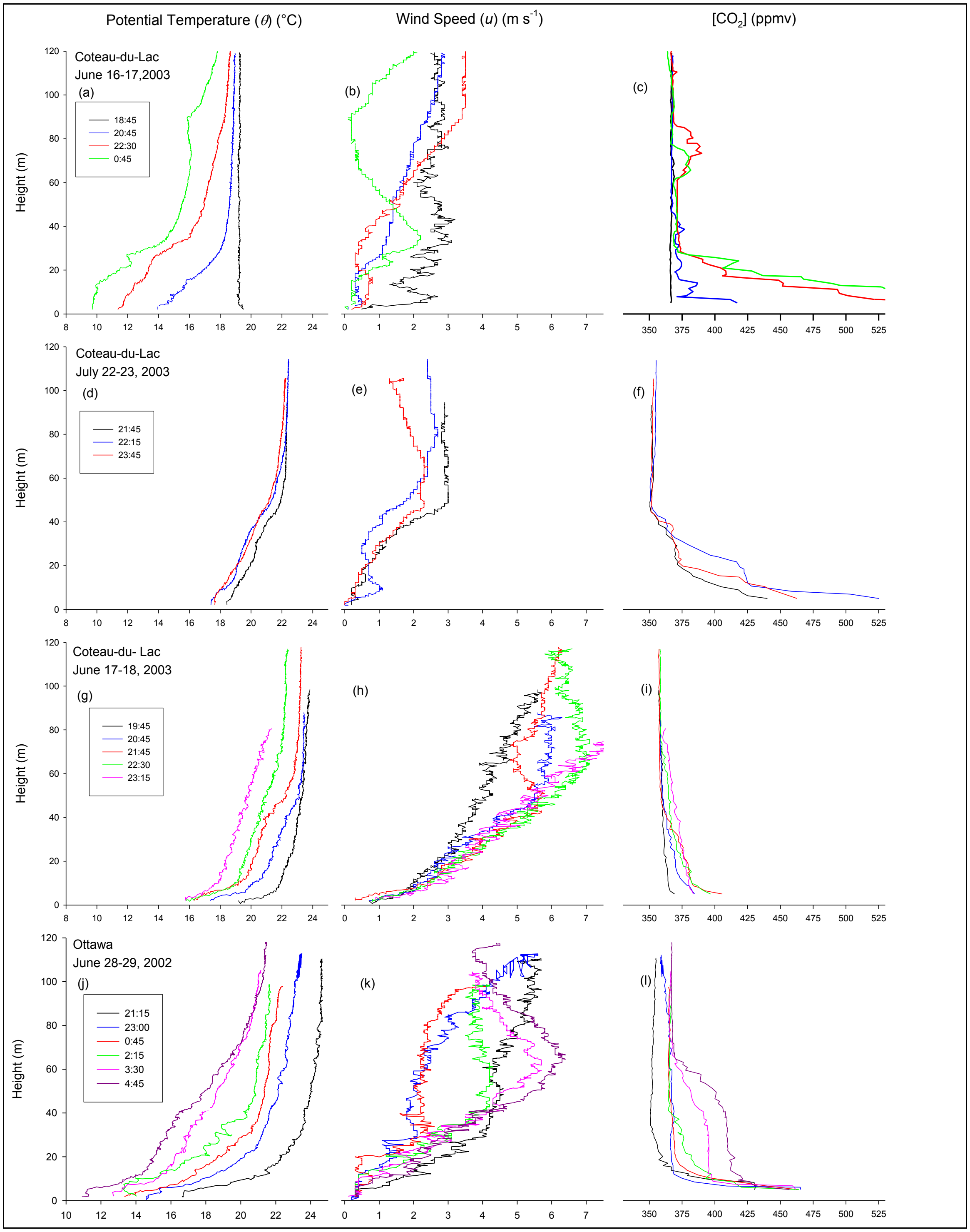

Figure 4.1 (a)-(l). Examples of NBL profiles of potential temperature (θ), horizontal wind speed (u), and CO_2 concentration ($[CO_2]$) for the Ottawa (2002) and Coteau-du-Lac (2003) field sites.

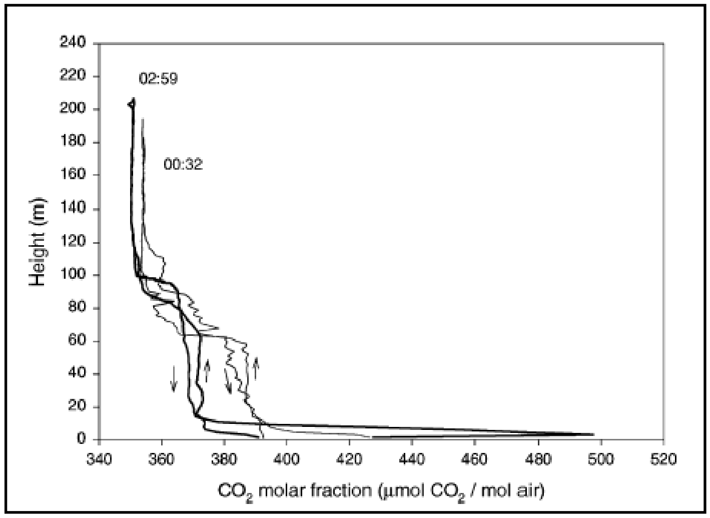

Figure 4.2. Carbon dioxide profile over agricultural field in Ottawa, ON, from Pattey *et al.* (2002). Arrows indicate balloon ascent and descent.

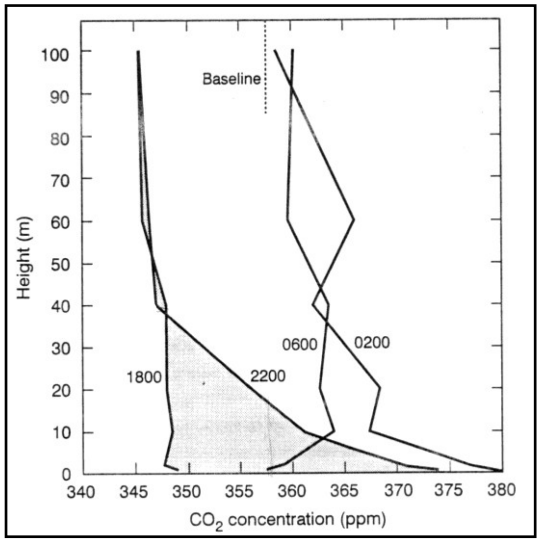

Figure 4.3. Profiles of nocturnal CO_2 concentrations over pasture in NSW, Australia, from Denmead *et al*. (1996). Shaded area represents the CO_2 accumulated between profile times.

Figure 4.4 (a-c). Case examples of u/Ri/CO_2 patterns from 22 NBL profile pairs that met criteria of constant upwind source area and intact NBL.

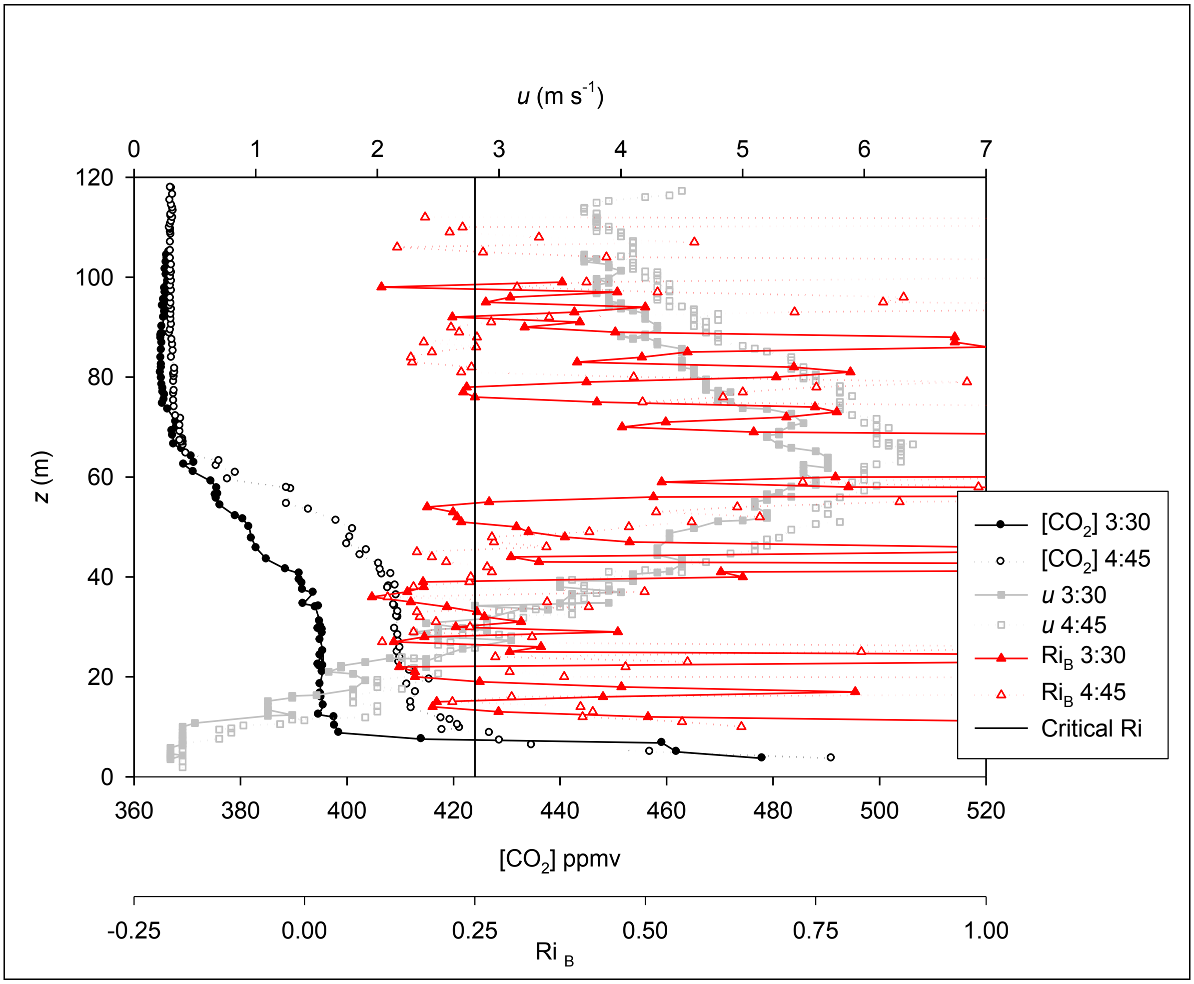

Figure 4.4 (a) Very stable upside-down boundary layer, decoupled low-level jet, $[CO_2]$ convergence: Ottawa, June 28-29, 2002.

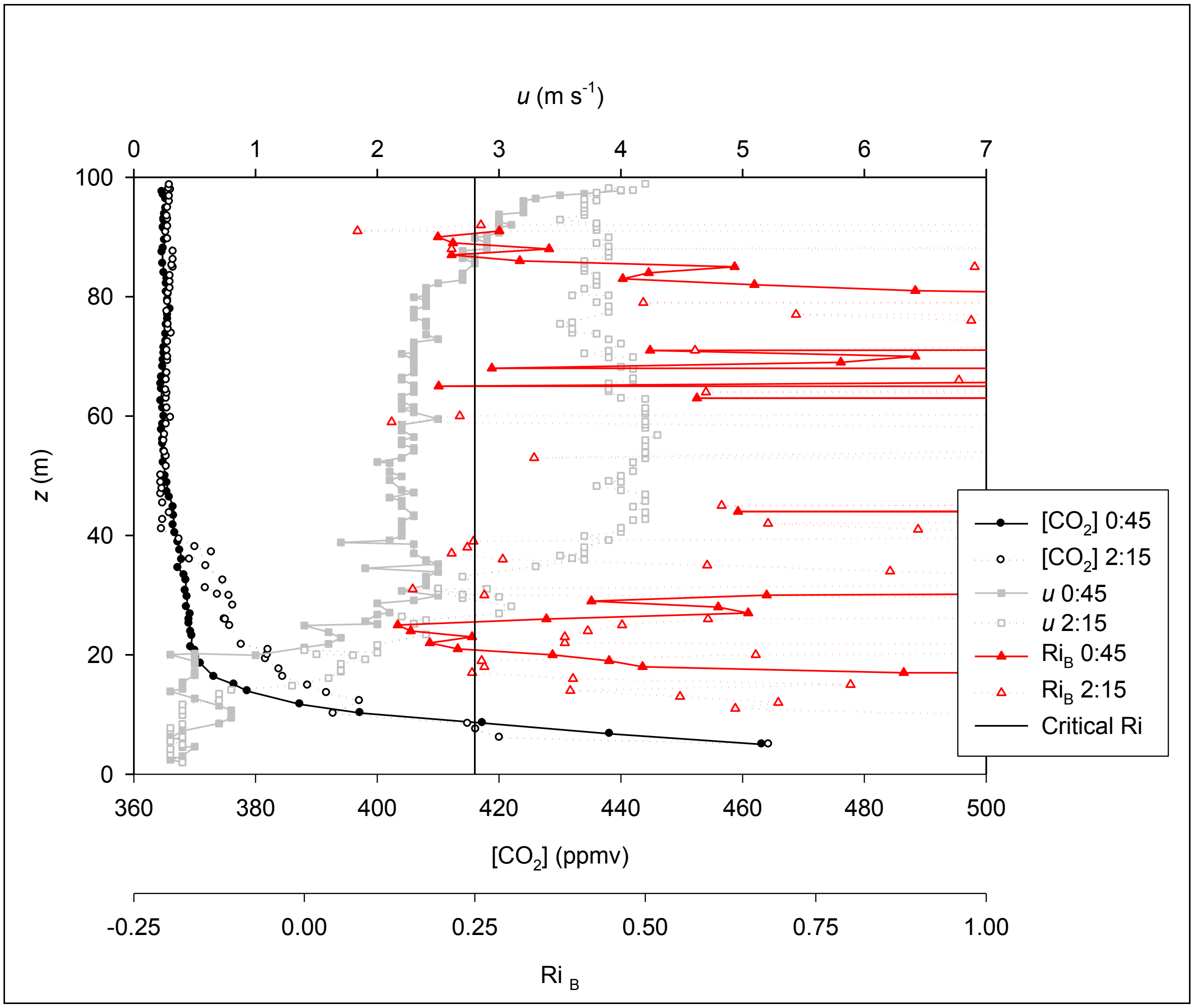

Figure 4.4 (b) Very stable upside-down boundary layer, *u* maxima, $[CO_2]$ convergence: Ottawa, June 28-29, 2002.

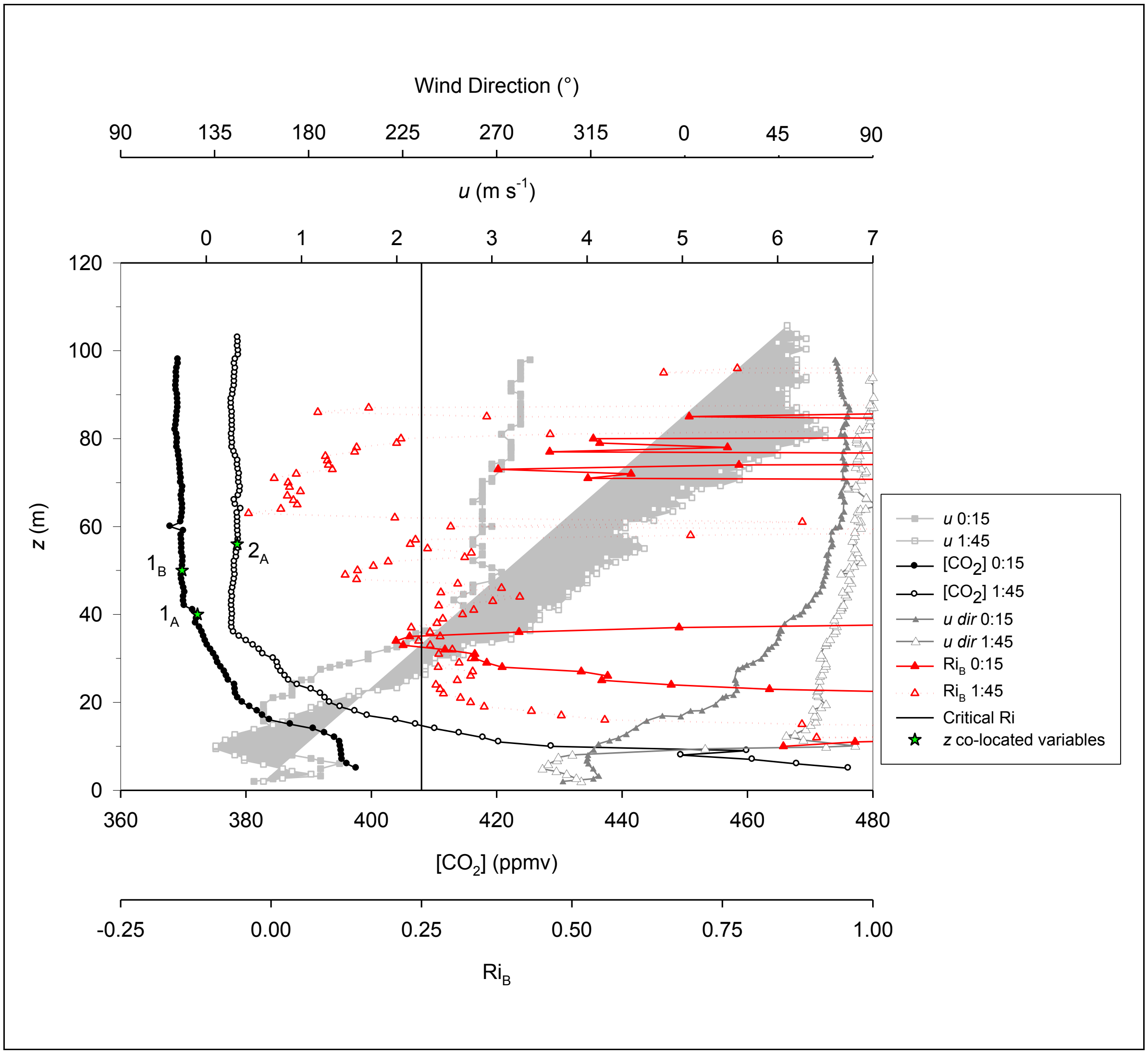

Figure 4.4 (c) Very stable upside-down boundary layer, non-convergent [CO_2] profiles: Coteau-du-Lac, July 9-10, 2003, with wind direction (*u dir*). Height of co-located variables using second approach for choosing integration height in suboptimal conditions (Section 4.5.2).

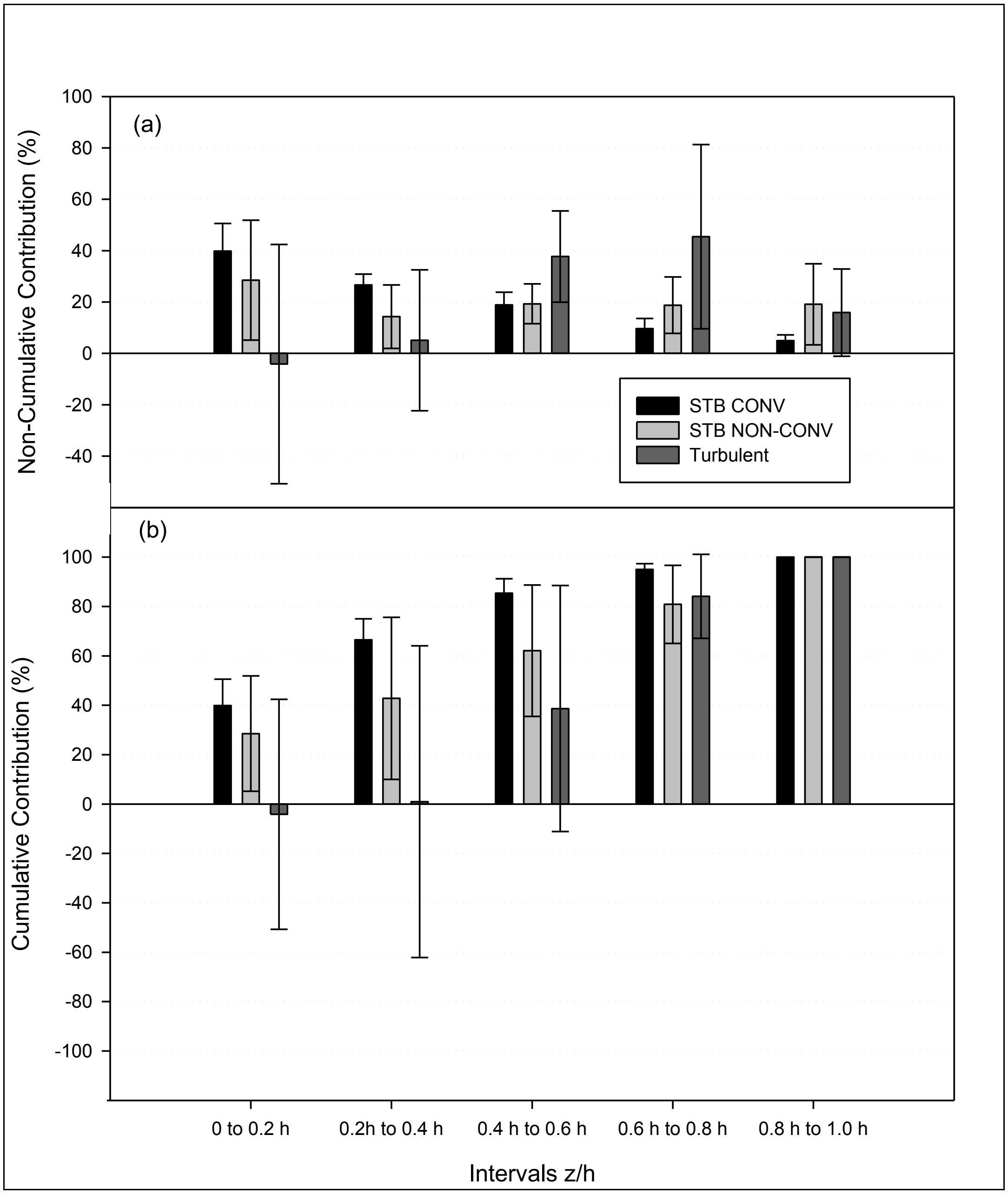

Figure 4.5. Non-cumulative (a) and cumulative (b) contribution (%) of normalized NBL height intervals (*z/h*) to total flux measured for the height interval z = 2.5 m to *h*, where *z* is measurement height and *h* is the height of the NBL (integration heigh). Data bars represent 3 situations of *u*/*Ri*/CO_2 patterns: STB CONV = very stable upside-down boundary layer with convergent CO_2 profiles, STB NON-CONV = very stable upside-

down boundary layer with non-convergent CO_2 profiles, Turbulent = turbulent layer at surface. Error bars are 95% confidence interval.

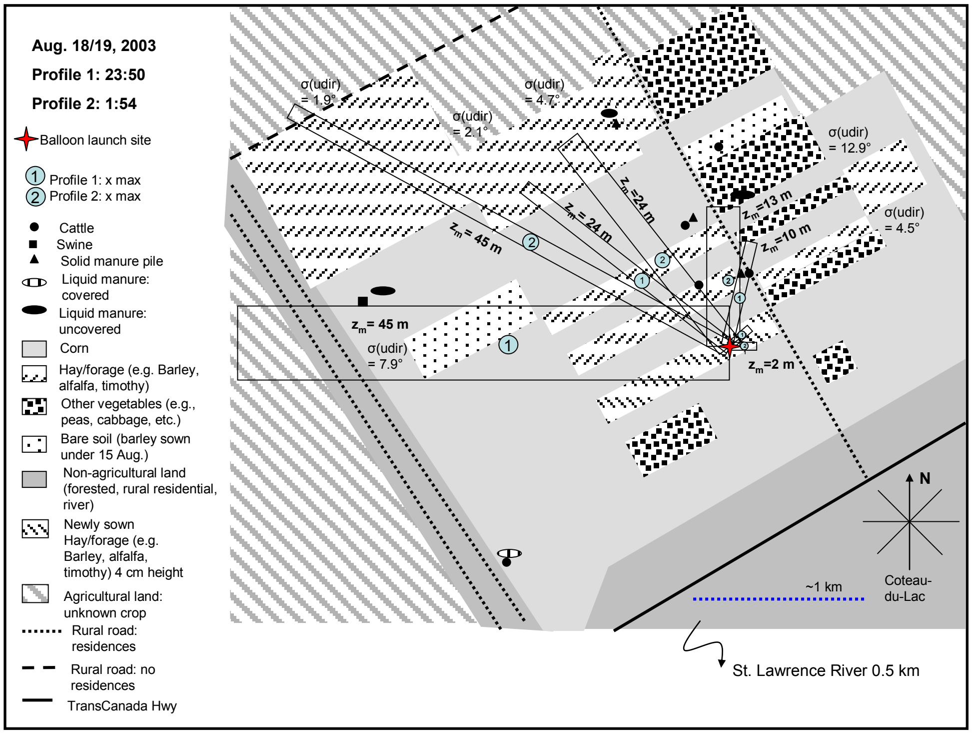

Figure 4.6. Detailed CH_4 profiles: Aerial photo labeled with crops, CH_4 point sources, overlain by 80% footprints and x_{max}, for given heights of detailed vertical CH_4 profiles on Aug. 18, 2003 (Coteau-du-Lac, QC).

5. NBL FLUXES OF CO_2, N_2O, AND CH_4 WITH SURFACE SPATIAL VARIABILITY

5.1 INTRODUCTION

In this chapter, field results are given for vertical profiles of the NBL budget. NBL-measured fluxes of CO_2, N_2O, and CH_4 are then given and overall results compared with near-in-time turbulent method fluxes and previously published results. NBL CO_2 flux data are then examined in detail with reference to near-in-time windy-night eddy covariance data and examined in terms of seasonality and bulk NBL state. Lastly, results for the spatial distribution of near-ground GHG concentrations at the field site are examined and their contribution to NBL budget method results discussed.

5.2 NBL BUDGET FOR CO_2, N_2O, AND CH_4

Examination of the NBL dataset has taught us that complete information on the state of the NBL (*e.g.,* wind, temperature, and CO_2 profiles) is required in order to produce meaningful NBL fluxes. Other studies (*e.g.,* Fisch *et al.,* 2000; Acevedo *et al.,* 2004) have sought to generalize properties of the NBL with regard to the measurement of GHG profiles, in order to be able to extrapolate profiles upward where only near-surface GHG measurements are convenient or available. We believe these types of extrapolations cannot be done reliably. NBL structure can vary greatly from one hour (or less) to the next. If a complete picture of NBL GHG flux is desired, one must perform a number of profiles throughout the night, always extending measurements up to a height where CO_2 (or other GHG) profile convergence can be reached most of the time. This ensures that the full flux profile can be collected and an appropriate integration height chosen with respect to concurrent NBL structure. For example, in our study, CO_2 convergence (due mostly to capping by u maxima) was seen within 100 m of the surface, most commonly around z = 20 to 60 m. All profiles were therefore measured up to 100-130 m, to capture the convergence height and a good portion of the NBL structure above it. As these typical heights may be specific to a measurement site, pre-study profiles going beyond the expected height can help determine these boundaries. Real-time wind speed and temperature data can also be used to verify this height at the time of NBL soundings.

5.2.1 CO_2 Fluxes

The overall mean NBL-measured CO_2 flux across the Ottawa sites (1998 and 2002) was 0.22 mg CO_2 m^{-2} s^{-1}, ranging from 0.07 to 0.40 mg CO_2 m^{-2} s^{-1}. The mean at the Coteau-du-Lac site was the same, 0.22 mg CO_2 m^{-2} s^{-1}, and, excluding the night of July 22-23, 2003, also ranged from 0.07 to 0.40 mg CO_2 m^{-2} s^{-1}, with a standard deviation of 0.10 mg CO_2 m^{-2} s^{-1} (Table 4.1). The reason for the similarity in fluxes between the two field sites is most likely a coincidence but could be due in part to the dominance of the same crop, corn, in both agricultural landscapes. Eddy covariance (EC) values during windy nighttime conditions ranged from 0.19 to 0.36 mg CO_2 m^{-2} s^{-1} at the Ottawa sites and from 0.29 to 0.46 mg CO_2 m^{-2} s^{-1} at the Coteau-du-Lac site (Table 4.1). Windy night EC results generally were within the same order of magnitude as NBL results, but were higher than NBL results. This difference in flux values is expected because of the difference in measurement scale, with the NBL footprint including contrasting respiration rates (*e.g.,* roads, buildings, various crops, grass, woody species) compared with the more homogeneous source in the footprint of the EC tower.

Overall, CO_2 results are similar to those for CO_2 emissions from agricultural areas measured in previous studies using the NBL method. Denmead *et al*. (1996) measured a nocturnal CO_2 flux of 0.05 mg CO_2 m^{-2} s^{-1} in a region of pasture and cereal crops. Pattey *et al*. (2002) reported nocturnal CO_2 fluxes of 0.04 to 0.92 mg CO_2 m^{-2} s^{-1} for soybean and corn fields near the Ottawa field site used for this study. Griffith *et al.* (2002), measured a mean flux of 0.15 +/- 0.05 mg CO_2 m^{-2} s^{-1} using a fixed, seven-point vertical profile up to z = 22 m, over a lucerne pasture. Acevedo *et al.* (2004) found nocturnal CO_2 fluxes ranging from 0.09 to 0.51 mg CO_2 m^{-2} s^{-1}, depending on the choice of boundary layer depth *(i.e.,* integration height), over a grass field in Brazil.

The NBL results of our study are similar to those having been obtained using other techniques as well. Kelliher *et al.* (2002), using a N_2O/CO_2 ratio method with data from Fourier transform infrared spectroscopy (N_2O) and chambers (CO_2) measured an average nighttime rate of 0.13 +/- 0.04 mg CO_2 m^{-2} s^{-1} on grazed farm pasture. Soegaard *et al.* (2003), using eddy covariance, measured nighttime CO_2 fluxes of approximately 0 to 0.09 mg m^{-2} s^{-1} (value integrated for a footprint-defined area containing wheat, barley, grass, and corn).

5.2.1.1 July 22-23, 2003 Results (Coteau-du-Lac)

Results from the night of July 22, 2003, a high positive flux (0.96 mg CO_2 m^{-2} s^{-1}) from 21:45 to 22:15 followed by a negative flux (-0.23 CO_2 mg m^{-2} s^{-1}) from 22:15 to 23:45 were not typical, despite capped conditions (Figure 4.1, d-f). A higher flux was echoed in EC measurements from one night before and after this night (0.46 mg CO_2 m^{-2} s^{-1}) (Table 5.1). No apparent breakdown of the NBL seemed to occur over the course of measurements as *Ri* profiles showed continued strong stability at the surface (Figure 5.1a) bearing in mind these are only snapshots of the NBL. Leakage through the top of NBL is not considered likely as CO_2 profiles converge quite cleanly. NBL method N_2O results for the period of approximately 23:00 to 0:00 (excluded from overall results in Table 5.1 due to a wind direction difference of 180° between profiles, with a change from W to E) gave a flux of 89 ng N_2O m^{-2} s^{-1}, higher than the Coteau-du-Lac average as well. A possibility for the elevated CO_2 (and N_2O flux) was that somewhere in the upwind source area for the second profile (NNE), some manure or slurry was applied to an agricultural field, resulting in a strong short-term flushing of CO_2 (*e.g.,* Rochette *et al.,* 2004); however, this is somewhat contradicted by windy night EC results which also showed a larger-than-normal flux and were presumably specific to the pea field, which had no new field management activities.

However, because the elevated CO_2 fluxes were measured by EC for more than one night, it lends credence to the elevated NBL-measured flux; the subsequent negative flux measured by the NBL method, then, could only be attributed to source area differences or intermittency or advection (at the surface or aloft) in the NBL.

While in general for CO_2 wind direction has not been considered critical as the agricultural landscape is very similar for Coteau-du-Lac to the east, north, and west, a change in surface wind direction may have had some role here. The surface wind direction measured by the sonde and the wind vane in this case conflicted by up to 45°. Wind direction has been found to meander somewhat due to slack pressure gradients and very low wind speeds in very stable conditions (Banta *et al.,* 2007). The discrepancy could therefore be due to a difference in instantaneous measurement vs. a half hourly average (although the wind direction histogram could not be reconciled either) or could be due to the low sensitivity of wind vanes to changes in wind direction at low wind speeds. In any case, according to the sonde, the wind at the surface came from the east for the first profile (note the tethersonde spun steadily from east through south to NW in the bottom 20 m of the profile), the NNE for the second profile, and the NW for the third profile, with the upper part of the profiles having a common direction of NW starting at z = 57 m (7 to 10 m above the convergence height) (Figure 5.1b).

Also out of the ordinary for this night and worth noting, the wind speed profile did show a small peak (approximately 1 m s^{-1} or less) consistently occurring at z = 5 to 10 m (*e.g.,* see Figure 4.1e, 22:15 profile) and this may be related to the relatively small decrease and, at times, slight increases, in surface temperature throughout the night. This may be an indication of some advective component (*e.g.,* drainage flow), which, in conjunction with the change in wind direction, contributed to the displacement of CO_2. If this is the case the results on this night should not be considered as representative of the farm.

5.2.2 N_2O Fluxes

N_2O fluxes were obtained during the 2002 and 2003 field campaigns (Table 5.1). In contrast to the CO_2 study, because of the smaller number of N_2O profiles obtained, N_2O flux data are presented for profiles even where a breakdown in the NBL may have occurred. However, the acceptance criterion of constant wind direction or source area type between successive profiles was maintained. For the most part, concurrent detailed CO_2 profiles were not available, due to limitations in the lift capacity of the tethered balloon.

With only the overall average N_2O concentration for each vertical profile, the height of N_2O accumulation, a major indicator of flux integration height, could not be ascertained as for CO_2. Instead, during optimal NBL conditions (*i.e.,* Type 1, stable NBL with converging CO_2 profiles), the height of CO_2 accumulation could be referred to as a proxy, under the assumption that the gas accumulation pattern would be the same along with other variables such as u and Ri. As long as the air sample collection included the height interval of CO_2 accumulation, the full flux would be captured. A simulation using typical vertical profile data (not shown) showed that the inclusion of the lower ambient gas concentrations above the gas accumulation height, would result in only a slightly lower measured flux, on the order of 1%. It was therefore considered acceptable to retain the height of bag collection as the flux integration height during optimal NBL conditions.

During suboptimal NBL conditions (*i.e.,* Type 2, stable NBL with non-converging CO_2 profiles), however, because of the non-zero difference between profile concentrations throughout the profile, the choice of flux integration height would make a larger difference. The situation was complicated further by the non-concurrent collection of N_2O bag sampling profiles and detailed CO_2 profiles. However, a very approximate flux integration height could be inferred from near-in-time detailed CO_2 measurements with their respective u and Ri profiles. There were three cases where N_2O and CO_2 data were available in suboptimal conditions (Table 5.1). A correction using concurrent or near-in-time detailed CO_2 data based on the difference between the flux calculated up to the CO_2 integration height and up to the bag collection height showed that these bag profiles may have overestimated the N_2O flux by 77% (June 28-29, 2002, 21:15-23:00), 16% (July 9-10, 2003, 23:30-0:45), and 20% (August 18-19, 2003, 1:15-3:00) (Table 5.1).

The mean NBL-measured N_2O flux (from all wind directions and type of farming management) was 30.3 ng N_2O m^{-2} s^{-1} for the 2002 Ottawa site (two nights with values ranging from -13.5 to 107.1 ng N_2O m^{-2} s^{-1}) and 26.5 ng N_2O m^{-2} s^{-1} for the 2003 Coteau-du-Lac site (five nights with values ranging from 2.7 to 50.4 ng N_2O m^{-2} s^{-1} giving a standard deviation of 14.5 ng N_2O m^{-2} s^{-1}) (Table 5.1). For the Ottawa site, N_2O flux gradient results from TDL for afternoons before and after our two nights of NBL measurements ranged from 3 ± 13 to as high as 1939 ± 479 ng N_2O m^{-2} s^{-1}, while for the night following the two NBL launches, values of 188 ± 57 and 27 ± 22 ng N_2O m^{-2} s^{-1}

were measured. At Coteau-du-Lac, daytime N_2O fluxes by TDL (afternoons before and after NBL measurement) ranged from -4.4 ± 64 to 89 ± 29 ng N_2O m^{-2} s^{-1}, while fluxes for the nights following NBL measurement ranged from 11 ± 43 to 189 ± 105 ng N_2O m^{-2} s^{-1}. Nighttime fluxes measured by the flux gradient method were generally higher than NBL-measured fluxes but in the same order of magnitude, with the exception of June 28-29, 2002, and June 16-17 and 17-18, 2003, where the flux gradient fluxes were one to two orders of magnitude greater, possibly because of comparatively heavier rainfall in days prior to these NBL launches (46.6 mm on day of June 27, 2002, and 58.4 mm from June 11-14, 2003) and the greater sensitivity of the flux gradient method to a smaller, specific source area of high N_2O production, compared with that of the NBL method over a larger, heterogeneous area with varying rates of N_2O production. Daytime flux gradient fluxes were also higher than NBL-measured results but on a few occasions quite close to NBL results[1]. In general, differences between the results of flux gradient and NBL methods can probably be attributed to scale differences and hence source area differences. While these areas are likely being exposed to the same precipitation, the two methods are seeing areas with different crops, soils (and microbes), and moisture levels.

Results for NBL-measured N_2O fluxes were, on average, higher than those measured in other studies for agricultural fields at the field scale. Pattey *et al.* (2006), at a site close to our Ottawa site, using a TDL to obtain a detailed NBL N_2O profile, measured a flux of 14 ng N_2O m^{-2} s^{-1}. Denmead *et al.* (2000b), using the flux gradient technique on windy nights measured an N_2O flux of 3.8 ± 3.1 ng N_2O m^{-2} s^{-1} over grazed pasture. Kelliher *et al.* (2002), using a N_2O/CO_2 ratio method with data from Fourier transform

[1] Overall N_2O flux results using TDL from 2002 and 2003 have been published in Grant and Pattey (2008) and Pattey *et al.* (2008).

infrared spectroscopy (N_2O) and chambers (CO_2), measured an average nighttime emission rate of 24 ± 5 ng N_2O m^{-2} s^{-1}, also over grazed pasture. Values for long-term average daily fluxes measured by Wagner-Riddle *et al.* (1996, 1997, 2007) were found to range from approximately -6 to 18 ng N_2O m^{-2} s^{-1} for various agricultural crops under different field management. Elevated values have been found following irrigation and rainfall (*e.g.,* up to 295 ng N_2O m^{-2} s^{-1}, Wagner-Riddle *et al.,* 2007).

The differences between NBL-measured and literature values despite similar crop types are likely precipitation- and field management-driven. The overall upwind region measured by the NBL budget method may have had areas more conducive to N_2O production, such as a sustained optimal water level in the soil to give a higher baseline N_2O production. Better knowledge of management events of all the farms in the upwind source area could also have helped to explain the higher fluxes, for example, N application and irrigation.

5.2.3 CH_4 Fluxes

Methane flux results for the Ottawa and Coteau-du-Lac sites ranged from -3.05 to 3.03 and -2.85 to 0.83 μg CH_4 m^{-2} s^{-1}, respectively (Table 5.1). The overall average fluxes measured, regardless were -0.43 μg CH_4 m^{-2} s^{-1} at the Ottawa site (data from eight profiles over two nights) and -0.36 μg CH_4 m^{-2} s^{-1} at Coteau-du-Lac (data from eleven profiles over five nights). Methane results, like those for N_2O, were included regardless of NBL state but the wind direction requirement was maintained: a difference between profiles of no more than approximately 45° (taking into consideration the difficulties of precise wind direction measurement at low wind speeds).

Agricultural lands (soils) usually display a slight uptake of atmospheric methane on the order of -0.0002 to -0.004 μg CH_4 m^{-2} s^{-1} (range of values from Lessard *et al.,* 1994; Boeckx *et al.,* 1997; Hansen *et al.,* 1993; Dorsch *et al.,* 2004; Jambert *et al.,* 1997; Gregorich *et al.,* 2005). Results here reflect the presence of significant point sources of CH_4 such as animal housing (non-ruminant), manure piles, and/or lagoons located near the launch site in Ottawa (within 150-500 m) and also further away (350 to 2000 m) at Coteau-du-Lac.

Unfortunately, methane fluxes measured by the NBL technique gave somewhat confusing results. Even if the wind direction remained very consistent throughout the night (say, within 20°), CH_4 fluxes over time could change from positive to negative, with seemingly no correlation to the presence of a point source. The fluxes appeared to be significant with respect to inter-replicate standard deviation most of the time (Table 5.1) (not tested). This was true even for profile pairs where a stable upside-down boundary layer appeared to remain intact.

This suggests that in the case of point sources in the vicinity of the tethered balloon launch site, a very precise reckoning of upwind source area needs to be obtained to explain the resulting fluxes. Wind direction (near the surface and aloft) needs to be measured continuously and more accurately than was possible here, with very low near-surface wind speeds and consequent slow reaction time of the blimp/tethersonde apparatus to any ephemeral wind direction change. Alternatively, wind vane or sonic anemometer data could be used to monitor the progression of wind direction close to the surface, but this is still not ideal as minimum wind speed and/or turbulence may render wind direction data questionable and half hourly averaging of data precludes having wind direction measured exactly concurrent to NBL measurement. Practically speaking, because of this challenge, it is apparent that the NBL method is not particularly suited to measuring GHGs from strong point sources. This is discussed further in Section 5.3.

Intermittency in turbulence especially near the surface also likely contributed to the resulting larger negative fluxes. If some CH_4 was displaced between profiles, it would appear as an "uptake" in the measured flux.

5.2.4 Comparison Between NBL Budget Method and Eddy Covariance Data

The NBL budget method, being used on calm nights in conditions of negligible vertical turbulent flux, measures the storage flux from the surface to the height of the NBL. The eddy covariance (EC) method is an established method that measures the vertical turbulent flux (and can be used on windy nights). Although a scale difference exists, a comparison of results from the NBL method with those from near-in-time EC data provides a check on the accuracy of the NBL budget method.

NBL budget fluxes from both the Ottawa and Coteau-du-Lac sites were compared with eddy covariance data during turbulent periods from within ± three nights of NBL measurement (this was extended to ± seven nights around Aug 27, 1998 because of exceptionally calm conditions). Valid EC data require turbulence and are available from windy nights only; they are therefore mutually exclusive of data from calm NBL budget nights. The overall average CO_2 fluxes from the two methods were compared by grouping with respect to the three NBL bulk structures seen on the NBL nights (Figure 5.2, Table 5.2). Overall, in comparison to EC, NBL-measured CO_2 fluxes were lower. NBL-measured CO_2 fluxes came closest (88%) to EC values during very stable upside-down boundary layer conditions with converging CO_2 profiles and were 69% of EC values during stable conditions with non-converging profiles. In conditions with turbulence at the surface, the NBL values were 41% of EC values. These results are similar to those of Chen *et al.* (2008) who found that regional estimates of GPP from concentration-derived flux from a tall tower in a boreal region were consistently smaller than local EC flux estimates. The annual difference between methods was 20-25% and was attributed to source area differences (concentration vs. flux footprint) (Chen *et al.,* 2008).

From these results, the NBL state generating a flux was closest to the EC flux) was the very stable upside-down boundary layer with converging CO_2 profiles, which was also the most frequently observed at 64% of our valid profile pairs. Even in very stable optimal NBL conditions, there still exist some periodic turbulent motions which will transport gas; this may lead to leakage within the NBL between profile measurements resulting in an underestimation. Horizontal flux divergence (advection) may be another possibility for the difference. Gioli *et al.* (2004) found a similar trend comparing EC- vs. aircraft-measured CO_2 flux and suggested that, in addition to source area differences, vertical flux divergence (where the flux decreases with height) might be responsible for the difference in results from the two methods.

Turbulent conditions within the NBL provided the least accurate NBL flux in comparison with EC. The presence of mixing down to the surface likely resulted in vertical turbulent flux of CO_2, reducing the build-up of CO_2 and thus a measurement of CO_2 storage (by the NBL budget) does not represent the net flux. These were the least desirable NBL conditions as not only were they insufficiently stable for accurate NBL fluxes, they were insufficiently turbulent for continuous successful measurement by EC.

5.2.5 Effects of Seasonality and NBL Structure on GHG Fluxes

Having established the relative accuracy of NBL vs. EC fluxes using CO_2 data, we may investigate further and ask whether NBL fluxes are more a function of the structure of the NBL or of seasonality (*e.g.,* soil temperature, crop growth stage)? We used data from the single year at the Coteau-du-Lac site to avoid the complication of inter-site differences. NBL profiles were bulk-grouped by month (June, July, August) and by NBL structure type (convergent, non-convergent, turbulent).

The effect of management practice and crop growth stage is shown in the monthly trend for CO_2 and N_2O (Table 5.3a). The average CO_2 flux was highest in July when the local surrounding crop systems (peas, corn) were in their peak growth stages and near-surface nighttime soil temperatures would have been highest and then decreased again later in August after the pea crop was harvested, the nearby corn fields were in their reproductive stages and nighttime temperatures would have begun to decrease. Average nitrous oxide flux, on the other hand, was greater in June, when N fertilizer had been recently applied for both crops (mid-to-late May). It dipped on average for the July measurements and increased again on average in the August measurements when the pea field was harvested, leveled, and manure applied. This trend is confirmed by the eddy flux data (Pattey *et al.,* 2008). No seasonality effect was seen in the monthly averaged methane results; this is not surprising as methane is not a diffuse source and wind direction would be a more important variable than time of year assuming that the number of animals in housing and size of manure piles were relatively constant.

The effect of NBL structure is indicated in the CO_2 flux results (Table 5.3b). During conditions displaying a very stable upside-down boundary layer, with both converging and non-converging CO_2 profiles, the average CO_2 flux is larger than during conditions where there is turbulence down to the surface from the underside of a u maximum. The mixing at the surface during the latter conditions, combined with a weak temperature gradient, appears to allow the entrainment of CO_2 upward through the u maximum, resulting in a lower measured flux value (Mathieu *et al*., 2005).

Average methane fluxes (which combine results from all wind directions) show uptake during very stable upside-down boundary layer conditions and emission during periods with turbulence at the surface (Table 5.3b). Arable agricultural land normally takes up methane at a rate of approximately -0.003 μg CH_4 m^{-2} s^{-1} (*e.g.,* Boeckx *et al.,* 1997; Hansen *et al.,* 1993; Dorsch *et al.,* 2004; Jambert *et al.,* 1997; Gregorich *et al.,* 2005). While the larger-than-expected average magnitude of uptake measured in this study was not correlated to changes in wind direction and the resultant inclusion or exclusion of known point sources of methane in the upwind source area, the displacement of existing CH_4 could be a possible factor. The methane flux was observed to change to a release during turbulent NBL conditions likely through upward mixing of CH_4 from drainage ditches which can be found surrounding fields throughout this agricultural region. Higher methane concentration in the stratified air existing above these water-filled ditches is mixed upward into the NBL by the intermittent turbulence penetrating to the surface. The introduction of higher methane concentrations can result in a positive flux (emission) being calculated between two successive ascents.

NBL structure appeared to have less of an influence on N_2O flux results (Table 5.3b) likely because in contrast to CO_2, nitrous oxide fluxes are governed very strongly by antecedent weather and field management activities (rainfall and N availability). Nitrous oxide fluxes during very stable upside-down boundary layer conditions with converging CO_2 profiles were nevertheless higher than during conditions with non-converging profiles or near-surface turbulence as was seen with the CO_2 fluxes.

5.3 NEAR-SURFACE SPATIAL VARIABILITY OF GHGS

A diffuse source of a GHG is one which is widely and evenly distributed across the landscape and the GHG is emitted relatively continuously at this scale. A point source is one which is localized and stands separately within the landscape. GHGs from point sources are therefore not emitted continuously at this scale.

The spatial distribution of any trace gas (flux or concentration) from a diffuse source/sink such as agricultural soil (*e.g.,* CO_2, from soil respiration, N_2O, from denitrification, or CH_4 uptake by methanotrophs), will still vary over a wide area and be most highly variable closest to the surface. This is also true for trace gas exchange from point sources (*e.g.,* N_2O from an anaerobic 'hot spot' in the soil, methane from ruminant housing or a manure storage facility). If we are interested in measuring GHG fluxes from the entire farm, concentrations measured at one location close to the surface might not adequately represent the contribution of these point sources. Therefore, in order to better capture the spatial variations in GHG fluxes at the surface and better reflect the spatial integration of the NBL budget, spatial averaging needs to be carried out.

Wind direction, as discussed previously, is a key factor in measuring GHG fluxes from point sources on a farm. This is true even in the gathering of spatial data for point sources. Of course, with respect to a single significant point source such as a manure pile, a spatial average for GHGs is only useful if the spatial measurements are actually downwind of this point source, *i.e.,* measurements should be made when the wind is coming from the point source. Now, it is expected that, to a certain extent, the mean wind acts to homogenize trace gas concentrations downwind of a source. But to what extent? Knowing this would further indicate whether there is a need for spatial sampling. To investigate this question, therefore, the sensitivity of measurements downwind from a significant point source to wind direction changes was obtained through near-surface field-scale spatial sampling of CH_4 at the Ottawa and Coteau-du-Lac sites, concomitantly with the spatial variability of CO_2 and N_2O, which originated mostly from the diffuse soil source.

5.3.1 Spatial Results: Ottawa, ON

Spatial measurements for the two Ottawa nights (June 24-25 and July 18-19, 2002) effectively demonstrate how sensitive the spatial distribution of a GHG may be with respect to animal-related sources and wind direction (Table 5.4, Figure 5.3 a to c). On both nights the wind principally came from the direction of a large manure pile approximately 150 m from the western edge of the field site (Figure 5.3 a to c).

The increased variability of CH_4 (18%) during the first transect on the first night (June 24-25, 2002) (Table 5.4) was due to higher concentration in one sample on the west side of the field (3.38 ppmv), which can be most likely be attributed to the manure pile (Figure 5.3a). N_2O, which also had a spatial CV of 18% during the first transect (Table 5.4), also showed a high concentration on the west side of the field (0.62 ppmv) but not in the same location as the high methane sample (Figure 5.3b). This would seem to suggest a source other than the manure pile. Interestingly, this sample was taken next to an area of brush bordering the farm field, where the trail was grassy, wet, and muddy because of 20 mm of rain that had fallen that afternoon. While still downwind of the manure pile, this N_2O may instead have come as a 'burst' from an anaerobic 'hot spot' in this area. In the second transect, however, the concentration at this location decreased toward the mean (Table 5.4), which may be a reflection the temporal variability of N_2O production. Studies using traditional chamber methods (with more appreciable changes in concentration over time) in agricultural fields have shown spatial variability of N_2O fluxes ranging from 37 to 90% (*e.g.,* Hénault *et al.,* 1998; Laville *et al.,* 1999), and even 217 % (Yanai *et al.,* 2003) and 282% (Ambus and Christensen, 1995). Clearly, the atmosphere will act to homogenize emissions spatially. It should be noted that while methane variability appears to be lower in the second transect, there were some key locations on the west side of the field where samples were not obtained; these samples, if taken, would perhaps have shown increased concentrations and therefore higher variability as in the first transect. CO_2 concentrations maintained the same variability (about 4%) from one transect to the next (Table 5.4). Van den Pol *et al.* (1998) also found that CO_2 fluxes were the least spatially variable compared to CH_4 and N_2O fluxes in a grassland on peat soil.

The period of rainfall on the afternoon of June 24, 2002, may also explain why the overall average methane concentration was considerably lower and the mean N_2O concentration slightly higher on this first night than on the second, drier night of July 18-19, 2002 (Table 5.4). The rainwater may have saturated pores in the surface of the manure pile so that methane from its anaerobic interior could not escape, thus resulting in lower emissions and a lower ambient concentration, except for one location close to the manure pile. On the other hand, the effect of an increase in water filled pore space in the soil around the field site may have provided more opportunity for optimum conditions for N_2O production, therefore slightly increasing overall ambient N_2O concentrations.

On the second night, July 18-19, 2002, CH_4 showed higher concentrations and increased variability for both transects, but N_2O did not (Table 5.4). Presumably the low variability of the latter is because of drier conditions which did not promote the formation of anaerobic 'hot spots' of increased N_2O production in the soil (although the most recent precipitation was 24 hours earlier, with 15 mm falling the evening of July 17, 2002, and prior to this, 27 mm on July 9, 2002). The variability of CH_4 around the field, on the other hand, can be explained by tracing the progression in wind direction over the course of the two transects (Figure 5.3c).

For the west half of the first transect, the mean surface wind was from the NW (see dashed line, Figure 5.3c, for division of transect), where air enriched in CH_4 originating from the manure pile and cattle feedlot are reflected in elevated concentrations (3.35, 4.28 ppmv). The shift in wind direction to WSW for the second half of the first transect is represented by an increase in CH_4 concentration at the opposite end of the field (2.74, 2.89 ppmv), which at that time came to be in the downwind path of the manure pile and feedlot. A gentle slope in the terrain from roughly west to east (a one meter drop over the 600 m length of the field) also favoured the near-ground downslope movement of CH_4 from the manure pile.

The mean wind for the second transect was from the W, with some contribution from S and SE (30% of the time). This resulted in lower concentrations by the manure ;.pile and feedlot, and a higher concentration close to the animal housing facility (3.59 ppmv) (Table 5.4, Figure 5.3c). The emission of methane from this facility housing approximately 200 sheep was estimated, using emission factors, to be 11.7 μg CH_4 m^{-2} s^{-1} (Environment Canada, 2004). There was also an overall (average) decrease of approximately 0.4 ppmv for the entire transect and a decrease by almost half in spatial variability to 11.5% (Table 5.4). The shift in wind direction may also explain the higher concentrations of CO_2 downwind of the animal housing facility which caused the variability of CO_2 to increase from 1.1 to 7.1% from the first to the second transect.

5.3.2 Spatial Results: Coteau-du-Lac

Compared to the Ottawa site, concentrations of all three gases around the Coteau-du-Lac field site were not very spatially variable, with overall %CV ranging from 0.9 to 7% (Table 5.4). This is because on the nights of measurement (August 18-19 and August 28-29, 2003), the sampling locations were not directly in the downwind path of the nearest manure piles and cattle housing facility found approximately 350 m to the N and NE of the nearest sampling locations (Figure 5.4).

5.3.3 Use of Spatial Results to Represent Surface Measurements in NBL Profile

Data from two concurrent vertical profiles and spatial transects (20:30 and 23:45) on the night of July 18-19, 2002 were used to replace the vertical profile concentrations in the first 10 m of the concurrent CO_2 vertical profile (Table 5.5). As a result, the CO_2 flux from 20:30 to 23:45 increased by 6%, from 0.44 to 0.47 mg CO_2 m^{-2} s^{-1}, reflecting the fact that the average spatial concentration was 4.3% lower than the average vertical concentration measured in the first 12 m of the 20:30 vertical profile (difference of about 30 mg m^{-3} or 16 ppmv) (Table 5.5).

An example illustrating the use of the spatial average of a highly spatially variable gas such as CH_4 on July 18-19, 2002, at the Ottawa site (11-20% CV) is not available, as no detailed vertical profile of CH_4 concentration was measured at this site. On nights at Coteau-du-Lac where a detailed vertical CH_4 profile was measured (August 18-19 and August 28-29, 2003), methane concentration exhibited low spatial variability on the same order of that of CO_2, for which an example was given above. The sensitivity of surface spatial measurements to wind direction in the case of CH_4 suggests, though, that where there are significant point sources, the overall NBL CH_4 profile will also be sensitive to small changes in wind direction, both at the surface and aloft. A CH_4 flux calculation using the NBL technique may therefore include changes in concentration that are not constant in origin and are therefore incorrect.

5.4 CONCLUSION

NBL budget results for CO_2 and N_2O fluxes fell within the range of literature values and were of the same order of magnitude of fluxes concurrently measured by eddy covariance and flux gradient methods, keeping in mind the scale differences. When compared to windy-night eddy covariance measurements at both sites, NBL CO_2 fluxes came to within 88% of EC-measured fluxes during very stable upside-down boundary layer conditions with converging CO_2 profiles. The lower values obtained with the NBL method were attributed to non-measured intermittent vertical turbulent flux, the possible presence of horizontal advection, and scale differences in flux source areas.

Methane fluxes, on the other hand, were considered invalid because of difficulties related to the sensitivity of measured CH_4 to wind direction. This sensitivity was confirmed by a spatial heterogeneity study performed at both field sites.

Trends in NBL fluxes of CO_2, N_2O, and CH_4 at the Coteau-du-Lac site were examined in terms of the three main bulk structures of the NBL and timing during the field season, revealing an interaction between NBL structure and measured CO_2 and CH_4 fluxes and also between timing of measurement and CO_2 and N_2O fluxes.

Our spatial sampling results show that an important distinction needs to be made in the measurement of 'whole farm' spatially representative gas concentrations, depending on the nature of the source or sink. For CO_2, a GHG of primarily diffuse, homogeneous emission at the field scale, the timing of sample collection (in conjunction with CO_2 NBL profiles) need not have any specific requirement such as a particular wind direction, as long as the landscape patchiness is homogeneous. For N_2O, the situation is slightly different: Depending on moisture conditions, and fertilizer level, anaerobic 'hot spots' may form at different locations, leading to increased spatial variability. Because of the relatively wider overall spatial distribution of emissions, wind direction would be a minor factor in capturing the 'whole farm' representative concentration. The NBL budget method, used in an agricultural landscape of 'homogeneous patchiness' and therefore not necessarily dependent upon constant wind direction, is therefore suitable to measure these gases coming from diffuse sources.

The NBL method, when used at one fixed location, is subject to wind direction change, which results in the inclusion or exclusion of point sources in the upwind source area from one profile to the next. In order to capture all emissions from the farm, downwind gas sampling needs to be maintained as the wind direction changes. This could be done by using a sampling setup which surrounds each point source on the farm, or even the entire farm, such as the mass balance method used, for example, by Denmead *et al.* (1998) and Wagner-Riddle *et al.* (2006). The NBL budget method, then, is not suited to measure GHG from strong point sources.

TABLES

Table 5.1 (see next page). Nitrous oxide (F_{N2O}) and CH_4 (F_{CH4}) fluxes using NBL method. Time intervals rounded to nearest quarter hour. CI 95 is 95% confidence interval, SD is standard deviation. FG means flux gradient-measured data (for N_2O), given as available. Three N_2O values for each night are given: (1) the afternoon prior to NBL measurements (12:00-18:00), (2) the next afternoon, and (3) the next night (21:00-4:30). Exceptions are footnoted. Integration height (h_i) is the height to which bags were filled. – is data not available (for N_2O, *u at* h_i, or for CH_4 where wind direction exceeded 45°). P1 is profile 1. *u* dir is mean wind direction from surface to z ≈ 20 m. Times are average profile times. Nightly flux is given for periods with constant source area type.

Location Date	Time Interval (hh:mm) (EST)	Recent Farm Management Events	Recent Precipitation (Date, mm)	F_{N2O} (NBL) ng m^{-2} s^{-1} ± CI 95	F_{N2O} (FG) ng m^{-2} s^{-1} ± CI 95	F_{CH4} (NBL) µg m^{-2} s^{-1} ± SD	h_i (m)	u at h_i (m s^{-1}) P1, P2	u dir P1, P2
				Ottawa					
June 28-29, 2002	21:15-23:00	N fertilizer applied May 15. Corn planted and 2nd N fertilizer injected May 22. (Neighbouring field: N fertilizer applied May 15; corn planted May 15-22.)	June 26, 13.6 June 27, 46.6	15.6 ± 3.4*	1939 ± 479 292 ± 76 188 ± 57	0.83 ± 0.09	80	3.2, 3.9	N, N
	23:00-0:45			40.9 ± 6.4		-0.34 ± 0.09	80	2.4, 3.2	N, N
	0:45-2:15			–		-0.60 ± 0.09	83	3.1, 3.8	N, N
	0:45-3:30			1.3 ± 2.0		1.24 ± 0.09	82	3.1, 4.5	N, N
	2:15-3:30			–		3.03 ± 0.09	80	3.8, 4.6	N, N
	3:30-4:45			107.1 ± 3.2		-2.93 ± 0.09	76	4.9, 5.8	N, N
nightly flux	23:00-0:45			–		-0.20 ± 0.09	76	2.3, 5.5	
July 18-19, 2002	20:30-22:15		July 17, 15.1	-13.5 ± 1.7	9 ± 10 3 ± 13 27 ± 22	-3.05 ± 0.11	72	3.0, 2.8	WSW, WSW
				Coteau-du-Lac					
June 16-17, 2003	21:30-0:00	Peas planted, N fertilizer applied May 22. (Neighbouring fields: Corn planted and N fertilizer injected May 6/ 7[a], and 18[b]. N fertilizer applied June 15[b], 18[a]. Irrigation for 3 weeks starting ~ June 20 [a].)	June 11-14, 58.4	50.4 ± 1.1	56 ± 18 42 ± 21 189 ± 105	-2.85[d]	76	2.8, 1.1	ENE, NNE
June 17-18, 2003	20:45-22:45			26.1 ± 1.5	42 ± 21[c] 189 ± 105[c] 32 ± 29[c] 43 ± 31[c]	-0.30[d]	80	6.0, 6.8	WNW, NNW
July 9-10, 2003	20:00-21:45		July 7, 0.5	–	23 ± 34 -4.4 ± 64 11 ± 43	-0.87 ± 0.06	74	7.0, 8.1	NNW, ENE
	21:45-0:45			–		0.07 ± 0.06	77	8.1, 5.2	ENE, ENE
	23:30-0:45			16.8 ± 2.4*		–	80	3.4, 5.2	W, NNE
nightly flux	20:00-0:45			–		-0.29 ± 0.06	77	7.2, 5.1	
July 30-31, 2003	20:15-21:30	Peas harvested July 24; Fields levelled July 25, 30.	July 29-30, 1.0	21.2 ± 1.9	63 ± 24 89 ± 29 66 ± 45	-0.29 ± 0.06	71	–	SE, SE
	21:30-23:00			24.7 ± 1.6		-0.02 ± 0.06	71	– , 5.9	SE,SE
	23:00-0:30			37.5 ± 1.7		0.34 ± 0.06	71	5.9, –	SE, E
	0:30-2:45			2.7 ± 1.4		0.83 ± 0.06	70	–, 3.3	E, E
Aug. 18-19, 2003	20:00-22:15	Manure incorporated Aug. 10, 11, cereals planted Aug. 12.	Aug. 16, 0.2	31.8 ± 0.3	87 ± 94 52 ± 34 26 ± 13	0.32 ± 0.07	85	6.1, 7.7	NW, W
	1:15-3:00			11.2 ± 0.3*		–	69	7.3, 5.3	SSE, ENE

a Neighbouring field to north.

b Neighbouring field to south.

c Values for (1) afternoon of June 17, 2003 (prior to NBL measurements), (2) night of June 17-18 (after NBL launches), and (3) afternoon following NBL measurements (June 18), and (4) the next night (June 18-19).

d single sample

***** Fluxes measured in suboptimal NBL conditions (Type 2, stable NBL with non-converging CO_2 profiles). A correction using concurrent or near-in-time detailed CO_2 data based on the difference between the flux calculated up to the CO_2 integration height and up to the bag collection height showed that these bag profiles may have overestimated the N_2O flux by 77% (June 28-29, 2002, 21:15-23:00), 16% (July 9-10, 2003, 23:30-0:45), and 20% (August 18-19, 2003, 1:15-3:00).

Table 5.2. Carbon dioxide fluxes: Comparison of NBL vs. eddy covariance (EC)-measured values at both Ottawa and Coteau-du-Lac sites. STB CONV = very stable upside-down boundary layer with convergent CO_2 profiles, STB NON-CONV = very stable upside-down boundary layer with non-convergent CO_2 profiles, TURBULENT = turbulent layer at surface. CI is the 95% confidence interval.

	EC (mg m^{-2} s^{-1})	NBL (mg m^{-2} s^{-1})	CI-EC (mg m^{-2} s^{-1})	CI-NBL (mg m^{-2} s^{-1})	NBL as % of EC
STB CONV	0.34	0.30	0.06	0.09	88
STB NON-CONV	0.27	0.19	0.03	0.20	69
TURBULENT	0.31	0.13	0.05	0.10	41

Table 5.3 (a) NBL flux data averages from Coteau-du-Lac, 2003, combined for all three observed NBL structures and sorted by month.

	JUNE	JULY	AUG
CO_2 (mg m^{-2} s^{-1})	0.20	0.26	0.18
N_2O (ng m^{-2} s^{-1})	38	16	22
CH_4 (µg m^{-2} s^{-1})	-1.58	0.21	0.11

Table 5.3 (b) NBL flux data averages from Coteau-du-Lac, 2003, combined for the entire season and sorted by observed NBL structure. STB CONV = very stable upside-down boundary layer with convergent CO_2 profiles, STB NON-CONV = very stable upside-down boundary layer with non-convergent CO_2 profiles, TURBULENT = turbulent layer at surface.

	STB CONV	STB NON-CONV	TURBULENT
CO_2 (mg m^{-2} s^{-1})	0.27	0.28	0.11
N_2O (ng m^{-2} s^{-1})	30	17	20
CH_4 (µg m^{-2} s^{-1})	-0.98	-0.22	0.28

Table 5.4. Results from spatial measurements of CO_2, N_2O and CH_4, where ST1 is spatial transect 1 (start time and duration of transects indicated in hh:mm local time). CI 95 is 95% confidence interval, SD is standard deviation, Rep is replicate.

Site/Night/Times	**Gas**	**ST1**					**ST2**				
		Ave. Conc. (ppmv)	**CI 95 (ppmv)**	**SD (ppmv)**	**Rep. % CV**	**Spatial % CV**	**Ave. Conc. (ppmv)**	**CI 95 (ppmv)**	**SD (ppmv)**	**Rep. % CV**	**Spatial % CV**
Ottawa											
June 24-25, 2002	CO_2	388.1	0.5	–	1.1	3.9	415.5	0.8	–	1.9	4.3
21:30 (73 min.)	N_2O	0.37	–	0.02	4.5	18.1	0.36	–	0.01	2.9	5.9
23:15 (41 min.)	CH_4	2.07	–	0.06	2.9	18.0	2.15	–	0.06	2.9	4.0
July 18-19, 2002	CO_2	357.1	0.4	–	0.7	1.1	443.3	0.8	–	1.1	7.1
20:30 (36 min.)	N_2O	0.36	–	0.02	5.0	3.3	0.35	–	0.02	4.5	2.6
23:45 (38 min.)	CH_4	2.97	–	0.06	2.0	19.9	2.55	–	0.11	4.1	11.5
Coteau-du-Lac											
Aug. 18-19, 2003	CO_2	443.1	5.4	–	1.9	4.3	609.2	5.7	–	1.5	7.0
21:30 (25 min.)	N_2O	0.33	–	0.01	2.8	1.7	0.34	–	0.01	2.5	1.0
2:45 (31 min.)	CH_4	2.23	–	0.06	2.6	1.2	2.39	–	0.06	2.3	0.9
Aug. 28-29, 2003	CO_2	n/a	n/a	n/a	n/a	n/a	n/a	n/a	n/a	n/a	n/a
20:45 (23 min.)	N_2O	0.32	–	0.01	2.6	5.3	0.32	–	0.01	3.1	4.3
21:45 (22 min.)	CH_4	2.42	–	0.11	4.4	5.5	2.32	–	0.11	4.9	1.6

Table 5.5. Carbon dioxide concentration (mg m^{-3}) in first 12 m of vertical profile, compared with spatial average at z =12 m, July 18-19, 2002.

	z (m)	20:30	Spatial Ave.	23:45	Spatial Ave.
CO_2 (mg m^{-3})	5	780.1	650.4	932.4	813.5
	6	723.1		869.5	
	7	670.3		810.7	
	8	658.0		775.3	
	9	655.8		763.0	
	10	654.2		760.0	
	11	649.1		764.1	
	12	641.2		766.6	
Average		679.0		805.2	

FIGURES

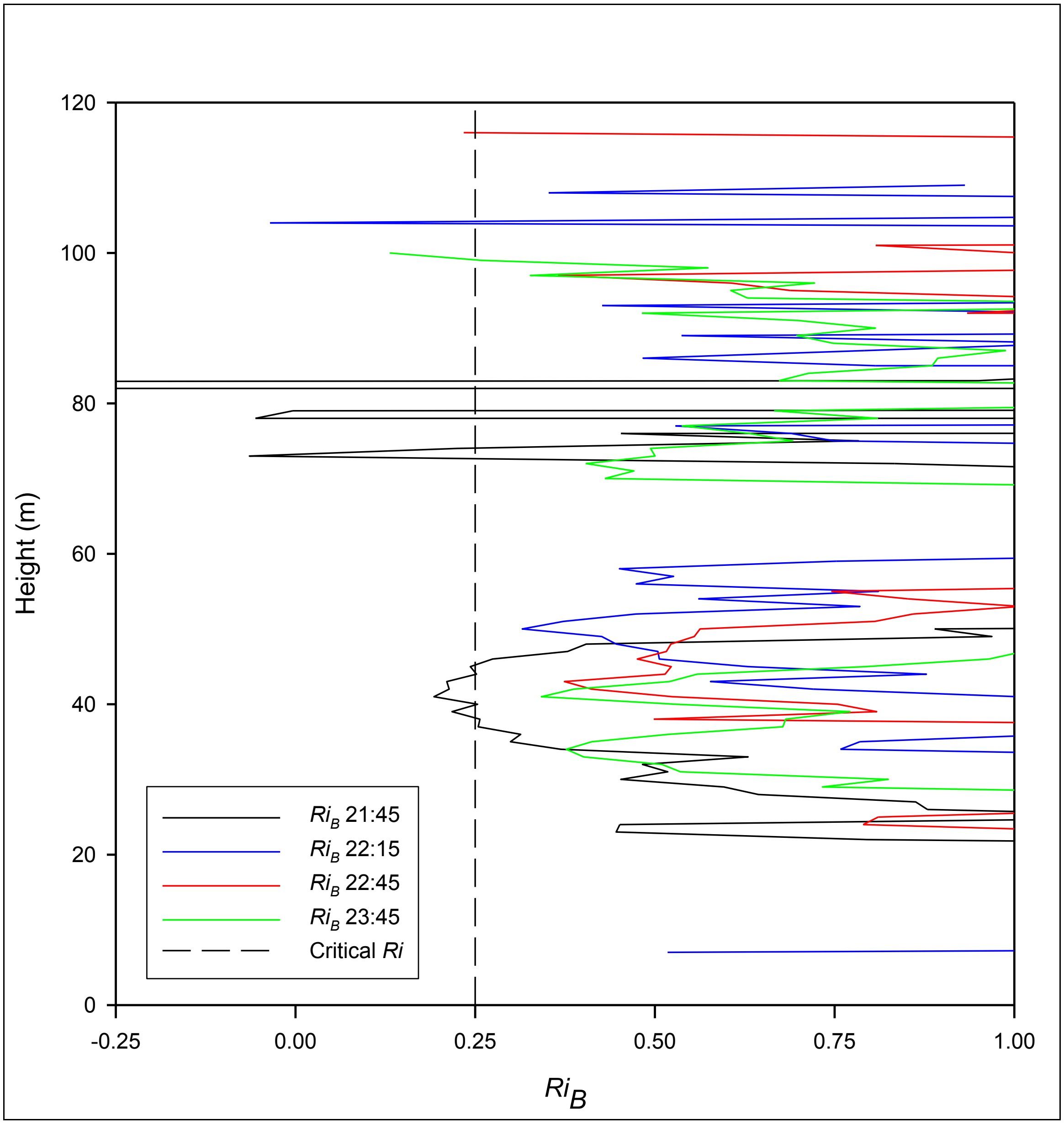

Figure 5.1 (a) Richardson number profiles for July 22-23, 2003, Coteau-du-Lac.

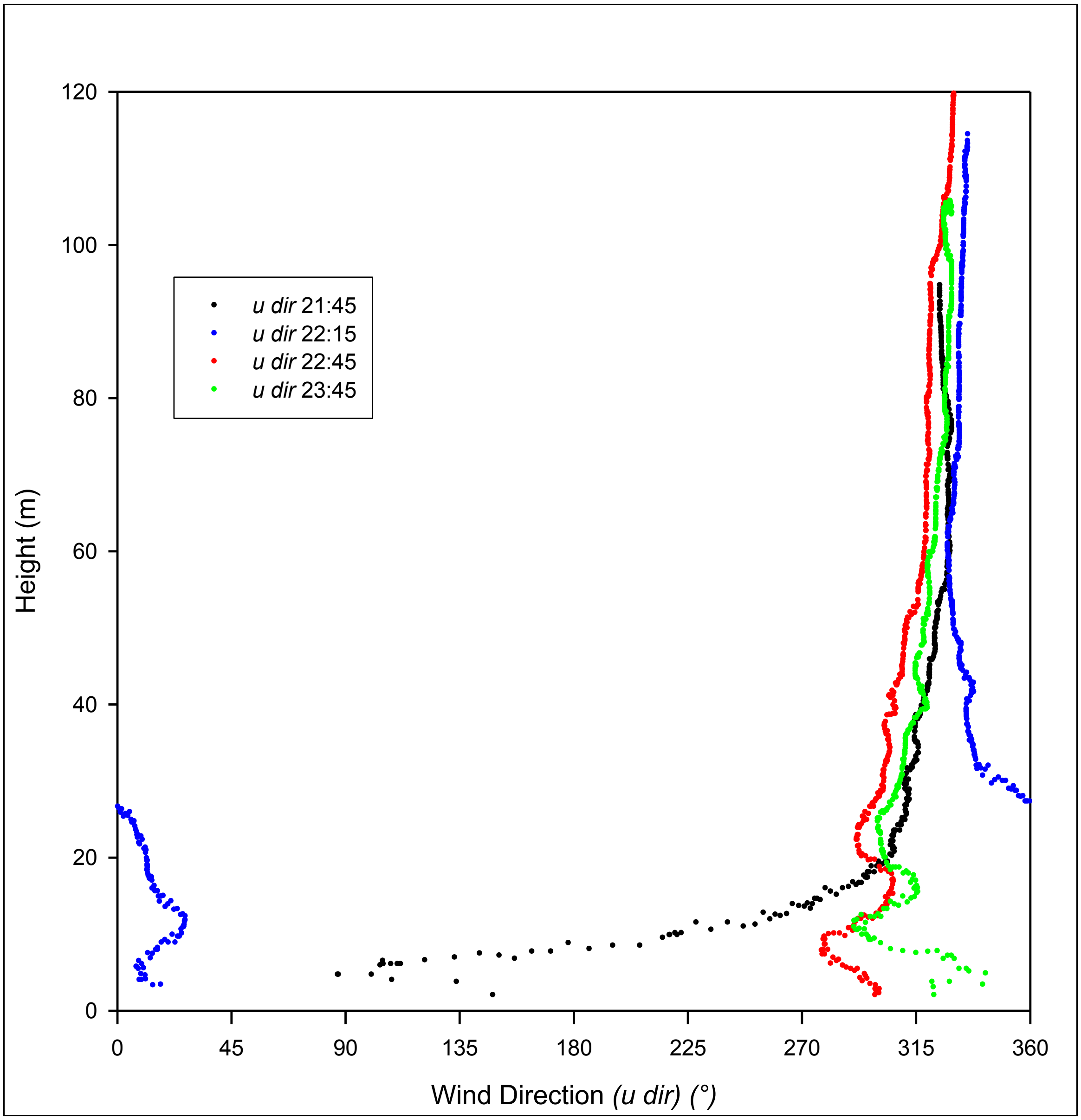

Figure 5.1 (b) Wind direction profiles, July 22, 2003, Coteau-du-Lac.

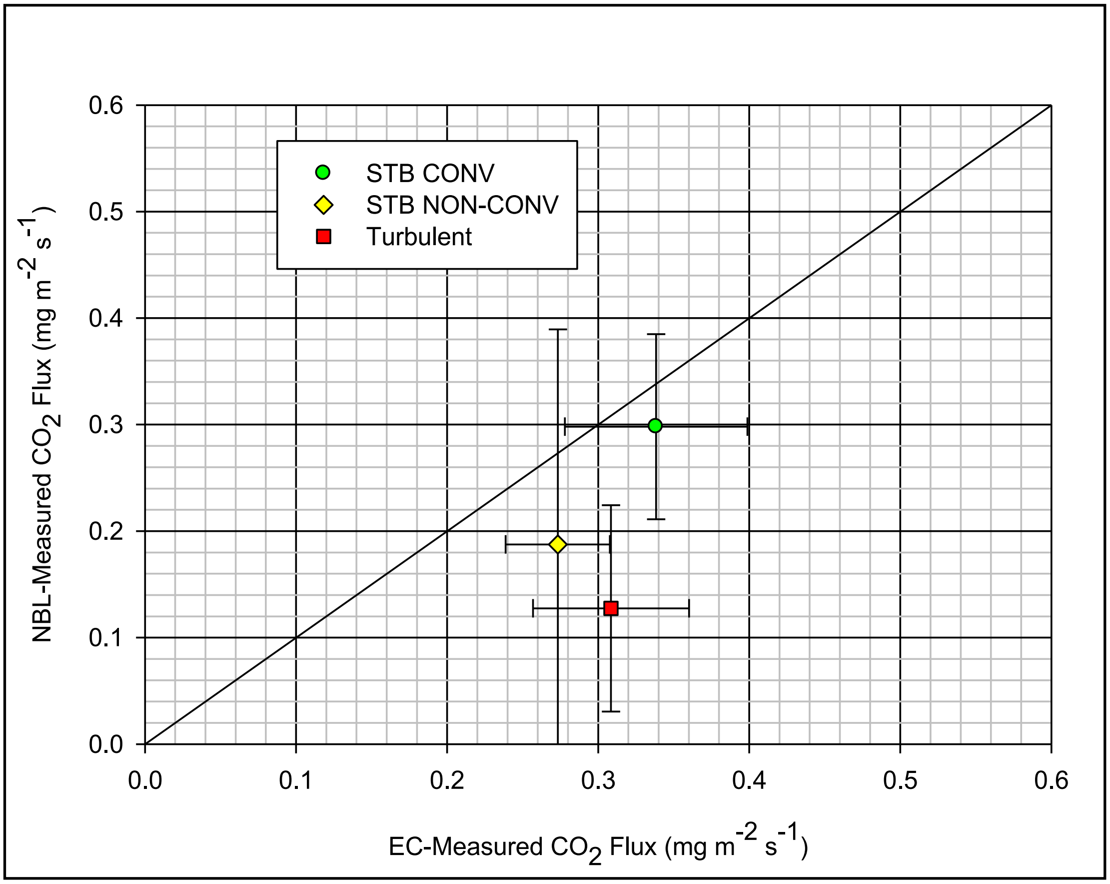

Figure 5.2 Comparison of NBL- and eddy-covariance (EC)-measured CO_2 fluxes plotted with 1:1 line. Error bars are 95% confidence interval. STB CONV = very stable upside-down boundary layer with convergent CO_2 profiles, STB NON-CONV = very stable upside-down boundary layer with non-convergent CO_2 profiles, Turbulent = turbulent layer at surface.

Figures 5.3 (a)-(c). Diagram depicting layout of spatial sampling at experimental site (approximately 450 × 600 m) at CFIA Farm, Ottawa, ON, Canada, June-July 2002. Star indicates blimp launch site. Dots indicate spatial sampling points. Striped triangle is location of manure pile, sheep in pentagon shape is sheep housing. Numbers in boxes at each sampling point indicate GHG concentrations. Top number is for first transect, bottom number is for second transect. Mean wind speeds and mean wind directions (dashed arrows in compass roses) are given for each transect (u_1 for ST1, u_2 for ST2). See Section 5.3.1 for explanation of wind direction. Times are given in Table 5.4.

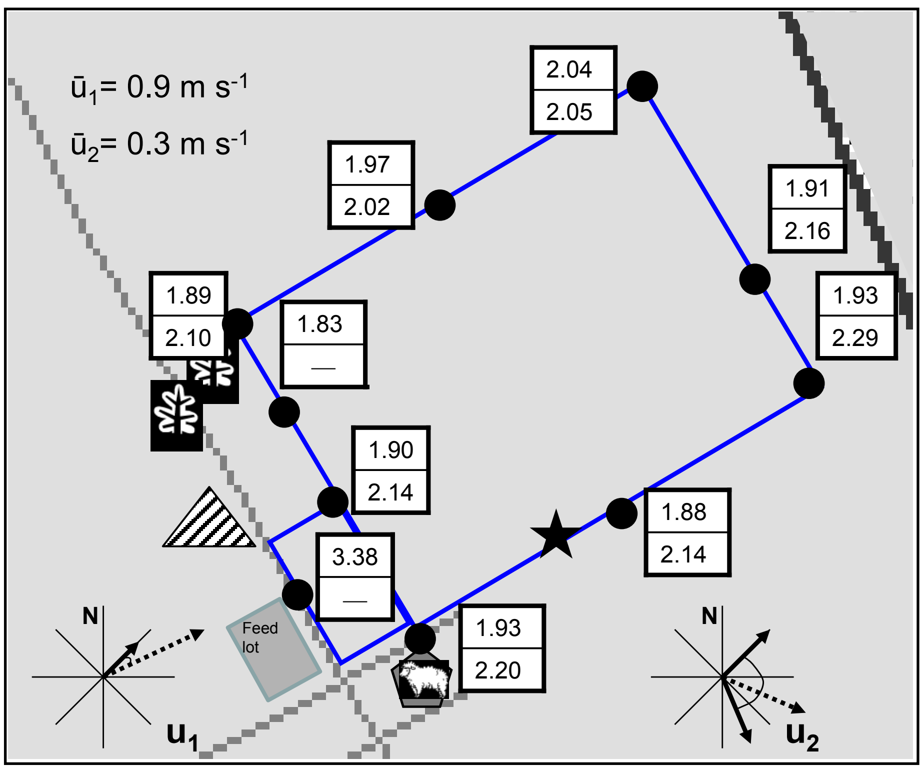

Figure 5.3 (a). Methane sampling at Ottawa site, June 24-25, 2002 (± 0.06 ppmv).

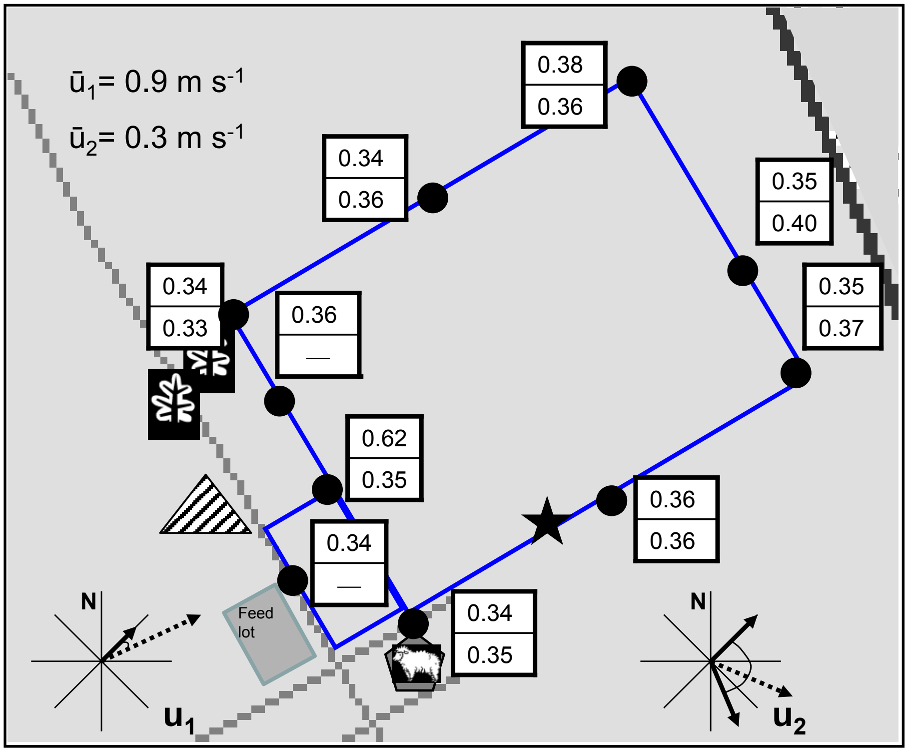

Figure 5.3 (b). Nitrous oxide sampling at Ottawa site, June 24-25, 2002 (± 0.01 ppmv).

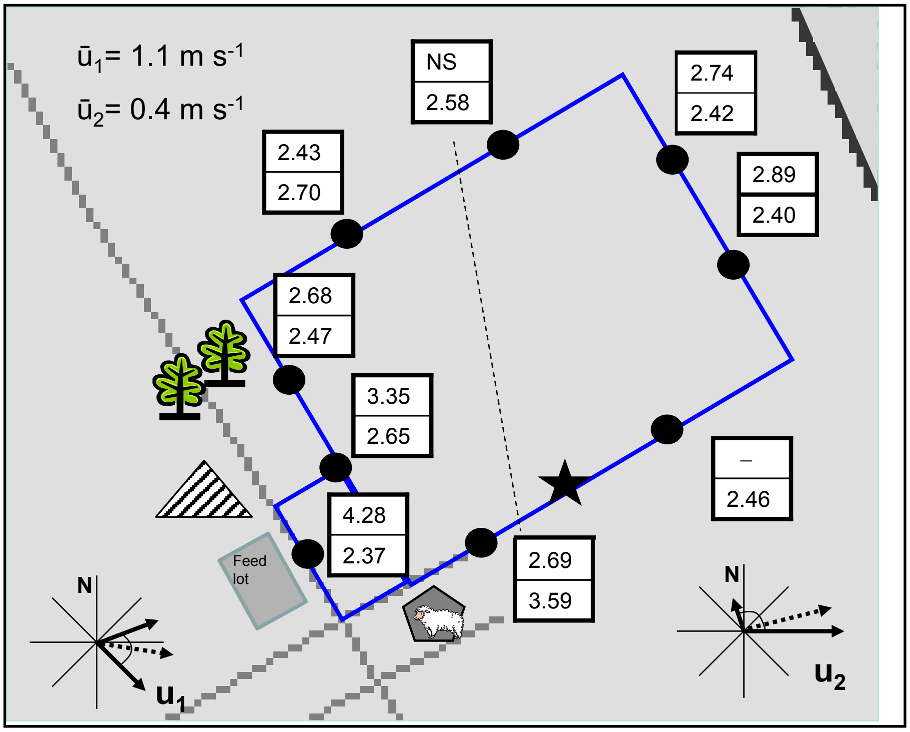

Figure 5.3 (c). Methane sampling at Ottawa site, July 18-19, 2002 (± 0.06 ppmv).

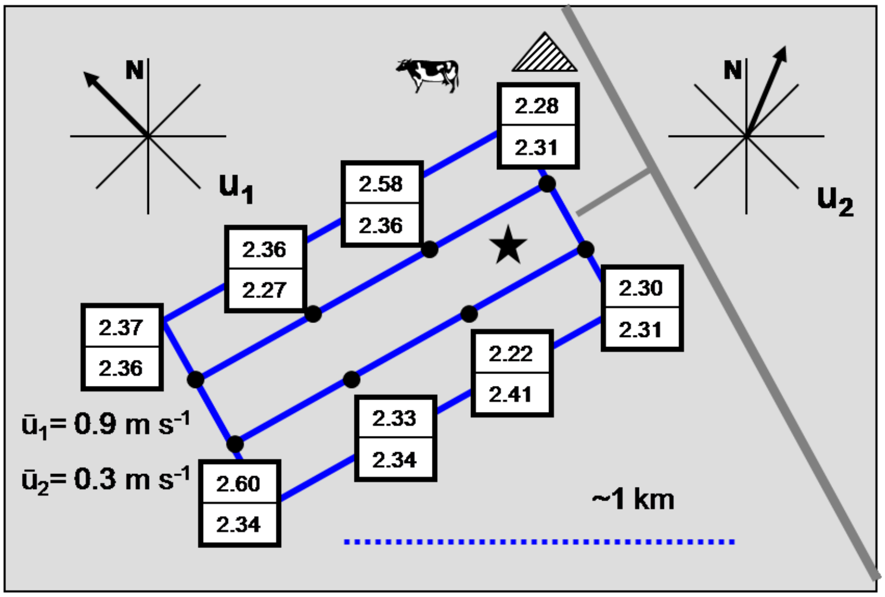

Figure 5.4. As in Figure 5.3 but for Coteau-du-Lac field site (240 × 1000 m). Cow indicates location of cattle housing. Numbers in boxes at each sampling point indicate CH_4 concentrations (+/- 0.06 ppmv) measured night of Aug. 28-29, 2003.

6. A 'BOTTOM-UP' VERIFICATION OF THE NBL BUDGET METHOD

6.1 INTRODUCTION

Chapter 5 provided preliminary ground-based verification of the NBL budget method using knowledge of ground-based methane point sources and detailed vertical profiles of methane concentration in an agricultural region of western Quebec, Canada.

However, the NBL-measured fluxes warrant more in-depth analysis. This can be done by comparing the values obtained by the 'top-down' NBL budget approach and corresponding ground-based, 'bottom-up' estimates. A 'bottom-up' approach has been defined by Bouwman *et al.* (1999) as the extension of 'calculations from an easily measured and reasonably well-understood unit to more encompassing processes'. A 'top-down' approach, on the other hand, is essentially the use of measurements at a higher scale to provide an integrative total which can be used as a constraint for smaller-scale flux estimates (Bouwman, *et al.,* 1999). Here, we will use a 'bottom-up' approach for scaling ground-based trace gas fluxes, comparing these results to those obtained using a 'top-down' approach as measured by the NBL budget method.

Aggregation or area-averaging of surface variables (*e.g.,* roughness length, Hasager and Jensen, 1999) or fluxes (*e.g.,* momentum, heat, or CO_2 flux) at small scales to yield large-scale regional estimates is usually necessary and commonly applied in the field of regional and global modeling of these processes over monthly or annual time scales (Bouwman, *et al.,* 1999). These studies use, for example, satellite imagery to determine areal proportions (*e.g.,* Roulet *et al.,* 1994; Kim *et al.,* 2006; Peng *et al.,* 2008). A mosaic or 'tile' approach can be used, where fluxes from different land-use classes are summed by arithmetically-weighting according to fractional proportion of a pre-defined regional area (*e.g.,* Roulet *et al.* 1994, Halldin *et al.,* 1999; Beyrich *et al.,* 2002, 2006;

Jochum *et al.,* 2006). Other studies have used footprint models to identify source areas of fluxes and to determine levels of contribution within this source area and associate these with mapped locations of land-use classes or vegetation types (*e.g.,* Ogunjemiyo *et al.,* 1999; Kim *et al.,* 2006; Griffis *et al.,* 2007; Chen *et al.,* 2008)

We use a combination of these two concepts: Ground-based flux estimates of CO_2 and N_2O obtained for a collection of individual areas within a relatively local footprint-defined area in an agricultural landscape were aggregated and compared to the larger-scale flux measured by the NBL method. Ground-based fluxes of CO_2 and N_2O were estimated from field measurements and literature data as well as IPCC emission factors. In the cases presented, the flux footprint distance for the NBL flux integration height, predicted by a Lagrangian-type model, was on the order of 1.5 to 4 km and the time scale, the time between profiles, was one to two hours.

The weighting of the contribution of individual areas within the total source area to the measured flux is done by weighting the different land-use sectors in the source area according to the flux footprint function with respect to their proportion within the footprint, taking into account the change in source area with increasing height. Similar approaches have been attempted previously. Soegaard *et al.* (2000; 2003) compared modelled respiration estimates from individual fields to areally weighted EC measurements of the same region. Gockede *et al.* (2004) and Rebmann *et al.* (2005) conducted a quality assessment of EC sites in the FLUXNET program which involved identifying the footprint of respective EC sites and weighting specific land use types and roughness elements. Reth *et al.* (2005), in a related study, scaled up chamber measurements from individual areas to compare with EC-measured fluxes. Neftel *et al.* (2008), using a bottom-up/top-down-type comparison, have developed a simple model for calculating fluxes from individual parts of a varied source area measured by EC towers. Gottschalk *et al.* (1999) compared mast measurements with area-averaged fluxes measured by aircraft. Griffis *et al.* (2007) explored the isotopic composition of ecosystem respiration by comparing flux gradient and mixing model approaches. Peng *et al.* (2008) apportioned heat fluxes to upwind source areas and Chen *et al.* (2008) investigated local and more distal contributions to concentration-profile-derived fluxes measured from tall towers. The current study is the first formal attempt to use ground-based evidence to support fluxes measured by the NBL budget method.

6.2 MATERIALS AND METHODS

6.2.1 Source Area Mapping

Information on the actual distribution of different crop/vegetation types in the area surrounding each NBL launch site was obtained from staff at Agriculture and Agri-Food Canada for the Ottawa site (2002) and from the private producer at the Coteau-du-Lac field site (2003). Similar to Göckede *et al.* (2004) and Rebmann *et al.* (2005) who also used a topographical map to obtain information for their footprint analysis, respective information from this study was plotted on an aerial photo of the Ottawa site (1: 21 500) and on a scaled map (1:20 000) of the Coteau-du-Lac region. While some studies have used satellite images to characterize a source area, Soegaard *et al.* (2000) pointed out that the coarser resolution of some of the less expensive commercially available images (equivalent to a scale of 1:45 000) are not suitable for study areas of small size as pixels may include more than one land-use type. Alternatively, high resolution satellite images such as QuickBird or IKONOS with spatial resolutions of 0.6 and 0.8 m representing a scale of 1:15 000 may be used, but as Kim *et al.* (2006) pointed out, these images can be fairly costly. The advantage of using a satellite image is the ability to digitally delineate homogeneous zones and to determine their contribution to the flux by overlaying the footprint function. However, while less precise, it is considered that the use here of a topographical map and aerial photo paired with assignment and proportioning of different crop/vegetation areas based on visual inspection, was convenient, inexpensive, and provided an adequate scale.

6.2.1.1 Farmland and Crops in Ottawa and Coteau-du-Lac Regions

Visual field scrutiny and farm records were used to determine the usage of as much of the agricultural land within the footprint as possible. For any remaining areas, statistical data was used to classify them into different crop types. According to Canada's 2001 agricultural census (Statistics Canada, 2004), 43% of the total land area of the Ottawa, Ontario, census subdivision (consisting of the greater Ottawa area, 2 779 km^2) was farmland (120 452 ha). Of this, 67% was in crops and 17% in pasture. The distribution of crops on farmland was 40% hay (barley, alfalfa, and other forage crops), 31% corn, and 16% soybean, with the remainder consisting mainly of wheat, oats, and mixed grains (Statistics Canada, 2004). Based on this crop distribution, areas of cultivated farmland located within the CFIA footprint with unknown crop type were assigned proportions of 50% hay, 35% corn, and 15% soybean, which corresponded well with the proportions of known crops and knowledge of other fields in the area. Although the experimental farm does tend to have a higher proportion of corn and soybean, rather than hay, the exact proportions were unknown and so the overall Ottawa farm proportioning was retained.

In the Vaudreuil-Soulanges county of Quebec, the area in farmland was 50 741 ha, about 59% of the total area for this census division (856 km^2) (Statistics Canada, 2004). Within Vaudreuil-Soulanges county, the subdivision of Coteau-du-Lac had a total area of 47 km^2, with 56% of this area in farmland (2645 ha) (Statistics Canada, 2004). Of the total farmland, 83% was in crops and 4% in pasture (Statistics Canada, 2004). The proportions within the cropped farm land were 47% corn, 22% hay (barley, alfalfa, and other forage crops), 21% soybean, and 5% consisting mostly of vegetables (sweet corn, green peas, cabbage), wheat, oats, and mixed grains (Statistics Canada, 2004). This distribution, with corn dominating the landscape, corresponds with the distribution of known crop fields around the Coteau-du-Lac field site. For simplicity, portions of the Coteau-du-Lac footprint with cultivated agricultural land of unknown crop were assigned 50% corn, 25% hay, and with the remaining 25% a combination of soybean and assorted vegetables.

6.2.2 Methods of Obtaining GHG Flux Estimates

Estimates of fluxes from sources within the CFIA and Coteau-du-Lac footprints were obtained using field data (ideally measured near-in-time) and where these were unavailable, literature values and/or IPCC emission factors were used (Environment Canada, 2006; 2008; IPCC, 2006). The GHG flux estimates used in the footprint aggregation, as well as the original sources of all estimates, are given in Table 6.2a.

6.2.2.1 Field-Based Estimates

Field-scale fluxes for corn, peas, and hay measured by eddy covariance (CO_2) and flux gradient (N_2O) methods at the same or similar sites were available for comparison to

NBL-measured fluxes. Data were taken from windy nights and where environmental conditions and crop growth stage were closest to those at the time of NBL measurement.

A small part of the footprint plotted for the 3:30-4:45AM NBL profiles on the night of June 28-29, 2002, at the Ottawa site extended into the surrounding suburban neighbourhoods. Summer nighttime CO_2 flux data from a suburban Montreal site with population density similar to Ottawa population density was also included in the analysis for the night of June 28-29, 2002 (Table 6.2a) obtained with permission from the Environmental Prediction in Canadian Cities (EPiCC) Network (2009). Fluxes were obtained at a private residence in the Roxboro-Pierrefonds area at a measurement height of approximately 25 m. Data used for the analysis were from nights of temperature similar to that of June 28-29, 2002, with a u_* of at least 0.3 m s^{-1}. Traffic count information was not available for the Montreal suburban area but was assumed to very low, with the suburban vegetation principally responsible for positive CO_2 fluxes through nighttime respiration.

6.2.2.2 Literature-Based Estimates

Published nocturnal flux data were selected with particular attention to environmental conditions and crop growth stage. For CO_2 flux estimates from agricultural or forested land, published soil or air temperature relationships with nighttime soil respiration were also used. Literature-based estimates of suburban CO_2 fluxes were also included in the analysis (Table 6.2a).

In general, considerably more flux data are published for corn as opposed to hay (grasses and forage crops), barley, peas, and other vegetable crops (*e.g.,* cabbage, peppers). For the portion of the footprint designated as a vegetable crop (July 9-10, 2003),

CO_2 fluxes for soybean were used due to the lack of available data for vegetables. Although soybean is a legume it was found in 21% of Vaudreuil-Soulanges farms in 2001 (Statistics Canada, 2004). This is not considered to have had a large impact on the flux aggregate as this portion was only 6% of the aggregate total.

6.2.2.3 IPCC Emission Factors

The estimation of total GHG emissions by applying a GHG emission factor (EF) per activity unit constitutes a 'bottom-up' approach (Bouwman *et al.,* 1999) and forms the basis of the IPCC (Intergovernmental Panel on Climate Change) methodology for individual countries to assess their GHG emissions (IPCC, 2006). This methodology aims to make it as simple as possible to compile the information required and to perform the necessary calculations to obtain GHG emissions estimates. Essentially, a participating country needs only to determine the activity data of a particular GHG from a particular process in a particular sector, be it transportation, agriculture, or forestry, *etc.* The IPCC has determined default (Tier 1) emission factors from available scientific data. As a result, individual countries may simply multiply their total activity units by the appropriate default emission factor to obtain the total emission of a particular GHG from a particular process.

If a country wishes to tailor the system of activity data and emission factors to its particular situation (*e.g.,* its unique climate, ecosystems, agricultural or industrial processes, *etc.*) it may modify the IPCC methodology accordingly, for example, creating new source categories and using custom emission factors, therefore increasing the level of complexity to Tier 2 (intermediate) or even Tier 3 (highest). The modified methodology must be published and changes to the original methodology made transparent. The result is a more accurate and more precise GHG inventory for that particular country.

Nitrous oxide fluxes from crops were estimated using an ecodistrict-specific Tier 2 emission factor (Environment Canada, 2007). An example of this calculation is shown in Table 6.2b. Total N input (kg N ha^{-1}) was estimated using recommended fertilizer input values for each crop, as well as estimates for N input from crop residue or information from the private producer. Each value for total N input was then multiplied by the ecodistrict-specific emission factor, the result giving the total N_2O emission for the frost-free season (April to October, according to climate normals). Indirect emissions of N_2O from leaching and volatilization were also estimated for N from synthetic fertilizer and manure application using the appropriate emission factors (Table 6.2b), which incorporates emissions from drainage ditches and rivers. In order to compare with NBL-measured fluxes, the total seasonal N_2O output (direct and indirect emissions) was then converted to ng N_2O m^{-2} s^{-1}. It is understood that this average value does not reflect a real-time response of the farmland, which in reality varies greatly over time and space.

As daytime CO_2 and N_2O flux estimates from vehicular traffic going into and out of the city of Ottawa, calculated using Tier 2 IPCC emission factors (Environment Canada, 2006, see Appendix E) were very low (0.06 mg CO_2 m^{-2} s^{-1} and 5.5 ng N_2O m^{-2} s^{-1}), it was assumed that because traffic from 3:00 to 5:00 is extremely low that nighttime fluxes from this source for the portion of the June 28-29, 2002, footprint falling on a suburban Ottawa area were negligible (Table 6.2a).

6.2.3 NBL Data

This section gives information about the nights for NBL fluxes used in this analysis. Methods for NBL data collection are as described previously in Chapter 4. NBL data used in this analysis are from the nights of June 28-29, 2002 (Ottawa, ON), June 17-18, 2003, and July 9-10, 2003 (Coteau-du-Lac, QC). Profiles from these nights were chosen for this analysis because they had a relatively constant wind direction both over time and height, from one profile to the next and from the surface to the top of the profile. On two of the three nights CO_2 was measured concurrently with N_2O.

6.2.3.1 Ottawa, ON, June 28-29, 2002— 23:00-0:45 (CO_2 and N_2O) (Figure 6.1a)

This exponentially-shaped profile pair showed peaks in wind speed at $z \approx 32$ m for both profiles with CO_2 convergence at approximately the same height (Figure 6.1a). The turbulence structure was that of a very stable upside-down boundary layer (stable surface layer with elevated turbulence) with peaks in *Ri* at the same heights as the wind speed maxima. Nitrous oxide fluxes were available for this period as well. The average concentration of N_2O from the surface to 80 m was measured collecting air samples over the vertical profile in bags (Pattey *et al.,* 2006b) for each of these profiles concurrently while the CO_2 was being measured. Because these were not detailed profiles of N_2O, it is assumed that N_2O was capped in the same fashion as CO_2 and that the interval above the height of CO_2 convergence had no effect on the flux calculation. The combined average wind direction for these profiles was 351°, with an overall standard deviation of 9°. The surface air temperature at 21:00 was approximately 20°C and decreased to 14.4°C by 4:30.

6.2.3.2 Ottawa, ON, June 28-29, 2002— 3:30-4:45 (CO_2 and N_2O) (Figure 6.1b)

This profile pair clearly exhibited the structure of a very stable upside-down boundary layer distinguished by the presence of a well-defined low-level nocturnal jet, whose maximum was at z = 65 m (Figure 6.1b). Carbon dioxide profiles demonstrate a clear convergence at this height and this was the chosen integration height. The combined average wind direction for these profiles was 338°, with an overall standard deviation of 8°. Nitrous oxide was measured for these profiles as well.

6.2.3.3 Coteau-du-Lac, QC, June 17-18, 2003—20:45, 21:45, 22:30 (CO_2 and N_2O) (Figure 6.1c)

Detailed CO_2 profiles were measured in all flights, with N_2O being measured concurrently in the 20:45 and 22:30 profiles by collecting air into sampling bags. Here, the NBL exhibited changes in structure with regards to Richardson number throughout these three profiles (Figure 6.1c). As a result, although wind speeds were comparable, CO_2 accumulation was less. The 20:45 profile exhibited a very stable upside down boundary layer. The 21:45 Ri profile showed surface mixing up to z = 10 m with subcritical Ri values. It is assumed that following this disturbance there was an upward migration of surface gases. As a result, the 22:30 CO_2 profile converged with previous profiles at a height of approximately z = 75 m.

The 20:45 and 21:45 CO_2 profiles demonstrated convergence at $z \approx 40$ m but in each profile $\Delta CO_2/\Delta z$ approached zero (less than -0.2 ppm m^{-1}) at $z \approx 49$ m. The latter height coincided with a strongly stable region ($Ri > 1$) in the 21:45 profile (z = 46 to 58 m) exhibiting a u maximum at z = 52 m. The flux calculated anywhere in this height interval yielded the same result, so the integration height chosen for these two profiles was $z = 46$ m (the start of the strongly stable region, closer to the convergence height).

We used the footprint for the 20:45-21:45 profiles for the 21:45-22:30 N_2O flux measurement footprint to avoid overestimating the upwind source area which could occur if we used the $z = 75$ m convergence height from the 22:30 profile (as it is thought that the gases accumulated to $z = 75$ m are the same that accumulated to $z = 40$ m but migrated upward). This is justifiable because the wind directions are virtually unchanged (average direction 262°), with an overall standard deviation of 8°. The surface air temperature at 21:00 was 19°C and decreased to 15.6°C by 4:30.

6.2.3.4 Coteau-du-Lac, QC, July 9-10, 2003—19:30-20:45 (CO_2 only) (Figure 6.1d)

Ri profiles for this night showed a mixed layer at the surface at 19:30 which then progressed to a very stable upside-down boundary layer by 20:45 (Figure 6.1d). While there was accumulation of CO_2, it was less than usual and profiles converged to within 1 ppmv at $z \approx 63$ m. Wind speeds were slightly higher than usual and u maxima were in the form of peaks in wind speed which stayed steady and then increased again with height. As a result, while there were intervals where Ri was greater than 1, shear was almost always present. In the 19:30 and 20:45 profiles, $Ri > 1$ at $z \approx 56$ m in both profiles. While $\Delta CO_2/\Delta z \approx 0$ in the second profile (20:45) occurred at $z \approx 42$ m, 56 m was chosen as the integration height as it was closer to the height of convergence. The wind direction (overall average 343°) was quite steady, with an overall standard deviation in wind direction ranging of 8°. The surface air temperature was much cooler than usual, 14.4°C at 21:00 decreasing to a minimum of 10.25°C.

6.2.4 Footprint Model Description, Assumptions, and Simplifications

The convenient on-line flux footprint parameterization of Kljun *et al.* (2004) (see also Chapters 2, 5) was used to give the distance from which 80% of the total contribution was made, at a given measurement height z_m. A basic description of the model, its input parameters, and the estimation of lateral distance were described in Chapter 5.

Göckede *et al.* (2004) give a good analysis of the assumptions, limitations, and possible errors involved in scaling up using a simple analytical footprint model (using Schmid's (1994, 1997) FSAM model in particular) for a heterogeneous source area. These involve, briefly, the effects of changes in roughness length across changing land use types and the effects of topography and advection.

Göckede *et al.* (2004) and Rebmann *et al.* (2005), in their footprint weighting for fluxes measured by EC, apportioned respective roughness lengths to individual portions (matrix cells) of their footprints, as surface roughness changes from one vegetation type to the next can have an effect on downwind diffusion patterns (Oke, 1987). Hasager and Jensen (1999) emphasized the importance of the effect of varying roughness lengths throughout a source area on aggregation results. Here, though, we simplify by using a composite value of roughness length for the entire footprint area. With increasing profile height, the effect of roughness change is less important as the roughness scale relative to the measurement height becomes smaller (Schmid, 1997). This means that the NBL footprint for measurement heights near the surface is more influenced by changes in roughness length, but we cannot characterize this without a footprint model with more flexible and comprehensive input procedures, as done with FSAM (Schmid, 1994; 1997) by Göckede *et al.* (2004; 2005; 2006) or Rebmann *et al.* (2005).

It is also assumed here that there is a uniform flux within each land use type (Göckede *et al.,* 2004). Other limitations and assumptions regarding the use of Kljun *et al.*'s (2002) model and others are as given in Chapters 2 and 5.

6.2.4.1 Footprint Parameterization Output

The on-line flux footprint parameterization of Kljun *et al.,* 2004, yields results in the form of a non-dimensional master footprint function and a real-scale footprint function, with the distances, in metres, given for the locations of maximum contribution, x_{max}, and the far end of the footprint. It then gives a plot showing the distribution of relative contribution. The values for the plot are supplied, consisting of the upwind distance x (m) and the crosswind-integrated footprint $f^y(x)$ (m^{-1}).

In contrast to the footprint pattern for convective conditions, attempts to model a flux footprint in weakly stable conditions or lower roughness length at the same measurement height show that while the majority of the contribution is still closest to the measurement location, it is spread over a significant distance with the remainder spread over an even larger distance (*e.g.,* Leclerc and Thurtell, 1990; Kljun *et al.,* 2002).

The flux footprint parameterization of Kljun *et al.* (2004), run with u_* of 0.2 m s^{-1}, a constant z_m of 30 m, and a varying roughness of 0.05 and 0.2 m showed this same pattern, with the footprint for the lower roughness extending farther (Figure 6.2a). If we consider again that this model is not optimized for very stable conditions, where, for example, u_* (friction velocity) can be below 0.1 m s^{-1} and σ_w (variation in vertical velocity) below 0.07 m s^{-1}, the contribution in these stratified atmospheric conditions is, in actuality, almost certainly spread even more evenly, over an even larger distance. The 50%-level contribution region comprised almost the entire 80% footprint, with the exception of the extreme near-field and slight downwind influence (an artifact of the simulation derived from stochastic particle movement) (Figure 6.2a). While absolute distances were different for each case (including an additional run with z_m = 10 m) (Figure 6.2a), when normalized with respect to total footprint distance the shape of the 50%-level contribution spread between the two ranges was identical (Figures 6.2b).

From this common pattern it could also be determined that for all footprints, the region of the footprint contributing at least 90% of the maximum (*i.e.,* the 90%-level contribution) was located in the interval of approximately 29% to 65% of the total footprint distance (Figure 6.2b).

Interestingly, for very stable upside-down boundary layer conditions, the vertical distribution of flux in the NBL profile tends to resemble that of the footprint function, with the greatest change in concentration occurring near the surface and decreasing with height (see flux distribution in Figure 5.2). Associating the flux within each of the five vertical profile segments with its respective footprint (Section 4.6) can also provide an approximation of how much of the total flux comes from what upwind distance.

6.2.5 Weighting of Source Area and Flux Aggregation

The NBL-measured flux was derived from detailed vertical profile measurements taken from the surface to the NBL height and not just a measurement at a single height at the top of the NBL. The blimp was therefore measuring the flux from different upwind source areas as it ascended in the NBL. In order to be able to partially account for the change in source area due to increasing measurement height and variations in wind direction as the blimp ascended, the vertical profile was divided into five equal segments reflecting height intervals from the surface to the NBL integration height (0.2 h to 1.0 h) with a corresponding total footprint area (see Chapter 5).

For each night/case, then, the flux footprint model was run for each height of the five segments of the vertical profile. The five individual footprints for each night/case were then combined to obtain one cumulative footprint representing the increase in source area as the tethered blimp ascended.

To achieve this, first, for each individual footprint 0.2h to 1.0h, the relative contribution with respect to the maximum contribution (x_{max}) was determined for each upwind distance x by:

$$Relative\ contribution\ (x) = \frac{f^y(x)}{f^y(x_{max})} \tag{6.1}$$

The footprint distances with their respective relative contributions were then plotted for the interval where the footprint was contributing at least 50% of x_{max}. A quadratic equation was fitted to each respective curve (r^2 = 0.999 in all cases); this equation was then used to obtain the relative contribution in all five footprints along common, 5-m increments, starting at the minimum 50%-level distance indicated by the first footprint (0.2 h). The cumulative footprint was then obtained by summing the relative contribution at each 5-m interval and dividing this by the maximum possible weight (5):

$$Cumulative\ footprint = \sum_{i=0.2h}^{1.0h} \frac{Relative\ contribution\ (x)}{Relative\ contribution\ (x_{\max})} \tag{6.2}$$

A plot of a cumulative footprint obtained following this procedure is shown in Figure 6.3. The cumulative footprint would be smoother if the footprint segments were smaller, for example, every 0.1 *h* instead of 0.2 *h*.

In order to visualize the proportion of sources contributing to the measured NBL flux, the cumulative footprint was overlaid on a map of each respective study area (Figures 6.4 (a) to (d)). The footprint was divided into weighted segments of 0-0.20, 0.20-0.40, 0.40-0.60, 0.60-0.80, and 0.80-1.00-0.80, 0.80-0.60, 0.60-0.40, 0.40-0.20, and 0.20-0 (a total of nine segments) (Table 6.1), following the rise in relative contribution from the beginning of the footprint to x_{max} and the decline in contribution toward the distal end of the footprint, in order to illustrate the relative contribution of different areas of the footprint. The plotted footprint was then visually examined and the fractional area of each source within each footprint-weighted segment was assigned (Table 6.1).

The total cumulative footprint flux estimate for each greenhouse gas was then obtained by summing the area-weighted contribution of all sources within each footprint-weighted segment of the total footprint:

$$Total\ footprint\ flux = \sum_{i=1}^{9} \sum_{j=1}^{n} \overline{weight_i} \cdot area_j \cdot flux_j \tag{6.3}$$

where $\overline{weight_i}$ is the mean footprint weight (normalized with respect to the total weight) for each footprint segment *i* (1 to 9), $area_j$ is the proportional area of each source *j* within each footprint segment *i,* and $flux_j$ is estimated flux for each source *j* found within each footprint segment *i*.

6.3 RESULTS AND DISCUSSION

6.3.1 Footprint-Aggregated Flux vs. NBL-Measured Flux

Footprint maps showing the flux-aggregated areas are provided in Figures 6.4 (a) through (d). Flux values from the two methods are summarized in Table 6.3.

6.3.1.1 Ottawa, ON, June 28-29, 2002—23:00-0:45 (Figure 6.4a)

In this example, the footprint extended to approximately 2.1 km upwind and included fields of corn and hay, and an area of cultivated farmland of unknown crop (Figure 6.4a).

The aggregated ground-based flux estimate for CO_2 (0.14-0.25 mg CO_2 m^{-2} s^{-1}) was greater than the NBL-measured value of 0.07 mg CO_2 m^{-2} s^{-1} (Table 6.3). The range in the aggregated flux estimate reflects the ranges in CO_2 flux estimates for corn and hay, which represent 44% and 32% of the total footprint, respectively (Table 6.2a). The NBL-measured flux was almost as low for the next set of profiles on this night, from 0:45-2:15 (0.09 mg CO_2 m^{-2} s^{-1}), with the same wind direction. The reason for these lower-than-average NBL-measured fluxes is not clear; Richardson number profiles for the time period of 23:00 to 2:45 (*e.g.,* Figures 5.1b and 6.1a) show that there were consistent, highly stable conditions at the surface with some occasional shear above, on the far upper side of the capping wind speed maximum. SODAR data (Mathieu *et al.,* 2005) showed only slight fluctuations in NBL height over this time period. Eddy covariance measurements, while not available for this extremely calm night, generally tended to show variable fluxes on nights with variable $u*$ and/or σ_w, but as these were both consistently close to zero throughout the night, this still does not explain the lower-than-average flux. Another possibility is advection: the 0:45 profile exhibited a small wind speed maximum between the heights of approximately 8 and 15 m (Figure 6.1a), which may have resulted in the transport of CO_2 out of the area. In fact, CO_2 concentrations closest to the surface dropped from 23:00 to 0:45 (Figure 6.1a) and did not increase from 0:45 to 2:15 (Figure 5.1b). Concentrations increased once again with the onset of the LLJ (Figure 5.1a). In any case, the NBL-measured values for the period of 23:00 to 2:15 are likely underestimating soil and plant respiration on this night.

On the other hand, for N_2O, the aggregated flux (16-21 ng N_2O m^{-2} s^{-1}) was smaller than the NBL-measured flux of 41 ng N_2O m^{-2} s^{-1} (Table 6.3). This may be because while accounting for N input into the soil, the aggregated flux value does not take into account climatic conditions leading to bursts of N_2O from the soil. In reality, ideal N_2O production conditions in the soil may have led to higher N_2O emission during this time period. It is well-known that N_2O emissions can become elevated during periods of optimum soil moisture content (about 60% water-filled pore space) (Linn and Doran, 1984) and it is therefore considered likely that the high NBL-measured value of 41 ng N_2O m^{-2} s^{-1} is probably related to the period of heavy rainfall (46 mm) that occurred on the afternoon of June 27, one day prior to NBL measurement. During drier days and nights, the NBL method would measure lower values more similar to the aggregated flux value.

Trends in field-scale N_2O fluxes measured by the flux gradient method taken at the Ottawa field site (Grant and Pattey, 2008) show the effect of rainfall on June 27, 2002. There was an increase in average nighttime N_2O fluxes from 87 and 100 ng N_2O m^{-2} s^{-1} on June 25-26 and 26-27, 2002, respectively, to a larger-than-average flux of approximately 1700 ng N_2O m^{-2} s^{-1} during the afternoon of June 28 (the afternoon prior to NBL measurement) to approximately 290 ng N_2O m^{-2} s^{-1} the following afternoon and 189 ng N_2O m^{-2} s^{-1} that following night. The reason the NBL N_2O value is not as high as the flux gradient value is likely because the NBL footprint was larger and included areas that did not contribute N_2O from increased denitrification as a result of the added rainfall, for example, the forested and suburban areas. Natural, non-managed (*i.e.,* non-fertilized) forests are only very small sources (and occasionally small sinks) of N_2O (Bowden *et al.,* 1990; Bowden *et al.,* 1991; Castro *et al.,* 1993; Corre *et al.,* 1996; Ambus and Robertson, 1999; Bowden *et al.,* 2000; Kellman, 2008). Nighttime nitrous oxide flux from vegetation and vehicular traffic in the suburban component was assumed to be negligible.

6.3.1.2 Ottawa, ON, June 28-29, 2002—3:30-4:45 (Figure 6.4b)

The majority of this footprint, which extended 4.3 km upwind, included fields of corn and hay, with a small patch of forest (Figure 6.4b). The uppermost portion of the profile extended to a suburban area adjacent to the agricultural zone. The aggregated flux for CO_2 (0.13-0.26 mg CO_2 m^{-2} s^{-1}), almost identical to that calculated for the 23:00-0:45 profile, was, this time, much lower than the NBL-measured value of 0.40 mg CO_2 m^{-2} s^{-1} (Table 6.3).

The range in values for the aggregated flux estimate mainly reflects the range in CO_2 flux estimates for corn and hay (Table 6.2a), whose area of maximum influence on the vertical profile was found between approximately 575 and 1000 m upwind of the measurement site. The lower and higher flux estimates for hay reflect fluxes from a young crop and a mature crop, respectively, for different sites with similar temperature ranges (Table 6.2a).

The suburban component of the footprint had a low enough weight that neither the IPCC-produced estimate (0.06 mg CO_2 m^{-2} s^{-1}) nor the literature/field data estimate

(0.005-0.44 mg CO_2 m^{-2} s^{-1}), had much impact on the total aggregated footprint flux. Likewise, even if the footprint were widened to include the forested park area adjacent to the suburban area (Figure 6.6), it would not likely have much effect on the total aggregated flux value. If the footprint, in reality, extended much farther into the urban/suburban part of Ottawa, however, a higher weight might be placed on this area, possibly increasing the aggregated flux value (if the Montreal-measured value of 0.44 mg CO_2 m^{-2} s^{-1} were used).

The aggregated N_2O flux value (16-20 ng N_2O m^{-2} s^{-1}) was slightly lower than the earlier profiles from this night (23:00-0:45) (Table 6.2a), which may be expected since the earlier footprint consisted only of agricultural land, while this footprint included a suburban component which most likely contributed almost no N_2O. The aggregated value for this footprint is in even greater contrast to the NBL-measured value (107 ng N_2O m^{-2} s^{-1}) than for the earlier profiles on this night (Table 6.3).

Why on this night were N_2O and CO_2 fluxes both considerably higher during the LLJ event compared to earlier in the evening? NBL measurements with the same wind direction, made the same night from 23:00 to 0:45, prior to jet formation and therefore having a smaller footprint which excluded the suburban area, gave fluxes of 0.07 mg CO_2 m^{-2} s^{-1} and 41 ng N_2O m^{-2} s^{-1}, while during jet formation fluxes of 0.40 mg CO_2 m^{-2} s^{-1} and 107 ng N_2O m^{-2} s^{-1} were measured. Friction velocity ($u*$) and/or σ_w remained consistently low throughout the night, with values between 0.00 and 0.04 m s^{-1}.

Regarding CO_2, we believe that the study of Karipot *et al.* (2006) reveals the reason behind this increase in NBL-measured flux: Within one night, they observed flushing of accumulated CO_2 from within a forest canopy at three separate onsets of a

LLJ following a period of calm conditions. Each time this resulted in an increase in the EC-measured CO_2 flux (*e.g.,* 0.40-0.66 mg CO_2 m^{-2} s^{-1}) above the forest canopy even though $u*$ increased only slightly (Karipot *et al.,* 2006). In our study we have three sources within the 4.3 km long June 28-29, 2002, 3:30-4:45 footprint that may have accumulated CO_2 during calm periods, including the forested areas, the suburban area, and the cultivated areas (especially mature corn canopies).

CO_2 distribution and fluxes within and from forest canopies have been well-studied; typically CO_2 concentrations increase at a faster rate within the canopy compared to above it (*e.g.,* Grace *et al.,* 1996; Goulden *et al.,* 1996; Lee, 1998; Sun *et al.,* 1998; Mahli *et al.,* 1999; Falge *et al.,* 2001; Massman and Lee, 2002; Baldocchi 2003; Karipot *et al.,* 2006). While, strictly speaking, only a small forested area was located within the footprint, larger areas were located close by, for example, to the immediate west of the suburban portion of the footprint (Figure 6.4b). Because the footprint width was somewhat arbitrarily determined, it is highly probable that in reality, some CO_2 was flushed upward from this area as well.

While nighttime CO_2 flux data from urban and suburban sites across Europe and North America have been generally shown to be low, *e.g.,* averages ranging from an almost zero flux to 0.44 mg CO_2 m^{-2} s^{-1} (Grimmond *et al.,* 2002; 2004; Nemitz *et al.,* 2002; Soegaard and Møller-Jensen, 2003; Walsh, *et al.,* 2004), concentrations do become elevated in stable conditions (*e.g.,* Grimmond *et al.,* 2002; 2004; Nemitz *et al.,* 2002; Walsh *et al.,* 2004; Valasco *et al.,* 2005). Unpublished data from the Montreal suburban site for June and July (EPiCC, 2009), show suburban lawns and foliage becoming a source of CO_2 at night, with afternoon to overnight increases ranging from approximately 20 to 70 ppmv, with peak concentrations commonly occurring just before sunrise.

Accumulation and venting of trace gases within cultivated crop canopies is less well-documented. Observations of the ejection or venting of accumulated CO_2 from within grass canopies at the onset of intermittent turbulent nocturnal events have been observed by Wohlfahrt *et al.* (2005) and Myklebust *et al.* (2008). It follows that the same should apply to corn and soybean canopies, especially as they mature. High surface CO_2 concentration next to the corn canopy (30-40 cm high at the time) was shown in our CO_2 profile data from this night. These profiles show an extremely sharp concentration gradient in the first 2.5-5 m (Figure 4.1(l)); if this were extrapolated down to the surface the concentration would be even higher, indicating a near-surface accumulation available to be vented upward at the onset of a turbulent event. With an open canopy, however, the effect would probably be of a lesser magnitude than a CO_2 burst from a closed forest canopy.

On the other hand, N_2O concentration is not likely to increase significantly in forest canopies or suburban areas even during the night. However, it may accumulate in crop canopies similarly to CO_2, so the elevated N_2O flux during this period may be attributable to LLJ-induced flushing as well.

Another possibility to consider for the elevated CO_2 flux during jet formation is the role of urban-rural circulation (Oke, 1987). This well-documented phenomenon comes about from the heat differential between the city (the urban heat island) and surrounding rural land. Macpherson *et al.* (1995) measured a daytime upward transport of CO_2 over an urban center and a downward transport of CO_2 over rural land, attributed to CO_2 uptake by vegetation. At nighttime, this effect could be even greater, as the city maintains an upward heat flux while the rural areas exhibit a downward heat flux, leading to an increased circulation of upper (hotter) air outward from the city to the country.

Combined with the effects of the low-level jet, CO_2 from the city of Ottawa could have been advected into the agricultural area of our Ottawa site on the night of June 28-29, 2002.

6.3.1.3 Coteau-du-Lac, QC, June 17-18, 2003—20:45-21:45 (Figure 6.4c)

The footprint for this profile pair, extending approximately 3 km just south of west, fell over areas of peas, corn, hay, barley, a rural residential road following a narrow, winding river (about 1.6 km long and 6 m wide within the footprint area), and an area of cultivated agricultural land of unknown crop (Figure 6.4c).

In this example, the NBL-measured value of 0.15 mg CO_2 m^{-2} s^{-1} was close to the lower end of the aggregated flux range of 0.18-0.27 mg CO_2 m^{-2} s^{-1} (Table 6.3). In this case the range in the aggregated flux estimate was due mainly to the range in CO_2 estimates for corn (0.15-0.23 mg CO_2 m^{-2} s^{-1}) (Table 6.2a), which was found in approximately 50% of the total footprint area. The corresponding EC flux value was 0.38 mg CO_2 m^{-2} s^{-1} (from the pea field) (table 6.2a), a value which was primarily responsible for making the aggregated value somewhat higher than that for the night of July 9-10, 2003 (Table 6.3).

Results from N_2O flux aggregation (14-18 ng N_2O m^{-2} s^{-1}) were fairly close to the NBL-measured flux of 26 ng N_2O m^{-2} s^{-1} (Table 6.3). Flux gradient measurements at the field site the following night averaged approximately 43 (±31) ng N_2O m^{-2} s^{-1}. While these fluxes are specific to the pea field at the launch site, they are also very close to the NBL flux. Again, environmental conditions promoting N_2O emission are not reflected in the aggregated estimate, for example the 46 mm of rain that fell 3-4 days prior to this NBL measurement. However, it is likely that the denitrification-promoting effect of this rainfall was diminished by the time the NBL-measurements were taken and that this NBL-measured value was again more representative of baseline N_2O values in the region, and is in fact exactly equal to the overall average NBL-measured N_2O flux at Coteau-du-Lac in 2003, 26 ng N_2O m^{-2} s^{-1}.

6.3.1.4 Coteau-du-Lac, QC, July 9-10, 2003—19:30-20:45 (CO_2 only) (Figure 6.4d)

The footprint for this profile pair, which extended about 3.7 km to the NNW, included areas of peas, corn, hay, vegetables, barley, and mixed deciduous forest patches within an area of cultivated agricultural land of unknown crop (Figure 6.4d).

Once again at this site, the aggregated flux value for CO_2 (0.13-0.15 mg CO_2 m^{-2} s^{-1}) was close to the NBL-measured value of 0.19 mg CO_2 m^{-2} s^{-1} (Table 6.3). While this night exhibited the lowest evening air temperature for the month of July 2002 (four degrees below average), the NBL value is still close to the overall average CO_2 flux measured at Coteau-du-Lac (0.22 mg CO_2 m^{-2} s^{-1}). Use of soil temperature/respiration relationships for corn (Suyker *et al.,* 2004) and soybean (Suyker *et al.,* 2005) gave lower CO_2 flux estimates for the flux aggregation. The estimate for the mixed deciduous forest patches, based on soil temperature total ecosystem respiration (TER) relationships (Knohl and Buchman, 2005; Knohl *et al.,* 2008), was the same as the NBL-measured flux, but its weight was not enough to influence the aggregated flux value.

6.4 CONCLUSION

In order to provide a ground-based validation of the NBL budget method for measuring agricultural trace gases, NBL-measured CO_2 and N_2O flux values were compared with aggregated flux values for four footprint-defined areas at two eastern Canadian agricultural field sites.

The 'bottom-up' aggregated method produced CO_2 and N_2O fluxes that in most cases were of the same order of magnitude as the top-down NBL-measured values. The notable exception was the night of June 28-29, 2002, when NBL-measured CO_2 fluxes were influenced by the onset of the LLJ and N_2O fluxes were increased overall because of heavy rainfall the preceding day. The aggregated flux values for the Coteau-du-Lac site fell within a standard deviation of the average CO_2 and N_2O flux measured at this location through the summer of 2003.

Better agreements were obtained in the two cases using Coteau-du-Lac data than the two cases from the Ottawa site; average absolute differences between the bottom-up aggregated flux and the 'top-down' NBL measurements ranged between 22% to 51% and 68% to 103%, for Coteau-du-Lac and Ottawa, respectively. For the cases at the Ottawa site, the inconsistent presence of a well-defined LLJ and heavy rainfall the day before NBL measurement at the Ottawa site produced short-term variations that were not accounted for by the flux aggregation method. For the cases at the Coteau-du-Lac site, the lack of both recent rainfall or farm management events in the immediate area and apparent intermittent NBL phenomena allowed the aggregated flux to be a good approximation of the NBL-measured flux.

With evidence that during typical baseline climatic and non-LLJ conditions, the 'top-down' and 'bottom-up' approaches provide similar nocturnal estimates of GHG exchange, the NBL budget method can be taken into consideration as a method to measure nocturnal fluxes over relatively homogeneous agricultural land when other methods used in turbulent conditions fail in calm conditions (*e.g.,* eddy covariance and flux gradient methods). There is the issue of scale, to be certain: the NBL method measures at scales many times larger than the other methods. If NBL conditions were to show capping at a relatively low height and if the source area were homogeneous, the flux measured by the NBL budget method should be the same as the turbulent method. Bouwman *et al.* (1999) give a good review of the errors involved in the spatial and temporal aggregation of fluxes within the scope of the compilation of emissions inventories. These errors generally arise from a lack of measurement data and the loss of spatial and temporal variability in the process of aggregation (both problems encountered here) (Bouwman *et al.,* 1999).

Three important improvements could be made to obtain a closer match. More frequent and complete NBL structure measurements (wind, temperature, GHGs) are required to better monitor changes in the NBL which would aid in the determination of NBL method fluxes as vertical profiles are only “snapshots” of the NBL. This is possible with the addition of continuous measurement techniques such as the use of a SODAR/RASS (available only periodically in this study). The recently established tall-tower super-sites in North America will provide continuous data collection in this regard at fixed levels through the lower atmosphere.

As previously outlined, the basic assumptions of footprint models (Chapter 2) are generally not met in real-life conditions. More work is needed to improve footprint models that are representative of calm nighttime conditions including the addition of the effects of the LLJ on surface-atmosphere exchange (Banta *et al.,* 2002; Karipot *et al.,* 2006). A tracer release study using a non-natural tracer gas could provide information on trace gas distribution in the NBL. Such knowledge would in turn improve weightings of the upwind contribution (*e.g.,* Kaharabata *et al.,* 1999).

Finally, more detailed information on the ground-based fluxes (*i.e.,* for each cover type or other point source) within the footprint could improve the aggregated flux estimates. Instead of obtaining estimates from methods complicated by different locations and time scales, the best accounting of the fluxes from all cover types and point sources within the footprint could in principle be made by directly measuring everything in the footprint, or at least for each cover type (*e.g.,* at the field scale, using a method not requiring turbulence, since good NBL budget nights are calm nights), concurrently to the NBL budget method measurement. Alternatively, fluxes for each cover type measured by turbulent methods (*e.g.,* Soegaard, *et al.,* 2000, and Soegaard and Møller-Jensen, 2003) on nights other than calm NBL nights may be more feasible. The use of IPCC emission factors also automatically introduces error through generalization, and even more so when input is estimated, *e.g.,* recommended vs. actual N fertilizer application.

TABLES

Table 6.1. Example of CO_2 flux aggregation with areal weighting of sources assigned within each footprint-weighted segment, 3:30 and 4:45 profiles, Ottawa, June 28-29, 2002. Segment and areal weightings listed here are applied to flux estimates for each source which are given in Table 6.2a, yielding a weighted flux for each footprint segment which is then summed to give the total flux for the footprint (Equation 6.3).

Cumulative Footprint-Weighted Contribution	Mean Weight of Footprint Segment (Normalized to Total Wt)	Source 1 Area Wt. CORN	Source 2 Area Wt. HAY	Source 3 Area Wt. FOREST	Source 4 Area Wt. RES	Segment/Area Weighted Flux ($mg\ m^{-2}\ s^{-1}$) (lower range)	Segment/Area Weighted Flux ($mg\ m^{-2}\ s^{-1}$) (upper range)
0.00-0.20	0.00	0.55	0.45	0.00	0.00	0.00	0.00
0.20-0.40	0.09	1.00	0.00	0.00	0.00	0.01	0.02
0.40-0.60	0.13	1.00	0.00	0.00	0.00	0.02	0.03
0.60-0.80	0.18	1.00	0.00	0.00	0.00	0.03	0.04
0.80-1.00-0.80	0.20	0.80	0.20	0.00	0.00	0.03	0.05
0.80-0.60	0.18	0.00	1.00	0.00	0.00	0.02	0.05
0.60-0.40	0.13	0.62	0.25	0.125	0.00	0.02	0.03
0.40-0.20	0.07	0.00	0.77	0.00	0.23	0.01	0.02
0.20-0.00	0.03	0.00	0.00	0.00	1.00	0.00	0.01
					Total Footprint Flux (mg CO_2 m^{-2} s^{-1})	0.13	0.26

Table 6.2 (a). Estimated fluxes of CO_2, and N_2O from sources within footprints on June 28-29, 2002, June 17-18, 2003, and July 9-10, 2003. Indirect sources of N_2O (from leaching, runoff, volatilization) are already included in estimates for each source.

Source	**Estimated Flux Value**	
	CO_2 (mg CO_2 m^{-2} s^{-1})	N_2O (ng N_2O m^{-2} s^{-1})
Ottawa, 2002	*June 28-29, 2002*	
Corn	0.15-0.23[a]	16-22 [h]
Hay	0.09[b], 0.30[c]	17[i]
Soybean	0.11[d]	18[i]
Mixed Deciduous Forest	0.32 [e]	1[j]
Suburban Residential	0.06 [f], 0.005-0.44[g]	6 [f]
Coteau-du-Lac, 2003	*June 17-18, 2003*	
Peas	0.38 [k]	1 [m]
Corn	0.15-0.23 [a]	16-22[h]
Barley	0.14-0.16 [l]	9 [i]
Hay	0.09[b], 0.30[c]	23[i]
Soybean	0.11 [d]	16 [i]
Mixed Deciduous Forest	0.32[e]	1[j]
Rural Residential	Assumed negligible	Assumed negligible
River	0.01-0.35[n]	Indirect emissions already included in other estimates
	July 9-10, 2003	
Peas	0.35[k]	N_2O not measured
Corn	0.12[o]	
Hay	0.10 [b] -0.21[c]	
Vegetables (Soybean)	0.11 [d]	
Mixed Deciduous Forest	0.19[e]	
Rural Residential	Assumed negligible	

a based on unpublished EC data, E. Pattey, 2002, for corn at launch site; Pattey *et al.,* 2002; Verma *et al., Ameriflux* data

b E. Pattey, 2003 (unpublished EC data) for a young crop of barley/alfalfa/timothy, 12 cm high, at launch site

c E. Pattey, 2004 (unpublished EC data) for a mature crop of alfalfa and timothy, 45-50 cm high

d Suyker *et al.,* 2005, soil temperature –respiration relationship

e Literature-derived value, based on soil temperature-respiration relationships for total ecosystem respiration (Knohl and Buchman, 2005; Knohl *et al.,* 2008)

f CO_2/N_2O from mobile emissions, calculated using IPCC Tier 2 emission factors for transportation (Environment Canada, 2006) (see Appendix E, Table E-1)

g Micrometeorologically-measured in urban/suburban settings: central Copenhagen by Soegaard and Møller-Jensen, 2003 (0.005 mg m^{-2} s^{-1}); suburban Montreal by EPiCC, 2009 (unpublished data obtained with permission) (0.26 to 0.44 mg m^{-2} s^{-1}). (http://www.epicc.uwo.ca/measurement/montrealsitegallery.asp).

h EF-derived estimate, range of recommended N fertilizer input (CPVQ, 2000) multiplied by ecodistrict-specific N_2O emission factor, plus indirect emissions (see Table 6.2b)

i EF-derived estimate, total N input multiplied by ecodistrict-specific N_2O emission factor, plus indirect emissions (see Table 6.2b for example)

j Direct N_2O emission very small for natural, unmanaged forest soils (IPCC, 2006); literature-derived value from: Bowden *et al.,* 1990; Bowden *et al.,* 1991; Castro *et al.,* 1993; Corre *et al.,* 1996; Ambus and Robertson, 1999; Bowden *et al.,* 2000; Kellman, 2008.

k E. Pattey, 2003, unpublished EC data for pea crop at launch site.

l Literature-derived values from: Eriksen and Jensen, 2001; Akinremi, *et al.,* 1999.

m EF-derived estimate, total N input (private producer's data for N fertilizer (G. Vincent, personal communication, 2003 multiplied by ecodistrict-specific emission factor, plus indirect emissions (see Table 6.2b for example).

n **L**iterature-derived estimate (range) for mid-latitude freshwater streams and rivers, from: Jones and Mulholland, 1998; Telmer *et al.,* 1999; Hope *et al.,* 2001; Vesala *et al.,* 2006; Silvennoinen *et al.,* 2008.

o Based on Suyker *et al.,* 2004, air temperature –respiration relationship

Table 6.2 (b). Example of N_2O calculation from crop fields, Ottawa, June 28-29, 2002.

Source	**Estimated TOTAL N input (kg N ha^{-1} season^{-1})**	**EF direct N_2O[c] (kg N_2O-N kg^{-1} N)**	**EF leaching/runoff[d] (kg N_2O-N kg^{-1} N) * Frac leach[d]**	**EF volatilization[d] (kg N_2O-N kg^{-1} N)[c] * Frac gas$_f$[d]**	**N_2O-N (kg N_2O-N ha^{-1} season^{-1})**	**N_2O (ng N_2O m^{-2} s^{-1})**
CORN	120-170[a]	0.0119	0.0075*0.3	0.01*0.1	1.82-2.58	16-22
HAY	135[b]	0.0119	0.0075*0.3	0.01*0.1	1.99	17

a range of recommended N fertilizer input (CPVQ, 2000)

b includes 75 kg synthetic N (CPVQ, 2000, requirements for hay <40% legumes) and 60 kg N from crop residue (standard practice CPVQ for hay)

c combined Quebec-Ontario ecodistrict emission factor (Environment Canada, 2008)

d Indirect N_2O emissions were estimated from synthetic fertilizer N only (in this case 75 kg N): EF leaching/runoff is emission factor EF_4 from the IPCC 2006 Guidelines (more recent than Canada's latest 2006 GHG Inventory), FRAC leach is the fraction of N lost due to leaching for a non-moisture deficit environment (IPCC, 2006; Environment Canada, 2008), EF volatilization is emission factor EF_5 (IPCC, 2006), and Frac gas$_f$ is the fraction of N_2O-N lost through volatilization of N from synthetic fertilizer (IPCC, 2006; Environment Canada, 2008). Volatilization of N from manure application was not applied here as manure application was unknown and could not be estimated for most of the footprint area.

Table 6.3. Results of flux aggregation vs. NBL flux measurements for Ottawa, June 28-29, 2002, and Coteau-du-Lac, June 17-18, 2003, and July 9-10, 2003.

Site	**CO_2 (mg CO_2 m^{-2} s^{-1})**		**N_2O (ng N_2O m^{-2} s^{-1})**	
	Flux Aggreg.	**NBL**	**Flux Aggreg.**	**NBL**
Ottawa, ON June 28-29, 2002 (23:00-0:45)	0.14-0.25	0.07	16-21	41
Ottawa, ON June 28-29, 2002 (3:30-4:45)	0.13-0.26	0.40	16-20	107
Coteau-du-Lac, QC June 17-18, 2003 (CO_2: 20:45-21:45) (N_2O : 20:45-22:30)	0.18-0.27	0.15	14-18	26
Coteau-du-Lac, QC July 9-10, 2003 (19:30-20:45)	0.13-0.15	0.19	—	—

FIGURES

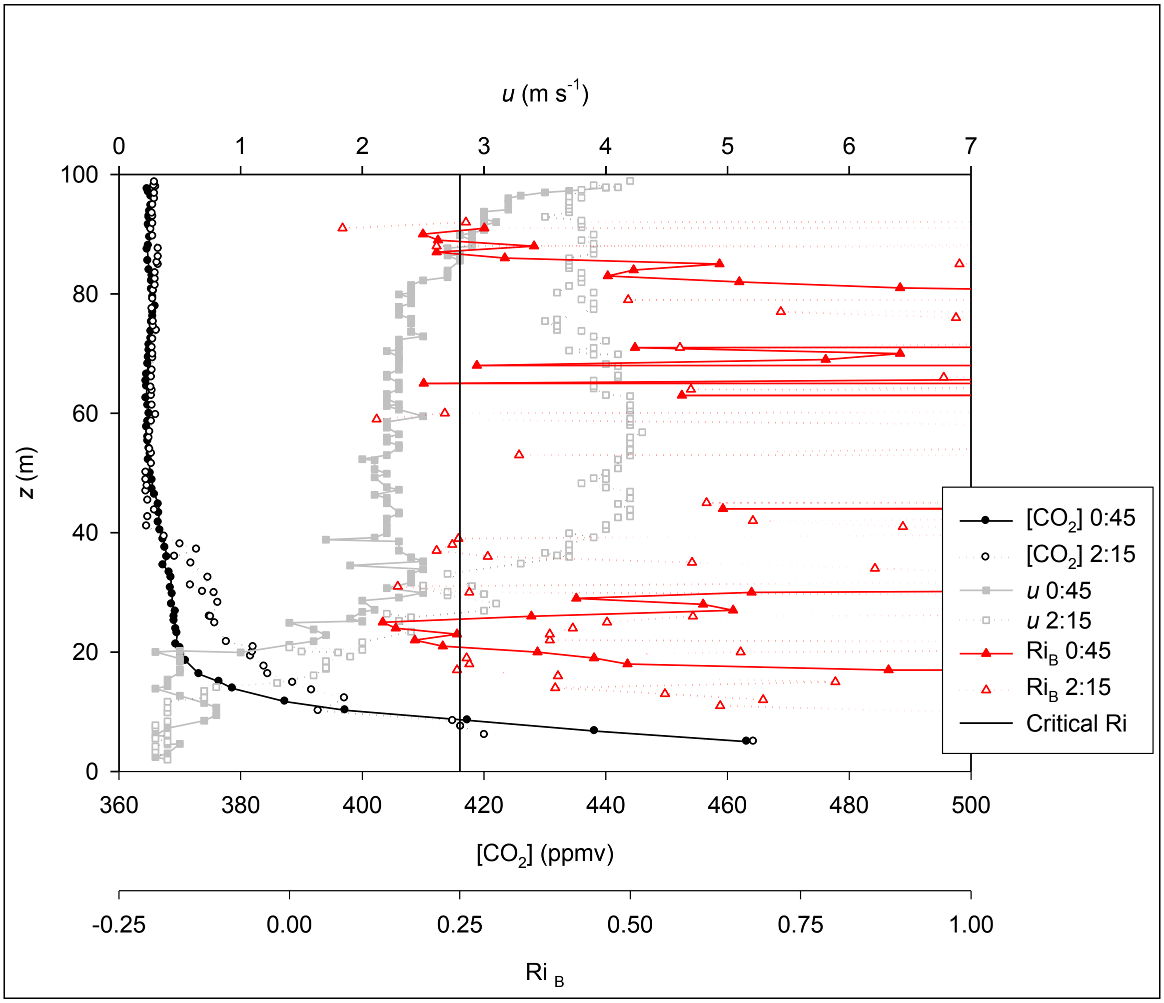

Figure 6.1 (a). Carbon dioxide, *u*, and *Ri* profiles for Ottawa, ON, June 28-29, 2002, 23:00-0:45.

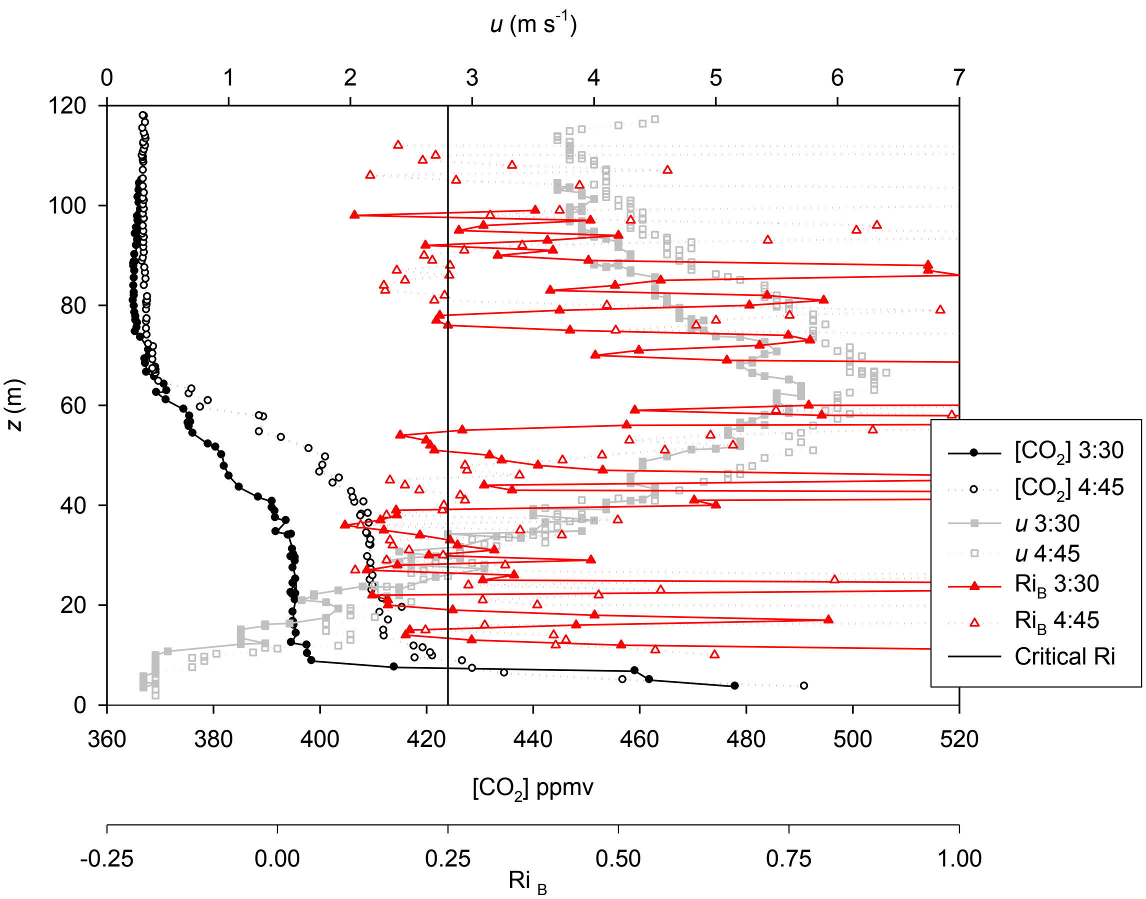

Figure 6.1 (b). Carbon dioxide, *u*, and *Ri* profiles for Ottawa, ON, June 28-29, 2002, 3:30-4:45.

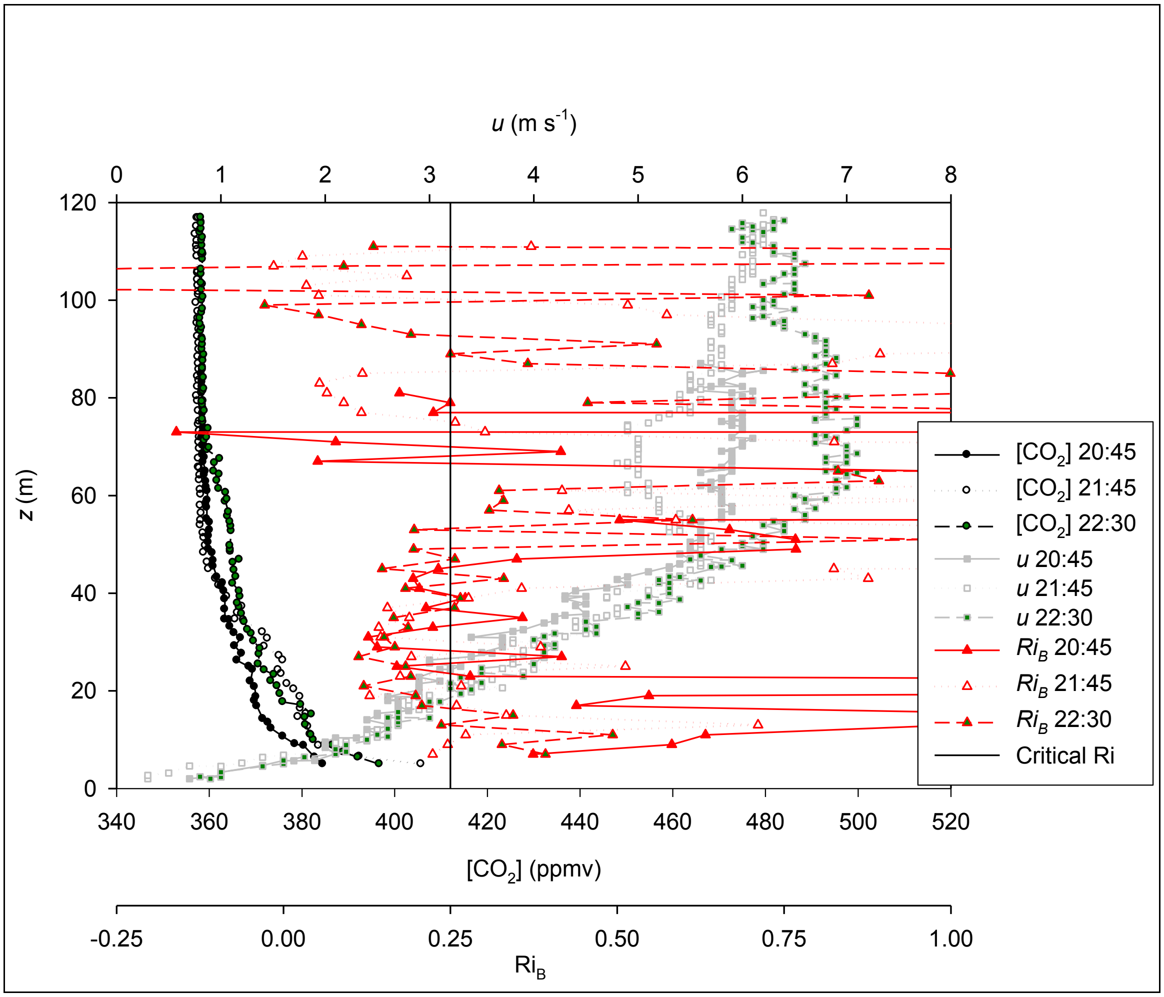

Figure 6.1 (c). Carbon dioxide, *u*, and *Ri* profiles for Coteau-du-Lac, QC, June 17-18, 2003, 20:45-22:30.

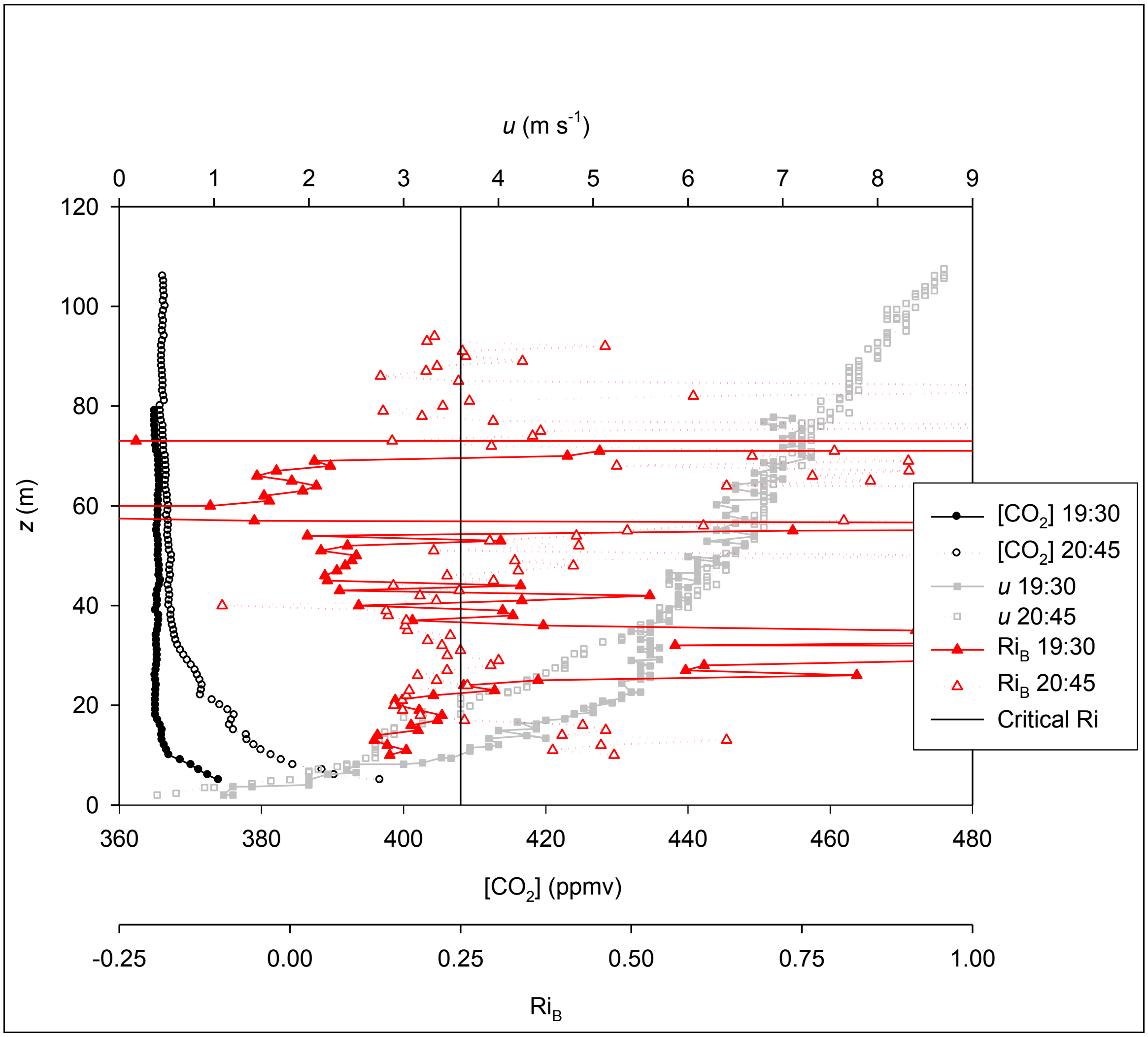

Figure 6.1 (d). Carbon dioxide, *u*, and *Ri* for Coteau-du-Lac, QC, July 9-10, 2003, 19:30-20:45.

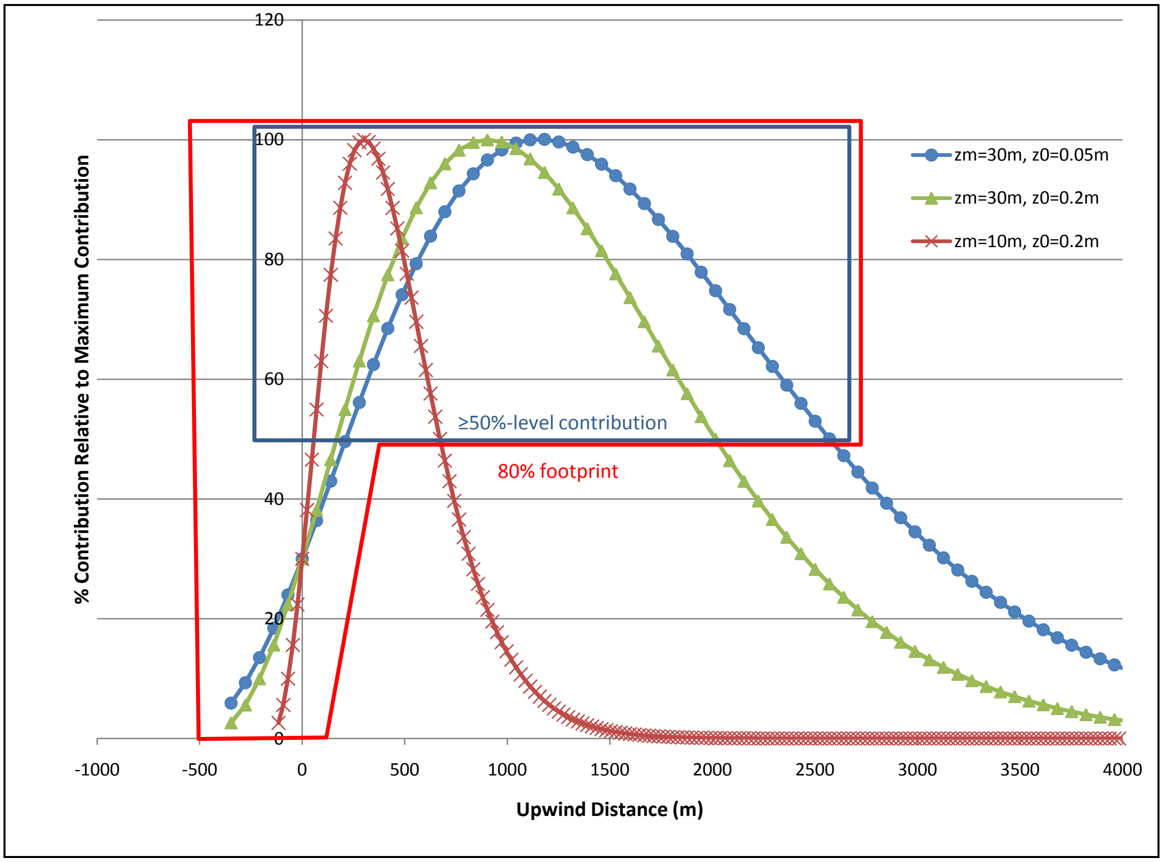

Figure 6.2 (a). Illustration of flux footprint parameterization-generated results, for u* = 0.2 m s^{-1}, σ_w = 0.07 m s^{-1}, and other settings indicated in figure.

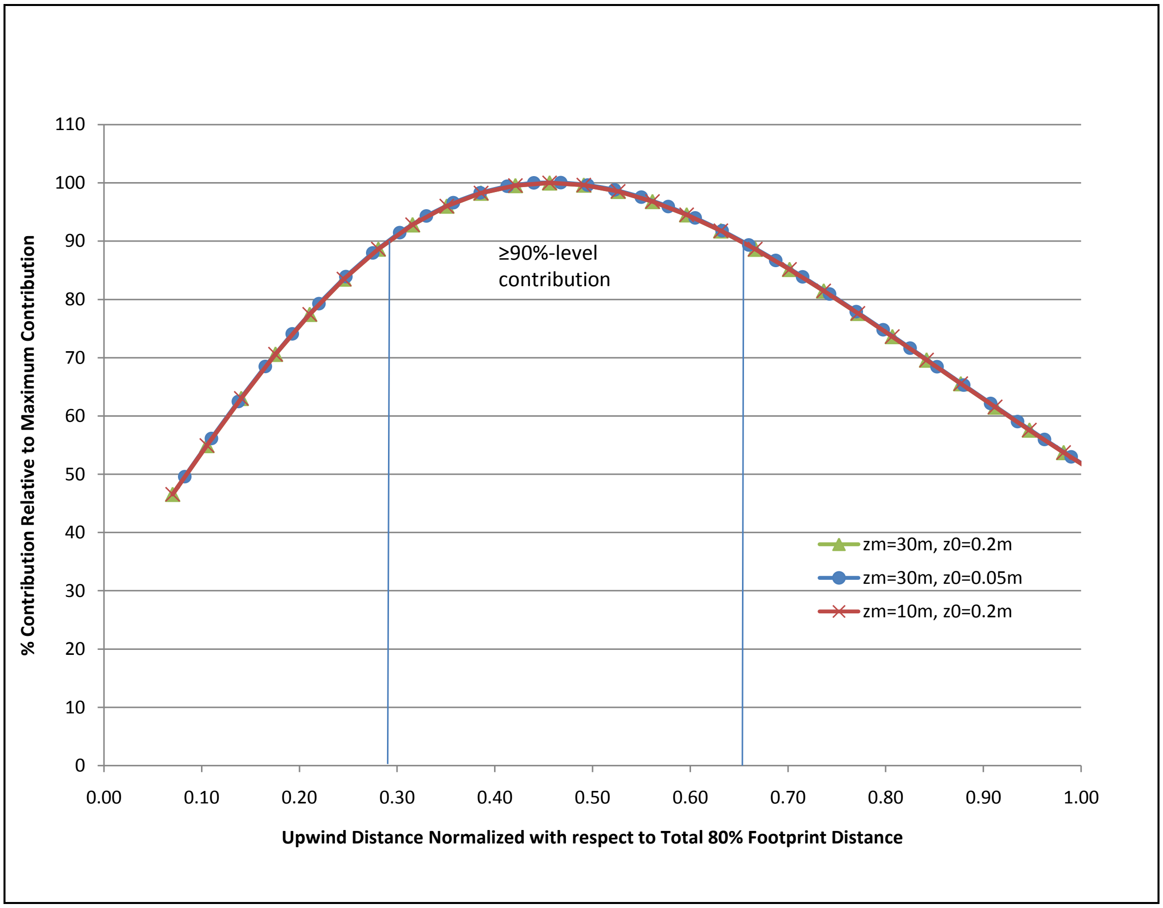

Figure 6.2 (b). Illustration of consistent relationship between relative upwind distance and relative contribution (same settings as 6.5 a).

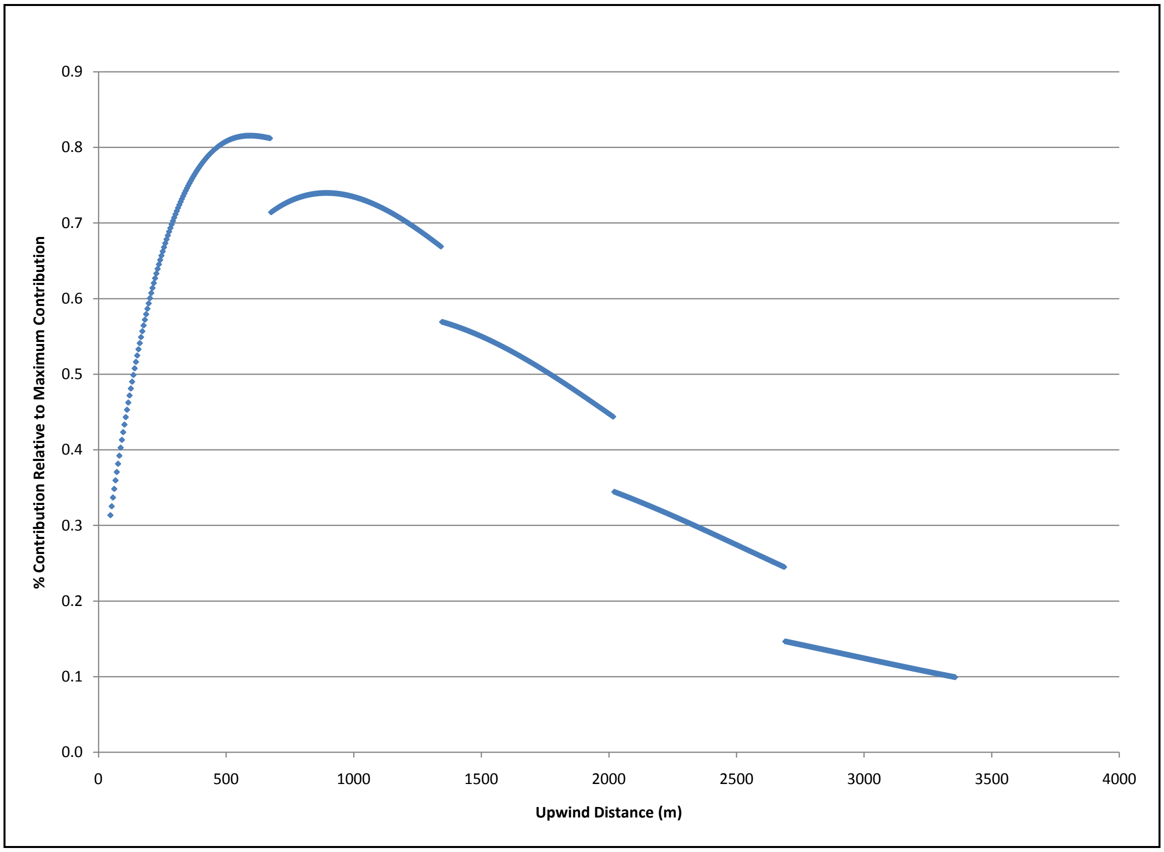

Figure 6.3. Example of cumulative 80% footprint obtained following procedure outlined in Section 6.2.5, for z_m = 10, 20, 30, 40, and 50 m (0.2 *h* to 1.0 *h*), $u*$ = 0.2 m s^{-1}, z_0 = 0.2 m, and σ_w of 0.07 m s^{-1}. Start of each gap signals drop below 50% level of previous footprint (*i.e.,* previous footprint is no longer included in cumulative weighting).

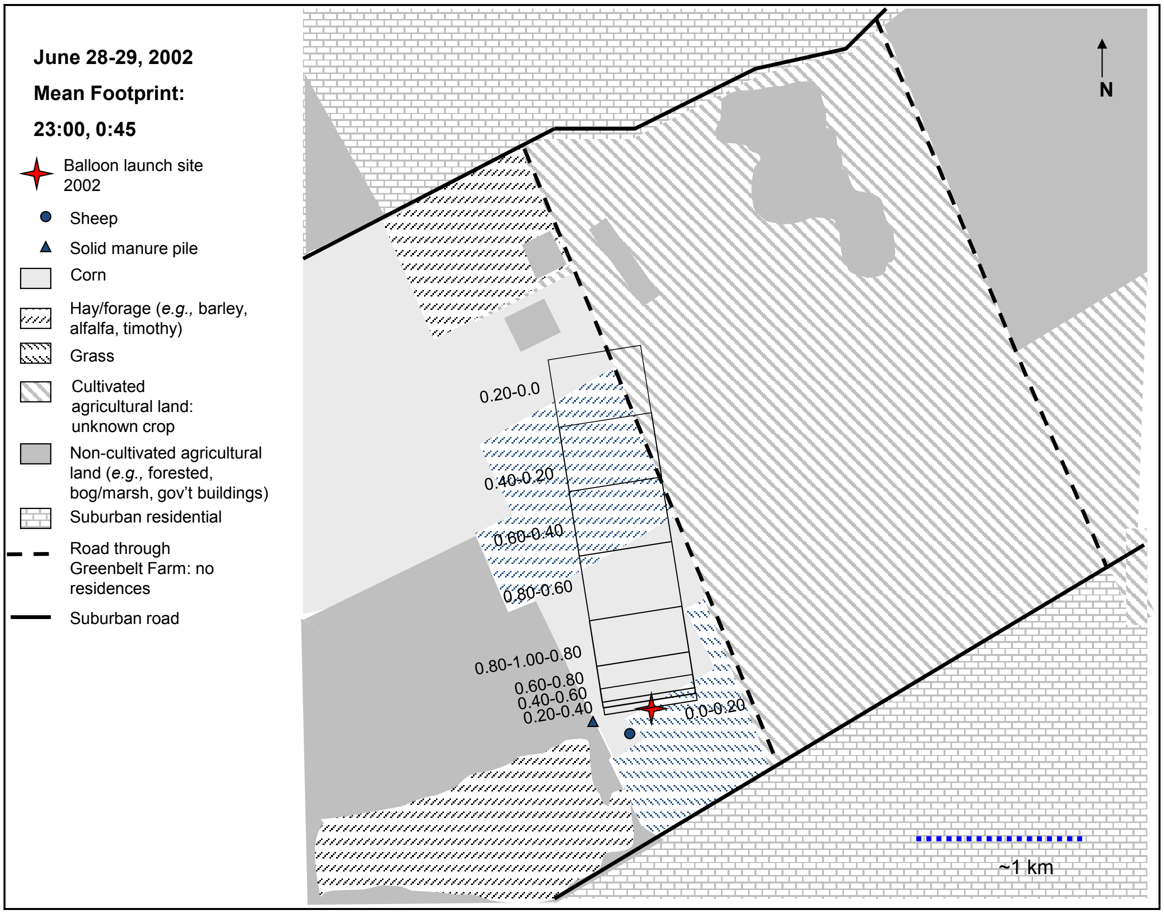

Figure 6.4 (a). Approximate flux footprint for Ottawa, ON, June 28-29, 2002, 23:00-0:45.

Numbers denote footprint weighting (relative contribution).

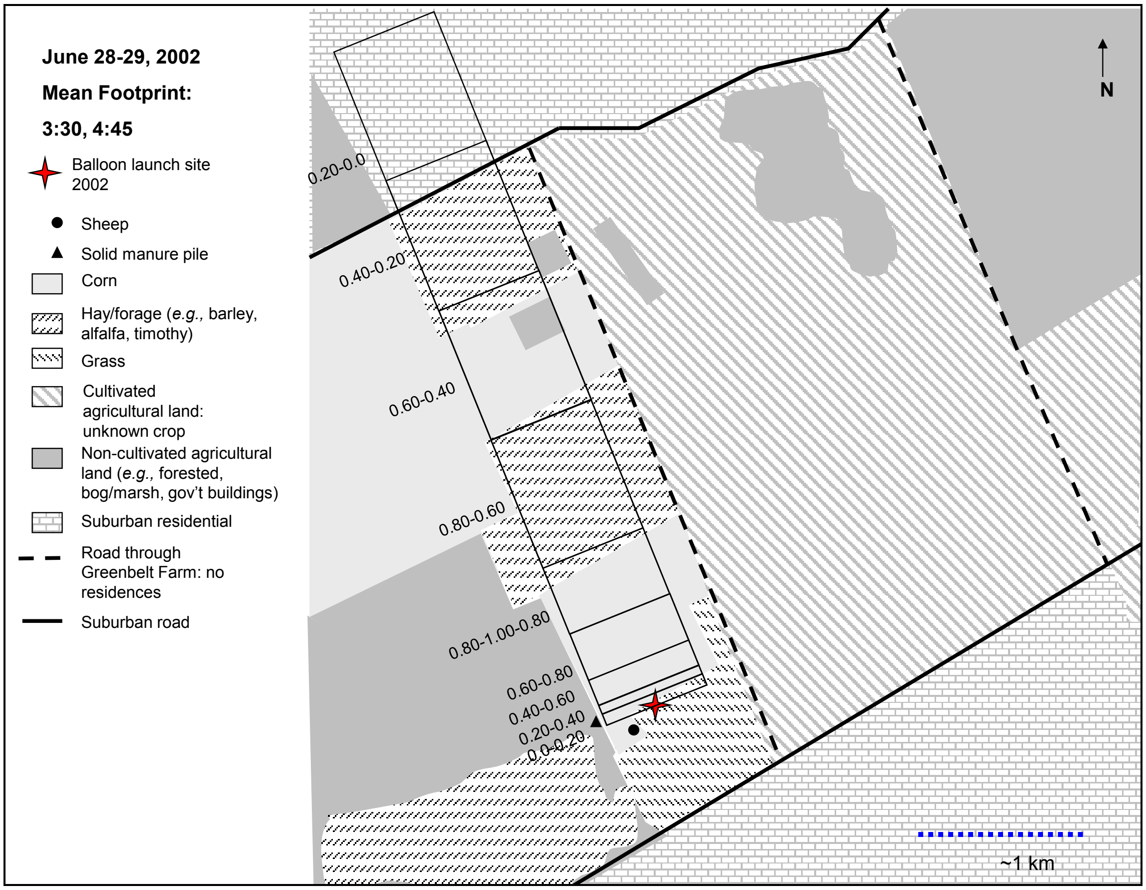

Figure 6.4 (b). Same as in (a), but for Ottawa, ON, June 28-29, 2002, 3:30-4:45.

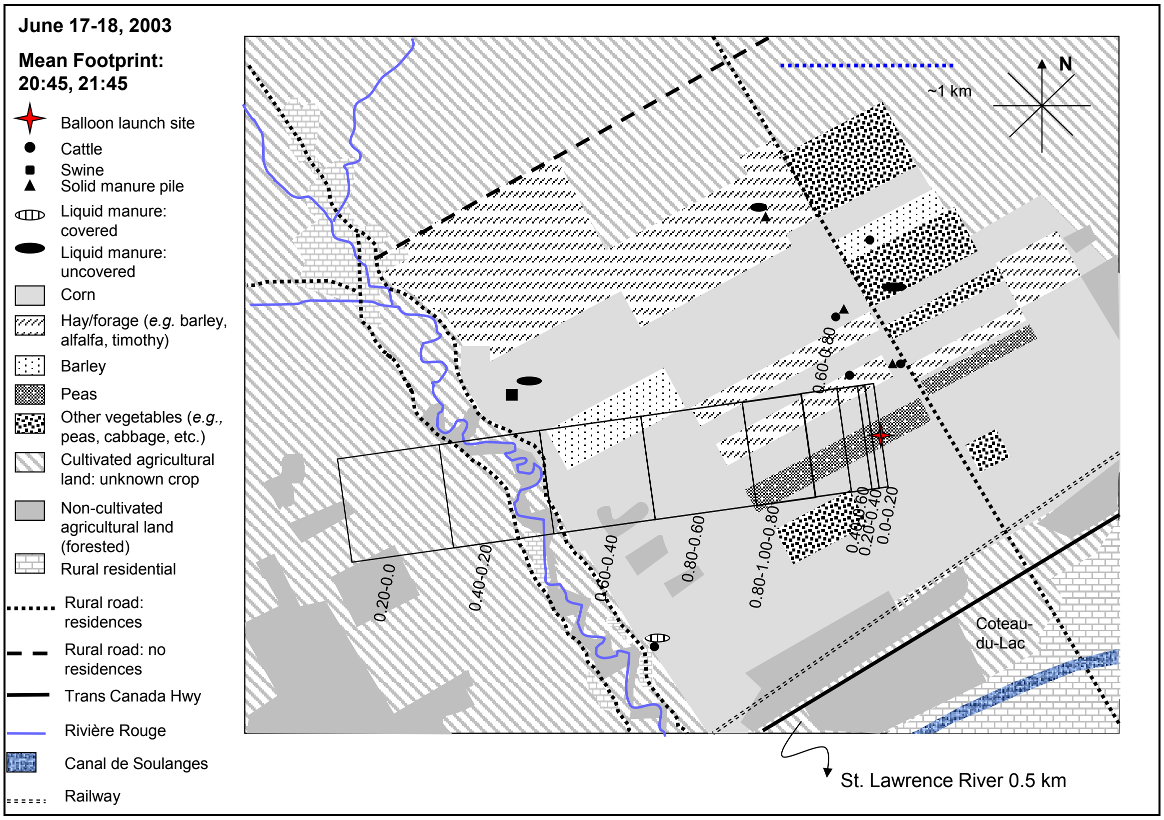

Figure 6.4 (c). Same as in (a) but for Coteau-du-Lac, QC, June 17-18, 2003, 20:45-21:45.

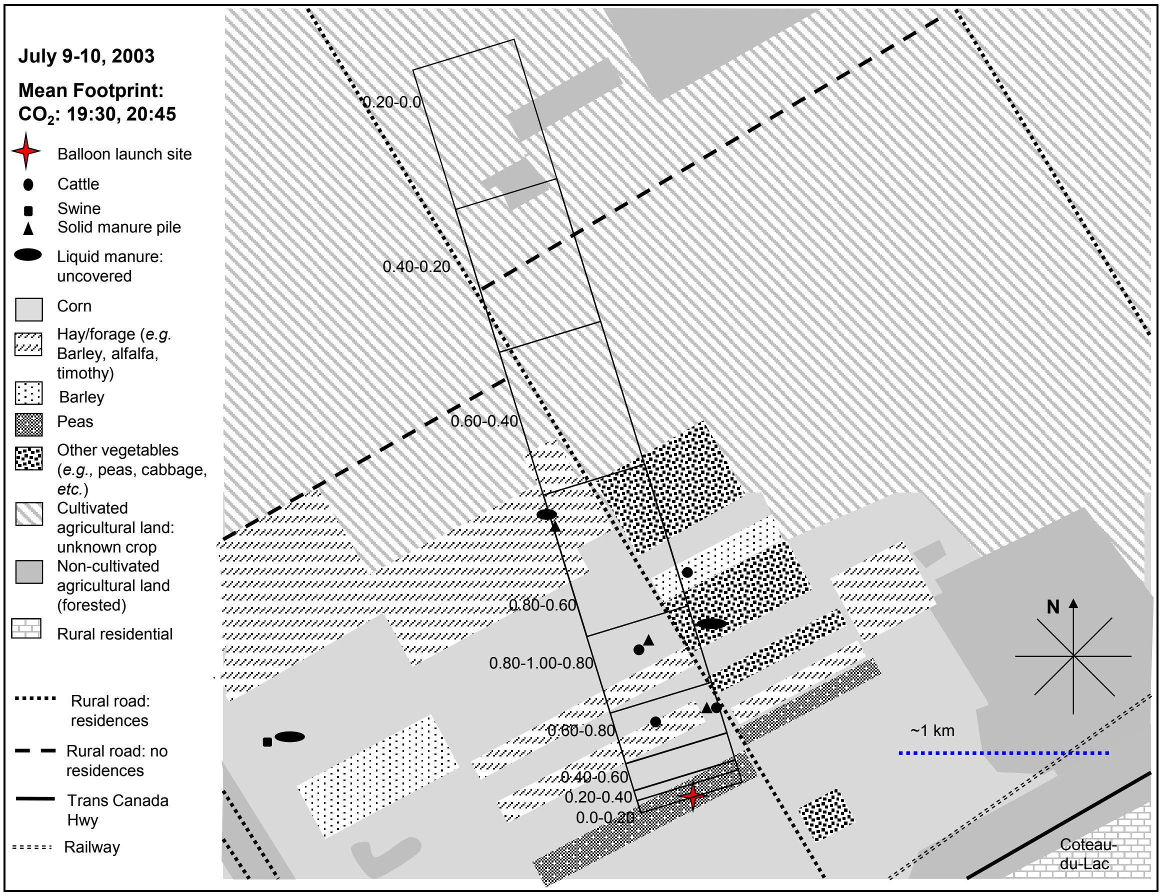

Figure 6.4 (d). Same as in (a) but for Coteau-du-Lac, QC, July 9-10, 2003, 19:30-20:45. St. Lawrence River is located approximately 2 km south of blimp launch site.

7. CONCLUSION

With the overall goal of refining the NBL budget method to obtain reliable flux estimates from agricultural farms, fluxes of the GHGs CO_2, N_2O, and CH_4 were measured using the NBL budget method at two agricultural farms in Eastern Canada in Ottawa, Ontario (2002) and in Coteau-du-Lac, QC (2003).

This study has shown that the NBL budget method, if performed according to the recommended methods in optimal or suboptimal conditions, can yield reasonable flux estimates from agricultural ecosystems for trace gases from relatively homogeneous and diffuse sources, such as CO_2 and N_2O, but not from strong point sources, such as CH_4. This is valuable in that it provides future users of the technique with information that can be used to obtain quality data, with increased confidence that fluxes are representative of the surface in question. It is also important as the NBL budget method can be taken into consideration as a method to measure nocturnal fluxes over continuous, relatively homogeneous agricultural land, when other methods based on turbulence fail. There is the issue of scale, to be certain: the NBL method measures at scales many times larger than other methods. The difference in scale from other methods could possibly be overcome if NBL conditions were to show a capping at a relatively low height, and if the source area were homogeneous and the same as that being measured by the turbulent method.

7.1 HYPOTHESES AND SUMMARY OF FINDINGS

The hypotheses proposed in Chapter 1 have been addressed as follows:

Hypothesis 1: During conditions demonstrating a sustained, very stable NBL, the NBL budget technique provides estimates of GHGs that are comparable to other methods of measurement (*e.g.,* eddy covariance, flux gradient methods, *etc.,* bearing in mind scale differences).

Conditions necessary for the application of the NBL budget method (Objective 1) were defined in Chapter 3, results showing typical NBL characterization were given in Chapter 4, and NBL-measured GHG fluxes were given in Chapter 5. The overall mean NBL budget-measured CO_2 flux at both the Ottawa and Coteau-du-Lac sites was 0.22 mg CO_2 m^{-2} s^{-1}. The mean N_2O flux (from all wind directions and type of farming management) was 30.3 ng N_2O m^{-2} s^{-1} for the Ottawa site and 26.5 ng N_2O m^{-2} s^{-1} for the Coteau-du-Lac site. Carbon dioxide and N_2O fluxes were comparable to agricultural GHG fluxes using other methods in the literature. NBL fluxes were compared to near-in-time windy-night eddy covariance- and flux-gradient-measured fluxes at both sites (Chapter 5). NBL-measured CO_2 fluxes came to within 88% of EC-measured CO_2 fluxes during optimal NBL conditions consisting of a very stable boundary layer with converging CO_2 profiles. The lower fluxes given by the NBL method were attributed to non-measured intermittent vertical turbulent flux, the possible presence of horizontal advection, and scale differences in flux source areas. An effect of seasonality and bulk NBL structure on measured NBL flux was also seen.

Methane results, on the otherhand, were determined to be invalid because of the apparent effect of small wind direction changes on measured concentrations from point sources as illustrated by a spatial sampling (Chapter 5). Hypothesis 1 is therefore rejected for CH_4.

Spatial measurements around our two field sites confirmed that the three GHGs (CO_2, N_2O, and CH_4) are spatially variable to differing degrees, confirming that a spatial average should be included as part of the NBL measured flux. An example using the spatial average in the NBL-measured flux calculation for CO_2 was given. Because of the relative strength and isolation of point sources of methane such as manure storage or cattle housing facilities, the emissions were not homogenized at the farm scale. The observed sensitivity of CH_4 concentration to point sources and wind direction leads us to conclude that the NBL budget method is not suited to measuring fluxes of gases from strong point sources.

Hypothesis 2: During suboptimal conditions consisting of elevated intermittent turbulence which may cause downward entrainment of trace gas-enriched air through the top of the NBL, the NBL budget technique can still produce representative estimates of GHG fluxes if the choice of integration height is made based on structural pattern indicators in the NBL.

By examining NBL structural pattern indicators including Richardson number, wind speed maxima, wind shear, and the change in gas concentration with height, the nightly state of the NBL was assigned to classes: 1) a very stable upside-down boundary layer with convergent profiles (optimal conditions); 2) a very stable upside-down boundary layer with non-convergent CO_2 profiles (suboptimal conditions); and 3) turbulence extending to the surface from the underside of a low-level jet or wind speed maximum (conditions not conducive to the NBL budget method) (Chapter 4). A process for choosing an integration height for optimal and suboptimal NBL conditions was presented (Chapter 4). The method used for suboptimal conditions, involving the choice of flux integration height based on the height of co-location of wind speed maxima, shear and turbulent layers, and where the change in CO_2 concentration with height goes to zero, did yield results that fell within the range of fluxes during optimal conditions (Objective 2). We may therefore accept Hypothesis 2.

Hypothesis 3: The trace gas source contribution to a vertical flux, under stable atmospheric conditions, varies spatially with the local sources exerting the most influence on the measured flux.

and

Hypothesis 4: The spatial scale of the fluxes measured using the NBL budget technique is in the range of the farm scale in Eastern Canada (*i.e.,* 1 km^2).

In Chapter 4, it was shown that the 80% of the measured NBL flux in the most prevalent, optimal NBL conditions was measured in the lowest 29.5 m of the vertical profile. Applying the flux footprint parameterization of Kljun *et al.* (2004) as a rough approximation of the upwind area of influence on this height interval gave an upwind distance of about 500-1000 m beyond the average farm length (1 to 1.5 km) of Coteau-du-Lac. However, local sources were still contributing heavily to the lowest portion of the profile, with 50% of the NBL-measured flux coming from within 1 km of the measurement site, which is within the typical farm size in Eastern Ontario and Western Quebec (Objective 3). Hypotheses 3 and 4 can therefore be accepted.

Hypothesis 5: The 'top-down' NBL budget method gives values that accurately reflect fluxes originating at the surface within a defined source area.

The validity of the NBL budget method was examined through a ground-based verification of 'top-down' NBL-measured fluxes (Objective 5). Detailed CH_4 profiles provided preliminary ground-based verification by showing that point sources were reflected in respective profiles as their footprints moved closer to and further from these areas (Chapter 4). A more in-depth analysis was performed by comparing NBL-measured flux values with weighted and aggregated flux values for four footprint model-defined areas across both field sites (Chapter 6). A 'bottom-up' aggregated method produced CO_2 and N_2O fluxes that in most cases were of the same order of magnitude as 'top-down' NBL-measured values. In comparison to the overall Coteau-du-Lac dataset, the aggregated fluxes calculated fell within a standard deviation of the average flux measured at this location through the summer of 2003. Better agreements were obtained with the Coteau-du-Lac data than those at the Ottawa site. At the Ottawa site, the inconsistent presence of a well-defined LLJ and heavy rainfall the day before NBL measurement at the Ottawa site produced short-term variations that were not accounted for by the flux aggregation method. At Coteau-du-Lac in contrast, the lack of both recent rainfall and farm management events and no apparent intermittent NBL phenomena allowed the aggregated flux to be a good approximation of the NBL-measured flux.

With evidence that the 'top-down' and 'bottom-up' approaches provide similar nocturnal estimates of GHG exchange, Hypothesis 5 is accepted in that the NBL budget method can be taken into consideration as a method to measure nocturnal fluxes over relatively homogeneous agricultural land.

7.2 SPECIFIC CONTRIBUTIONS FURTHERING THE ADVANCEMENT OF NBL BUDGET RESEARCH

The current study has built upon the work of previous NBL budget researchers, in particular that of Denmead *et al.* (1996), Pattey *et al.* (2002), and Mathieu *et al.* (2005) by examining: 1) the use of the NBL budget method in suboptimal NBL conditions where intermittent turbulence may cause downward entrainment of trace gases through the top of the NBL, 2) the extent of the spatial representation of the NBL budget, and 3) the validity of the NBL budget method by conducting a detailed ground-based verification of the fluxes it measures.

A number of advances were made, in particular:

An operational methodology was presented to simultaneously measure CO_2, N_2O, and CH_4 (previously measured only separately) by concomitantly measuring vertical concentration profiles of these gases in the NBL using a portable CO_2 analyzer and a bag air sampling system for N_2O and CH_4. It was also shown that during specifically defined suboptimal NBL conditions, where intermittent turbulence may cause the downward entrainment of trace gas-enriched air through the top of the NBL, the NBL budget technique can still be used to produce representative estimates of GHG fluxes through careful choice of the flux integration height by examining in detail the progression of vertical profiles over time, with specific reference to the co-location of the following: (1) u maxima, (2) shear and turbulent layers, and (3) where $\Delta CO_2/\Delta z$ approaches zero for a given profile. The height-contribution within the vertical profile of NBL-measured GHG flux has not previously been examined in relation to the upwind area of influence. It was shown that the trace gas source contribution to the vertical flux, under stable atmospheric conditions, varies spatially with the local sources exerting the most influence on the measured flux by identifying the contribution of vertical profile height intervals to the total measured NBL flux at both field sites, during optimal conditions exhibiting a sustained, very stable NBL and by using a footprint model to show that 50% of the flux came from local sources within 1 km upwind and that 80% of the flux came from within 2 km upwind of the launch site. This thesis also showed, as supported by spatial sampling data, that the NBL budget method as performed here with vertical concentration profiles in a single location fails to measure trace gas fluxes from strong point sources such as methane. Lastly, prior to this study, no ground-based verification of the NBL budget method had been conducted. This thesis verifies the ‘top-down’ NBL budget method using two ‘bottom-up’ approaches by showing that point sources within two to three km were reflected in respective detailed CH_4 concentration profiles as their footprints moved closer to and further from these sources, and by comparing and showing the agreement, during baseline atmospheric and farm management conditions, between NBL-measured fluxes of CO_2 and N_2O and footprint-weighted and aggregated individual ground-level sources of these gases, within four footprint model-defined upwind source areas.

7.3 SCOPE FOR FUTURE STUDY

To enhance the results of this study, more work with detailed N_2O and CH_4 profiles using more sensitive instruments, such as a TDL-TGA (tunable diode laser trace gas analyzer) would be necessary to confirm that vertical distribution of these gases is similar to CO_2 (preferably by measuring these three gases simultaneously), with the opportunity to perform spatial measurements in order to see the effect of substituting them in the near-surface vertical profile interval. More frequent profiles of the NBL, ideally even continuous sampling, instantaneous over the height of the NBL, would improve overall certainty in the NBL budget method, by precisely tracking the evolution of the NBL and movement of gases within it. This is possible with the addition of continuous measurement techniques such as the use of a SODAR/RASS. The recently established tall-tower super-sites in North America will provide continuous data collection in this regard at fixed levels through the lower atmosphere. A study of within-canopy GHG storage and release at the onset of turbulent events (particularly LLJs) as well as a detailed study of the contributions of advection in the form of drainage flow would provide more insight into trace gas exchange in the NBL and give a more complete representation of fluxes from the agricultural landscape. More work is needed to improve footprint models that are representative of nighttime conditions. A tracer release study using SF_6 (a non-natural tracer gas) could provide information on trace gas distribution in the NBL.

LITERATURE CITED

Acevedo, O.C., Moraes, O.L.L, Da Silva, R., Fitzjarrald, D.R., Sakai, R.K., Staebler, R.M., and Czikowskyw, M.J., 2004. Inferring nocturnal surface fluxes from vertical profiles of scalars in an Amazon pasture. Global Change Biol., 10, 886–894.

Akinremi, O. O., McGinn, S. M., and McLean H. D. J., 1999. Effects of soil temperature and moisture on soil respiration in barley and fallow plots. Can. J. Soil Sci. 79: 5–13.

Allaire, S. E., Dufour-L'Arrivée, C., Lafond, J. A., Lalancette, R. and Brodeur, J., 2008. Carbon dioxide emissions by urban turfgrass areas. Can. J. Soil Sci., 88: 529-532.

Ambus, P., and Christensen, S., 1995. Spatial and seasonal nitrous oxide and methane fluxes in Danish forest-, grassland-, and agroecosystems. J. Environ. Qual., 24: 993-1001.

Ambus, P., and Robertson, G.P., 1999. Fluxes of CH_4 and N_2O in aspen stands grown under ambient and twice-ambient CO_2. Plant Soil, 209: 1-8.

Amon, B., Amon, Th., Boxberger, J., and Alt, Ch., 2001. Emissions of NH_3, N_2O and CH_4 from dairy cows housed in a farmyard manure tying stall (housing, manure storage, manure spreading). Nutr. Cycl. Agroecosys., 60: 103–113.

André, J.C., and Mahrt, L., 1982. The nocturnal surface inversion and influence of clear-air radiative cooling. J. Atmos. Sci., 39: 864-878.

Andreas, E.L., Claffey, K.J., and Makshtas, A.P., 2000. Low-level atmospheric jets and inversions over the western Weddell Sea. Boundary-Layer Meteorol., 97: 459–486.

Aubinet, M., 2008. Eddy covariance CO_2 flux measurements in nocturnal conditions: an analysis of the problem. Ecol. Appl., 18: 1368-1378.

Baldocchi, D., 1997. Flux footprints within and over forest canopies. Boundary-Layer Meteorol., 85: 273-292.

Baldocchi, D., 2003. Assessing the eddy covariance technique for evaluating carbon dioxide exchange rates of ecosystems: past, present, and future. Global Change Biol., 9: 479-492.

Baldocchi, D., Valentini, R., Running, S., Oechel, W., and Dahlman, R., 1996. Strategies for measuring and modelling carbon dioxide and water vapour fluxes over terrestrial ecosystems. Global Change Biol., 2: 159-168.

Banta, R.M., Mahrt, L., Vickers, D., Sun, J., Balsley, B.B., Pichugina, Y.L., and Williams E.J., 2007. The very stable boundary layer on nights with weak low-level jets. J. Atmos. Sci., 64: 3068-3090.

Banta, R.M., Newsom R.K., Lundquist J.K., Pichugina Y.L., Coulter R. L., and Mahrt., L., 2002. Nocturnal low-level jet characteristics over Kansas during CASES-99. Boundary-Layer Meteorol., 105: 221–252.

Banta, R.M., Pichugina, Y.L., and Brewer, W.A., 2006. Turbulent velocity-variance profiles in the stable boundary layer generated by a nocturnal low-level jet. J. Atmos. Sci., 63: 2700–2719.

Batjes, N.H., 1998. Mitigation of atmospheric CO_2 concentrations by increased carbon sequestration in the soil. Bio. Fertil. Soils, 27: 230-235.

Beauchamp, E.G., 1997. Nitrous oxide emission from agricultural soils. Can. J. Soil Sci., 77: 113-123.

Beswick, K.M., Simpson, T.W., Fowler, D., Choularton, T.W., Gallagher, M.W., Hargreaves, K.J., Sutton, M.A., and Kayes, A., 1998. Methane emissions on large scales. Atmos. Environ., 32(19): 3283-3291.

Beyrich, F., Leps, J.-P., Mauder, M., Bange, J., Foken, T., Huneke, S., Lohse, H., Lüdi, A., Meijninger, W.M.L., Mironov, D., Weisensee, U., Zittel, P., 2006. Area-averaged surface fluxes over the LITFASS region based on eddy-covariance measurements. Boundary-layer Meteorol., 121: 33-65.

Beyrich, F., Richter, S.H., Weisensee, U., Kohsiek, W., Lohse, H., de Bruin, H.A.R., Foken, T., Göckede, M., Berger, F., Vogt, R., and Batchvarova, E., 2002. Theor. Appl. Climatol., 73: 19-34.

Blackadar, A.K., 1957. Boundary layer maxima and their significance for the growth of nocturnal inversions. Bull. Am. Meterol. Soc., 38: 283-290.

Boeckx, P., van Cleemput, O., and Villaralvo, I., 1997. Methane oxidation in soils with different textures and land use. Nutr. Cycl. Agroecosys. 49: 91–95.

Bouwman, A.F., Derwent, R.G., and Dentener, F.J., 1999. Towards reliable global bottom-up estimates of temporal and spatial patterns of emissions of trace gases and aerosols from land-use related and natural sources. In: Bouwman, A.F. (Ed.). Approaches to Scaling Trace Gas Fluxes in Ecosystems. Elsevier Science B.V.

Bowden, R.D., Melillo, J.M., Steudler, P.A., and Aber, J.D., 1991. Effects of nitrogen additions on annual nitrous oxide fluxes from temperate forest soils in the northeastern United States. J. Geophys. Res., 96(D5): 9321-9328.

Bowden, R.D., Rullo, G., Stevens, G.R., and Steudler, P.A., 2000. Soil fluxes of carbon dioxide, nitrous oxide, and methane at a productive temperate deciduous forest. J. Environ. Qual., 29: 268-276.

Bowden, R.D., Steudler, P.A., Melillo, J.M., and Aber, J.D., 1990. Annual nitrous oxide fluxes from temperate forest soils in the northeastern United States. J. Geophys. Res.. 95(D9): 13997-14005.

Brady, N.C., and Weil, R.R., 2002. The Nature and Properties of Soils. (13th ed.). Prentice Hall, NJ.

Bronick, C.J., and Lal., R., 2005. Manuring and rotation effects on soil organic carbon concentration for different aggregate size fractions on two soils in northeastern Ohio, USA. Soil Till. Res. 81: 239–252.

Brost, R.A., and Wyngaard, J.C., 1978. A model study of the stably stratified planetary boundary layer. J. Atmos. Sci. 35: 1427-1440.

Brown, H. A., Wagner-Riddle, C., and Thurtell, G. W., 2000. Nitrous oxide flux from solid dairy manure in storage as affected by water content and redox potential. J. Environ. Qual. 29: 630–638.

Brown, H. A., Wagner-Riddle, C., and Thurtell, G. W, 2002**.** Nitrous oxide flux from a solid dairy manure pile measured using a micrometeorological mass balance method. Nutr. Cycl. Agroecosyst., 62: 53–60.

Brown, L., Syed, B., Jarvis, S.C., Sneath, R.W., Phillips, V.R., Goulding, K.W.T., and Li, C., 2002. Development and application of a mechanistic model to estimate emission of nitrous oxide from UK agriculture. Atmos. Environ., 36: 917-928.

Burton, D.L., and Beauchamp, E.G., 1994. Profile nitrous oxide and carbon dioxide concentrations in a soil subject to freezing. Soil Sci. Soc. Am. J., 58: 115-122.

Burton, D.L., Bergstrom, D.W., Covert, J.A., Wagner-Riddle, C., and Beauchamp, E.G., 1997. Three methods to estimate N_2O fluxes as impacted by agricultural management. Can. J. Soil Sci., 77: 125-134.

Businger, J. A., 1973. Turbulent transfer in the atmospheric surface layer’. In: D. H. Haugen (Ed.). Workshop on Micrometerology. American Meteorological Society, Boston, MA, pp. 67–100.

Businger, J.A., 1986. Evaluation of the accuracy with which dry deposition can be measured with current micrometeorological techniques. J. Climate Appl. Meteorol. **25**: 1100–1124.

Cai, X., and Leclerc, M.Y., 2007. Forward-in-time and backward-in-time dispersion in the convective boundary layer: The concentration footprint. Boundary-Layer Meteorol., 123: 201-218.

Castro, M.S., Steudler, P.A., Melillo, J.M., Aber, J.D., and Millham, S., 1993. Exchange of N_2O and CH_4 between the atmosphere and soils in spruce-fir forests in the northeastern United States. Biogeochem., 18: 119-135.

Caughey, S.J., Wyngaard, J.C., and Kaimal, J.C., 1979. Turbulence in the evolving stable boundary layer. J. Atmos. Sci., 36: 1041-1052.

Chen, J.M., Chen, B., and Tans, P., 2007. Deriving daily carbon fluxes from hourly CO_2 mixing ratios measured on the WLEF tall tower: An upscaling methodology. J. of Geophys. Res., 112: G01015.

Chen, B., Chen, J.M., Gang, M., Black, T.A., and Worthy, D.E.J., 2008. Comparison of regional carbon flux estimates from CO2 concentration measurements and remote sensing based footprint integration. Global Biogeochem. Cycles, 22: GB2012.

Choularton, T.W., Gallagher, M.W., Bower, K.N., Fowler, D., Zahniser, M., and Kaye, A., 1995. Trace gas flux measurements at the landscape scale using boundary-layer budgets. Phil. Trans. R. Soc. Lond. A, 351: 357-369.

Corre, M.D., van Kessel, C., and Pennock, D.J., 1996. Landscape and seasonal patterns of nitrous oxide emissions in a semiarid region. Soil Sci. Soc. Am. J., 60: 1806-1815.

Coulter, R.L., 1990. A case study of turbulence in the stable nocturnal boundary layer. Boundary-Layer Meteorol., 52 (1-2): 75-91.

CPVQ (Conseil des productions végétales du Québec), 2000. Fertilizer Recommendations. (1st Ed.).

Dalal, R.C., Allen, D.E., Livesley, S.J., and Richards, G. 2008. Magnitude and biophysical regulators of methane emission and consumption in the Australian agricultural, forest, and submerged landscapes: a review. Plant Soil, 309: 43–76.

Del Grosso, S. J., Ojima, D. S., Parton, W. J., Mosier, A. R., Peterson, G. A. and Schimel, D. S. 2002. Simulated effects of dryland cropping intensification on soil organic matter and greenhouse gas exchanges using the DAYCENT ecosystem model. Environ. Pollut. 116: S75-S83.

Denmead, O.T., Leuning, R., Griffith, D.W.T., Jamie, I.M., Esler, M.B., Harper, L.A., and Freney, J.R., 2000a. Verifying inventory predictions of animal methane emissions with meteorological measurements. Boundary-Layer Meteorol., 96: 187-209.

Denmead, O.T., Leuning, R., Jamie, I.M., Griffith, D.W.T., 2000b. Nitrous oxide emissions from grazed pastures: Measurements at different scales. Global Change Biol., 2: 301-312.

Denmead, O.T., and Raupach, M.R., 1993. Methods for measuring atmospheric gas transport in agricultural and forest systems. In: Harper, L.A., Mosier, A.R., Duxbury, J.M., and Rolston, D.E. (Eds.). Agricultural Ecosystem Effects on Trace

Gases and Global Climate Change. ASA Special Publication Number 55, Madison, Wisconsin.

Denmead, O.T., Raupach, M.R., Dunin, F.X., Cleugh, H.A., and Leuning, R., 1996. Boundary-layer budgets for regional estimates of scalar fluxes. Global Change Biol., 2: 255-264.

Denmead, O.T., Harper, L.A., Freney, J.R., Griffith, D.W.T., Leuning, R., and Sharpe, R.R., 1998. A mass balance method for non-intrusive measurements of surface-air trace gas exchange. Atmos. Environ., 32: 3679-3688.

Derbyshire, S.H., 1990. Nieuwstadt's stable boundary layer revisited. Q. J. R. Meteorol. Soc., 116: 127-158.

Derbyshire, S.H., 1995. Stable boundary layers- Observations, models and variability. 1. Modelling and measurements. Boundary-Layer Meteorol., 74(1-2):19-54,

Desjardins, R.L., Denmead, O.T., Harper, L., McBain, M., Masse, D., and Kaharabata, S., 2004. Evaluation of a micrometeorological mass balance method employing an open-path laser for measuring methane emissions. Atmos. Environ., 38: 6855–6866.

Desjardins, R.L., MacPherson, Schuepp, P.H., 2000. Aircraft-based flux sampling strategies. In: Meyers, R.A. (Ed.), Encyclopedia of Analytical Chemistry. John Wiley & Sons, Ltd., Chichester, pp. 3573-3588.

Dörsch, P., Palojarvi, A., and Mommertz, S., 2004. Overwinter greenhouse gas fluxes in two contrasting agricultural habitats. Nutr. Cycl. Agroecosys., 70: 117–133.

Dunfield, P., Knowles, R., Dumont, R., and Moore, T.R., 1993. Methane production and consumption in temperate and subarctic peat soils–Response to temperature and pH. Soil Biol. Biochem. 25: 321-326.

Environment Canada, 1999. Canada's Greenhouse Gas Inventory: 1997 Emissions and Removals with Trends. Environment Canada: Greenhouse Gas Division, Pollution Data Branch, Air Pollution Prevention Directorate, Ottawa.

Environment Canada, 2002. Canada's Greenhouse Gas Inventory: 1990-2000. Environment Canada, Greenhouse Gas Division, Ottawa.

Environment Canada, 2005. Environmental Sustainability of Canada's Agricultural Soils: Technical Supplement- Fertilization and Nutrient Balance (residual nitrogen). Environment Canada, Knowledge and Strategies Integration Division, Ottawa. National Environmental Indicator Series webpage <http://www.ec.gc.ca/soer-ree/English/Indicators/Issues/Agriculture/Tech_Sup/agsup1_e.cfm> accessed Nov. 2006, based on: T.McRae, C.A.S. Smith, and L.J. Gregorich (eds.) 2000. Environmental Sustainability of Canadian Agriculture: Report of the Agri-Environmental Indicator Project. Agriculture and Agri-Food Canada.

Environment Canada, 2006. National Inventory Report: Greenhouse Gas Sources and Sinks in Canada 1990-2004. Greenhouse Gas Division, Environment Canada. <http://www.ec.gc.ca/pdb/ghg/inventory_report/2004_report/ta8_3_e.cfm>

Environment Canada, 2007. National Inventory Report: Greenhouse Gas Sources and Sinks in Canada 1990-2005. Greenhouse Gas Division, Environment Canada. <http://www.ec.gc.ca/pdb/ghg/inventory_report/2005_report/2005_report_e.pdf>

Environment Canada, 2008. National Inventory Report: Greenhouse Gas Sources and Sinks in Canada 1990-2006. Greenhouse Gas Division, Environment Canada. <http://www.ec.gc.ca/pdb/ghg/inventory_report/2006_report/2006_report_e.pdf>

Eriksen, J., and Jensen, L.S., 2001. Soil respiration, nitrogen mineralization and uptake in barley following cultivation of grazed grasslands. Biol. Fertil. Soils, 33:139–145.

Eugster, W., and Siegrist, F., 2000. The influence of nocturnal CO_2 advection on CO_2 flux measurements. Basic and Applied Ecol. 1(2): 177-188.

Falge, E., Baldocchi, D., Olson, R.J., Anthoni, P., Aubinet, M., Bernhofer, C., Burba, G., Ceulemans, R., Clement, R., Dolman, H., Granier, A., Gross, P., Greunwald, T., Hollinger, D., Jensen, N.-O., Katul, G., Keronen, P., Kowalski, A., Ta Lai, C., Law, B.E., Meyers, T., Moncrieff, J., Moors, E., Munger, J.W., Pilegaard, K., Rannik, €UU, Rebmann, C., Suyker, A., Tenhunen, J., Tu, K., Verma, S., Vesala, T., Wilson, K., Wofsy, S., 2001. Gap filling strategies for defensible annual sums of net ecosystem exchange. Agric. For. Meteorol., 107: 43–69.

Finn, D., Lamb, B., Leclerc, M.Y., Horst, T.W., 1996. Experimental evaluation of analytical and Lagrangian surface-layer flux footprint models. Boundary-Layer Meteorol. 80, 283–308.

Finnigan, J., 2004. The footprint concept in complex terrain. Agric. For. Meteorol., 127: 117-129.

Finnigan, J., 2008. An introduction to flux measurements in difficult conditions. Ecol. Appl., 18: 1340-1350.

Fisch, G., Culf, A.D., Malhi, Y., Nobre, C.A., and Nobre, A.D., 2000. Carbon dioxide measurements in the nocturnal boundary layer over Amazonian tropical forest. In:

R. Lal, J.M. Kimble, and B.A. Stewart (Eds.). Global Climate Change and Tropical Ecosystems. CRC Press LLC, Boca Raton, Florida, pp. 391-403.

Flesch, T.K., Wilson, J.D., and Yee, E., 1995. Backward-time Lagrangian stochastic dispersion models and their application to estimate gaseous emissions. J. Appl. Meteorol., 34: 1320-1332.

Foken, T., 2008. The energy balance closure problem: an overview. Ecol. Appl., 18: 1351-1367.

Foken, T., and Leclerc, M.Y., 2004. Methods and limitations in validation of footprint models. Agric. For. Meteorol., 127: 223–234.

Fortin, M.-C., Rochette, P., and Pattey, E., 1996. Soil carbon dioxide fluxes from conventional and no-tillage small-grain cropping systems. Soil Sci. Soc. Am. J. 60: 1541-1547.

Frolking, S.E., Mosier, A.R., Ojima, D.S., Li, C., Parton, W.J., Potter, C.S., Priesack, E., Stenger, R., Haberbosch, C., Dörsch, P., Flessa, H. & Smith, K.A., 1998. Comparison of N_2O emissions from soils at three temperate agricultural sites: simulations of year-round measurements by four models. Nutr. Cycl. Agroecosys., 52(2): 77-105

Funk, J.P., 1960. Measured radiative flux divergence near the ground at night. Q. J. R. Meteorol. Soc., 86: 382-389.

Garratt, J.R., 1992. The Atmospheric Boundary Layer. Cambridge University Press, Cambridge, England.

Gioli, B., Miglietta, F., De Martino, B., Hutjes, R.W.A., Dolman, H.A.J., Lindroth, A., Schumacher, M., Sanz, M.J., Manca, G., Peressotti, A., and Dumas, E.J., 2004.

Comparison between tower and aircraft-based eddy covariance fluxes in five European regions. Agric. For. Meteorol., 127: 1-16.

Göckede, M., Markkanen, T., Hasager, C.B., and Foken, T., 2006. Update of a footprint-based approach for the characterization of complex measurement sites. Boundary-Layer Meteorol., 118: 635-655.

Göckede, M., Markkanen, T., Mauder, M., Arnold, K., Leps, J-P., Foken, T., 2005. Validation of footprint models using natural tracer measurements from a field experiment. Agric. For. Meteorol., 135: 314–325.

Göckede, M., Rebmann, C., and Foken, T., 2004. A combination of quality assessment tools for eddy covariance measurements with footprint modeling for the characterization of complex sites. Agric. For. Meteorol., 127: 175-188.

Goodroad, L.L., and Keeney, D.R., 1984. Nitrous oxide emission from forest, marsh, and prairie ecosystems. J. Environ. Qual., 13: 448-452.

Gottschalk, L., Batchvarova, E., Gryning, S.-E., Lindroth, A., Melas, D., Motovilov, Y., Frech, M., Heikinheimo, M., Samuelsson, P., Grelle, A., Persson, T., 1999. Scale aggregation—comparison of flux estimates from NOPEX. Agric. For. Meteorol., 98-99: 103-119.

Goulden, M.L., Munger, J.W., Fan S.M., and Daube, B.C., 1996. Measurements of carbon sequestration by long-term eddy covariance: Methods and a critical evaluation of accuracy. Global Change Biol., 2: 169-182.

Grace, J., Y. Malhi, J. Lloyd, J. McIntyre, A.C. Mirand, P. Meir, and Miranda, H.S., 1996. The use of eddy covariance to infer the net carbon dioxide uptake of Brazilian rain forest. Global Change Biol., 2: 209-217.

Grachev, A.A., Fairall, C.W., Persson, P.O.G., Andreas, E.L., and Guest, P.L., 2005. Stable boundary-layer scaling regimes: The SHEBA data. Boundary-Layer Meteorol., 116: 201-235.

Grant, R. F. and Nalder, I. A., 2000. Climate change effects of a boreal aspen-hazelnut forest: estimates from the ecosystem model *ecosys*. Global Change Biol. 6: 183-200.

Grant, R.F., and Pattey, E., 1999. Mathematical modeling of nitrous oxide emissions from an agricultural field during spring thaw, Global Biogeochem. Cycles, 13(2), 679-694.

Grant, R.F., and Pattey, E., 2003. Modelling variability in N_2O emissions from fertilized agricultural fields. Soil Biol. Biochem., 35: 225–243.

Grant, R.F., and Pattey, E., 2008. Temperature sensitivity of N_2O emissions from fertilized agricultural soils: Mathematical modelling in ecosys. Global Biogeochem. Cycles, 22: GB4019.

Gregorich, E.G., Rochette, P., van den Bygaart A.J., and Angers, D.A., 2005. Greenhouse gas contributions of agricultural soils and potential mitigation practices in Eastern Canada. Soil Tillage Res., 83: 53–72.

Griffis, T.J., Zhang, J., Baker, J.M., Kljun, N., and Billmark, K., 2007. Determining carbon isotope signatures from micrometeorological measurements: Implications for studying biosphere-atmosphere exchange processes. Boundary-Layer Meterol., 123: 295-316.

Griffith, D.W.T., Leuning, R., Denmead, O.T., and Jamie, I.M., 2002. Air–land exchanges of CO_2, CH_4 and N_2O measured by FTIR spectrometry and micrometeorological techniques. Atmos. Environ., 36, 1833–1842.

Grimmond, C.S.B., King, T.S., Cropley, F.D., Nowak, D.J., and Souch, C., 2002. Local-scale fuxes of carbon dioxide in urban environments: methodological challenges and results from Chicago. Environ. Poll., 116: S243–S254.

Grimmond, C.S.B., Salmond, J.A., Oke, T.R., Offerle, B., and Lemonsu, A., 2004. Flux and turbulence measurements at a densely built-up site in Marseille: Heat, mass (water and carbon dioxide), and momentum. J. Geophys. Res., 109: D24101.

Groffman, P.M., Brumme, R., Butterbach-Bahl, K., Dobbie, K.E., Mosier, A.R., Ojima, D., Papen, H., Parton, W.J., Smith, K.A., and Wagner-Riddle, C., 2000. Evaluating annual nitrous oxide fluxes at the ecosystem scale. Global Biogeochem. Cycles, 14(4): 1061-1070.

Halldin, S., Gryning, S.-E., Gottschalk, L., Jochum, A., Lundin, L.-C., van de Griend, A.A., 1999. Energy, water and carbon exchange in a boreal forest landscape—NOPEX experiences. Agric. For. Meteorol., 98-99: 5-29.

Hansen, S., Maehlum, J.E., and Bakken, L.R., 1993. N_2O and CH_4 fluxes in soil influenced by fertilization and tractor traffic. Soil Biol. Biochem., 25: 621-630.

Hao, X.Y., Chang, C., Carefoot, J.M., Janzen, H.H., and Ellert, B.H., 2001a. Nitrous oxide emissions from an irrigated soil as affected by fertilizer and straw management. Nutr. Cycl. Agroecosys., 60: 1-8.

Hao, X.Y., Chang, C., Larney, F. J. and Travis, G. R., 2001b. Greenhouse gas emissions during cattle feedlot manure composting. J. Environ. Qual. 30: 376–386.

Hasager, C.B., and Jensen, N.O., 1999. Surface-flux aggregation in heterogeneous terrain. Q.J.R. Meteorol. Soc., 125: 2075-2102.

Helgason, B.L., Janzen, H.H., Chantigny, M.H., Drury, C.F., Ellert, B.H., Gregorich, E.G., Lemke, R.L., Pattey, E., Rochette, P., and Wagner-Riddle, C., 2005. Toward improved coefficients for predicting direct N_2O emissions from soil in Canadian agroecosystems. Nutr. Cycl. Agroecosys., 72: 87–99.

Hellebrand, H.J., Kern, J., and Scholz, V., 2003. Long-term studies on greenhouse gas fluxes during cultivation of energy crops on sandy soils. Atmos. Environ., 37: 1635–1644.

Hénault., C., Devis, X., Lucas, J.L., and Germon, J.C., 1998. Influence of different agricultural practices (type of crop, form of N-fertilizer) on soil nitrous oxide emissions. Biol. Fertil. Soils 27, 299–306.

Hope, D., Palmer, S.M., Billett, M.F., Dawson, J.J.C., 2001. Carbon dioxide and methane evasion from a temperate peatland stream. Limnol. Oceanogr., 46: 847-857.

Horst, T.W., 1999. The footprint for estimation of atmosphere-surface exchange fluxes by profile techniques. Boundary-Layer Meteorol. 90:171-188.

Horst, T.W., and Weil, J.C., 1992. Footprint estimation for scalar flux measurements in the atmospheric surface layer. Boundary-Layer Meteorol., 59: 279-296.

Horst, T.W., and Weil, J.C., 1994. How far is far enough?: The fetch requirements for micrometeorological measurement of surface fluxes. J. Atmos. Oceanic Technol., 11: 1018-1025.

Houghton, J.T., Ding, Y., Griggs, D.J., Noguer, M., van der Linden, P.J., Dai, X., Maskell, K., and. Johnson, C.A. (Eds.). 2001. Climate Change 2001: The Scientific Basis: Summary for Policymakers. Contribution of Working Group I to the Third Assessment Report of the Intergovernmental Panel on Climate Change. Cambridge University Press, UK. http://www.ipcc.ch/pub/tar/wg1/index.htm. Accessed April 18, 2002.

Houghton J.T., Meira Filho, L.G., Lim, B., Treanton, K., Mamaty, I, Bonduki, Y., Griggs, D.J., and Callender, B.A. (Eds.). 1997. Revised 1996 IPCC Guidelines for National Greenhouse Gas Inventories. IPCC/OECD/IEA, UK Meteorological Office, Bracknell.

Husted, S., 1994. Waste management: Seasonal variation in methane emission from stored slurry and solid manures. J. Environ. Qual., 23:585-592.

Hutchinson, J.J., Rochette, P., Verge, X., Desjardins, R., and Worth, D., 2007. Uncertainties in methane and nitrous oxide emissions from Canadian agroecosystems using Crystal Ball, Research Branch of Agriculture and Agri-Food Canada, Preliminary Report Submitted to Greenhouse Gas Division of Environment Canada.

IPCC, 2006. 2006 IPCC Guidelines for National Greenhouse Gas Inventories. Prepared by the National Greenhouse Gas Inventories Programme, Eggleston H.S., Buendia L., Miwa K., Ngara T. and Tanabe K. (eds). Published: IGES, Japan.

IPCC, 2007. Summary for Policymakers. In: Climate Change 2007: The Physical Science Basis. Contribution of Working Group I to the Fourth Assessment Report of the Intergovernmental Panel on Climate Change [Solomon, S., D. Qin, M. Manning, Z. Chen, M. Marquis, K.B. Averyt, M.Tignor and H.L. Miller (eds.)]. Cambridge University Press, Cambridge, United Kingdom and New York, NY, USA.

Jambert, C., Delmas, R., Serça, D., Thouron, L., Labroue, L., and Delprat, L., 1997. N_2O and CH_4 emissions from fertilized agricultural soils in southwest France. Nut. Cyc. Agroecosys., 48: 105-114.

Janzen, H.H., Desjardins, R.L., Asselin, J.M.R., and Grace, B., 1998. The Health of our Air: Toward Sustainable Agriculture in Canada. Agriculture and Agri-Food Canada, Research Branch, Ottawa.

Janzen, H.H., Desjardins, R.L., Rochette, P., Boehm, M., and Worth, D., 2008. Better Farming, Better Air: A Scientific Analysis of Farming Practice and Greenhouse Gases in Canada. Agriculture and Agri-Food Canada, Research Branch, Ottawa.

Jochum, M.A.O., de Bruin, H.A.R., Holtslag, A.A.M., and Belmonte, A.C., 2006. Area-averaged surface fluxes in a semiarid region with partly irrigated land: Lessons learned from EFEDA. J. Appl. Meteorol., 45: 856-874.

Jones, J.B., Jr., and Mulholland, P.J., 1998. Influence of drainage basin topography and elevation on carbon dioxide and methane supersaturation of stream water. Biogeochem., 40: 57-72.

Judd, M.J., F.M. Kelliher, M.J. Ulyatt, K.R. Lassey, K.R. Tate, I.D. Shelton, M.J. Harvey, and Walker, C.R., 1999. Net methane emissions from grazing sheep. Global Change Biol., 5: 647-657.

Kaharabata, S.K., Schuepp, P. H. and Desjardins, R. L., 1998. Methane emissions from above ground open manure slurry tanks. Global Biogeochem. Cycles 12: 545–554.

Kaharabata, S.K., Schuepp, P.H., and Fuentes, J.D., 1999. Source footprint considerations in the determination of volatile organic compound fluxes from forest canopies. J. Appl. Meteorol., 38: 878-884.

Kaimal, J. C., 1973. Turbulence spectra, length scales and structure parameters in the stable surface layer. Boundary-Layer Meteorol., 4: 289-309.

Karipot, A., Leclerc, M. Y., Zhang, G., Martin, T., Starr, G., Hollinger, D., McCaughey, J. H., and Hendrey, G. R., 2006. Nocturnal CO_2 exchange over a tall forest canopy associated with intermittent low-level jet activity. Theor. Appl. Climatol., 85 (3-4): 243-248.

Kebreab, E., Clark, K., Wagner-Riddle, C., and France, J. 2006. Methane and nitrous oxide emissions from Canadian animal agriculture: A review. Can. J. Anim. Sci., 86: 135-158.

Kelliher, F.M., Reisinger, A.R., Martin, R.J., Harvey, M.J., Price, S.J., and Sherlock, R.R., 2002. Measuring nitrous oxide emission rate from grazed pasture using Fourier-transform infrared spectroscopy in the nocturnal boundary layer. Agric. For. Meteorol., 111: 29-38.

Kellman, L., and Kavanaugh, K., 2008. Nitrous oxide dynamics in managed northern forest soil profiles: is production offset by consumption? Biogeochem., 90:115-128.

Kim, J., Guo, Q., Baldocchi, D.D., Leclerc, M.Y., Xu, L., and Schmid, H.P., 2006. Upscaling fluxes from tower to landscape: Overlaying flux footprints on high-resolution (IKONOS) images of vegetation cover. Agric. For. Meteorol., 136: 132-146.

Kinsman, R., Sauer, F.D., Jackson, H.A., and Wolynetz, M.S., 1995. Methane and carbon dioxide emissions from dairy cows in full lactation monitored over a six-month period. J. Dairy Sci., 78: 2760-2766.

Kirschbaum, M.U.F., 1995. The temperature dependence of soil organic matter decomposition, and the effect of global warming on soil organic C storage. Soil Biol. Biochem., 27: 753-760.

Knohl, A., and Buchman, N., 2005. Partitioning the net CO_2 flux of a deciduous forest into respiration and assimilation using stable carbon isotopes. Global Biogeochem. Cycles, 19: GB4008.

Knohl, A., Søe, A.R.B., Kutsch, W.L., Göckede, M., and Buchmann, N., 2008. Representative estimates of soil and ecosystem respiration in an old beech forest. Plant Soil, 302: 189-202.

Knowles, R., 1982. Denitrification. Microbiol. Rev., 46: 43-70.

Kljun, N., Calanca, P., Rotach, M.W., and Schmid, H.P., 2004. A simple parameterisation for flux footprint predictions. Boundary-Layer Meteorol., 112, 503-523. On-line model: http://footprint.kljun.net/index.php.

Kljun, N., Rotach, M.W., and Schmid, H.P., 2002. A three-dimensional backward Lagrangian footprint model for a wide range of boundary-layer stratifications. Boundary-Layer Meteorol., 103: 205-226.

Kormann, R., and Meixner, F.X., 2001. An analytical footprint model for non-neutral stratification. Boundary-Layer Meteorol., 99: 207-224.

Kuhlmann, A.J., Worthy, D.E.J., Trivett, N.B.A., and Levin, I., 1998. Methane emissions from a wetland region within the Hudson Bay Lowland: An atmospheric approach. J. Geophy. Res., 103(D13): 16009-16016.

Laville, P., Jambert, C., Cellier, P., and Delmas, R., 1999. Nitrous oxide fluxes from a fertilized maize crop using micrometeorological and chamber methods. Agric. For. Meteorol., 96:19-38.

Leclerc, M.Y., Karipot, A., Prabha, T., Allwine, G., Lamb, B., and Gholz, H.L., 2003a. Impact of non-local advection on flux footprints over a tall forest canopy: A tracer flux experiment. Agric. For. Meteorol., 115: 19-30.

Leclerc, M.Y., Meskhidze, N., Finn, D., 2003b. Comparison between measured tracer fluxes and footprint model predictions over a homogeneous canopy of intermediate roughness. Agric. For. Meteorol., 117: 145–158.

Leclerc, M.Y., Shen, S., and Lamb, B., 1997. Observations and large-eddy simulation modeling of footprints in the lower convective boundary layer. J. Geophys. Res., 102 (D8): 9323-9334.

Leclerc, M.Y., and Thurtell, G.W., 1990. Footprint prediction of scalar fluxes using a Markovian analysis. Boundary-Layer Meteorol., 52: 247-258.

Lee, X., 1998. On micrometeorological observations of surface-air exchange over tall vegetation. Agric. For. Meteorol., 91: 39-49.

Lemus, R., and Lal, R., 2005. Bioenergy crops and carbon sequestration. Crit. Rev. Plant Sci., 24(1): 1-21.

Lessard, R., Rochette, P., Gregorich, E.G., Desjardins, R.L., and E. Pattey., 1997. CH_4 fluxes from a soil amended with dairy cattle manure and ammonium nitrate. Can. J. Soil Sci., 77: 179-186.

Lessard, R., Rochette, P., Topp, E., Pattey, E., Desjardins, R.L., and Beaumont, G., 1994. Methane and carbon dioxide fluxes from poorly drained adjacent cultivated and forest sites. Can. J. Soil Sci., 74: 139-146.

Lettau, H.H., and Davidson, B. (Eds.), 1957. Exploring the Atmosphere's First Mile: Proceedings of the Great Plains Turbulence Field Program, 1 August to 8 September 1953, O'Neill, Nebraska. Volume 2: Site Description and Data Tabulation. 1st ed., Pergammon Press, London.

Li, C., Frolking, S. and Frolking, T. A., 1992a. A model of nitrous oxide evolution from soil driven by rainfall events: 1. Model structure and sensitivity. J. Geophys. Res. 97: 9759- 9776.

Li, C., Frolking, S. and Frolking, T. A., 1992b. A model of nitrous oxide evolution from soil driven by rainfall events: 2. Model applications. J. Geophys. Res. 97: 9777-9783.

Li, C., Frolking, S. and Harris, R., 1994. Modeling carbon biogeochemistry in agricultural soils. Global Biogeochem. Cycl. 8: 237-254.

Liebig, J., 1840. Chemistry in its Application to Agriculture and Physiology. 1st ed.

Linn, D. M., and Doran, J. W., 1984. Effect of water-filled pore space on carbon dioxide and nitrous oxide production in tilled and non-tilled soils. Soil Sci. Soc. Am. J., 48: 1267-1272.

Long, I.F., Monteith, J. L., Penman, H.L., and Szeicz, G., 1964. The plant and its environment. Meteorol. Rundsch. 17: 97-101.

Macpherson, J.I., Desjardins, R.L., Schuepp, P.H., and Pearson, R., Jr., 1995. Aircraft-measured ozone deposition in the San Joaquin Valley of California. Atmos. Environ., 29: 3133-3145.

Mahrt, L., 1981. The early evening boundary layer transition. Quart. J. Roy. Meteorol. Soc. 107: 329-343.

Mahrt, L., 1996. The bulk aerodynamic formulation over heterogeneous surfaces. Boundary-Layer Meteorol., 78: 87-119.

Mahrt, L., 1998. Stratified atmospheric boundary layers and breakdown of models. Theor. Comp. Fluid Dyn., 11: 263-279.

Mahrt, L., 1999. Stratified atmospheric boundary layers. Boundary-Layer Meteorol., 90: 375-396.

Mahrt, L., Heald, R.C., Lenschow, D.H., Stankov, B.B., and Troen, I.B., 1979. An observational study of the structure of the nocturnal boundary layer. Boundary-Layer Meteorol., 17: 247-264.

Mahrt, L., Lee, X., Black, A., Neumann, H., and Staebler, R.M., 2000. Nocturnal mixing in a forest subcanopy. Agric. For. Meteorol., 101:67-78.

Mahrt, L., Sun, J., Blumen, W., Delany, T., and Oncley, S., 1998. Nocturnal boundary-layer regimes. Boundary- Layer Meteorol., 88: 255-278.

Mahrt, L. and Vickers, D., 2002. Contrasting vertical structures of nocturnal boundary layers. Boundary-Layer Meteorol., 105: 351–363.

Mahrt, L., and Vickers, D., 2006. Extremely weak mixing in stable conditions. Boundary-Layer Meteorol., 119: 19-39.

Mahrt, L., Vickers, D., Nakamura, R., Soler, M.R., Sun, J., Burns, S., Lenschow, D.H., 2001. Shallow drainage flows. Boundary-Layer Meteorol., 101: 243-260.

Malhi, Y., Baldocchi, D., and Jarvis, P., 1999. The carbon balance of tropical, temperate and boreal forests. Plant Cell Environ., 22:715-740.

Martens, D.A., Reedy, T.E., and Lewis, D.T., 2003. Soil organic carbon content and composition of 130-year crop, pasture and forest land-use managements. Global Change Biol., 10: 65–78.

Mason, P.J., 1988. The formation of areally-averaged roughness lengths. Q.J.R. Meteorol. Soc., 114: 399-420.

Massé, D. I., Croteau, F., Patni, N. K. and Masse, L., 2003. Methane emissions from dairy cow and swine manure slurries stored at 10ºC and 15ºC. Can. Biosyst. Engin. 45: 6.1–6.6.

Massman, W. J., and Lee, X. 2002. Eddy covariance flux corrections and uncertainties in long term studies of carbon and energy exchanges. Agric. For. Meteorol., 113: 121–144.

Mathieu, N., Strachan, I.B., Leclerc, M.Y., Karipot, A., and Pattey, E., 2005. Role of low-level jets and boundary-layer properties on the NBL budget technique. Agric. For. Meteorol., 135: 35-43.

McCann, T.J., and Associates, 1994. Uncertainties in Canada's 1990 Greenhouse Gas Emission Estimates. Independent consultant's report prepared for Environment Canada, Pollution Data Branch, Hull.

Mengel, K., 1992. Nitrogen: Agricultural productivity and environmental problems. In: Mengel, K., and Pilbeam, D.J. (Eds.). Nitrogen Metabolism of Plants. Oxford University Press, New York, 1-16.

Meyer, C.P., Galbally, I.E., Griffith, D.W.T., Weeks, I.A., Jamie, I.M., and Wang, Y.-P., 1997. Trace gas exchange between soil and atmosphere in southern NSW using flux chamber measurement techniques. In: Leuning, R., Denmead, O.T., Griffith, D.W.T., Jamie, I.M., Isaacs, P., Hacker, J., Meyer, C.P., Galbally, I.E., Raupach, M.R., Esler, M.B. (Eds.) Assessing Biogenic Sources and Sinks of Greenhouse Gases at Three Interlinking Scales. Consultancy Report 97-56, CSIRO Land and Water, Canberra, Australia.

Michalski, L., Eckersdorf, K., Kucharski, J., McGhee, J., 2001. Temperature Measurement. (2nd Ed.) John Wiley & Sons Ltd., Chichester, England.

Moeng, C.-H., 1984. A large-eddy-simulation model for the study of planetary boundary-layer turbulence. J. Atmos. Sci., 41: 2052-2062.

Molina, J.A.E., Clapp, C.E., Shaffer, M.J., Chichester, F.W., and Larson, W.E., 1983. NCSOIL, a model of nitrogen and carbon transformations in soil: Description, calibration, and behaviour. J. Environ. Qual., 3: 391-396

Moore, T.R., and Knowles, R., 1989. The influence of water table levels on methane and carbon dioxide emissions from peatland soils. Can. J. Soil Sci., 69: 33-38.

Monteny, G.J., Groenestein, C.M., and Hilhorst, M.A., 2001. Interactions and coupling between emissions of methane and nitrous oxide from animal husbandry. Nutr. Cycl. Agroecosys., 60: 123-132.

Mosier, A., Schimel, D., Valentine, D., Bronson, K., and Parton, W., 1991. Methane and nitrous oxide fluxes in native, fertilized, and cultivated grasslands. Nature, 350: 330-332.

Myklebust, M.C., Hipps, L.E., and Ryel, R.J., 2008. Comparison of eddy covariance, chamber, and gradient methods of measuring soil CO_2 efflux in an annual semi-arid grass, *Bromus tectorum*. Agric. For. Meteorol., 148: 1894–1907.

Natural Resources Canada, 2000. National Private Vehicle Use Survey - October 1994 to September 1996 - Summary Report; Catalogue No. M92-190/2000. Natural Resources Canada, Office of Energy Efficiency, Ottawa.

Natural Resources Canada, 2004. Fuel Efficiency Benchmarking in Canada's Trucking Industry. Natural Resources Canada, Office of Energy Efficiency, Ottawa. <http://oee.nrcan.gc.ca/transportation/business/documents/case-studies/fuel-effic-benchm.cfm?attr=16>, Accessed on-line: Nov. 2006.

Natural Resources Canada, 2006. Fuel Consumption Ratings Tool. Natural Resources Canada, Office of Energy Efficiency, Ottawa. <http://oee.nrcan.gc.ca/transportation/tools/fuelratings/ratings-search.cfm?attr=8>, Accessed on-line: Nov. 6, 2006.

Neftel, A., Spirig, C., and Ammann, C., 2008. Application and test of a simple tool for operational footprint evaluations. Environ. Pollut., 152: 644-652.

Nemitz, E., Hargreaves, K.J., McDonald, A.G., Dorsey, J.R., and Fowler, D., 2002. Micrometeorological measurements of the urban heat budget and CO_2 emissions on a city scale. Environ. Sci. Technol., 36: 3139-3146.

Nicholas, J.V., and White, D.R., 2001. Traceable Temperatures: An Introduction to Temperature Measurement and Calibration. (2^{nd} ed.). John Wiley & Sons, Ltd., Chichester, England.

Nieuwstadt, F.T.M., 1984. The turbulent structure of the stable, nocturnal boundary layer. J. Atmos. Sci., 41: 2202-2216.

Nyborg, M., Laidlaw, J.W., Solberg, E.D., and Malhi, S.S., 1997. Denitrification and nitrous oxide emissions from a Black Chernozemic soil during spring thaw in Alberta. Can. J. Soil Sci., 77:153-160.

Nyhan, J.W., 1976. Influence of soil temperature and water tension on the decomposition rate of carbon-14 labelled herbage. Soil Sci., 121: 288-293.

Ogunjemiyo, S.O., Kaharabata, S.K., Schuepp, P.H., MacPherson, I.J., Desjardins, R.L., Roberts., D.A.. 2003. Methods of estimating CO_2, latent heat and sensible heat fluxes from estimates of land cover fractions in the flux footprint. Agric. For. Meteorol., 117: 125–144.

Oke, T.R., 1987. Boundary Layer Climates. Methuen and Co., Ltd., Cambridge, England.

Ontario Ministry of Transportation, 2004. Preliminary Design Study and Environmental Assessment, Highway 417 (Ottawa Queensway), from Highway 416 to Anderson Road. G.W.P. 663-93-00 C.A. 4005-A-000090 Traffic Operations Report, December 30, 2003. <http://www.mto.gov.on.ca/english/engineering/417ea/traffic/data.htm#2-2>, Accessed on-line: Nov. 7, 2006.

Ontario Ministry of Transportation, 2006. Ontario Road Safety Annual Report 2004: 5. The Vehicle. <http://www.mto.gov.on.ca/english/safety/orsar/orsar04/chp5_04.htm>, Accessed on-line: Nov. 2006.

Parsons, L.L., Murray, R.E., and Scott Smith, M., 1991. Soil denitrification dynamics: spatial and temporal variations of enzyme activity, populations, and nitrogen gas loss. Soil Sci. Soc. Am. J., 55: 90-95.

Parton, W. J., Hartman, M. D., Ojima, D. S. and Schimel, D. S., 1998. DAYCENT: its land surface submodel-description and testing. Global Planet. Change 19: 35-48.

Pasteur, L., 1857. Mémoire sur la fermentation appeleé lactique. In: Mémoires de 1a Société des Sciences, de l'Agriculture et des Arts de Lille, Séance du 3 août 1857, 2e Série, V, 13-26.

Patterson, Vince, 2006. Senior Project Manager, Transportation – Strategic Planning, City of Ottawa. Personal communication *via* e-mail.

Pattey, E., Blackburn, L. G., Strachan, I. B., Desjardins, R. and Dow, D., 2008. Spring thaw and growing season N_2O emissions from a field planted with edible peas and a cover crop. Can. J. Soil Sci. 88: 241-249.

Pattey, E., Desjardins, R.L., and Dow, D., 1998. Measuring nighttime CO_2 flux. In: Proceedings of the 23rd Conference on Agricultural and Forest Meteorology, 2-6 November 1998. Albuquerque, New Mexico. 433-435.

Pattey, E., Desjardins, R.L., and St-Amour, G., 1997. Mass and energy exchanges at a southern old black spruce site during key periods of BOREAS 1994. J. Geophys. Res., 102(D24): 28967-28976.

Pattey, E., Edwards G.C., Desjardins, R.L., Pennock, D.J., Smith, W., Grant, B., and MacPherson, J.I., 2007. Tools for quantifying N_2O emissions from agroecosystems. Agric. For. Meteorol., 142: 103-119.

Pattey, E., Edwards, G., Strachan, I.B., Desjardins, R.L., Kaharabata, S.K,, Wagner-Riddle, C., 2006a. Towards standards for measuring greenhouse gas emissions from whole farms. Can. J. Soil Sci., 86:373–400.

Pattey, E., Strachan, I.B., Boisvert, J.B., Desjardins, R.L., and McLaughlin, N.B., 2001. Detecting effects of nitrogen rate and weather on corn growth using micrometeorological and hyperspectral reflectance measurements. Agric. For. Meteorol., 108: 85-99.

Pattey, E., Strachan, I.B., Desjardins, R.L., Edwards, G.C., Dow, D., and MacPherson, J.I., 2006b. Application of a tunable diode laser to the measurement of CH4 and N2O fluxes from field to landscape scale using several micrometeorological techniques. Agric. For. Meteorol., 136: 222-236.

Pattey, E., Strachan, I.B., Desjardins, R.L., and Massheder, J., 2002. Measuring nighttime flux over terrestrial ecosystems using eddy covariance and nocturnal boundary layer methods. Agric. For. Meteorol., 113: 145-158.

Paustian, K., Andrén, O., Janzen, H.H., Lal, R., Smith, P., Tian, G., Tiessen, H., van Noordwijk, M., and Woomer, P.L., 1997. Agricultural soils as a sink to mitigate CO_2 emissions. Soil Use Manage., 13: 230-244.

Pelletier, L., Moore, T. R., Roulet, N., Garneau, T. M., and Beaulieu-Audy, V., 2007. Methane fluxes from three peatlands in the La Grande Rivière watershed, James Bay lowland, Canada, J. Geophys. Res., 112, G01018.

Peng, G., Cai, X., Zhang, H., Li, A., Hu, F., Leclerc, M.Y., 2008. Heat flux apportionment to heterogeneous surfaces using flux footprint analysis. Adv. Atmos. Sci., 25: 107-116.

Petersen, S. O., Lind, A.-M. and Sommer, S. G., 1998. Nitrogen and organic matter losses during storage of cattle and pig manure. J. Agric. Sci. 130: 69–79.

Piomelli, U., 1999. Large-eddy simulation: Achievements and challenges. Prog. Aerosp. Sci., 35: 335-362.

Prescott, L.M., Harley, J.P., and Klein, D.A., 1993. Microbiology. (2nd ed.). Wm. C. Brown Publishers, IA.

Prior, S.A., Raper, R.L., and Runion G.B., 2004. Effect of implement on soil CO_2 efflux: Fall vs. spring tillage. TASAE., 47(2): 367−373.

Rannik, Ü., Aubinet, M., Kurbanmuradov, O., Sabelfeld, K.K., Markkanen, T., and Vesala, T., 2000. Boundary-Layer Meteorol., 97: 137-166.

Rannik, Ü., Markkanen, T., Raittila, J., Hari, P. and Vesala, T., 2003. Turbulence statistics inside and over forest: Influence on footprint prediction. Boundary-Layer Meteorol., 109: 163-189.

Rastogi, M., Singh, S., and Pathak, H., 2002. Emission of carbon dioxide from soil. Curr. Sci. India, 82(5): 510-517.

Raven, P.H., Evert, R.F., and Eichhorn, S.E., 1992. Biology of Plants. (5th ed.). Worth Publishers, New York.

Rebmann, C., Göckede, M., Foken, T., Aubinet, M., Aurela, M., Berbigier, P., Bernhofer, C., Buchmann, N., Carrara, A., Cescatti, A., Ceulemans, R., Clement, R., Elbers, J.A., Granier, A., Grünwald, T., Guyon, D., Havránková, K., Heinesch, B., Knohl, A., Laurila, T., Longdoz, B., Marcolla, B., Markkanen, T., Miglietta, F., Moncrieff, J., Montagnani, L., Moors, E., Nardino, M., Ourcival, J.-M., Rambal, S., Rannik, Ü., Rotenberg, E., Sedlak, P., Unterhuber, G., Vesala, T., and Yakir, D., 2005. Quality analysis applied on eddy covariance measurements at complex forest sites using footprint modelling. Theor. Appl. Climatol., 80: 121-141.

Reth, S., Göckede, M., and Falge, E., 2005. CO_2 efflux from agricultural soils in Eastern Germany – comparison of a closed chamber system with eddy covariance measurements. Theor. Appl. Climatol., 80: 105-120.

Roberson, T., Reddy, K.C., Reddy, S.S., Nyakatawa, E. Z., Raper, R. L., Reeves, D. W., and Lemunyon, J., 2008. Carbon dioxide efflux from soil with poultry litter applications in conventional and conservation tillage systems in Northern Alabama. J. Environ. Qual., 37: 535-541.

Richardson, R.F., 1920. The supply of energy from and to atmospheric eddies. Proc. R. Soc. London, A97: 354–373.

Rochette, P. and Bertrand, N., 2003. Soil air sample storage and handling using polypropylene syringes and glass vials. Can. J. Soil Sci., 83, 631–637.

Rochette, P., and Côté, D., 2000a. CH_4 fluxes and soil CH_4 concentration following application of pig slurry for the 19th consecutive year. Can. J. Soil Sci., 80: 387-390.

Rochette, P., and Côté, D., 2000b. Soil surface carbon dioxide fluxes induced by spring, summer, and fall moldboard plowing in a sandy loam. Soil Sci. Soc. Am. J., 63: 621-628.

Rochette, P., Desjardins, R.L., and Pattey, E., 1991. Spatial and temporal variability of soil respiration in agricultural fields. Can. J. Soil Sci., 71: 189-196.

Rochette, P., Ellert, B., Gregorich, E.G., Desjardins, R.L., Pattey, E., Lessard, R., and Johnson, B.G., 1997. Description of a dynamic closed chamber for measuring soil respiration and its comparison with other techniques. Can. J. Soil Sci., 77:195-203.

Roulet, N.T., Jano., A., Kelly, A., Klinger, L.F., Moore, T.R., Protz, R., Ritter, J.A., and Rouse, W.R., 1994. Role of Hudson Bay lowland as a source of atmospheric methane. J. Geophys. Res., 99(D1): 1439-1454.

Sartori, F., Lal, R., Ebinger, M.H., and Parrish, D.J., 2006. Potential soil carbon sequestration and CO_2 offset by dedicated energy crops in the USA. Crit. Rev. Plant Sci., 25(5): 441- 472.

Saurette, D. D., Chang, S. X. and Thomas, B. R., 2006. Some characteristics of soil respiration in hybrid poplar plantations in northern Alberta. Can. J. Soil Sci., 86: 257–268.

Schloesing, T., and Müntz, A., 1877. *Sur la nitrification par les ferments organisés.* Compt. Rend., lxxxiv., 301-303.

Schmid, H.P., 1994. Source areas for scalars and scalar fluxes. Boundary-Layer Meteorol., 67: 293-318.

Schmid, H.P., 1997. Experimental design for flux measurements: matching scales of observations and fluxes. Agric. For. Meteorol., 87: 179-200.

Schmid, H.P., 2002. Footprint modeling for vegetation atmosphere exchange studies: a review and perspective. Agric. For. Meteorol., 113: 159-183.

Schmid, H.P., and C.R. Lloyd, 1999. Spatial representativeness and the location bias of flux footprints over inhomogeneous areas. Agric. For. Meteorol., 93: 195-209.

Schmid, H.P., and Oke, T.R., 1990. A model to estimate the source area contributing to turbulent exchange in the surface layer over patchy terrain. Q.J.R. Meteorol. Soc., 116: 965-988.

Schuepp, P.H., Leclerc, M.Y., Macpherson, J.I., and Desjardins, R.L., 1990. Footprint prediction of scalar fluxes from analytical solutions of the diffusion equation. Boundary-Layer Meteorol., 50: 355-373.

Schulze, E.-D., Lloyd, J., Kelliher, F.M., Worth, C., Rebmann, C., Lühker, B., Mund, M., Knohl, A., Milyukova, I.M., Schulze, W., Ziegler, W., Varlagin, A.B., Sogachev, A.F., Valentini, R., Dore, S., Grigoriev, S., Kolle, O., Panfyorov, M.I., Tchebakova, N., Vygodskaya, N.N. 1999. Productivity of forests in the Euro-Siberian boreal region and their potential to act as a carbon sink – A synthesis. Global Change Biol., 5: 703–722.

Silvennoinen, H., Liikanen, A., Rintala, J., and Martikainen, P.J., 2008. Greenhouse gas fluxes from the eutrophic Temmesjoki River and its Estuary in the Liminganlahti Bay (the Baltic Sea). Biogeochem., 90:193-208.

Smedman, A-S., 1988. Observations of a multi-level turbulence structure in a very stable atmospheric boundary layer. Boundary-Layer Meteorol. 44: 231–253.

Smith, W.N., Desjardins, R.L., and Grant, B. 2001. Estimated changes in soil carbon associated with agricultural practices in Canada. Can. J. Soil Sci., 81: 221-227.

Smith, W.N., Desjardins, R.L., Grant, B., Li, C., Lemke, R., Rochette, P., Corre, M.D., and Pennock, D., 2002. Testing the DNDC model using N_2O emissions at two experimental sites in Canada. Can. J. Soil Sci., 82: 365-374.

Smith, W. N., Grant, B. B., Desjardins, R. L., Rochette, P., Drury, C. F. and Li, C., 2008. Evaluation of two process-based models to estimate soil N_2O emissions in Eastern Canada. Can. J. Soil Sci. 88: 251-260.

Soegaard, H., Jensen, N.O., Boegh, E., Hasager, C.B., Schelde, K., and Thomsen, A., 2003. Carbon dioxide exchange over agricultural landscape using eddy correlation and footprint modelling. Agric. For. Meteorol., 114: 153-173.

Soegaard, H., and Møller-Jensen, L., 2003. Towards a spatial CO_2 budget of a metropolitan region based on textural image classification and flux measurements. Remote Sens. Environ., 87: 283-294.

Soegaard, H., Nordstroem, C., Friborg, T., Hansen, B.U., Christensen, T.R., and Bay, C., 2000. Trace gas exchange in a high Arctic valley. 3. Integrating and scaling CO_2 fluxes from canopy to landscape using flux data, footprint modeling, and remote sensing. Global Biogeochem. Cycles, 14(3): 725-744.

Sogachev, A., and Lloyd, J.J., 2004. Using a one-and-a-half order closure model of the atmospheric boundary layer for surface flux footprint estimation. Boundary-Layer Meteorol., 112: 467-502.

Sogachev, A., Menzhulin, G., Heimann, M., and Lloyd, J., 2002. A simple three dimensional canopy-planetary boundary layer simulation model for scalar concentrations and fluxes. Tellus, 54B: 784-819.

Sorbjan, Z., 1989. Structure of the Atmospheric Boundary Layer. Prentice-Hall, New Jersey.

Spokas, K.A., and Bogner, J.E., 1996. Field system for continuous measurement of landfill gas pressures and temperatures. Waste Manage. Res. 14: 233–242.

Statistics Canada, 2003. Canadian Vehicle Survey: Annual, 2002. Catalogue no. 53-223-XIE. Statistics Canada, Transportation Division, Ottawa. Accessed on-line: http://www.statcan.ca/english/freepub/53-223-XIE/53-223-XIE2002000.pdf, Nov. 2006.

Statistics Canada, 2004. 2001 Agricultural Community Profiles. Accessed on-line: <http://www25.statcan.ca:8081/AgrProfile/acphome.jsp>, Mar. 1, 2007.

Statistics Canada. 2007. Ottawa, Ontario (table). 2006 Community Profiles. 2006 Census. Statistics Canada Catalogue no. 92-591-XWE. Ottawa. Released March 13, 2007. http://www12.statcan.ca/census-recensement/2006/dp-pd/prof/92-591/index.cfm?Lang=E (accessed February 4, 2009).

Steele, L.P., Krummel, P.B., and Langenfelds, R.L., 2007. Atmospheric CO_2 concentrations from sites in the CSIRO Atmospheric Research GASLAB air sampling network (August 2007 version). In: Trends: A Compendium of Data on Global Change, Carbon Dioxide Information Analysis Center, Oak Ridge National Laboratory, U.S. Department of Energy, Oak Ridge, TN, U.S.A. Accessed on-line: < http://cdiac.ornl.gov/trends/co2/csiro/csiro-alt.html>, Oct. 2008.

Stull, R.B., 1988. An Introduction to Boundary Layer Meteorology. (1st Ed.). Kluwer Academic Publishers, Dordrecht, Netherlands.

Sun, J., R. Desjardins, L. Mahrt, and I. MacPherson., 1998. Transport of carbon dioxide, water vapor, and ozone by turbulence and local circulations. J. Geophys. Res., 103 (D20): 25873-25885.

Sun, J., Lenschow, D.H., Burns, S.P., Banta, R.M., Newsom, R.K., Coulter, R., Frasier, S., Ince, T., Nappo, C., Balsley, B.B., Jensen, M., Mahrt, L., Miller, D., Skelly, B., 2004. Intermittent turbulence in stable boundary layers and the processes that generate it. Boundary-Layer Meteorol., 110: 255–279.

Suyker, A.E., Verma, S.B., Burba, G.G., Arkebauer, T.J., 2005. Gross primary production and ecosystem respiration of irrigated maize and irrigated soybean during a growing season. Agric. For. Meteorol., 131: 180–190.

Suyker, A.E., Verma, S.B., Burba, G.G., Arkebauer, T.J., Walter, D.T., and Hubbard, K.G., 2004. Growing season carbon dioxide exchange in irrigated and rainfed maize. Agric. For. Meteorol., 124: 1–13.

Swift, R.S., 2001. Sequestration of carbon by soils. Soil Sci., 166(11): 858-871.

Teepe, R., Brumme, R., Beese, F., 2001. Nitrous oxide emissions from soil during freezing and thawing periods. Soil Biol. Biochem. 33, 1269–1275.

Telmer, K., and Veizer, J., 1999. Carbon fluxes, pCO_2 and substrate weathering in a large northern river basin, Canada: carbon isotope perspectives. Chem. Geol., 159: 61-86.

Tenuta, M., Barry, D.A.J., Fairchild, G., and Beauchamp, E.G., 2001. Nitrous oxide production by manure samples collected from six manure-handling systems. Can. J. Soil Sci., 81: 33-38.

Topp, E., and Pattey, E., 1997. Soils as sources and sinks for atmospheric methane. Can. J. Soil Sci., 77:167-178.

Touraine, B., Daniel-Vedele, F., and Forde, B., 2001. Nitrate uptake and its regulation. In: Lea, P.J., and Morot-Gaudry, J.-F. (Eds.). Plant Nitrogen. Springer-Verlag Berlin Heidelberg, Paris, 1-36.

Velasco, E., Pressley, S., Allwine, E., Westberg, H., Lamb, B., 2005. Measurements of CO_2 fluxes from the Mexico City urban landscape. Atmos. Environ., 39: 7433–7446.

van Bochove, E., Gerald Jones, H., Bertrand, N., and Prévost, D., 2000. Winter fluxes of greenhouse gases from snow-covered agricultural soil: Intra-annual and interannual variations. Global Biogeochem. Cycles, 14(1): 113-125.

van den Pol-van Dasselaar, A., Corre, W.J., Prieme, A., Klemedtsson, A.K., Weslien, P., Stein, A., Klemedtsson, L., and Oenema, O., 1998. Spatial variability of methane, nitrous oxide, and carbon dioxide emissions from drained grasslands. Soil Sci. Soc. Am. J., 62: 810-817.

van Niel C.B., 1929. Photosynthesis in bacteria. In: Contribution to Marine Biology. Stanford University Press, Stanford, California, 161-169.

van Spanning, R.J.M., Delgado, M.J., and Richardson, D.J., 2005. The nitrogen cycle: Denitrification and its relationship to N_2 fixation. In: Werner, D. and Newton, W. E. (Eds.). Nitrogen Fixation in Agriculture, Forestry, Ecology, and the Environment. Springer Netherlands, 277-342.

Verma, S., Schimelfenig, T., and Suyker, A. (Principal Investigators for Mead, Nebraska AmeriFlux site), 2006. Ameriflux data from rainfed maize site accessed on-line: <http://public.ornl.gov/ameriflux/>, August 2006. This research was supported by the Office of Science (BER), U.S. Department of Energy, Grant No. DE-FG02-03ER63639.

Vesala, T., Huotari, J., Rannik, Ü., Suni, T., Smolander, S., Sogachev, A., Launiainen, S., and Ojala, A., 2006. Eddy covariance measurements of carbon exchange and latest and sensible heat fluxes over a boreal lake for a full open-water period. J. Geophys. Res., 111: D11101.

Vesala, T., Kljun, N., Rannik, U., Rinne, J., Sogachev, A., Markkanen, T., Sabelfeld, K., Foken, Th., and Leclerc. M.Y., 2007. Flux and concentration footprint modelling: state of the art. Environ. Poll., 152: 653-666.

von Wirén, N., Gojon, A., Chaillou, S., and Raper, D., 2001. Mechanisms and regulation of ammonium uptake in higher plants. In: Lea, P.J., and Morot-Gaudry, J.-F. (Eds.). Plant Nitrogen. Springer-Verlag Berlin Heidelberg, Paris, 61-78.

Wagner-Riddle, C., Furon, A., McLaughlin, N.L., Lee, I., Barbeau, J., Ayasundara, S.J., Parkin, G., Von Bertoldi, P., and Warland, J., 2007. Intensive measurement of nitrous oxide emissions from a corn–soybean–wheat rotation under two contrasting management systems over 5 years. Global Change Biol., 13: 1722–1736.

Wagner-Riddle, C., Park, K.-H., Thurtell, G.W., 2006. A micrometeorological mass balance approach for greenhouse gas flux measurements from stored animal manure. Agric. For. Meteorol., 136: 175–187.

Wagner-Riddle, C., Thurtell, G.W., Kidd, G.K., Beauchamp, E.G., and Sweetman, R., 1997. Estimates of nitrous oxide emissions from agricultural fields over 28 months. Can. J. Soil Sci., 77: 135-144.

Wagner-Riddle, C., Thurtell, G.W., King, K.M., Kidd, G.E., and Beauchamp, E.G., 1996. Nitrous oxide and carbon dioxide fluxes from a bare soil using a micrometeorological approach. J. Environ. Qual., 25: 898-907.

Walsh, C.J., Oke, T.R., Grimmond, C.S.B., Salmond, J.A., 2004. Fluxes of atmospheric carbon dioxide over a suburban area of Vancouver. In: Fifth Symposium on the Urban Environment, 23–27 August 2004, Vancouver, Canada.

Wang, F.L., and Bettany, J.R., 1995. Methane emission from a usually well-drained prairie soil after snowmelt and precipitation. Can. J. Soil Sci., 75: 239-241.

Wang, W.J., and Dalal, R.C., 2006. Carbon inventory for a cereal cropping system under contrasting tillage, nitrogen fertilisation and stubble management practices. Soil & Till. Res., 91: 68–74.

Warburg, O.H., 1919-1920 Ober die Gesehwindigkeit der photochemischen Kohlensfiurezersetzung in lebenden Zellen (I and II). Biochem. Z., 100:230-270; 103:188-217.

Warington, R., 1878-1891. On nitrification. Parts I-IV. Journ. Chem. Soc., 33: 44-51; 35: 429-56; 45: 637-72; 59: 484-529.

West, T.O., and Post, W.M., 2002. Soil organic carbon sequestration rates by tillage and crop rotation: a global data analysis. Soil Sci. Soc. Am. J., 66: 1930–1946.

Wilson, J.D., and Swaters, G.E., 1991. The source area influencing a measurement in the planetary boundary layer: The “footprint” and the “distribution of contact distance”. Boundary-Layer Meteorol., 55: 25-46.

Wilson, J.D., Thurtell, G.W., Kidd, G.E., and Beauchamp, E.G., 1982. Atmos. Environ., 16: 1861-1867.

Wilson, J.S. (Ed.), 2005. Sensor Technology Handbook. Elsevier, pp. 531-561.

Winogradsky, S. 1890-1891. Recherches sur les organismes de la nitrification. Annales de l’Institut Pasteur. 4: 215–231, 257–275, 760–811; 5: 92–100, 577–616.

Wohlfahrt, G., Anfang, C., Bahn, M., Haslwanter, A., Newesely, C., Schmitt, M., Drosler, M., Pfadenhauer, J., Cernusca, A., 2005. Quantifying nighttime ecosystem respiration of a meadow using eddy covariance, chambers and modeling. Agric. For. Meteorol., 128: 141–162.

Wood, N., and Mason, P.J., 1991. The influence of static stability on the effective roughness lengths for momentum and heat transfer. Q.J.R. Meteorol. Soc., 117: 1025-1056.

Worth, Devon, 2006. Technician, Agriculture and Agri-Food Canada (Environmental Health), Ottawa. Personal communication *via* e-mail.

Worthy, D.E.J., Levin, I., Trivett, N.B.A., Kuhlmann, A.J., Hopper, J.F., and Ernst, M.K., 1998. Seven years of continuous methane observations at a remote boreal site in Ontario, Canada. J. Geophys. Res., 103(D13): 15995-16007.

Yanai, J., Sawamoto, T., Oe, T., Kusa, K., Yamakawa, K., Sakamoto, K., Naganawa, T., Inubushi, K., Hatano, R., and Kosaki, T., 2003. Spatial variability of nitrous oxide emissions and their soil-related determining factors in an agricultural field. J. Environ. Qual., 32: 1965-1977.

Zinchenko, A.V., Paramonova, N.N., Privalov, V.I., and Reshetnikov, A.I., 2002. Estimation of methane emissions in the St. Petersburg, Russia, region: An atmospheric nocturnal boundary layer budget approach. J. Geophys. Res., 107(D20), 4416-4427

APPENDIX A: EXETAINER TUBE EVACUATION EFFICIENCY TEST

A.1 PROCEDURE FOR EVACUATION EFFICIENCY TEST

A.2 EVACUATION TEST RESULTS AND DISCUSSION

A.1. PROCEDURE FOR EVACUATION EFFICIENCY TEST

A.1.1. Goal of Procedure

To verify the degree of evacuation by an in-house-developed tube evacuation system and the maintenance of evacuation of 12-mL Exetainer-brand air sampling tubes sealed with both the manufacturer's septum and an additional PTFE septum, after three punctures (typical in preparation of tubes for field sample collection).

A.1.2. Materials

- in-house-developed evacuation apparatus w/ pressure indicator, capable of evacuating 10 Exetainer air sampling tubes simultaneously (Figure A.1). Vacuum pressure gauge: units not indicated, assumed psi.
- 80 12 mL Exetainer-brand glass air sample collection tubes (Labco, High Wycombe, UK)
- small vaccuum pump
- water
- beaker 600 mL or bigger
- 26G stainless steel Luer-Lok needles, 20 mL and 30 mL Becton-Dickinson polypropylene syringes
- 2 or 3 decimal balance
- tube rack

A.1.3. Procedure Followed (with notes from actual conduct of test), after Rochette and Bertrand (2004)

July 3, 2003: 40 tubes were tested for same-day evacuation efficiency after 3 septum punctures (as required in preparation of tubes for typical field use).

1. The initial evacuation of 4 sets of 10 tubes. Set of 40 tubes divided into 4 sets of 10 on tube rack:

1st row: 422-415-423-441-475-481-494-495-401-403;
2nd row: 500-454-420-442-417-438-436-444-434-424;
3rd row 456-421-416-492-439-425-414-493-405-480;
4th row: 460-455-419-437-406-440-497-402-418-404.

2. Tubes were placed onto evacuation apparatus by placing septum end of tubes onto 26 G needles found on apparatus (1 puncture on fresh double-septum). Evacuated each set of ten tubes for five minutes:

1st row: evacuation time from 9:37:09-9:42:09/9:42:37; 5min to 5 min 28 sec; *
2nd row: evacuation time from 9:45:15-9:50:15; ~5min;**

3rd row evacuation time from 9:54:29-9:59:29; ~5min; ***
4th row: evacuation time from 10:03:16-10:08:16; ~5min. ****

*note, evacuation system was shut down after the valves were closed at ~5min
**note, evacuation system was shut down at ~5min, however the valves were closed before the machine was closed, which caused confusion and the valves were reopened by a second party. The vacuum pressure dropped to 0.5 psi before they were all reclosed.
***note, evacuation system was shut down before the valves were closed at ~5min, they were closed in the order from 456 to 480. Pressure dropped from 28 to around 20 psi.
****note, evacuation system was shut down before the valves were closed at ~5min, they were closed in the order from 460 to 404. Pressure dropped from 28 psi to around 20 psi.

3. Filled tubes with 20 mL of N_2 (2nd puncture on septum).
   -a 26G 30mL syringe was flushed 3 times w/ N_2
   -the syringe was then filled to 20mL
   -the Exetainer sample tubes were then injected with 20mL of N_2, the volume initially pulled in by the vacuum was noted
   -the tubes were then over-pressurized with N_2 to inject a total volume of 20mL*
   *except for tubes 455 and 402 that have respectively only 11.5 and 9.8mL. (forgot to over-pressurize- no impact)

   (***caps were tightened***)

4. Evacuated each set of ten tubes for five minutes **again** (3rd puncture on septum).
   1st row: evacuation time from 11:46:41-11:51:41/11:52:12; 5min to 5 min 36s;*
   2nd row: evacuation time from 11:54:25-11:59:25/11:59:36; ~5min;**
   3rd row evacuation time from 12:48:00-12:53:00; ~5min; ***
   4th row: evacuation time from 12:55:50-1:00:50; ~5min. ****

   *note, evacuation system was shut down before the valves were closed at ~5min

5. Weighed all the empty vacuumed tubes to 2 decimals and noted weight.
   -the soils lab balance of 3 decimals was used.

6. Filled tubes with water, using a 26G 20mL syringe.
   -the tube was to take in the amount of water the vacuum suction would permit, the water was **not** to be injected
   -noted the amount of water taken in

7. Re-weighed all tubes partially filled with water to its vacuum capacity of suction. Recorded to 2 decimal.
   -again it was the 3 decimal soil lab balance that was used to maintain consistency

8. Filled all tubes to capacity with water:

-used a clean 600mL beaker filled with tap water, i.e. the same that was used to fill the tubes
-plunged the exetainer tube into the beaker
-opened cap under water
-waited till the tube is completely filled (no bubbles)
-closed cap while tube is still under water

9. Re-weighed all tubes completely filled with water, recorded to 2 decimals.
-again it was the 3 decimal soil lab balance that was used to maintain consistency

10. Calculated percent differences, averages, %C.V. with data.

July 18, 2003: Started over experiment testing evacuation efficiency (after 3 septum punctures) at different time intervals after initial evacuation (4, 7, 13, and 18 days).

1. Divided the 40 fresh tubes into 4 sets:
1st row: 405-480-402-440-406-437-419-455-460-497;
2nd row: 404-418-425-439-414-493-456-421-416-492;
3rd row 403-424-436-444-438-417-442-420-500-422;
4th row: 401-434-494-495-481-475-441-423-415-454.

2. Evacuated each set of ten tubes for five minutes
1st row: evacuation time from 13:09:02-13:14:02; ~5min ;
2nd row: evacuation time from 13:15:51-13:20:51; ~5min;
3rd row evacuation time from 13:22:19-13:27:19; ~5min;
4th row: evacuation time from 13:29:04-13:34:04; ~5min.

-for all evacuations done, the tubes were simultaneously (3 to 4 tubes at a time, till all ten were removed) removed at ~5min before the pump was shut. Pressure never fell below 25 psi.

3. Filled tubes with 20mL of N_2.
-a 26G 30mL syringe was flushed 3 times w/ N_2
-the syringe was then filled to 20mL
-the exetainers were then injected with 20mL of N_2, the volume initially pulled in by the vacuum was noted
-the exetainers were then over pressured with N_2 to inject a total volume of 20mL

(***caps were tightened***)

4. Evacuated each set of ten tubes for five minutes **again**
1st row: evacuation time from 14:04:57-14:09:57;
2nd row: evacuation time from 14:11:56-14:16:56; 3rd row evacuation time from 14:18:30-14:23:30;
4th row: evacuation time from 14:25:00-14:30:00.

5. Weighed all the empty vacuumed tubes to 2 decimals and note weight.
   -the soils lab balance of 3 decimals was used.

6. The predetermined amount of time was allowed to pass for each row of tubes (i.e., Row 1: 4 days, Row 2: 7 days, Row 3: 13 days, Row 4: 18 days).

7. Remaining steps same as for previous test: July 3, 2007, steps 7 to 10.

A.2. EVACUATION TEST RESULTS

A.2.1. July 3, 2003

The overall same-day evacuation efficiency attained was 93.1% evacuation with a standard deviation of 1.1%. A possible trend was noted in the order that stopcocked valves were closed at the end of evacuation: Tubes where the valves were closed first had slightly greater evacuation (as high as 94.7%); it decreased in a matter of the seconds it took to finish closing the valves to as little as 91%. This trend was not statistically tested.

A.2.2. July 18, 2003

The overall evacuation efficiency attained was as follows:

Date tested (Day post evacuation)	Evacuation Result	
	Average (% evacuated)	Std. Deviation (%)
July 22, 2003 (Day 4)	94.7	0.7
July 25, 2003 (Day 7)	93.7 [a]	2.1 [a]
July 31, 2003 (Day 13)	94.3	1.2
August 5, 2003 (Day 18)	94.3	1.3

[a] One unusually low value of 88.9% was seen in this group. If this outlier is removed, the average increases to 94.2% and the standard deviation decreases to 1.4%.

It can be noted here that there was virtually no decrease in evacuation state 18 days after the initial evacuation and the standard deviation remained fairly constant. The results are actually slightly better than the July 3, 2003 test, probably because of an adjustment in the procedure whereby the tubes were all removed (pulled off very quickly) while the vacuum was still in operation (and stopcock valves were left open). The trend in higher evacuation for tubes pulled off the vacuum first was not seen in these tests.

A.2.3. Discussion

It can be presumed that the principal reason 100% evacuation was not attained was due to the healing time of the double-septum, which can take from 9 to 25 s according to Rochette and Bertrand (2004). Other issues might include a leaky system and thus imperfect vacuum (maximum not reached). In comparison, Rochette and Bertrand (2004) had better results with their evacuation system (97.6% evacuation after 14 days). They also found that there might be a slight loss in N_2O due to reactivity with the inside of the glass vial and rubber septum. This was monitored in this study by taking field samples of a reference gas of known concentration at the same time unknown air samples were being collected. The loss in gas concentration was taken into account when unknown samples were analyzed.

Based on these results, the recommended procedure for use of the A.E.R. Lab in-house Exetainer evacuation apparatus would include the following steps:

1) Place a few grains of dessicant in the bottom of each 12 mL Exetainer tube.
2) Remove manufacturer's grey-black rubber septum from Exetainer, insert white PTFE silicone septum (hard side up), and replace rubber septum beneath it.
3) Screw cap back on firmly but carefully (cap can become crooked if screwed on too much).
4) Evacuate tubes for 5 minutes, removing tubes quickly at the end of this time, without shutting off the vacuum pump.
5) Fill tubes with 20 mL of N_2 (goal being to flush out any ambient air possibly left in tube).
6) Evacuate tubes a second time (5 minutes), removing tubes quickly at the end of this time, without shutting off the vacuum pump.

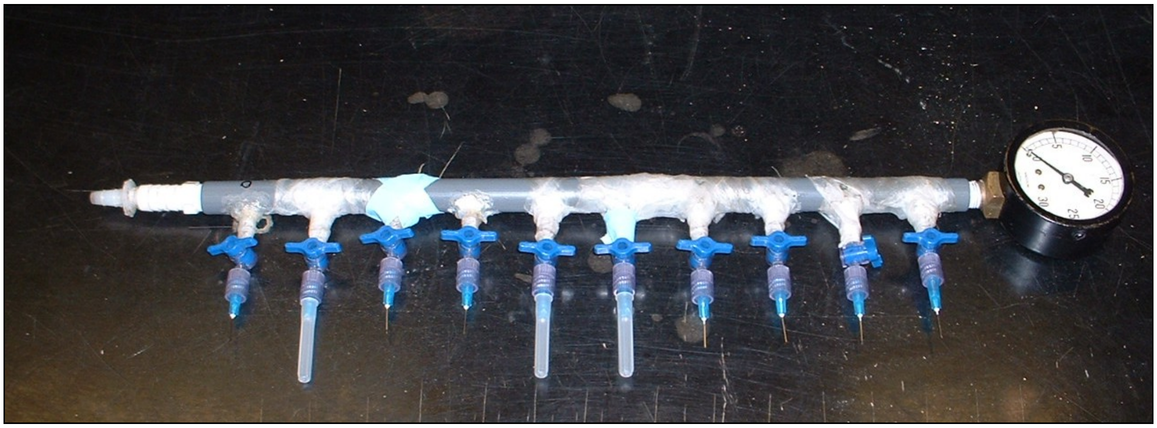

Figure A-1. In-house assemble evacuation manifold, consisting of ten 26G needles on Luer-Lok ports, inserted into a plastic tube and fastened with silicone, vacuum pressure gauge, and end connector for tubing from vacuum pump (not shown). Additional taping to minimize leaks at joints where sampling ports meet plastic tube. A double septum-sealed Exetainer tube is inserted on each sampling port and the vacuum pump turned on.

APPENDIX B: ANALYTICAL METHODS FOR GAS CHROMATOGRAPHY

B.1 CH_4 METHOD FOR SHIMADZU GC-8AIF (FLAME IONIZATION DETECTOR-FID)

B.2 N_2O METHOD FOR HP 5890 (ELECTRON CAPTURE DETECTOR-ECD)

B.3 COMPARISON OF RESULTS GENERATED BY GC AND TDL-TGA

B.1 CH_4 METHOD FOR SHIMADZU GC-8AIF (FLAME IONIZATION DETECTOR-FID)

This method was established following a series of validation tests performed in June 2002.

Chromatographic Conditions

Compressed Air (regulator pressure)	50 psi
Hydrogen (regulator pressure)	30 psi
Carrier Gas: Helium (regulator pressure)	50 psi
Column (packed)	Porapak Q 80/100
Column Head Pressure	1.25 kg/cm^2
Carrier Gas Flow Rate	30 mL/min
Oven Temp. (COL)	50°C
Injector/Detector Temp. (INJ/DET)	150°C
Integrator settings [2]	pk wd = 0.04, thrsh = 2, att^2 (peak attenuation)=1, chart speed= 5
Integrator functions	INT(0) at 0.4 mins (reset baseline) INT(8) at 0 mins (start tick marks)
Sample Size[3]	3 cc/injection
Sample Loop Size	~ 900 µL (0.9 mL)
Retention Time	~ 0.5 mins
Run Time[4] (set on integrator)	At least 1min

Turning on GC (at least 1 hour before sample analysis-note time you turn it on):

1. Turn on compressed air, hydrogen, and helium cylinders.
2. As per manual: Supply carrier gas to GC (toggle at rear of GC).
3. Set carrier pressure to 1.25 kg/cm^2 (CARRIER GAS 2).
4. Set INJ/DET temperature to 150°C and set COL to 50°C. Leave temp readout in COL position.
5. Turn power on.
6. Switch temp readout to INJ/DET.
7. Feed air and H_2 to detector (toggle at rear of GC). For ignition: "Air"=0.2 kg/cm^2, "Hydrogen 1" =0.9 kg/cm^2.
8. Light detector "DET 1" with flame igniter. **Never turn on the oven or the detector without turning on the carrier flow first. Check ignition with shiny object (condensation should form).
9. Set both air and H_2 to 0.5 kg/cm^2.

Integrator:

1. Check ink. Use paper clip to prime ink cartridge.
2. Verify peak width (pk wd), threshold (thrsh), att^2, and chart speed by pressing the "LIST" button twice.
3. Set date and time. Type "d-a-t-e mm/dd/yyyy" and enter, and " t-i-m-e hh:mm:ss" and enter.
4. Chart attenuation at 0 or can be adjusted (integration not affected). See integrator manual.
5. Integrator may be set to show "tick" marks denoting start and end of peak integration.
6. Set/Verify run time on integrator:

   TO VERIFY timed functions: "LIST" "TIME" enter.
   TO SET RUN TIME: "TIME" (time) "STOP" enter.
   TO SET INT FUNCTIONS: "TIME" (time) "INT()" (number) enter.

Sample Handling Prior to Injection:

---

[2] Chosen in accordance with integrator manual instructions, for the peaks seen during testing.
[3] Suggested in order to flush out sample loop. Minimum injection volume at least 3 mL.
[4] Suggested to avoid incomplete integrations (especially at high concentrations).

1. Use a syringe/needle that has been flushed with N_2 just prior to drawing in the sample. Syringes/needles can be reused for replicates of the same sample, as well as for blanks and reference standards as long as they are labeled and devoted to their respective contents. (i.e., “blank” syringe is just for blanks, 0.5 ppm is just for 0.5 ppm).
2. Special attachment, “stopcock”, is required to be attached to the syringe (where the needle would be) to inject a sample into the GC.
3. Attach needle to the stopcock, open stopcock, and withdraw sample into syringe. Close stopcock.

Sample Injection

1. Sample injection port handle should be set to “LOAD”.
2. Remove needle from stopcock, and screw end of stopcock into the sample injection port (onto the needle).
3. Open stopcock on syringe. Load contents of syringe into injection port.
4. Switch injection port to “INJECT”.
5. IMMEDIATELY press RUN/START on the integrator keyboard. Wait 5 seconds and switch handle back to “LOAD”.
6. Note it is important to keep the timing of this sequence consistent because retention time changes with “injection” and “start run” synchronization.
7. Wait until completion of run time (set on integrator).
8. After injection of a set of replicates, flush syringe/stopcock/needle with N_2 before moving on to next set of replicates.

Suggested Injection Sequence:

One (1) blank (pure nitrogen N_2) (cylinder found in Soils lab)

Standard Curve[5]

NOTE: For each std there should be at least 3 readings within 5% of each other, verify this as you go:
At least three (3) reps of low standard (*e.g.,* 1 ppm), verify that they are within 5% C.V.
At least three (3) reps of mid std (will be compared against field std) (*e.g.,* 10 ppm)
At least three (3) reps of high standard (*e.g.,* 20 ppm)
Flush syringe with N_2.

Samples:

Set of replicate injections for first field sample[6]
Ideally flush syringe with N_2 between each set
Set of replicate injections for next field sample
…etc. …etc.

Standard Curve (optional):

Three (3) reps of low std (again within 5% CV)
Three (3) reps of high std

END

Shutting Down GC (in this order, on a daily basis):

1. Set COL to 20°C, push reset, open oven door.
2. Turn off recorder.
3. Toggle off H_2 supply (will extinguish detector flame).
4. INJ/DET lowered to 0 °C.
5. Wait until INJ/DET and COL are lowered to at least 100 – 150°C.
6. Turn off power.
7. Toggle off compressed air and helium.
8. Close valves for all cylinders.

[5] Standard curve may be injected at beginning and end of run in order to verify there is no detector drift. FID is known to be very linear (and so mid-std may be left out in second curve). However, for very short analyses (*i.e.,* less than 2 hours’ worth) there is no need to inject a second standard curve.
[6] Inject as many replicates as possible for a field sample (at LEAST 3), to avoid relying on one or two values for your sample, one of which may be anomalous. (The GC does give a weird number occasionally).

B.2 N_2O METHOD FOR HP 5890 (ELECTRON CAPTURE DETECTOR-ECD)

This method was established following a series of validation tests performed in Winter and Spring 2002.

Chromatographic Conditions

Compressed Air (regulator pressure)	60 psi
Carrier Gas 5% Argon in Methane (regulator pressure)	60 psi
Column (packed)	Poropak Q 80/100 (L= ?, O.D. = ?)
AUX Gas	On
Set Column Head Pressure	24 psi
Total Flow Rate[7] (carrier + aux gas)	76-79 mL/min
Carrier Gas Flow Rate[1]	15-18 mL/min
Oven Temp.	70°C
Detector Temp.	400°C
Integrator [8]	pk wd = 0.10, thrsh = -1
Sample Size[9]	10 cc/injection
Sample Loop Size	250 µL (0.25 mL)
Retention Time	~ 5.0 mins
Run Time[10]	6 mins

<u>Turning on GC (at least 2 hours before sample analysis or night before):</u>

10. Turn on compressed air (60 psi) if not already on (runs pneumatics of GC).
11. Turn on carrier flow (60 psi) (Ar/Me).
12. Turn on AUX gas.
13. Set column head pressure to 24 psi.
14. Turn on GC oven. Set oven temp. to 70°C.
15. Turn on detector B (ECD). Verify detector temp. is 400°C. **Never turn on the detector without turning on the carrier flow first.

<u>Starting analysis:</u>
<u>Integrator</u>:

7. Check ink. Use paper clip to prime ink cartridge.
8. Verify peak width (pk wd) and threshold (thrsh) by pressing the "LIST" button twice. Threshold may need to be decreased to -2 for 0.1 ppm std to be detected (see during sample run).
9. Check date and time. See integrator manual for adjustment.
10. Chart attenuation at 0 or can be adjusted (integration not affected). See integrator manual.
11. Integrator may be set to show "tick" marks denoting start and end of peak integration.

<u>Sample Handling Prior to Injection:</u>

4. Use a new syringe/needle for each individual field sample. Syringes/needles can be reused for replicates of the same sample, as well as for blanks and reference standards as long as they are labeled and devoted to their respective contents. (i.e., "blank" syringe is just for blanks, 0.5 ppm is just for 0.5 ppm).

---

[7] Flow rate can be verified using a bubble flowmeter. Turn off detector when checking flow rate (especially if AUX gas is turned off, as there needs to be a minimum of 20 mL/min going through the detector).
[8] Chosen in accordance with integrator manual instructions, for the peaks seen during testing.
[9] Suggested in order to flush out sample loop. Minimum injection volume at least 3 mL.
[10] Suggested to avoid incomplete integrations (especially at high concentrations).

5. The needle may get blocked with septum debris. If this happens, remove needle, expel contents of syringe, place new needle on syringe, and re-take your sample. (i.e., if you have any sample left to re-take. If you use what is in your syringe after having removed the needle, there is a chance it will be contaminated.)
6. As well, an accumulation of moisture was sometimes noted in the syringes after about 5 uses, so monitor this and perhaps discard your reused syringes if this is seen.
7. The septum in the sample injection port should also be changed occasionally as it must maintain a seal.

Sample Injection[11]

1. Inject contents of syringe into injection port (through septum).
2. Press START on GC control panel.
3. Wait until completion of run time before injecting the next sample.

Suggested Injection Sequence:

Two (2) blanks[12,13]

Standard Curve[14]:

Six (6) reps of low standard (e.g., 0.1 ppm)
Six (6) reps of medium standard (e.g., 0.5 ppm)
Six (6) reps of high standard (e.g., 1.0 ppm)
One (1) blank[15]

Samples:

Set of replicate injections for first field sample[16]
One blank
Set of replicate injections for next field sample
One blank
…etc. …etc.
One blank

Standard Curve:

Six reps of low std
Six reps of mid std
Six reps of high std

END

Shutting Down GC (in this order, on a daily basis):

9. Turn off detector.
10. Turn off oven.
11. Turn off carrier gas (small valve).
12. Leave compressed air on (it will not be used if GC is not used).
13. Leave integrator on (turning it off resets the date, time, and any other settings).
14. If turning off the GC for an extended period of time (i.e., a week), shut off all regulators completely.

---

[11] Note there is a back-flushing of the GC pre-column at 1.75 mins. into the run (valve 2 shuts off).
[12] Blank is 100% N_2, chosen because this is the balance gas in the N_2O gas standards (e.g., 0.5 ppm N_2O in N_2). There is a large N_2 cylinder for this purpose.
[13] Blanks at beginning of run are recommended to flush column of whatever remains from a previous analysis. At concentrations of 1 ppm or lower, one blank may be used to clear the column to prevent potential carryover.
[14] Standard curve is injected at beginning and end of run in order to verify there is no detector drift (according to literature, ECD signal is known to drift).
[15] Injection of one blank is recommended when going from higher to lower concentrations as well as between sets of replicates of individual field samples to prevent contamination from one sample to the next.
[16] Inject as many replicates as possible for a field sample (at LEAST 3), to avoid relying on one or two values for your sample, one of which may be anomalous. (The GC does give a weird number occasionally).

B.3 COMPARISON OF RESULTS GENERATED BY GC AND TDL-TGA

A cross-comparison of results obtained from GC and TDL-TGA was made for CH_4 and N_2O measurements.

2002 results from the N_2O GC were considered erroneous as they yielded fluxes far higher than the TDL values (1-3 orders of magnitude) and far higher any expected values using the NBL method in an agricultural landscape. GC analysis for N_2O was therefore stopped for 2003 and TDL analysis maintained. It is surmised that despite the testing and development of a method to yield better results, the ambient N_2O concentrations were too close to the limit of detection of the GC to be accurate.

GC results for methane were much more in correspondence with TDL results (see Table B.1 and Figure B.1). Values were within one order of magnitude and only differed in sign three out of eight times. Based on these results, CH_4 TDL was stopped and GC continued.

Table B-1. Methane results: GC vs. TDL

CH_4 Flux ($\mu g/m^2/s$)			
DATE	Profile	GC	TDL
06/24/02	A-B	0.32	-0.91
06/28/02	A-B	-0.35	0.63
	B-C	-0.34	-0.33
	C-D	-0.60	
	D-E	3.03	
	E-F	-2.93	-0.32
	A-F	-0.24	
	C-E	1.24	-0.02
07/28/02	A-B	-3.05	-6.82
	B-C	-2.81	
	C-D	1.07	0.31
	D-E	-0.82	
	E-F	1.91	0.40

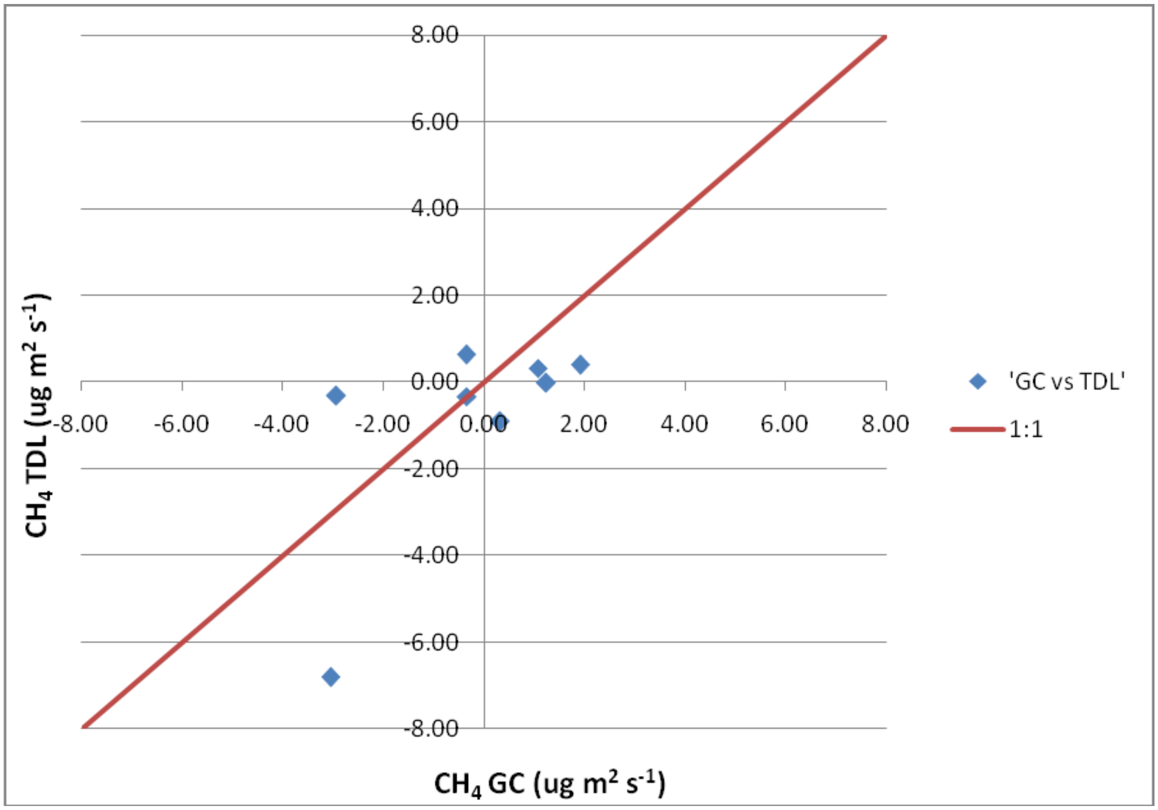

Figure B-1. Correspondence of GC to TDL values for methane.

APPENDIX C: SOURCES OF ERROR AND UNCERTAINTY IN CO_2 FLUX CALCULATION

C.1. COORDINATION BETWEEN INSTRUMENTS

Slight uncertainties in flux calculation may arise due to the necessity to coordinate readings between the CIRAS-SC IRGA and the tethersonde. This was necessary because the CIRAS-SC IRGA could not record pressure to at least one decimal, and so we could not derive measurement height from this instrument alone. Further potential differences arose because the CIRAS measurement frequency was not as high as tethersonde and also physically the instruments were by necessity placed about 1 m apart from each other on the tetherline. Measures were taken to minimize any discrepancies between instruments by attempting to fix start heights to the actual height each instrument was physically upon launching the balloon and matching this height to signs in the data that indicated start of ascent (*e.g.* , decrease in pressure or CO_2 concentration, increase in temperature, etc.). However, when looking at the data it was sometimes not extremely obvious where to pin down the start of ascent, due to fluctuations in measurements of pressure by the tethersonde. The tethersonde was physically at a height of 2 m from the ground so all ascent starts were adjusted for start at that height. The CIRAS was actually about 3 m above the ground (1 m above the sonde) but its first measurements upon launching often had to be ignored due to: 1) adjustment from compressed air to ambient air, and 2) because measurements were only recorded every ten seconds, the balloon's ascent rate (on average 0.12 m/s) meant that the next measurement would be approximately 1.2 m above this, and so the start height of measurements (waiting two readings so that the CIRAS was stabilized) was taken to be approximately 2.5-5 m. Once the start heights were determined it was necessary to filter the tethersonde data to correspond to CIRAS data in order to use tethersonde pressure with CIRAS water vapor pressure in the hypsometric height calculation for CIRAS. To do this, first the start heights were determined for both instruments (2 m for tethersonde, 5 m for CIRAS). Once the measurement associated with the 5 m height had been determined for the CIRAS, the CIRAS time at this measurement was synchronized with the tethersonde time at 5 m. Then the tethersonde measurements were placed in a Microsoft Access table, and were filtered by query for readings at every hh:mm:10, hh:mm:20, hh:mm:30, etc., +/- 2 seconds because that was when the CIRAS recorded its readings. These readings were then matched with the sonde +/- 2 sec. and so were not always a precise match and could be sometimes as much as 4 seconds off, translating into an almost 0.5 m difference.

This type of height uncertainty could be eliminated with the development of lightweight portable instruments concurrently measuring gas concentration (*e.g.,* CO_2, CH_4, N_2O) and height (along with appropriate environmental variables).

C.2. INTERPOLATION OF CO_2 CONCENTRATION TO GLOBAL Z AXIS

Once the CO_2 and tethersonde data were filtered and synchronized, because each profile had different z values as measured by the tethersonde, it was considered convenient to interpolate CO_2 concentrations from all profiles to fit to a global z axis of z = 1 to 120 m, with fixed intervals of 1 m. This procedure allowed easy graphical plotting of all profiles together and helped to determine CO_2 convergence heights along with concurrent temperature and *u* profiles. A comparison between fluxes calculated with the average of concentration differences calculated at each 1 m of the global z axis vs. the difference in average CO_2 concentration (subtracting the average concentration up to the integration height of the first profile from that of the second profile) revealed that they were identical.

C.3. CONVERSION FROM ppmv TO mg m^{-3}

The CIRAS gives CO_2 concentration in ppmv (parts per million by volume) based on an internally dried air sample at a fixed internal temperature and pressure. This output was converted to mg m^{-3} reflecting actual atmospheric pressure and temperature conditions as the balloon was ascending.

A significant difference in flux value was also seen depending at which point the conversion of CO_2 concentrations from ppmv to mg m^{-3} took place. In the first method, the average difference in concentration was calculated first in ppmv and this value was then converted to mg m^{-3} (based on an average molar volume for the profile). When this was compared to first converting concentrations at all heights to mg m^{-3} and then computing the average difference in concentration, it resulted in differences of 6 to 62% in the flux value, with the average being about 20%. It is considered that the second method is more precise and was therefore used.

A test was also done to see the effect of using an average profile molar volume vs. molar volumes calculated at each height throughout the vertical profile on the ppmv to mg m^{-3} conversion. The difference between these two methods was minimal (average difference of 0.6%).

C.4. NON-STATIONARITY

Lastly, non-stationarity of atmospheric variables within a vertical profile should be not be forgotten, as gas concentrations, temperature, wind speed and direction could all be changing from top to bottom within the 10-15 minute ascent period. However, this error cannot really be evaluated unless compared with an instrument that measures the same variables in the same way, instantaneously for the entire height of the profile.

APPENDIX D: IMPACT OF TETHERSONDE TEMPERATURE HYSTERESIS ON NOCTURNAL SOUNDINGS

D.1 INTRODUCTION

Air temperature measurement is key to the application of the NBL budget method. The temperature profile, together with the horizontal wind speed profile, determines the bulk structure of the nocturnal boundary layer. Low wind speeds and rapidly decreasing air temperature from the surface upward (due to longwave radiation loss) form the basic elements allowing the establishment of a very stable nocturnal boundary layer and the accumulation of trace gases.

Correct measurement of air temperature is necessary to the NBL technique to obtain (1) the correct height of tethered balloon measurements, using the hypsometric equation (Equations 3.1 to 3.3) (Stull, 1988), (2) through the potential temperature profile (Equation 3.4), an accurate characterization of the degree of stability of the NBL (*i.e.,* the rapidity of surface temperature decline and consequent air density decline with height) (Stull, 1988), and (3) the location of turbulent layers found using the Richardson number (*Ri*) for the NBL profile (Equation 3.5) (Mahrt *et al.,* 1979; Stull, 1988) which may delimit the height of accumulation of GHGs in the NBL (Mathieu *et al.,* 2005).

It was therefore considered particularly desirable to verify temperature measurement by the tethersonde system (Model 4A , A.I.R., Boulder, CO) which provided the backbone of the NBL measurement system. This system concomitantly measured air temperature using a bead thermistor, atmospheric pressure, relative humidity, horizontal wind speed using a cup anemometer, and compass direction, at 0.5 Hz. All signals were transmitted to a ground-based receiver and displayed in real time on a laptop computer at the experimental site, allowing immediate viewing and evaluation of NBL conditions.

D.2 TETHERSONDE TEMPERATURE SENSOR: THE THERMISTOR

A thermistor ("thermally sensitive resistor") is a semi-conductor-type temperature sensor made of various metal oxides in which changes in electrical resistance are inversely correlated with changes in temperature (Nicholas and White, 2001; Michalski *et al.,* 2002; Wilson, 2005). Thermistors are normally encased in a sheath and have an operating range of approximately -50°C to 300°C (Michalski *et al.,* 2002).

Both thermocouples and thermistors appear to have a fast thermal response, or thermal time constant (Wilson, 2005), with time constants for thermistors ranging typically from 0.4 to 25 s (the time it takes to reach 63% of the equilibrium temperature) (Michalski *et al.,* 2002). Thermistors, though, would theoretically be the preferred temperature sensor for the NBL budget method as they offer a much higher sensitivity to temperature change (due to a large change in resistance per degree change in temperature) than the thermocouple and are less affected by external electrical interferences (Spokas and Bogner, 1996; Michalski et al., 2002; Nicholas and White, 2001; Wilson, 2005).

D.3 EXPERIMENTAL SET-UP

A test was performed in the micrometeorological laboratory of Agriculture and Agri-Food Canada (Ottawa, ON) on three tethersondes (Model 4A, A.I.R., Boulder, CO.) to verify the accuracy of their temperature readings and their response time to changes in temperature. The sondes' air temperature sensors consisted of a bead thermistor coated in a white epoxy sheath, inside an open-ended cylindrical metal cover (about 3 cm long and 1 cm in diameter). They were connected to a laptop downloading data in real time, and were placed within 5-10 cm of a thermocouple (with no cylindrical metal cover) connected to a datalogger (CR23X, Campbell Scientific, Logan, UT). The individual sondes transmitted temperature readings approximately every eight seconds while the thermocouple data were collected every five seconds. The clock on the tethersonde acquisition computer was synchronized with the datalogger clock. After all instruments showed equilibrium at the ambient temperature of the lab (23°C), the set-up was moved to an isolated room with a temperature maintained at 15°C. After re-equilibrium, the instruments were moved to a location with an ambient temperature of 29°C and then following equilibrium, moved back to the same cold room and then finally after re-equilibrium back to the original lab.

D.4 RESULTS

The various locations generated a succession of ambient temperature steps of 8 and 14°C (Figure D-1). The temperature reading correlation between each sonde and the thermocouple during times of sensor stabilization is shown in Figure D-2. Sensor stabilization time was defined as the time when, following a temperature change, the standard deviation of readings from the sensor over a 16 to 20-second period (readings +/- 8 to 10 s) returned to less than 0.175°C. Readings from all three sondes were highly correlated with those of the thermocouple (Figure D-2). Temperature readings of Sondes 1 and 2 were fairly consistent with each other and were consistently slightly greater than the thermocouple wire (Figures D-1, D-2). Sonde 3 was consistently slightly lower than the other sondes and the thermocouple wire (Figures D-1, D-2). The absolute temperature differences between the sondes and the thermocouple are given in Table D-1. Sonde 2 had both the smallest overall absolute temperature difference (0.27°C) and a very high correlation with the thermocouple ($r^2 = 0.9995$) and was therefore chosen to be used in the field for NBL measurements.

Relative humidity (% RH) was also plotted for all three sondes (Figure D-3). Sonde 2 was the least stable overall, showing much scatter, while Sonde 3 was the most stable comparatively (Figure D-3). Unfortunately, absolute values of %RH were quite different between the sondes (Figure D-3), particularly in the cold room where temperature was controlled. Sonde 3 actually showed the best data capture overall with, by far, the least amount of missing data.

D.4.1 Rate of Response to Temperature Change

The rates of response to temperature change were calculated from the stable point (SD temp < 0.175 °C) prior to the onset of the temperature change to the stable point (SD temp < 0.175 °C) at the end of the temperature transition, for each sensor. These points match what is seen graphically in the temperature difference between instruments (see example using Sonde 2, Figure D-4). The peaks and dips in temperature difference represent the hysteresis displayed by the sonde (Figure D-4). Response rates for the thermocouple and three sondes are shown in Table D-2. While both sensors showed hysteresis, or a certain amount of time to reach stabilization, the thermocouple responded the most rapidly to each temperature change, at three to five times as fast as all the sondes (Table D-2). The rate of change (s $°C^{-1}$) to reach 100% stabilization for all three sondes was on average 1.7 times faster when going from cold to warm than from warm to cold (excluding the last temperature change). This means that the sondes “gained” heat faster than they lost it. However, rate of change to reach 63.2% T change (across all three sondes) showed contradictory results. The rate of response for the thermocouple showed no trends in either direction (warm/cold, cold/warm) whether for reaching 63.2% or 100% equilibrium.

D.4.2 Rate of Response to Relative Humidity Change

A slower rate in the sondes' response from warm to cold was also seen in the %RH, but data scatter in Sondes 1 and 2 prevented a precise determination of the rate. On the other hand, examination of wind speed data on ascent and descent revealed no consistent pattern indicating possible under- or overestimation.

D.4.3 Step-Change During Last Temperature Transition

During the last temperature transition (15 to 23 °C) all three sondes showed a step-like delay in warming before finally reaching the stabilization temperature (Figure D-1). For all three sondes there was a relatively slow increase from 15°C to about 20°C (over 5 minutes) and then a rapid jump (over 2°C in half a minute) at precisely the same time, before eventually stabilizing at about 23-24°C. This delay was not observed in the thermocouple data nor in any sonde temperature data for the first transition from cold to warm. A similar delay pattern, however, was seen in relative humidity data and is clearest for Sonde 3 (no missing data), with a maximum in %RH change at the same time as the temperature change maximum (Figure D-3). Possible reasons for this step-delay are discussed below and the data not included in this temperature response analysis.

D.5 DISCUSSION

The observed sonde temperature response was far larger than the typical thermal response time indicated for this type of thermistor (0.4 to 25 s to reach 63.2% of final temperature) (Wilson, 2005). Why is this?

The heat dissipation constant of thermistors depends on the temperature of the medium of the heat transfer, for example, air, as well as the instantaneous temperature measured by the sensor (Michalski *et al.,* 2002). So heat constants will vary with varying heat transfer conditions (Michalski *et al.,* 2002). Errors due to self-heating may also occur (Michalski *et al.,* 2002; Wilson, 2005). For example, as the air temperature increases, the resistance of the thermistor decreases, increasing the self-heating effect (Wilson, 2005). However, if the sensor mass and thermal conductivity are sufficient, this effect will apparently be negligible; but depending on accuracy requirements, they should be considered (Wilson, 2005). Thermal inertia related to sensor size may also affect the heat constant; the smaller the sensor size the faster the response (Wilson, 2005). Protective covering should also be considered (Wilson, 2005).

In fact, in the test done here, the issue of the flow of air across the sensors probably did influence the rapidness of the response. The air flow was less for the sonde thermistors as they were surrounded by a cylindrical metal cover, where the thermocouple wire was not. Response time, then, might have been improved by having a fan blow air onto the sensors.

However, this probably would not have prevented the measured difference in response for heating vs. cooling. Furthermore, in the strongly stable NBL the wind speed near the ground is negligible (*i.e.,* 0-1 m s^{-1}) so this experiment was a close replicate of the very low-to-negligible near-surface wind speed conditions expected in the field. Perhaps, then, a self-heating error is responsible for the faster attainment of the stabilization temperature when going from cold to warm air.

Regarding the step-delay in temperature change for the last transition, perhaps this occurred because energy was being used to evaporate condensed water on the sensor (or on the cylindrical sensor cover) instead of increasing the air temperature near the sensor. The reason why this would occur only for the second transition from cold to warm is unclear. Perhaps it is related to the smaller degree of temperature change (i.e., going from 15°C to 23°C instead of 29°C as in the first transition). In turn, this could influence the rate of evaporation of water on the sonde sensor/cover. In a field situation, the temperature change would not be this extreme in so short a time and so it is doubtful that such a step-delay would occur.

What does this imply for the NBL vertical profile? During nighttime periods, the surface cools rapidly due to longwave radiation loss and a radiative temperature inversion ensues. The temperature profile takes on a positive exponential shape with a sharp increase with height at the surface (see example in Figure 3.3). From our observations, this temperature decrease can be as much as 0.5 °C m^{-1} at the surface and likely 0.1 °C m^{-1} at 20 m height. It was desirable to have the fastest response time possible to give the most accurate instantaneous temperature readings in this quickly changing region of the temperature profile. If the response time was not rapid enough, a steep temperature gradient would not be captured and a false indication of NBL stability would be given.

With the winch unwinding the tetherline at a speed of 0.12 m/s and the sonde taking readings every 2 seconds (i.e., 1 reading every 0.24 m), the response times necessary to capture a temperature gradient of 0.5 °C m^{-1} (steeper gradient) and 0.1 °C m^{-1} (milder gradient) would be 17 s $°C^{-1}$ and 83 s $°C^{-1}$, respectively. The response time of the sonde from cold to warm (21 s $°C^{-1}$) was slightly slower than required but was far better than the response time going from warm to cold. We therefore chose to use only NBL ascent data where the sonde would be consistently measuring an increase in temperature with height.

In fact, it was found, after examining the tethersonde data from all launches, that every launch (with a few exceptions) showed that the temperature on the descent was greater than on the ascent (typically by about 0.5 – 1°C). This shows again the hysteresis of the sonde's thermistor response to temperature changes from warm to cold.

D.6 CONCLUSION

While it is acknowledged that more repetitions of this test would have more fully confirmed these results, they nonetheless have implications for previous applications of the A.I.R. tethersonde in measuring in conditions of rapidly decreasing temperature. For example, when used to collect NBL profile data, as demonstrated here, using descent data (and therefore going from warmer to colder temperatures) or using too rapid an ascent rate (that would not provide the sonde with enough time to respond to the steep temperature gradient) could give a false indication of the strength of the sensible heat flux and the NBL inversion, and hence the NBL stability. The closer to the ground, the steeper the gradient, and the more serious this effect would be. This could lead to sub-critical Richardson numbers (indicating regions of turbulence) where none actually exist, leading, in the NBL budget method, for example, to misinterpretations of the accumulation of gases near the surface. It is also possible that advection or a change in wind direction could cause a sudden drop in temperature higher up in the profile. Again, depending on profiling direction (up or down) and the ascent speed, the sonde may not be able to respond quickly enough and therefore give misleading information as to the height of the onset, and the degree, of the temperature decline and might even miss a very brief interval of temperature decline completely.

TABLES

Table D-1. Temperature difference (T diff): Three tethersondes (TS) vs. thermocouple reference.

	Ave. T diff (Overall) (°C)	Ave. T diff (Stabilized areas) (°C)	SD T diff. (Stabilized areas) (°C)
TS 1	0.32	0.29	0.22
TS 2	0.27	0.23	0.20
TS 3	-0.28	-0.22	0.20

Table D-2. Response times and rates for tethersonde (TS) and thermocouple (TC) for temperature (T) change when moving from warm to cold to warm locations.

TIME for T (min) to reach 100% of stabilization temperature				
	Warm to Cold	Cold to Warm	Warm to Cold	Cold to Warm
TC	1.2	1.6	1.9	0.8
TS 1	5.0	4.9	8.9	7.2
TS 2	5.3	3.4	8.8	6.2
TS 3	5.4	7.7	9.7	5.8
TIME for T (s) to reach 63.2% of stabilization temperature				
	Warm to Cold	Cold to Warm	Warm to Cold	Cold to Warm
TC	21	44	63	23
TS 1	66	150	157	305
TS 2	59	124	134	217
TS 3	133	216	140	273
RESPONSE RATE for 100% stabilization (sec $°C^{-1}$ change in T)				
	Warm to Cold	Cold to Warm	Warm to Cold	Cold to Warm
TC	9	9	9	6
TS 1	38	22	41	52
TS 2	40	18	40	47
TS 3	47	36	45	47
RESPONSE RATE for 63.2% stabilization (sec $°C^{-1}$ change in T)				
	Warm to Cold	Cold to Warm	Warm to Cold	Cold to Warm
TC	4	6	8	4
TS 1	13	18	19	58
TS 2	12	17	16	43
TS 3	30	27	17	58

FIGURES

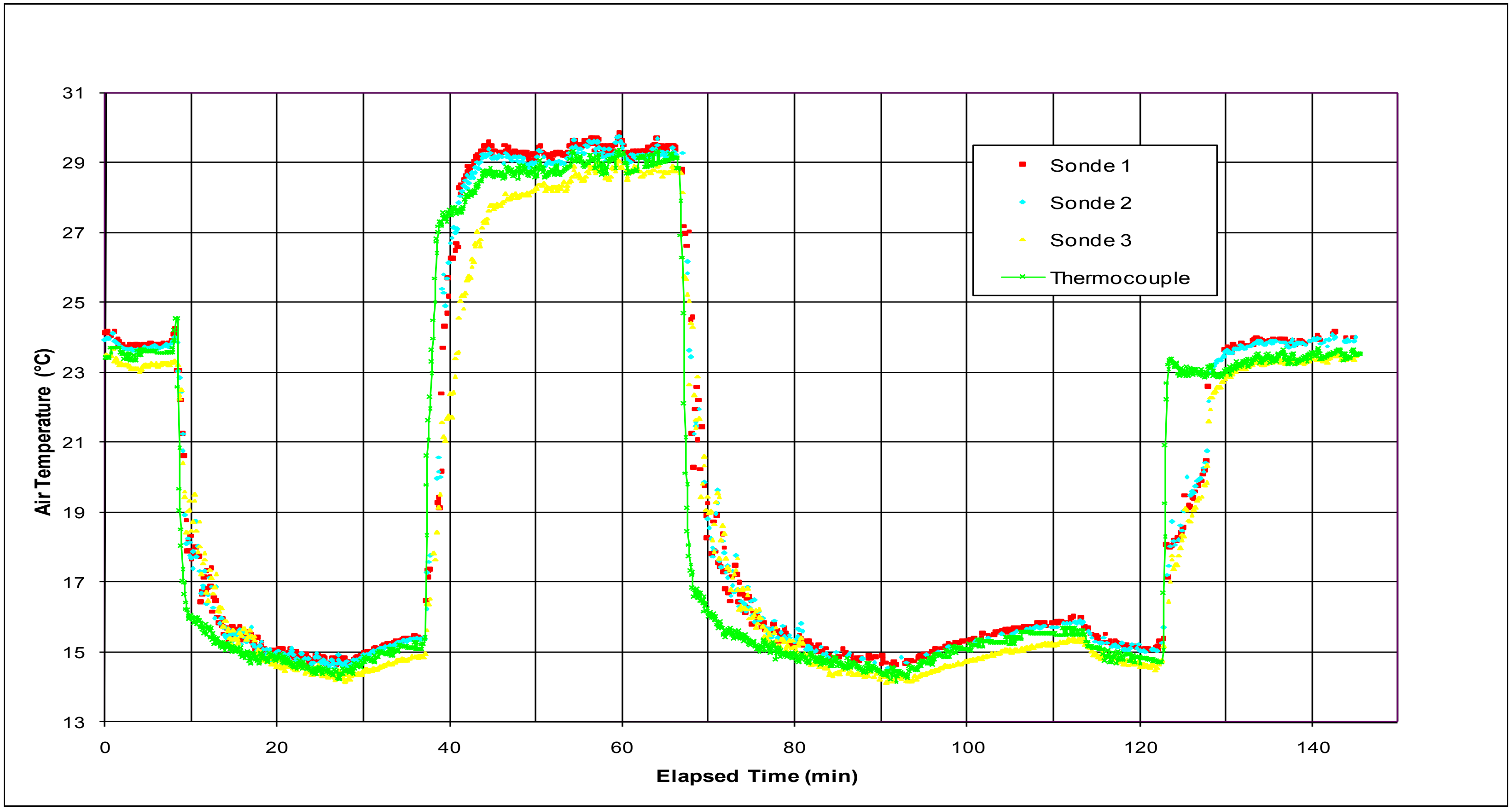

Figure D-1. Air temperature over time for three tethersondes and a thermocouple, moved between several locations varying in ambient temperature.

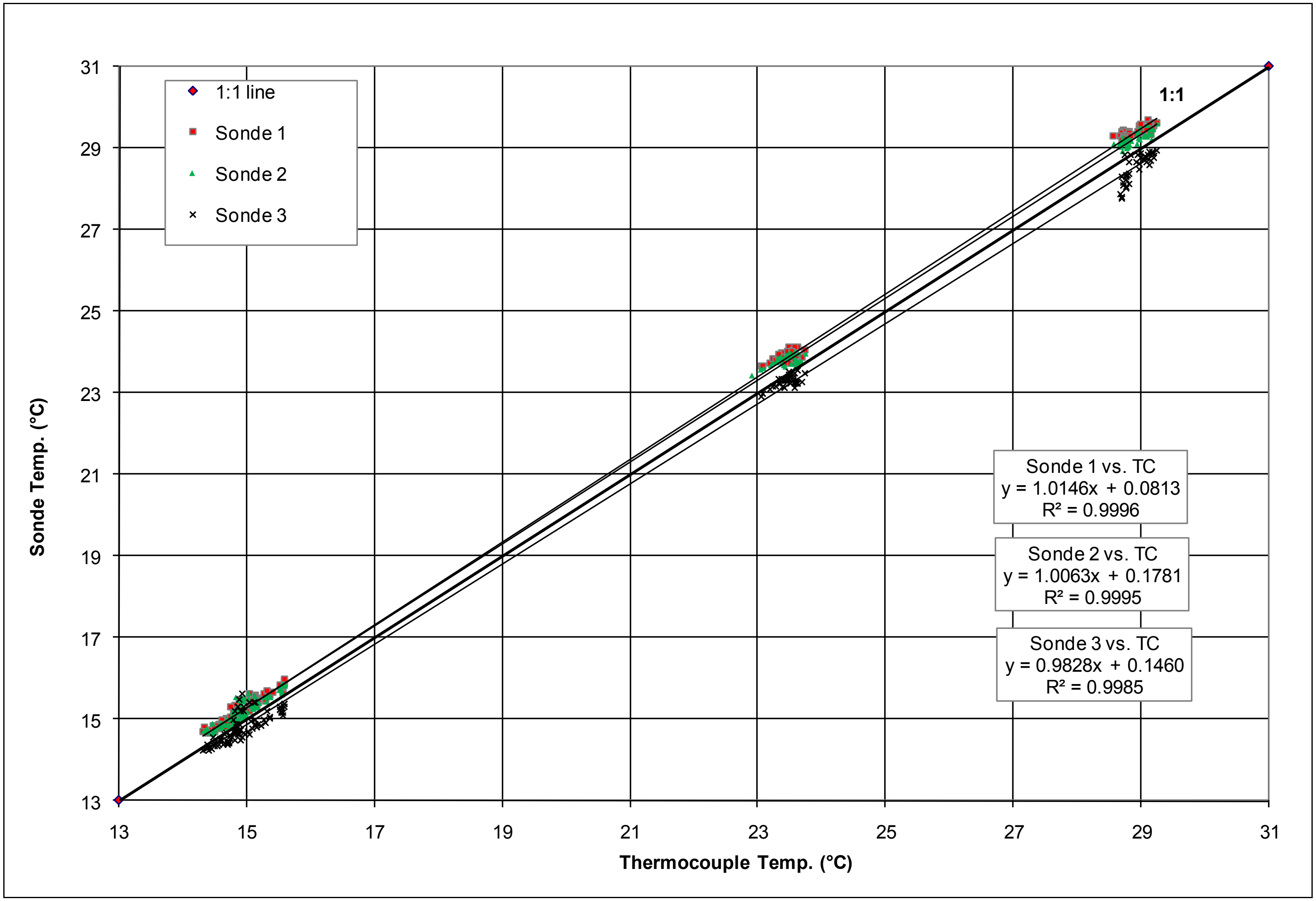

Figure D-2. Correlation of tethersonde and thermocouple results outside of transition periods.

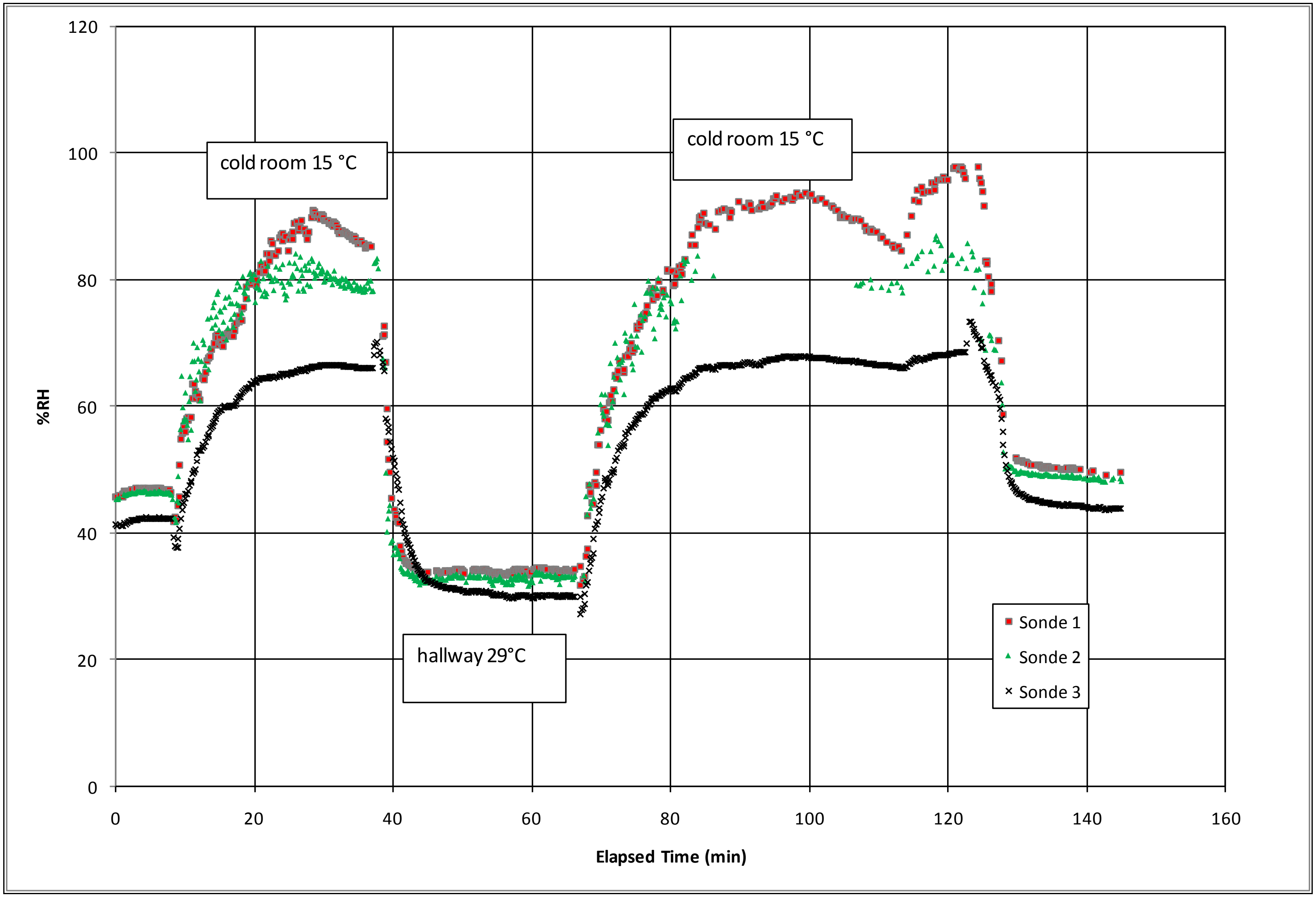

Figure D-3. %RH plotted for three sondes over time and across varying locations.

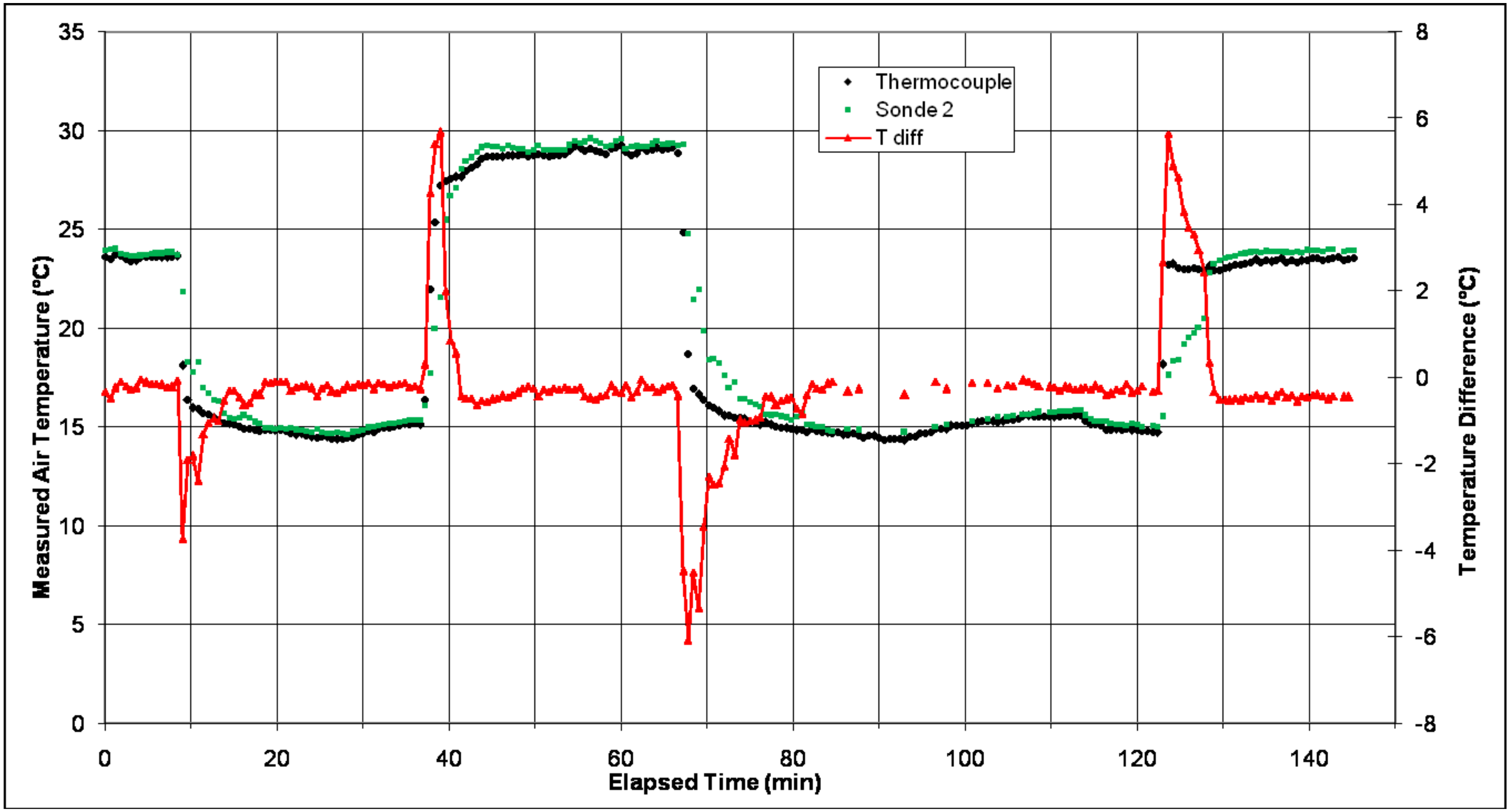

Figure D-4. Temperature difference (red line) between thermocouple wire and sonde 2. Peaks and dips in T diff correspond to periods where the SD in temperature for each respective sonde was greater than 0.175 °C.

APPENDIX E. GHG SOURCE STRENGTH CALCULATION

E.1. TABLE 5.1 Footnotes: Height, wind direction (*u* dir) with variation, concentrations, and comparative source strength from detailed CH_4 profiles measured on the night of August 18-19, 2003, at Coteau-du-Lac, QC.

a Most footprints include drainage ditches but this source probably gets very diluted in the larger footprints (so not included in point source column in table) except for the closest local drainage ditch on the eastern edge of the launch site field. Nighttime sampling of air right above water in ditch gave CH_4 concentration of 3.0 ppmv. Hensen *et al*. (2006) measured up to 250 g CH_4 m^{-2} day^{-1} in ditches next to animal housing.

b Literature suggests a value of 300 g LU^{-1} day^{-1} is typical for dairy cattle housed in naturally ventilated barns (includes manure in barn) (*e.g.,* Kinsman *et al*, 1995; Sneath *et al*., 1997; Kaharabata and Schuepp, 2000; Jungbluth *et al*., 2001). 1 LU (livestock unit) cattle ≈ 500 kg.

c Based on IPCC Tier 2 emission factors for CH_4 emission from beef cattle (90 kg CH_4 $head^{-1}$ $year^{-1}$) and beef cattle manure management (3.5 kg CH_4 $head^{-1}$ $year^{-1}$) (Table A3-6, 2004 Canadian GHG Inventory (Environment Canada, 2006)).

d Estimated at 107 t (based on a typical bulk density of dry cattle manure of about 830 kg m^{-3} and internal temperature of 35°C in month of August (study in Germany by Amon et al., 2001).

e Equation from Amon *et al* (2001), Figure 5.3, used to estimate emissions from dry cattle manure pile closest to launch site shows contribution is much smaller than from the animals themselves.

f Based on IPCC Tier 1 emission factor for CH_4 emission from swine (1.5 kg CH_4 head^{-1} year^{-1}, Table A3-6, 2004 Canadian GHG Inventory (Environment Canada, 2006)). Swine endogenous CH_4 emission is less than 1% of digestible feed intake vs. 10% for ruminants (Corré and Oenema, 1998) but sheer numbers make the emissions comparable.

g Range of values sampled from Kaharabata *et al*. (1998), Zahn *et al*. (2001), Sharpe *et al*. (2002), Wagner-Riddle *et al*. (2006), using micrometeorologically-based methods from outdoor uncovered swine slurry tanks. Wide variation can be explained by differences in manure volume, temperature, and tank surface area (Sharpe *et al*., 2002; Park *et al*., 2006).

h Range based on Sharpe *et al*. (2002) per LU slurry estimate in August 1997 (32.4 kg LU^{-1} year^{-1}). 1 LU swine ≈ 500 kg.

i Based on IPCC Tier 2 emission factors for CH_4 emission from swine manure management (Table A3-6, 2004 Canadian GHG Inventory (Environment Canada, 2006)). This swine farm (2500 head) is assumed to have had equal proportions of pigs under 20 kg (1.8 kg CH_4 head^{-1} year^{-1}), pigs 20-60 kg (5.1 kg CH_4 head^{-1} year^{-1}), and pigs over 60 kg (7.9 kg CH_4 head^{-1} year^{-1}).

E.2. Calculation Method for CO_2 and N_2O Contributions from Daytime Vehicular Traffic in Suburban Portion of Flux Footprint: Ottawa, ON, June 28-29, 2002.

To obtain the daytime estimates of CO_2 and N_2O contributions from vehicular traffic into and out of the city of Ottawa, vehicle count information (7 AM to 7 PM, May to July 2002) was obtained from Mr. Vincent Patterson (Senior Project Manager, Transportation – Strategic Planning, City of Ottawa). Nighttime vehicle count data was not available. The number of vehicles was divided by the proportion of cars, light trucks, and heavy trucks and each category (Environment Canada, 2006) and then multiplied by an estimated average fuel efficiency (L/100 km, city driving) (Natural Resources Canada, 2006) based on an estimated daily travel distance of 80 km, into and out of the Ottawa Greenbelt area (estimated at 2 779 km^2). The total amount of fuel consumed was then multiplied by the appropriate emission factor to obtain the amount of CO_2 generated by fuel combustion. Table E-1, in Appendix E, summarizes the calculation. In any case, it should be noted that the literature estimate for urban CO_2 flux (0.44 mg CO_2 m^{-2} s^{-1}), being taken from micrometeorological field observations, is an integration of CO_2 produced by different sources in a city (*e.g.,* vehicles, industry, vegetation) and may therefore better reflect the true Ottawa urban value than the IPCC-estimated flux from mobile combustion (0.06 mg CO_2 m^{-2} s^{-1}) (Table 6.2a). The literature value is very similar to summer nighttime EC-measured CO_2 flux from a suburban Montreal site with similar population density to the city of Ottawa (EPiCC, 2009, unpublished data).

In the case of N_2O, the vehicle population (cars, light trucks, and heavy trucks) was further subdivided by age of vehicle (Statistics Canada, 2003), which was used to approximate the most likely type of catalytic converter on the vehicle. This determined the appropriate N_2O emission factor (Table E-1.).

Table E-1 summarizes the calculation of daytime CO_2 and N_2O emissions from the City of Ottawa, ON. Methane estimates from mobile combustion are also given in Table E-1 but are not addressed in the main text.

Table E-1. Calculation of CO_2, N_2O, and CH_4 emissions from mobile fuel combustion (vehicular traffic) from National Capital Region.

Vehicle Type/Age[a]	Catalyst Type[a]	Population[a]	Fuel Economy[b]	Daily Distance Travelled[c]	Daily Fuel Used[d]	EF (CO_2)[e]	EF (CH_4)[e]	EF (N_2O)[e]	City Area[f]	CO_2 Emission[g]	*12-h daytime*[h]	CH_4 Emission[g]	*12-h daytime*[h]	N_2O Emission[g]	*12-h daytime*[h]
		Entering/ Leaving Greenbelt	**(L/100 km) (city)**	**thru Ottawa (km)**	**L**	**g/L fuel**	**g/L fuel**	**g/L fuel**	**(km^2)**	**g/km^2/day**	**mg/m^2/s**	**g/km^2/day**	**µg/m^2/s**	**g/km^2/day**	**ng/m^2/s**
Cars															
1995-present	Tier 1	108210	10	80	8	2360	0.12	0.26	2,779	735252	0.0170	37	0.00043	81	0.93753
1985-1994	Tier 0, Aged	40664	11	80	8.8	2360	0.32	0.58	2,779	303932	0.0070	41	0.00048	75	0.86453
<1985	Oxid Cat	5711	15	80	12	2360	0.42	0.2	2,779	58209	0.0013	10	0.00012	5	0.05709
SUVs, PICK-Ups, Vans															
1995-present	Tier 1	69461	16	80	12.8	2360	0.22	0.41	2,779	755144	0.0175	70	0.00081	131	1.51841
1985-1994	Tier 0, Aged	26103	16	80	12.8	2360	0.41	1	2,779	283777	0.0066	49	0.00057	120	1.39172
<1985	Oxid Cat	3666	19	80	15.2	2360	0.44	0.2	2,779	47329	0.0011	9	0.00010	4	0.04642
Freight transport trucks, buses															
Gas	Three-way	4377	40	80	32	2360	0.17	1	2,779	118972	0.0028	9	0.00010	50	0.58347
	Non-catalyst	274	40	80	32	2360	0.29	0.046	2,779	7449	0.0002	1	0.00001	0	0.00168
Diesel	Advanced, Moderate, Uncontrolled	9444	40	80	32	2730	0.13	0.08	2,779	296915	0.0069	14	0.00016	9	0.10070
	TOTAL:	**267911**			**166**					**2606979**	**0.06**	**241**	**0.0028**	**475**	**5.5**

a Categories based on Table A-13-5, Environment Canada (2006). Information on vehicle age, catalyst type, and vehicle population and traffic information (May to July 2002) compiled from the following: Environment Canada (2006), Mr. Vince Patterson, Transportation – Strategic Planning, City of Ottawa (2006), Statistics Canada (2003), Ontario Ministry of Transportation (2004, 2006), and Natural Resources Canada (2000).

b Fuel economy information from Natural Resources Canada (2004, 2006).

c Estimated daily commute through Ottawa

d Calculated as: Fuel economy (L/100km) /100 × distance traveled (km)

e Emission factors based on Table A13-5, Environment Canada (2006). New emission factors are available for 2007 Table A12-7, Environment Canada, 2008) but as changes are not extreme, numbers here have not been updated.

f Wikipedia, November 2006. <http://en.wikipedia.org/wiki/Ottawa>

g Calculated as: Daily fuel used × respective EF /City area

h Calculated for 12 hour traffic period (7AM to 7 PM).